Development and characterization of novel transgenic techniques for the study of neuronal circuitry

By:
Victoria Heimer-McGinn
Department of Biochemistry
University College Cork, Ireland

A thesis presented to the National University of Ireland
for the degree of Doctor of Philosophy

April 2013

Head of department: Thomas D. Cotter, PhD
Thesis supervisor: Paul Young, PhD

Table of Contents

I. Declaration

I hereby declare that the work presented in this thesis is original and entirely my own. This dissertation, to the best of my knowledge and belief, has not been previously submitted, in part or in whole, to the National University of Ireland, Cork or any other university for any degree.

Wherever contributions of others are involved, every effort has been made to indicate this clearly; with due reference to the literature, and acknowledgement of collaborative research and discussions.

_____

Victoria Heimer-McGinn

April 2013

II. Table of Abbreviations

Abbreviation	Description
AD	Alzheimer's disease
AMPA	2-amino-3-(3-hydroxy-5-methyl-isoxazol-4-yl)propanoic acid
AMPAR	AMPA receptor
ABPs	actin binding proteins
BAC	bacterial artificial construct
BDNF	brain-derived neurotrophic factor
BoNT	botulinum neurotoxin
bp	base pair
Ca	calcium ion
CA1	cornu ammonis 1
CA2	cornu ammonis 2
CA3	cornu ammonis 3
CaMKII	calcium-calmodulin-dependent kinase II
CAMs	cell adhesion molecules
cDNA	complementary deoxyribonucleic acid
CFP	cerulean fluorescent protein
ChR2	channelrhodopsin-2
Cl	chloride ion
CMV	cytomegalovirus
CNS	central nervous system
Cre	causes recombination
DAPI	4',6-diamidino-2-phenylindole
DEPC	diethylpyrocarbonate
DIG	digoxygenin
DNA	deoxyribonucleic acid
dox	doxycycline
DRG	dorsal root ganglion
DSCAM	Down syndrome cell adhesion molecule
EPSC	excitatory postsynaptic current
ER	estrogen receptor
ES	embryonic stem cells
ESC	embryonic stem cells
FLEx	flip excision
fmi	Flamingo
FP	fluorescent protein
GAP	GTPase activating proteins
GAPDH	glyceraldehyde 3-phosphate dehydrogenase
GEF	guanine exchange factor
GFAP	glial fibrillary acidic protein
GFP	green fluorescent protein
GKAP	guanylate kinase-associated protein
GluCl	Glutamate-gated Cl- channels
GOI	gene of interest
GPCR	G protein coupled receptor
ICC	immunocytochemistry
IHC	immunihistochemistry
IP	immunoprecipitation
IRES	internal ribosomal entry site
ISH	*in situ* hybrydization

K	potassium ion
kDa	kilodalton
Kir	inward rectifying potassium channel
LBD	ligand-binding domain
LTD	long-term depression
LTP	long-term potentiation
MADM	mosaic analysis with double markers
mEPSC	mini EPSC
MIST	molecules for inactivation of synaptic transmission
mRNA	messenger ribonucleic acid
Ms	mouse
Na	sodium ion
NBT/BCIP	Nitro blue tetrazolium / 5-Bromo-4-chloro-3-indolyl phosphate
NeuN	neuronal nuclei
NMDA	N-methyl-D-aspartate
NMDAR	NMDA receptor
NMJ	neuromuscular junction
OLIG2	oligodendrocyte transcription factor 2
PAGE	polyacrylamide gel electrophoresis
PBS	phosphate-buffered saline
pBSII-SK$^+$	pBlueScriptII-SK$^+$
PCR	polymerase chain reaction
PFA	paraformaldehyde
PFC	prefrontal cortex
PLP	proteolipid protein
PNS	peripheral nervous system
PR	progesterone receptor
PSD	postsynaptic density
PVA	polyvinyl alcohol
Ras	abbreviation of "rat sarcoma"
RasGAP	RAS p21 protein activator
RASSL	receptor activated solely by a synthetic ligand
Rb	rabbit
RCG	retinal ganglion cell
RFP	red fluorescent protein
RMCE	recombinase-mediated cassette exchange
RNA	ribonucleic acid
rtTA	reverse tTA
SA	spine apparatus
SAPAP	synapse-associated protein 90/postsynaptic density-95-associated protein
SB	Southern blotting
SDS	sodium dodecyl sulphate
SER	smooth endoplasmic reticulum
SHANK	SH3 and multiple ankyrin repeat domains protein
SLICK	single-neuron labeling with inducible Cre-mediated knockout
SNARE	soluble NSFattachment protein (SNAP) receptors; NSF is N-ethylmaleimide-sensitive fusion
SOB	super optimal broth
SSR	site-specific recombination
SSR	site-specific recombination
SynGAP	Synaptic Ras GTPase-activating protein

SZ	Schizophrenia
TBS	Tris-buffered saline
TBST	TBS-Tween
TeNT	tetanus neurotoxin
tet	tetracycline
tetO	tet operon
TetoxLC	tetanus toxin light chain
tTA	tetracycline transactivator
VAMP	vesicle-associated membrane protein
WB	western blotting
X-gal	5-bromo-4-chloro-indolyl-β-D-galactopyranoside
YFP	yellow fluorescent protein
β-gal	β-galactosidase

III. Published work arising from this thesis

Papers:

VICTORIA HEIMER-MCGINN & PAUL YOUNG. 2011. Efficient inducible Pan-neuronal Cre-mediated recombination in SLICK-H transgenic mice. *Genesis,* 49**,** 942-9.
(Discussed in Chapter 3)

Manuscript in progress:
VICTORIA HEIMER-MCGINN, JUN CHUL KIM, SUSAN M. DYMECKI, PAUL YOUNG
Decreased dendritic spine density as a consequence of tetanus toxin light chain expression in single neurons *in vivo*
(Discussed in Chapter 5)

Posters:

VICTORIA HEIMER-MCGINN, GUOPING FENG & PAUL YOUNG
SLICK-H Transgenic Mice for Inducible Neuron-Specific Cre-Mediated Recombination
7th FENS Forum (Federation of European Neuroscience Societies)
2010 – Amsterdam, The Netherlands

VICTORIA HEIMER-MCGINN & PAUL YOUNG
Decreased dendritic spine density as a consequence of tetanus toxin light chain expression in single neurons *in vivo*
7th Annual of Neuroscience Ireland
2012 - Royal College of Surgeons, Dublin, Ireland

IV. Abstract

Modern neuroscience relies heavily on sophisticated tools that allow us to visualize and manipulate cells with precise spatial and temporal control. Transgenic mouse models, for example, can be used to manipulate cellular activity in order to draw conclusions about the molecular events responsible for the development, maintenance and refinement of healthy and/or diseased neuronal circuits. Although it is fairly well established that circuits respond to activity-dependent competition between neurons, we have yet to understand either the mechanisms underlying these events or the higher-order plasticity that synchronizes entire circuits. In this thesis we aimed to develop and characterize transgenic mouse models that can be used to directly address these outstanding biological questions in different ways.

We present SLICK-H, a Cre-expressing mouse line that can achieve drug-inducible, widespread, neuron-specific manipulations *in vivo*. This model is a clear improvement over existing models because of its particularly strong, widespread, and even distribution pattern that can be tightly controlled in the absence of drug induction. We also present SLICK-V::Ptox, a mouse line that, through expression of the tetanus toxin light chain, allows long-term inhibition of neurotransmission in a small subset (<1%) of fluorescently labeled pyramidal cells. This model, which can be used to study how a silenced cell performs in a wildtype environment, greatly facilitates the *in vivo* study of activity-dependent competition in the mammalian brain. As an initial application we used this model to show that tetanus toxin-expressing CA1 neurons experience a 15% - 19% decrease in apical dendritic spine density. Finally, we also describe the attempt to create additional Cre-driven mouse lines that would allow conditional alteration of neuronal activity either by hyperpolarization or inhibition of neurotransmission. Overall, the models characterized in this thesis expand upon the wealth of tools available that aim to dissect neuronal circuitry by genetically manipulating neurons *in vivo*.

Chapter 1 Introduction

1.1 Activity-Dependent Refinement of Neuronal Networks

The human brain is composed of ~80 billion neurons interconnected by a vast network of synapses and another ~80 billion supporting glial cells (Azevedo et al., 2009). Neurons extend axonal projections and dendritic arbors to form complex but specific patterns. This connective specificity is guided by molecular cues and further refined as synapses are eliminated, added, stabilized, strengthened or weakened. This synaptic plasticity enables cells to undergo short- and long-term modifications in response to synaptic activity and experience. At the core of several forms of plasticity, like long-term potentiation (LTP), long-term-depression (LTD), and homeostasis, are the postsynaptic dendritic spines. These small protrusions that extend from dendritic branches receive most of the excitatory neurotransmission in the brain. Their unique structural and functional properties make them an ideal potential substrate for higher cognitive functions like memory and learning. This introduction will focus on the wiring of the brain and on the activity-dependent refinement of these synapses. Particular attention is given to the involvement of the postsynaptic terminal in synaptic plasticity. Finally, the role of synaptic failure or deficiency in disease is highlighted.

1.1.1 Neuronal circuit development

The vast and intricate networks of the brain require precise connectivity in order to function properly. Throughout the human lifespan, neurons form and refine synaptic connections in the following general pattern: (1) during fetal development, axonal and dendritic arborization is established with the aid of environmental guidance cues, (2) synaptic innervation increases during infancy, peaking at 1-2 years to as much as 50% above the adult mean, (3) throughout adolescence this number decreases sharply as axonal and dendritic arbors are pruned in response to synaptic activity, (4) the adult brain retains relatively stable synaptic connections but can also undergo a substantial amount of activity-dependent plasticity (Huttenlocher, 1979, Zuo et al., 2005, Pan and Gan, 2008).

1.1.1.1 *Axonal arbor formation and refinement*

1.1.1.1.1 Growth cone function

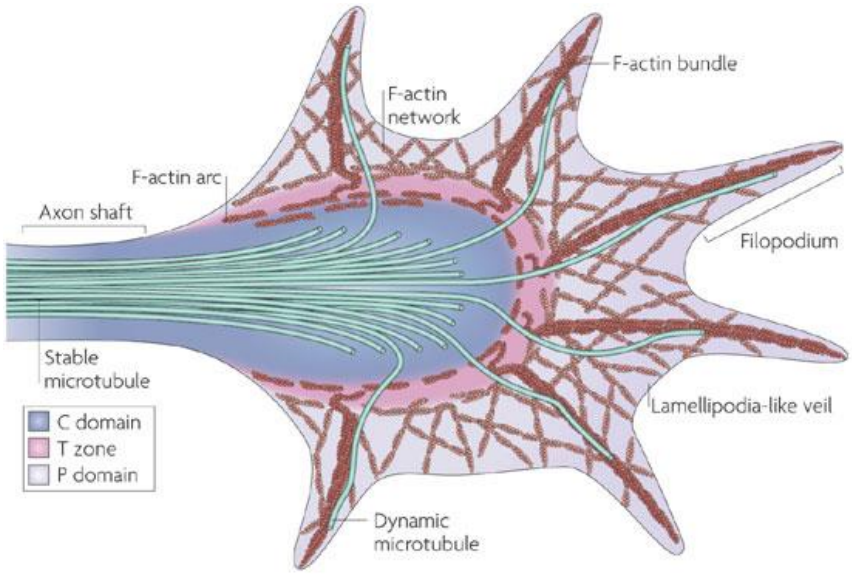

Figure 1.1 – The structure of the growth cone
The leading tip of the axon consists of dynamic, finger-like filopodia separated by sheets of membrane called lamellipodia. The dynamics of these cytoskeletal components determine its shape and movement. From Lowery and Van Vactor (2009)

The growth cone is a dynamic structure located at the tip of migrating axons that responds to environmental cues and is critical to axonal pathfinding (Tojima, 2012). Its task is to steer axons towards their final target locations, sometimes farther than a thousand times the diameter of their cell body (Tessier-Lavigne and Goodman, 1996). The growth cone contains a mobile cytoskeleton composed of filopodia (thin extensions of bundled F-actin) and lamellipodia (flat web-like extensions of meshed F-actin) whose mobility in response to

environmental cues is responsible for directing axonal growth (Fig 1.1) (Dent and Gertler, 2003). Axon progression occurs in three steps called protrusion, engorgement, and consolidation (Goldberg and Burmeister, 1986). During consolidation microtubules facilitate axonal advance by transiently entering the growth cone and forming a new axonal segment (Dent and Gertler, 2003). The process of axonal pathfinding occurs in several contexts, including topographic map formation in the developing nervous system (Udin and Fawcett, 1988) and repair and regeneration in the mature brain (Giger et al., 2010).

1.1.1.1.2 Guidance molecules

There are many different types of environmental guidance molecules that can act as repulsive or attractive signals for the growth cone (Maskery and Shinbrot, 2005). Adhesive cues like cell adhesion molecules (CAMs) and extracellular matrix molecules pave a physical path through which axons can navigate (Maness and Schachner, 2007, Evans et al., 2007), membrane-bound proteins such as slits and ephrins, prevent the axons from deviating from their path (Chilton, 2006) and a wide range of diffusible chemotropic signals, including semaphorins, netrins, morphogens, growth factors, transcription factors, neurotrophic factors and neurotransmitters provide further specificity to individual axons (Zou and Lyuksyutova, 2007, Butler and Tear, 2007, Sanford et al., 2008, Mattson et al., 1988). When axons reach their target locations, axonal arborization is initiated by instructive neurotrophic signals like nerve growth factor (Lentz et al., 1999, Patel et al., 2000). Many of these molecules can impose either repellant or attractive cues depending on the spatiotemporal specificity of expression (Lowery and Van Vactor, 2009). These guidance cues are responsible for activating or modulating signaling pathways within the growth cone that affect its motility; these include kinases, phosphatases, Ca^{2+}, and Rho-family GTPases, as well as endo/exocytotic machinery (Tojima, 2012).

1.1.1.1.3 Activity-dependent axonal refinement

Upon initial axonal arbor formation, which is regulated by guidance cues and axonal growth cones, an overabundance of connections is formed that is further refined in response to synaptic activity (Spitzer, 2006). The morphology of arborization, described in terms of branch number, length and order, can be modified by pruning or by branch additions (Gibson and Ma, 2011). In the visual system, for example, axons originating from the retina of both eyes converge onto the lateral geniculate nucleus (LGN) and then segregate into eye-specific layers (Wong, 1999, Huberman et al., 2008). Similarly, axons originating from the LGN form ocular dominance columns in the primary visual cortex according to eye preference. Both of these patterns arise from a refinement process by which inappropriately

placed branches are eliminated in response to spontaneous wave activity in the retina, LGN, and visual cortex (Huberman et al., 2008). A vast amount of studies have built on this knowledge. During synaptogenesis, for example, activity leads to the preferential formation of new branches (Meyer and Smith, 2006, Ruthazer et al., 2006). A time-lapse study in the *Xenopus* retina showed that neuronal activity promotes axon branch elimination during topographic map formation in an NMDAR-dependent manner (Ruthazer et al., 2003). Another time-lapse study performed in thalamocortical slice cultures showed that global pharmacological suppression reduces axonal arbor size by preventing branch addition (Uesaka et al., 2007). These studies, among many others, demonstrate that axonal branching and development are subject to activity-dependent processes.

Finally, activity-dependent axonal modulation has been widely proven to be a competitive process. A classic example of how activity-dependent competition shapes connectivity is the neuromuscular junction, where several axons initially innervate an immature muscle fiber and then compete with each other until ultimately a single axon innervates a mature fiber (Sanes and Lichtman, 1999). Several key studies that make observations of cells under manipulation show that these processes take place in the central nervous system as well (Buffelli et al., 2003, Yu et al., 2004, Hua et al., 2005, Gosse et al., 2008, Ben Fredj et al., 2010, Yasuda et al., 2011, Plazas et al., 2013). Ample evidence, for example shows that suppressing the excitability or synaptic release of single neurons places them at a competitive disadvantage to wildtype cells, and that the phenotype produced is not observed under global suppression (Fig 1.2) (Yu et al., 2004, Hua et al., 2005, Yasuda et al., 2011, Plazas et al., 2013).

Most studies of this nature have found that when a neuron is selectively silenced in a competitive environment, axonal arbors are reduced in size and complexity (Fig 1.2) and that this can lead to eventual cell death, although axonal targeting is generally unaffected (Yu et al., 2004, Hua et al., 2005, Yasuda et al., 2011). In some studies, global suppression by tetrodotoxin eliminates the competitive disadvantage and restores normal arborization (Hua et al., 2005, Yasuda et al., 2011). Along these lines, chimeric zebrafish in one study were engineered to contain only one retinal ganglion cell (RGC) in each eye in order to eliminate the effects of normal competition. Complementing previous studies, these single RCG axons innervated properly but did not undergo pruning, suggesting that competition plays a role in branch elimination (Gosse et al., 2008).

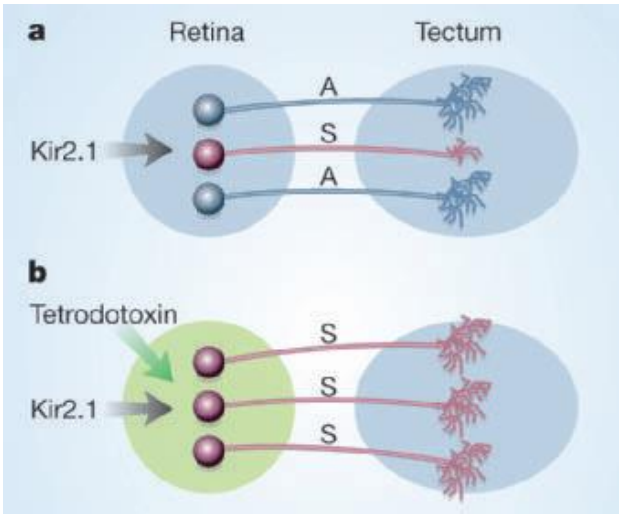

Figure 1.2 – Competition in the brain. Competition between neighboring axons plays a part in the growth and branching of axon arbors. Retinal ganglion cells convey information from the retina to the optic tectum in the zebrafish brain. **a**: Individual retinal ganglion cells silenced by transfection with the potassium channel Kir2.1. develop reduced axonal arbors compared to adjacent wildtype cells. **b**: Silencing of all retinal ganglion cells by injecting the neurotoxin tetrodotoxin into the eye restores the ability of the Kir2.1-expressing cell to grow a normal-sized axonal arbor. (S – silenced cell, A – active cell). From Ottersen (2005)

On the other hand, some studies have found that arbors are increased in size and complexity when silenced (Ruthazer et al., 2003, Ben Fredj et al., 2010, Dong and Aizenman, 2012). These inconsistencies may arise from differences in the experimental setup or in the area of the brain examined, but in any case they suggest a complex role for the mechanisms by which competition shapes axonal branching. Although specific mechanisms are not yet clear, some potential players are brain-derived neurotrophic factor (BDNF) with its receptor p75 (Singh et al., 2008, Grimbert and Cang, 2012, Je et al., 2012), the semaphorins SEMA3A with its receptors (Yaron et al., 2005, Plazas et al., 2013), and netrin and its receptor UNC-40 (Alexander et al., 2010, Hao et al., 2010). These molecular mechanisms governing activity-dependent competition are currently under intense investigation.

1.1.1.2 *Dendritic arbor formation and refinement*

On the postsynaptic end of a neuron, dendritic arbor development is similarly a dynamic "trial and error" process where filopodia expand and contract in response to their environment (Dailey and Smith, 1996). Dendrite arborization patterns are cell-type specific, so for example, pyramidal neurons in the cortex and hippocampus are characterized by a prominent apical dendrite from which higher order branches extend (Parrish et al., 2007). These type-specific dendritic arbor patterns partly arise from the different types,

combinations and amounts of intrinsic transcription factors for each cell-type (Parrish et al., 2006, Jan and Jan, 2010). Similarly to axons, dendrites also respond to extrinsic factors, including CAMs, slits, ephrins, semaphorins, netrins, trophic factors and neurotransmitters that either attract or repel growing dendrites in order to further shape the dendritic tree (Jan and Jan, 2010, Kulkarni and Firestein, 2012). The precise mechanisms by which these molecules promote arborization are not well understood but include signaling pathways like kinases, phosphatases, and small GTPases (Jan and Jan, 2010). Interestingly, the chemotropic signals involved in neurite guidance can elicit different responses between dendrites and axons, between dendrites from different cell-types and even between dendrites of the same neuron (Parrish et al., 2007).

1.1.1.2.1 Dendritic fields

An important factor in dendritic arbor formation is the organization of dendritic fields. Dendrites of the same neuron tend to avoid each other (self-avoidance), as do dendrites of same-type neurons (tiling), while dendrites from different neuronal types can inhabit the same regions (coexistence) (Jan and Jan, 2010, Grueber and Sagasti, 2010). An example of these dendritic properties can be seen in the mammalian retina where each of the 50+ neuronal types covers the retinal surface completely but without overlapping with same-type branches (Masland, 2001). The ability to selectively avoid same-type dendrites without repelling other neuronal types is partly attributed to Down syndrome cell adhesion molecule (DSCAM)-mediated homotypic binding, although the specificity of this mechanism is not fully understood in mammalian systems (Fuerst et al., 2008, 2009). This is in contrast to dendritic development in *Drosophila* where the large abundance of DSCAM splice variants allows each cell type to possess a unique “bar code” involved in homotypic repulsion (Wojtowicz et al., 2004). Other adhesion molecules like N-cahderin and Flamingo (fmi) are also speculated to play a part in mammalian dendritic tiling (Zhu and Luo, 2004, Kimura et al., 2006). Arbor size is another factor in dendritic development. In some neurons, like cerebellar Purkinje cells, dendritic arbor complexity increases in proportion to the organism’s growth (Wen et al., 2009). Several signaling cascades, including secretory, endocytic, and cytoskeletal pathways are beginning to emerge as regulators of this dendritic scaling (Jan and Jan, 2010).

1.1.1.2.2 Activity-dependent dendritic refinement

Similarly to axonal branching, dendritic arborization is shaped, refined and maintained by synaptic activity (Katz and Shatz, 1996, Sanes and Lichtman, 1999, Lichtman and Colman, 2000, Hashimoto and Kano, 2005). The growth and branching of dendritic arbors is steered by synaptic activity in a repetitive general pattern: (a) newly extended filopodia form a new

synapse, (b) most of these are eliminated but (c) a fraction of them are maintained, (d) these filopodia become stabilized, and finally (e) mature into new dendritic branches (Cline, 2001, Niell et al., 2004). Activity deprivation results in reduced stability of dendritic branches and consequently leads to reduced arborization (Haas et al., 2006, Tyler et al., 2007, Cline and Haas, 2008). Although less intensely studied than axonal competition, activity-dependent competition also shapes dendritic arbors. In hippocampal cultures, activity suppression in a small subset of cells (by potassium channel overexpression) leads to reduced synaptic inputs as measured by dendritic spine density and excitatory postsynaptic current (EPSC) amplitude; this effect is not observed following global suppression by tetrodotoxin (Burrone et al., 2002). Moreover, a homeostatic increase in synaptic input is observed when suppression is induced after synaptic connectivity has been established (Burrone et al., 2002).

More recent studies investigating the effects of activity-dependent competition on synaptic inputs find slightly different results. In rat cortical layers 2/3, an siRNA-based knockdown of Na^+ channels in a small subset of pyramidal neurons reveals an increase in spine density attributed to the cells' inability to prune immature filopodia (Komai et al., 2006). In the *Xenopus* visual system, potassium channel overexpression in a small population of cells does not affect dendritic arborization, although axonal arbors were found to be significantly larger than usual (Dong and Aizenman, 2012). These results vary considerably but are based in different organisms, areas of the brain and developmental timepoints, and also employ different methods of activity suppression. This may indicate that dendritic activity-dependent competition is not universally regulated among regions in the CNS or throughout different developmental stages.

1.1.1.3 *Synapse formation and refinement*

As mentioned before, synaptogenesis occurs at a high rate during human fetal development and childhood, as neurons attempt to innervate the immature brain (Huttenlocher, 1979). The period of adolescence, however, is dominated by synapse elimination/pruning; although new synapses continue to be formed, there is a large net loss of synaptic connections (Lichtman and Colman, 2000). Throughout adulthood, the balance between synaptogenesis and synapse elimination results in a slow but steady net loss of synaptic connectivity (Pan and Gan, 2008). Studies performed in mice show that throughout an animal's lifespan, a

large portion of dendritic spines are stabilized and maintained (Zuo et al., 2005), presumably forming the cellular basis for memory (Kasai et al., 2010). Moreover, the highly dynamic nature of synapses during childhood could provide the molecular basis for early learning (Pan and Gan, 2008).

1.1.1.3.1 Synapse recognition and assembly

As described previously, filopodia of developing neurites (axons and dendrites) constantly probe the environment in search of suitable synaptic connections. Synaptic recognition between potential partners is mediated by several factors including homophilic binding of synaptic adhesion molecules, repulsion signals from non-synaptic partners, transient synaptic partners that provide cues for target field selection, glial cells that secrete guidance cues and also serve as intermediary targets, and morphogenic gradients that prevent neurites from innervating prematurely (Shen and Scheiffele, 2010). Once appropriate pre- and postsynaptic partners come together, an array of signaling pathways is responsible for the process of synaptic differentiation, which can occur in a bidirectional, anterograde, or retrograde manner (Shen and Scheiffele, 2010). Finally, activity-dependent competition drives the elimination of redundant synapses to ensure connective specificity in the brain (Shen and Scheiffele, 2010).

Adhesion complexes, which physically hold the synapse together also play an important role in assembling the functional components of both pre- and postsynaptic machinery. Neurexin and neuroligin, for example, contain PDZ-binding motifs at their C-terminals (Gerrow and El-Husseini, 2006) that allow them to interact with key proteins at both the presynaptic terminal, where they trigger the accumulation of synaptic vesicles and active zone components (Dean et al., 2003), and at the postsynaptic terminal, where they promote dendritic spine formation and recruit key scaffolding proteins involved in post synaptic density (PSD) assembly (Gerrow et al., 2006).

In addition to adhesive molecules, anterograde (presynaptic-derived) and retrograde (postsynaptic-derived) signals facilitate postsynaptic and presynaptic differentiation, respectively (Shen and Scheiffele, 2010). Axonally secreted pentraxins, for example, recruit postsynaptic glutamate receptors by interacting with the extracellular N-terminal domain of AMPA receptor subunits (Passafaro et al., 2003, Sia et al., 2007). Presynaptic ephrin ligands cluster postsynaptic ephrin receptors, which in turn bind to and cluster NMDA receptor subunits (Kayser et al., 2008, Dalva et al., 2000). In the opposite direction, postsynaptic factors like Wnt7a and the fibroblast growth factor FGF22 are released upon synapse

formation and induce presynaptic modifications like synaptic vesicle accumulation (Hall et al., 2000, Umemori et al., 2004).

1.1.1.3.2 Synapse elimination

In the immature brain, more connections are established than are ultimately maintained (Katz and Shatz, 1996, Sanes and Lichtman, 1999, Hua and Smith, 2004). Many lines of evidence indicate that (a) synapse elimination is an integral and crucial feature of early circuit development and that (b) activity-dependent synaptic elimination continues to refine neuronal connections in the adult brain (Lichtman and Colman, 2000, Buffelli et al., 2003, Luo and O'Leary, 2005, Pan and Gan, 2008). In postmortem human tissue, for example, a high rate of synapse formation during childhood is followed by a massive reduction in synaptic connections throughout adolescence (Pan and Gan, 2008). In the developing mouse cortex, 13%-20% of excitatory synapses are eliminated during postnatal weeks 4-6 with only 5%-8% formed during the same period; moreover a net loss of 25% occurs between 1 and 4 months (Zuo et al., 2005). Importantly, sensory deprivation preferentially reduces the rate of spine elimination in these mice (Zuo et al., 2005).

Although it is well established that synapse elimination is activity-dependent, there is a poor understanding of how synapses are tagged for elimination, the precise cellular mechanisms for synapse elimination, and how synapse elimination leads to branch pruning (Stephan et al., 2012). One potential tagging system for synapses undergoing elimination is the complement protein cascade, classically an immune system phagocytic process (Stevens et al., 2007). In line with this, glial cells have been shown to engulf presynaptic terminals in response to the compliment cascade in an activity-dependent manner (Schafer et al., 2012, Chung and Barres, 2012). Secreted semaphorins and their receptors have also been found to influence synapse elimination mechanisms (Liu et al., 2005). This is currently an area of intense research and its importance is underscored by the fact that several diseases, including Fragile X syndrome, are associated with deficiencies in synapse elimination and axonal or dendritic pruning (Kulkarni and Firestein, 2012).

1.1.1.3.3 Synapse stability and turnover

Aside from synapse elimination, two important aspects of neuronal circuit remodeling are the ability for synapses to strengthen and stabilize and the adaptive capacity for synaptic turnover (Grutzendler et al., 2002, Trachtenberg et al., 2002, Holtmaat et al., 2005, Xu et al., 2009, Yang et al., 2009, Roberts et al., 2010, Lai et al., 2012). Both of these processes occur in response to neuronal activity. Long-term two-photon studies in mice reveal that up to

96% of excitatory synapses in the adult cortex remain stable over a one-month period (Grutzendler et al., 2002), and that over an 18-month period 70% of synapses can be stably maintained (Zuo et al., 2005). In the mouse barrel cortex 60%-70% of stable synapses are predicted to persist throughout an animal's lifespan; this includes synapses that were established during development and survived elimination, as well as synapses that were established later in life (Yang et al., 2009). Some studies reveal lower rates of stably maintained synapses (Trachtenberg et al., 2002, Holtmaat et al., 2005), although these inconsistencies are attributed to the use of cranial window versus thinned-skull techniques (Xu et al., 2007). The smaller but significant population of synapses that undergoes constant turnover in the mature brain endows neuronal circuits with a substantial capacity for experience-dependent modification (Caroni et al., 2012). Importantly, sensory deprivation alters synapse dynamics in several of these studies showing the activity-dependent nature of synapse stability and turnover (Pan and Gan, 2008, Yang et al., 2009). Taken together, these data reiterate that synapses are plausible substrates for long-term information storage (Caroni et al., 2012).

1.1.2 The role of dendritic spines in postsynaptic plasticity

1.1.2.1 *Dendritic spine morphology and biochemistry*

1.1.2.1.1 General morphology

Dendritic spines are the postsynaptic sites for most of the glutamatergic/excitatory connections in the brain. They are small membranous protrusions that generally extend from the dendritic shaft by a thin "neck" and terminate in a spine "head" (Lee et al., 2012). Spine structures (Fig 1.3) vary greatly but can be broadly classified as "mushroom-like" (defined neck and head), "stubby" (no neck, head protrudes directly from the shaft) or "thin" (long and thin, no clear neck/head distinction) (Peters and Kaiserman-Abramof, 1970). These morphological differences are thought to reflect functional changes in synaptic strength and maturity (Yuste and Bonhoeffer, 2001, Kasai et al., 2003, Hayashi and Majewska, 2005). The spine head membrane contains the post-synaptic density (PSD), an electron rich conglomeration of proteins and molecules responsible for most of the excitatory synaptic transmission in the brain (Gold, 2012). The spine possesses a dynamic actin cytoskeleton that is thought to underlie structural plasticity of the spine (Penzes and Rafalovich, 2012). It also contains several supporting organelles like mitochondria (Li et al., 2004), endocytic vesicles (Kelly et al., 2011), spine apparatus (Vlachos, 2012) and smooth endoplasmic reticulum (Spacek and Harris, 1997). The thin neck of the spine is thought to provide biochemical and electrical compartmentalization; this isolation is thought to account for the relationship between spine morphology and synaptic function, and for synapse-specific plasticity (Lee et al., 2012, Yuste, 2011).

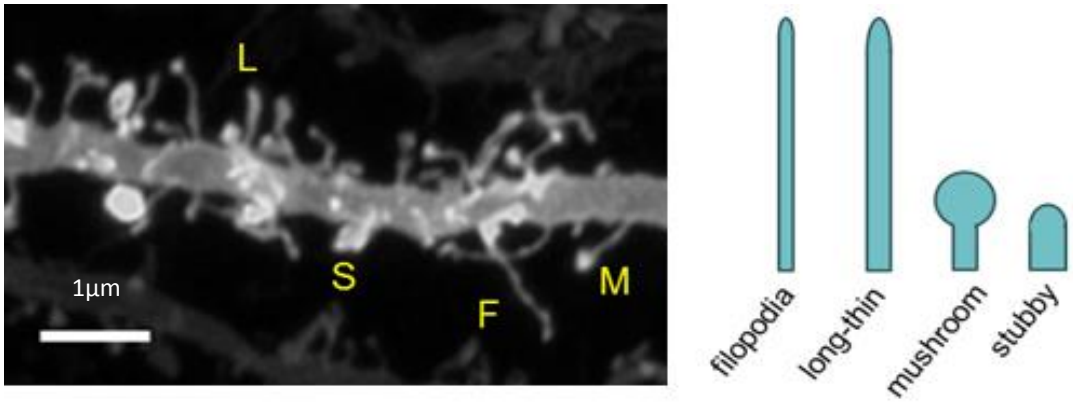

Figure 1.3 – Dendritic spine classifications
Laser-scanning confocal micrograph shows distal primary apical dendrite from a Layer 5 cortical pyramidal neuron in an adult Fmr1-KO mouse. Filopodia-like (F), long-thin (L), mushroom (M) and stubby (S) spines are identified based on structural measures. From www.psychogenics.com.

1.1.2.1.2 The post-synaptic density (PSD)

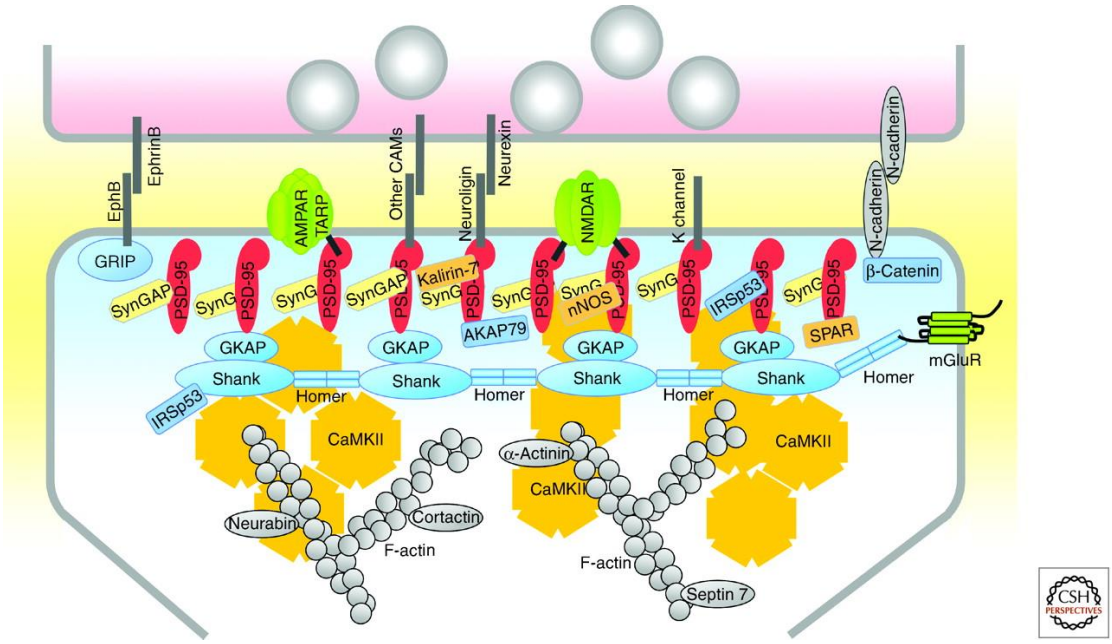

Figure 1.4 - Molecular organization of the PSD of excitatory synapses
Schematic diagram of the major proteins of the PSD, with protein interactions indicated by direct contacts or overlaps. The relative numbers of the proteins shown correlate roughly with their relative abundance in PSDs of forebrain. Copy numbers of most adhesion molecules and ion channels are unknown (dark gray lines). Each CaMKII shape represents a dodecamer. From Sheng and Kim (2011)

The postsynaptic density (PSD; Fig 1.4) is a membrane specialization that generally occurs at the tip of dendritic spine heads, is directly apposed to the presynaptic active zone, and contains hundreds of proteins involved in excitatory synaptic transmission (Sheng and Kim, 2011). The core functional proteins of the PSD are the glutamate receptors (Husi et al., 2000): *N*-methyl-D-aspartate receptors (NMDAR), α-amino-3-hydroxy-5-methyl-4-isoxazolepropinoic acid receptors (AMPAR), and metabotropic glutamate receptors (Traynelis et al., 2010). Signaling proteins such as kinases (e.g. CaMKIIα), phosphatases (e.g. tyrosine phosphatases) and small GTPases (e.g. Ras, Rac, Rho) are responsible for regulating various biochemical pathways in response to synaptic activity (Kennedy et al., 2005, Sheng and Hoogenraad, 2007). This includes actin-cytoskeleton reorganization, local protein synthesis, neuronal apoptosis, regulation of glutamate receptors, and others (Kennedy et al., 2005, Murakoshi and Yasuda, 2012). Small GTPases act as binary molecular switches that are turned "on" by guanine exchange factors (GEF; e.g. kalirin/ RhoGEF) and turned "off" by GTPase activating proteins (GAP; e.g. SynGAP/RasGAP) (Takai et al., 2001). Cell adhesion molecules like neuroligins and N-cadherin help to anchor the PSD into close proximity with the presynaptic active zone and are also important for synapse specificity (Missler et al.,

2012). Finally, key scaffolding proteins like PSD-95, GKAP/SAPAP, Shank and Homer cluster proteins into a dynamic laminar structure (Valtschanoff and Weinberg, 2001) that allows glutamate receptor activity to be coupled to its downstream signaling pathways (Sheng and Kim, 2011). The activity of key PSD proteins is thought to underlie the cellular mechanisms for several forms of synaptic plasticity including long-term potentiation/depression (LTP/LTD) and homeostatic plasticity (Malenka and Bear, 2004, Matsuzaki, 2007, Turrigiano, 2012).

1.1.2.1.3 Organelles

Dendritic spines contain several organelles that support its biochemical functions locally (Sheng and Hoogenraad, 2007). Smooth endoplasmic reticulum (SER), for example, is widespread in dendritic shafts and extends its network into a large subset of spines (Spacek and Harris, 1997). Their main function is most likely related to local calcium storage and release, as well as protein transport to the postsynaptic membrane (Horton and Ehlers, 2004). Another organelle called the spine apparatus (SA) is composed of stacked SER and is present at mature dendritic spines (Gray, 1959, Segal et al., 2010). The SA is thought to be involved in local calcium storage and protein synthesis/recycling, although mechanistic evidence remains to be found (Sheng and Hoogenraad, 2007, Vlachos, 2012). Although postsynaptic proteins are generally created in the cell body and then transported to the spine (Horton and Ehlers, 2004), some mRNAs are known to be translated locally in dendrites (Schuman et al., 2006), including the mRNAs for AMPARs to some extent (Ju et al., 2004). Consistent with this notion, polyribosomes are present in the dendrite shaft (Gardiol et al., 1999) and have been shown to translocate into the spine following LTP (Ostroff et al., 2002). These translation-related organelles are thought to play an important role in synaptic plasticity (Sheng and Hoogenraad, 2007).

Endocytic machinery components such as clathrin-coated vesicles, multi-vesicular bodies, and tubular compartments are also essential to synaptic function. (Racz et al., 2004, Park et al., 2004, Brown et al., 2005). The endocytic zone, located on the extrasynaptic membrane (lateral to the PSD) is a site where synaptic proteins are endocytosed, exocytosed, recycled or degraded (Blanpied et al., 2002, Racz et al., 2004). Recycling endosomes, for example, can provide a local supply of AMPA receptors; evidence shows that these endosomes are translocated into the spine following NMDAR activation to increase the number of membrane-bound AMPARs (Park et al., 2004, 2006). Endosomal recycling thus facilitates fast

NMDAR-mediated recruitment of AMPARs during LTP, as well as trafficking of other receptors at the postsynapse (Kelly et al., 2011).

Finally, an increasing body of evidence shows that mitochondria, which are recruited to the spine in response to electrical stimulation, are essential to the morphological plasticity of dendritic spines (Li et al., 2004, Sheng and Hoogenraad, 2007). Although a precise mechanism of action has not yet been revealed, their ability to buffer intracellular calcium levels is likely to be relevant (Chan, 2006). Some recent studies look at postsynaptic mitochondrial dysfunction in the context of Alzheimer's disease and find that it is correlated with spine reduction and dendritic branch loss (Rui et al., 2010, Baloyannis, 2011). A mitochondrial role in AMPA receptor trafficking to the postsynaptic membrane has also been suggested (Rui et al., 2010).

1.1.2.2 *Postsynaptic plasticity in dendritic spines*

A generally accepted model for LTP in dendritic spines is reviewed by Nicoll and Roche (2013) and goes as follows: (1) NMDA receptors are activated when presynaptic glutamate is coupled with postsynaptic depolarization. (2) NMDAR activation induces rapid Ca^{2+} influx, which (3) promotes activation of calcium/ calmodulin-dependent protein kinase II (CaMKII) and (4) leads to the rapid recruitment of additional AMPA receptors to the postsynaptic membrane, which in turn (5) results in a long-lasting increase in excitatory postsynaptic current (EPSC) amplitude. Strong evidence suggests that activation of CaMKII, which is highly abundant in the PSD (Cheng et al., 2006), is one of the most crucial steps in LTP (Lisman et al., 2012). The multiple roles that CaMKII plays at the synapse are reviewed by Lisman et al and include: (a) it binds to the NMDAR subunit NR2B, (b) it phosphorylates the AMPAR subunit GluR1 and its associated protein stargazin in order to enhance AMPAR trafficking to the postsynaptic membrane, and (c) bundles and stabilizes actin filaments, thus regulating actin cytoskeletal modifications. Importantly, NMDAR-CaMKII complex formation is necessary for LTP to occur, as is NMDA activation (Barria and Malinow, 2005). Although some forms of plasticity have been identified that are not NMDAR-dependent, notably at hippocampal mossy fibers (Nicoll and Malenka, 1995), the vast majority of studies focus on the CA1 where LTP is particularly robust (Nicoll and Roche, 2013).

1.1.2.2.1 Molecular basis of synaptic plasticity

One of the most prominent features of biochemical plasticity in dendritic spines is the reorganization of several PSD proteins (Murakoshi and Yasuda, 2012). During LTP, for example, CaMKII and AMPAR levels increase immediately and in proportion with spine volume changes (Lee et al., 2009, Patterson et al., 2010) whereas the opposite occurs in LTD (Zhou et al., 2004). Several hours after LTP induction, the scaffolding proteins PSD-95 and Shank are enriched and the PSD enlarges in proportion to spine volume, which is thought to have a stabilizing effect (Knott et al., 2006). During LTD loss of PSD-95 occurs immediately and is coupled with a shrinking spine volume (Woods et al., 2011).

These biochemical processes are regulated by signaling pathways that include kinases like CaMKII, ERK (extracellular signal-related kinase) and PAK (p-21 activated kinase), as well as small GTPases such as Ras and the Rho family GTPases RhoA, Cdc42 and Rac. CaMKII activity is upstream of many of these GTPase pathways (Murakoshi et al., 2011) and although the relationship between the two pathways is not yet clear, it has been suggested that CaMKII may regulate GEFs and/or GAPs (Stornetta and Zhu, 2011). CaMKII also facilitates AMPAR trafficking by directly phosphorylating its subunits (Kristensen et al., 2011).

1.1.2.2.2 Structural plasticity

In dendritic spines morphological changes are thought to reflect physiological changes in synaptic strength and maturity of the spine (Matsuzaki, 2007). In general, spines with larger heads are more stable and promote stronger synaptic connections while smaller spines are more dynamic and therefore undergo synaptic plasticity more readily (Kasai et al., 2003, Matsuzaki et al., 2004). In line with this, LTP and LTD are associated with respective enlargement or reduction of dendritic spine size (Okamoto et al., 2004, Zhou et al., 2004), PSD volume (Kasai et al., 2003), and amount of membrane-bound AMPARs (Malinow and Malenka, 2002, Kessels and Malinow, 2009). Although under certain conditions spines have the ability to deviate from form-function coupling, the strong correlation between structural and functional plasticity implies that they share a common molecular mechanisms (Lee et al., 2012). Finally, compartmentalization provided by the dendritic spine neck could be responsible for this form-function relationship (Lee et al., 2012).

Rapid actin cytoskeleton remodeling is thought to underlie morphological plasticity in dendritic spines (Penzes and Rafalovich, 2012, Bosch and Hayashi, 2012). LTP causes fast actin polymerization whereas LTD is accompanied by actin depolymerization (Okamoto et

al., 2004). Moreover, mutating actin filaments blocks LTP and suppresses spine enlargement (Matsuzaki et al., 2004). Actin treadmilling, whereby actin monomers are polymerized at one end and depolymerized at the other, is thought to drive these activity-dependent morphological changes (Star et al., 2002, Honkura et al., 2008, Frost et al., 2010). During LTP, endosomal exocytosis is believed to be crucial for adding membrane area to the spine (Park et al., 2006) while simultaneously delivering AMPARs to the synaptic membrane (Kessels and Malinow, 2009, Makino and Malinow, 2009).

These changes are regulated by a complex signaling network that relays input information from membrane receptors like NMDARs to the actin-binding proteins (ABPs) that directly polymerize/ depolymerize actin (Okamoto et al., 2004, Murakoshi and Yasuda, 2012). CaMKII bundles F-actin to regulate its stability (Okamoto et al., 2007) and also regulates the activity of small GTPases (Murakoshi et al., 2011) like Rho family GTPases, which in turn regulate APB activity (Penzes and Rafalovich, 2012). Rho activation for example, inhibits actin polymerization and causes spine loss/shrinkage while activation of Cdc42 and Ras promotes actin polymerization and leads to increased spine number (Saneyoshi et al., 2010). Epigenetic mechanisms like methylation, acetylation, and micro-RNA regulation also play a role in activity-dependent spine remodeling (Penzes and Rafalovich, 2012). Finally, microtubules have also been found to contribute to dendritic spine plasticity (Jaworski et al., 2009).

1.1.2.2.3 Biochemical and electrical compartmentalization

Rapid actin cytoskeletal reorganizations are thought to not only reflect biochemical changes in dendritic spines but also to actively facilitate functional plasticity. Morphological modifications to the spine neck, which isolates spines from their parent dendrites, could attenuate the way in which spines respond to synaptic activity.

The idea of a biochemical compartment was first proposed when NMDAR-mediated calcium influx was shown to be tightly restricted to the spine under certain conditions (Muller and Connor, 1992). It was later established that calcium diffusion into the dendritic shaft is restricted in spines with thin necks but not in spines with wider neck diameters (Noguchi et al., 2005). Similar to intracellular diffusion, the lateral mobility of membrane proteins is also restricted by spine neck morphology (Choquet, 2010). AMPA receptors, for instance, exhibit a twofold decrease in lateral diffusion out of the spine when a defined neck is present (Ashby et al., 2006).

Biochemical compartmentalization is not absolute, however, as spines need to retain the ability to communicate with the parent dendrite. Although precise regulation mechanisms remain to be elucidated, it is clear that spines can differentially regulate diffusion of several signaling molecules. For example, during LTP CamKII and Cdc42 are restricted to the spine head (Harvey et al., 2008, Lee et al., 2009) whereas Ras and RhoA diffuse into the parent dendrite and spread into neighboring synapses (Harvey et al., 2008, Murakoshi et al., 2011). Several studies also point out that GFP also experiences restricted diffusion and lateral motility through the spine neck, suggesting that the obstruction is caused by geometric parameters, and not by intrinsic trafficking properties of the proteins involved (Bloodgood and Sabatini, 2005, Ashby et al., 2006). These forms of biochemical isolation facilitate synapse-specific plasticity by providing autonomy to individual synapses.

Until recently, the idea of an electrical compartment was mostly dismissed based on the prediction that the spine neck would provide only negligible ohmic resistance (Koch and Zador, 1993, Svoboda et al., 1996). A recent study, however, measures spine neck resistance to be up to ~500MΩ for subsets of dendritic spines (Harnett et al., 2012). This study shows that spine neck resistance amplifies synaptic depolarization locally (1.5-45 fold), which increases the activity of voltage-dependent (i.e. NMDAR-mediated) pathways within the spine (Harnett et al., 2012). If longer/thinner spine necks provide a higher ohmic resistance and therefore produce a more intense local depolarization (Harnett et al., 2012), this would be consistent with the fact that thinner spines are more prone to LTP (Matsuzaki et al., 2004).

Aside from facilitating synapse-specific plasticity, electrical isolation could also serve to linearize dendritic input integration; this would avoid “electrical shunting” and subsequent reduction to the cell’s overall excitability (Tsay and Yuste, 2004, Yuste, 2011). One study shows that input amplitudes received by the soma are inversely proportional to the neck length of individual synapses and independent from spine location or head size (Araya et al., 2006). In addition, computational models predict that spine neck isolation can preserve local excitatory postsynaptic potentials (EPSPs), thereby protecting spines from the location-dependent variability of dendritic impedance (Gulledge et al., 2012).

Taken together, these findings suggest that spines can in fact act as both biochemical and electrical compartments capable of locally filtering and processing synaptic inputs (Harnett et al., 2012, Yuste, 2011). Moreover, the ability of the cytoskeleton to rapidly modify neck shape/length endows dendritic spines with the capacity to control the geometric parameters that affect its response to synaptic activity (Lee et al., 2012).

1.1.2.3 *Dendritic spine pathology*

Dendritic spine anomalies (size, shape and density) are prominent in several neuropsychiatric diseases that involve information-processing deficits and impairments to neuronal plasticity and connectivity (Fig 1.5) (Penzes et al., 2011). Among these are schizophrenia (SZ), Alzheimer's disease (AD), autism spectrum disorders, addiction, Down's syndrome, Fragile X syndrome, Rett's syndrome, and non-syndromic intellectual disability (Russo et al., 2010, Kulkarni and Firestein, 2012); some of these are detailed below. These diseases are characterized by varying degrees of cognitive and behavioral impairment including distorted perception, memory loss, and socio-linguistic deficiencies; at the molecular level, they exhibit dendritic arbor anomalies and altered spine density/size, albeit expressed in different regions of the brain and at different developmental timepoints (Penzes et al., 2011). The similarities between these diseases, with spines as a common substrate, further strengthen the idea that dendritic spine function is at the core of certain cognitive processes (Kasai et al., 2010).

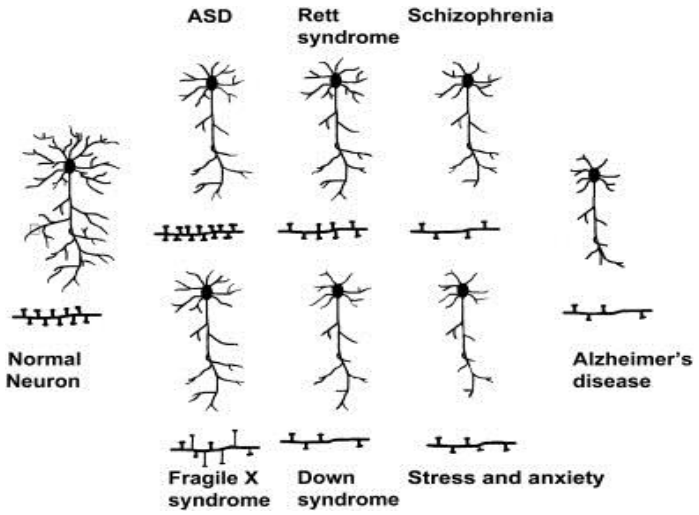

Figure 1.5 - Schematic representation of dendritic spines and branching abnormalities in diseased brains. From Kulkarni and Firestein (2012)

1.1.2.3.1 Dendritic spine anomalies in schizophrenia

Schizophrenia is a genetically heterogeneous disease that affects thought, perception, emotion and cognition and emerges in late adolescence or early adulthood (Silveira et al., 2012). Despite its heterogeneity, a common pathology in SZ is substantial loss of gray matter in the prefrontal cortex (PFC) (Zipursky et al., 1992) that is caused by a decrease in dendritic arborization and spine density instead of neuronal death (Selemon and Goldman-Rakic, 1999, Glausier and Lewis, 2012). In human postmortem tissue spine density is severely decreased, specifically in the PFC (Garey et al., 1998, Glantz and Lewis, 2000), auditory cortex (Sweet et al., 2009), striatum (Roberts et al., 1996) and CA3 (Kolomeets et al., 2005, 2007). Cortical deficits occur only in layer 3 (Kolluri et al., 2005), which is noteworthy considering that layer 3 neurons undergo more pruning during adolescence than other layers (Bourgeois et al., 1994). Taken together, these findings may suggest that synapse elimination during adolescence is a prominent and common feature of the disease (Penzes et al., 2011).

1.1.2.3.2 Dendritic spine anomalies in Alzheimer's disease

Alzheimer's disease arises much later in life and is clinically indicated by severe memory loss and mood alterations (Yu and Lu, 2012). At the molecular level it is characterized by the presence of neurofibrillary tangles and amyloid beta oligomers, by neuronal death and by dendritic branch and spine anomalies in the hippocampus and cortex (Tackenberg et al., 2009, Yu and Lu, 2012). Postmortem human tissue reveals spine density decrease in all cortical layers, in both pyramidal and non-pyramidal neurons (Davies et al., 1987, el Hachimi and Foncin, 1990), as well as in the hippocampus (Ferrer and Gullotta, 1990, Baloyannis et al., 2004, 2011). In transgenic mice, human-derived amyloid-beta oligomers can potently inhibit LTP, enhance LTD, and reduce spine density (Shankar et al., 2008). Particularly interesting are the findings that spine loss is more highly correlated to cognitive function than are neuronal death or number of tangles or oligomers (DeKosky and Scheff, 1990, Terry et al., 1991). This evidence has led to the idea that synaptic dysfunction occurs early in AD and may be a causative pathology rather than an outcome of disease (Selkoe, 2002, Arendt, 2009, Penzes et al., 2011).

1.1.2.3.3 Dendritic spine anomalies in intellectual disability and mental retardation

Several neuropsychiatric diseases related to intellectual disability and mental retardation also have synaptic origins but vary in their exact pathologies (Levenga and Willemsen, 2012). For example, autism spectrum disorders and Fragile X syndrome experience an increase in spine density (Hutsler and Zhang, 2010, He and Portera-Cailliau, 2012) whereas Down's and

Rett's syndromes exhibit decreased spine density (Kaufmann and Moser, 2000). Fragile X not only displays an increased spine density, but also an increased proportion of long/thin spines that are considered to represent immature synapses (Irwin et al., 2001). Down's syndrome displays irregularly sized spines, both larger and smaller, in addition to decreased density (Marin-Padilla, 1972, 1976, Takashima et al., 1981, 1989). The similarity in synaptic pathologies across neuropsychiatric diseases supports the belief that spine function underlies higher cognitive processes like memory and learning (Kasai et al., 2010).

1.2 Molecular tools for the *in vivo* study of neuronal networks

1.2.1 Visualizing the brain

The ability to visualize neurons in precise detail is an important cornerstone of modern neuroscience. Classical neuroanatomical studies that traced neuronal connectivity relied heavily on silver stains like Golgi and "Nauta-Gygax" stains, Nissl staining, and others (Heimer, 2003, Switzer, 2000, Jones, 2007). Many of these staining methods are still relevant today and serve to compliment modern techniques. The Golgi stain is still used in the study of dendritic spines (Dagnino-Subiabre et al., 2012, Bianchi et al., 2012) and Nissl staining is still used to map cellular populations following immunocytochemical detection (Kadar et al., 2009). These classical staining methods, however, are restricted by their toxicity and by the fact that they cannot selectively stain with brain area- or cell type-specificity.

As an alternative, retrograde tracers became popular in the 1970's, beginning with the use of horseradish peroxidase (Kristensson and Olsson, 1971). Fluorescent dyes followed, for example, lucifer yellow (Maranto, 1982), nuclear yellow, fast blue (Bentivoglio et al., 1980), and lipophilic carbocyanine dyes like DiI, DiO and DiD (Honig and Hume, 1989). These dyes can be introduced by several methods including microinjection and ballistics (Lo et al., 1994). The particle-mediated ballistic delivery of carbocyanine dyes is termed "DiOlistic" labeling (Gan et al., 2000). Although these types of labeling are widely used even today (Jung et al., 2013), their application is limited to slices and cell culture. In the last two decades, methods that deliver genetically encoded markers have allowed neuronal visualization in intact organisms as well. For example, genes for LacZ (Soriano, 1999, Kiernan, 2007) or alkaline phosphatase (Cordell et al., 1984) can be genetically introduced as cell markers for any specific cell-type. However, LacZ is only expressed in the cell body and alkaline phosphatase requires an enzymatic reaction. The discovery of green fluorescent protein (GFP), a non-toxic, uniformly expressed protein whose fluorescence does not require exogenous factors, overcame many of the limitations of its predecessors and revolutionized the field of fluorescent imaging.

GFP, from the jellyfish *Aequorea Victoria*, produces strong and stable fluorescence when expressed exogenously in prokaryotic or eukaryotic cells (Chalfie et al., 1994). Because GFP is a protein, its coding sequence can be incorporated directly into the genome of an

organism and its expression thereby becomes inheritable (Feng et al., 2000). Importantly, it can be fused to a protein of interest with minimal disruption to the system (Chalfie et al., 1994). Unlike other staining methods, the GFP chromophore relies only on protein expression and does not require activation by cofactors or substrates (Chalfie et al., 1994). Since it is a relatively small protein (26.9kDa), it is able to diffuse throughout the entire cell without the need for peptide fusions that facilitate transport (Feng et al., 2000, Rodriguez et al., 1999). GFP is not toxic and does not perturb cellular activity, morphology or synaptic connectivity, even when expressed long-term *in vivo* in neurons (Feng et al., 2000). Finally, GFP cDNA has been mutated to produce spectral variants, called XFPs, that allow co-labeling of more than one cell population (Chalfie, 1995, Day and Davidson, 2009).

Since the discovery of GFP, many fluorescent proteins (FPs) from several origins and spanning the entire spectral palette have been engineered to achieve proteins that are brighter and more photostable (Day and Davidson, 2009). Two example are DsRed from the sea anemone *D. striata* and mCherry, a third generation monomeric derivative of DsRed (Baird et al., 2000, Campbell et al., 2002, Shaner et al., 2004). The availability of FPs has also brought about new techniques, like optical highlighting, which enables the temporal study of proteins and cells (Dickson et al., 1997, Miyawaki, 2004). By exploiting the photophysical properties of certain fluorescent proteins, like photoactivation, photoconversion and photoswitching, some FPs can now be used to track temporal expression patterns, turnover rates and other time-dependent processes (Lippincott-Schwartz et al., 2003, Lukyanov et al., 2005). The field of calcium imaging has also benefited from engineered FPs that can modulate their fluorescence in response to intracellular Ca^{2+} concentration (Zhao et al., 2011b). In addition, voltage-sensitive fluorescent proteins facilitate the analysis of electrical activity at genetically defined neuronal populations (Akemann et al., 2010).

The development of methods that utilize fluorescent proteins has been instrumental in the field of neurobiology as it allows dynamic cellular processes to be studied in a controlled and selective manner *in vivo*. Shortly after the discovery of GFP, fluorescent proteins became widely used to study cells and molecules in a vast range of species (Tsien, 1998), and to study neuronal processes in transgenic models (Knobel et al., 1999, Dynes and Ngai, 1998, Murray et al., 1998, van den Pol and Ghosh, 1998, Rodriguez et al., 1999). As described in more detail below, the use of Cre-based fluorescent labeling has also become an essential tool (Feng et al., 2000). For example, the Brainbow technique, which uses the Cre/*lox*P

system, produces multicolor mosaicism by stochastic combinatorial expression of three or more XFPs (Livet et al., 2007). With up to 89 distinguishable colors, this method facilitates the visualization of cellular interactions in areas of high neuronal density (Havekes and Abel, 2009). In addition to Brainbow, there are currently over 300 available lines of transgenic mice that use fluorescent proteins (www.jax.org, www.gensat.org).

1.2.2 Genetic Manipulation of Neurons

1.2.2.1 *Site-specific recombination*

Site-specific recombination (SSR) has greatly facilitated the large-scale study of mammalian gene function. Recombinases like Cre and Flp (Tyr recombinases) and ϕC31 (Ser recombinase) are commonly used in the field of mouse genetics because they allow for the accurate insertion, deletion or inversion of DNA (Branda and Dymecki, 2004, Turan and Bode, 2011). Recently, novel recombinases have also been characterized in *Drosophila* and mice (Nern et al., 2011). When used in combination with other elements such as cell-type specific promoters and modified steroid receptor ligand binding domains, site-specific recombination has the power to render both spatial and temporal control of genetic manipulation.

1.2.2.1.1 Cre & Flp recombinase

Cre (short for "causes recombination") is a recombinase protein derived from the bacteriophage P1 genome that recognizes target sites called *lox*P (locus of crossover in P1) (Abremski and Hoess, 1984). When two *lox*P sites are present, Cre catalyzes recombination between them in order to delete, invert or integrate DNA (Hamilton and Abremski, 1984). A *lox*P site consist of two 13 basepair (bp) palindromic sequences separated by an 8bp asymmetric spacer (Hoess et al., 1982). Similarly, Flp recombinase, from the 2µm plasmid of *Saccharomyces cerevisiae* , catalyzes recombination between FRT target sites (Cox, 1983). FRT target sites are similar in structure to loxP sites but differ in their precise nucleotide sequence (McLeod et al., 1986).

In both systems, the asymmetry of the spacer sequence provides directionality to the site and thus recombination is only possible when the two target sites are properly aligned (Hoess et al., 1986). This means that the relative orientation of the two *lox*P or FRT sites determines the outcome of recombination (Fig 1.6). DNA that is flanked by two *lox*P sites ('floxed") or by two FRT sites ("flirted") is deleted when the sites are oriented in the same direction (parallel) and inverted when the sites are in opposite directions (antiparallel). Two sequences, each containing its own target site, can also be integrated; for example, a circular donor sequence into genomic DNA (Golic and Lindquist, 1989) or interchromosomal crossover (Van Deursen et al., 1995, Zong et al., 2005).

DNA excisions are the most basic of the modifications catalyzed by recombinases because they are essentially irreversible. Since this technique is accurate and stable, it is widely used in the production of transgenic and knockout mice (Branda and Dymecki, 2004). Recombinase-mediated excisions can be used to either delete a gene by flanking it, or insert a gene by placing it downstream of a flanked STOP cassette. Insertions, however, result in a floxed or flirted DNA sequence that is susceptible to further deletion and/or inversion. Likewise, inversions can switch indiscriminately between conformations. Several methods attempt to rectify these problems, including the use of heat-shock promoters to control reaction time (Morris et al., 1991), as well as target site modification (Senecoff and Cox, 1986).

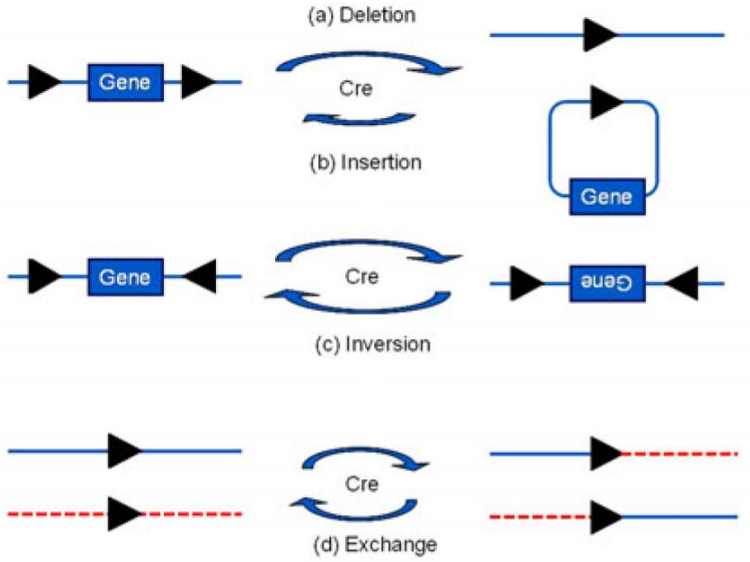

Figure 1.6 – DNA manipulations controlled by Cre and loxP directions or locations
(a) If the two loxPs are in the same direction on one DNA molecule, the DNA between them will be deleted. (b) When one loxP is on a linear DNA while another is on a circular DNA, the circular DNA will integrate into the linear DNA at the target. Small circular DNA is easily lost in cells; hence, the reaction in (a) happens more easily than that in (b). (c) If two loxPs are opposite, the DNA fragment between them will be inverted. (d) The DNA molecules will exchange a segment if both loxPs lie on linear DNA molecules. The black triangles are loxP sites, and indicate the direction. The length of the arrows indicates the relative tendency of reactions. From Zhang et al. (2012)

Target site modifications fall into two categories, the first being spacer variants. RMCE (recombinase-mediated cassette exchange) and FLEx (flip excision) are two strategies that take advantage of the fact that *lox*P and FRT sites tolerate certain point mutations within their core (Hoess et al., 1986) and that only two identical sites can be recombined effectively (Senecoff et al., 1988). In general, two heterotypic sites containing different spacer sequences will not recombine efficiently (Senecoff et al., 1988). Spacer variants used in these two strategies have been developed for both Cre- and Flp-mediated recombination

(Lee and Saito, 1998, Langer et al., 2002, Schlake and Bode, 1994). In RMCE, a DNA sequence flanked by antiparallel heterotypic sites (e.g. "→DNA←") can be inserted into a sequence containing the same combination of sites. The product is a newly replaced sequence flanked by heterotypic sites that cannot cross-react. RMCE is commonly used to replace selectable markers in embryonic stem (ES) cells used for gene targeting (Branda and Dymecki, 2004). In FLEx, a DNA sequence to be inverted is placed within two pairs of antiparallel homotypic sites (e.g. →→DNA←←). An inversion of either pair of homotypic sites leaves one site trapped for excision by the second pair of homotypic sites (e.g. "→AND←←←"). The product is an inverted sequence flanked by non-reacting heterotypic sites (→AND←).

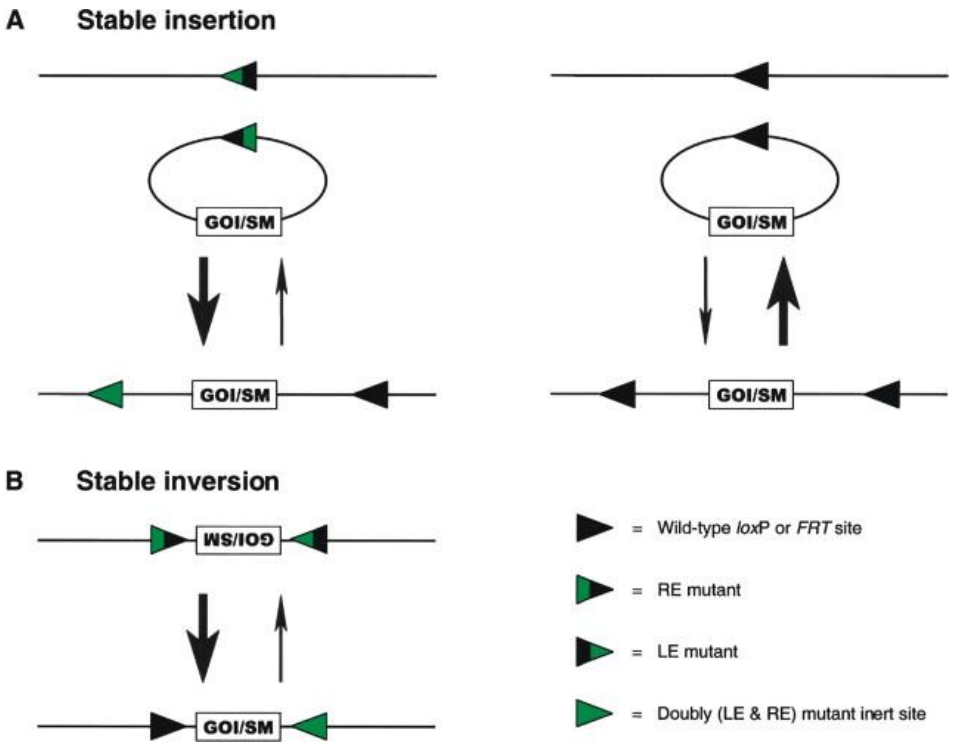

Figure 1.7 - Use of inverted repeat-variant target sites to achieve stable DNA Insertion or inversion
Stable DNA insertions (A) or inversions (B) may be achieved by exploiting lox or FRT sites that contain established substitutions in either the left or right inverted repeat, also referred to as the left element (LE) or right element (RE), respectively. While two wild-type (wt) target sites can recombine with each other repeatedly, an LE and RE mutant site will recombine efficiently only once, creating two different sites, a wild-type and a doubly (LE & RE) mutant inert site, that cannot recombine efficiently with each other. SM, selectable marker; GOI, gene-of-interest. From Branda and Dymecki (2004)

In the second category of target site modifications, called inverted-repeat variants (Fig 1.7), a point mutation is made on one of the palindromic (inverted) sequences (Branda and Dymecki, 2004). A target site containing a nucleotide substitution on its left inverted repeat (LE mutant site) will recombine with a site that contains an analogous substitution on its right inverted repeat (RE mutant site). This strategy is often used to insert circular plasmid

DNA into chromosomal DNA, where one possesses an LE mutant site and the other an RE mutant site (Branda and Dymecki, 2004). The result is an inserted DNA sequence flanked by one wildtype target site and one double-mutant site (both RE and LE mutations). This strategy can also be used to invert a sequence flanked by one RE and one LE mutant site. The result is a stable inverted sequence flanked by one wildtype and one doubly mutant site.

Advances in SSR technology have also focused on the recombinases themselves. Several modifications aim to enhance recombinase expression levels and enzymatic activity in mammalian cell culture and transgenic mouse models (Buchholz and Stewart, 2001, Voziyanov et al., 2003). A modified version of Flp called Flpe, for example, increases the protein's thermostability and enhances its recombination efficiency four-fold (Buchholz et al., 1998). A modified version of Cre called iCre (improved Cre), is more compatible with eukaryotic systems and has a slightly elevated recombination efficiency (Shimshek et al., 2002). Because unmodified Cre recombinase is substantially more efficient at 37^{o}C than Flp, the Cre/*lox*P system has traditionally been favored in the field of mouse genetics. Improved versions of Flp, however, have recently shifted preference in favor of modified recombinases like Flpe and Flpo (Turan et al., 2011, Raymond and Soriano, 2007).

1.2.2.1.2 ΦC31 recombinase

In cultured ES cells, a more recent alternative to Cre and Flp is the *Streptomyces* phage-derived ϕC31, which produces insertions that are inherently stable (Groth et al., 2000, Thyagarajan et al., 2001). ΦC31 catalyzes recombination between attP (39bp) and attB (34bp), which have similar but not identical inverted arm sequences, and produces two new sites termed attL and attR (Groth et al., 2000, Thorpe and Smith, 1998). ΦC31 by itself is unable to catalyze recombination between attR/attL, which means the reaction is unidirectional. Reversal of this recombination event has recently been found to be possible in human and mouse cells (Farruggio et al., 2012). The use of this recombinase in chromosomal engineering and gene therapy has recently gained popularity (Zhang et al., 2012).

1.2.2.2 *Inducible genetic manipulation*

The field of genetics has greatly benefited from the use of inducible techniques that provide temporal control of genetic manipulations. In transgenic models, these strategies make it possible to bypass any embryonic lethality, early developmental defects or secondary compensatory mechanisms due to modified gene function. Genetic modifications can therefore be analyzed in both the developing and adult brain. Temporal control can be achieved using transcriptional strategies, such as the tetracycline (tet), lac and GAL4/UAS systems, or by the use of ligand-induced recombination. Tetracycline and estrogen based ligand-inducible variants of Cre recombinase are most commonly used in transgenic mice (Saunders, 2011). Both of these are binary systems, wherein two genetically modified mice, a "driver" and a "reporter", are mated in order to obtain double heterozygous mice that can undergo conditional genetic manipulation (Lewandoski, 2001). In these strategies, the driver line carries either tet-regulated transactivation factors or a drug-sensitive recombinase and the reporter line carries a gene of interest whose expression relies on activation by tet or Cre (Saunders, 2011).

1.2.2.2.1 Ligand-induced recombinases

In this method, the mutated ligand-binding domain (LBD) of a steroid receptor is fused to a recombinant protein so its catalytic activity becomes ligand-dependent (Logie and Stewart, 1995, Metzger et al., 1995). The binding domains of these fusion proteins are engineered to be resistant to their natural ligands and sensitive to synthetic equivalents (Feil et al., 1996, Zhang et al., 1996, Kellendonk et al., 1996). This is particularly important in mammalian systems where endogenous steroids are present and could activate recombination. Estrogen receptor (ER) chimeras are insensitive to βestradiol and responsive to its synthetic equivalent 4-OH tamoxifen. The most popular ligand-induced recombinase, $CreER^{T2}$, contains a triple mutation to the LBD and is ~10 fold as efficient as other CreER fusions (Feil et al., 1997, Indra et al., 1999, Feil et al., 2009). Over 300 Cre-based transgenic mouse lines have been developed, characterized and used successfully to study gene function (http://cre.jax.org, www.gensat.org/cre.jsp). A $FlpeER^{T2}$ variant has also been developed but is not as commonly used as CerERs (Hunter et al., 2005). The progesterone receptor (PR) has also been used to design ligand-dependent recombinases, albeit with limited success *in vivo* (Wunderlich et al., 2001). Chimeras CrePR1 and Cre*PR are insensitive to endogenous progesterone but sensitive to the synthetic steroid RU 486 (Kellendonk et al., 1996, Wunderlich et al., 2001).

1.2.2.2.2 Tetracycline-inducible system for genetic manipulations

A second method of temporal control uses tetracycline (tet) to regulate transcription (Fig 1.8) (Gossen and Bujard, 1992). This method requires two components; a transactivator gene that binds tetracycline, and a fusion of the tetracycline operon (tetO) and a gene of interest (GOI) (St-Onge et al., 1996, Strathdee et al., 1999). In the tet-Off system, the transactivator tTA binds to tetO to initiate transcription in the absence of tetracycline (Gossen and Bujard, 1992). Constant administration of tetracycline, or its analog doxycycline (dox), must therefore be maintained to repress expression of the GOI. Gene transcription can be induced by discontinuing drug administration, although complete clearance of doxycycline in mice may take up to seven days (Kistner et al., 1996). In the tet-ON system, rtTA (reverse tTA) binds tetO to initiate transcription only in the presence of tetracycline (Gossen et al., 1995). This method relies on delivery of tetracycline or doxycycline in order to initiate GOI transcription. In adult transgenic mice, gene expression can be detected within an hour of drug administration (Hasan et al., 2001, Schonig et al., 2002).

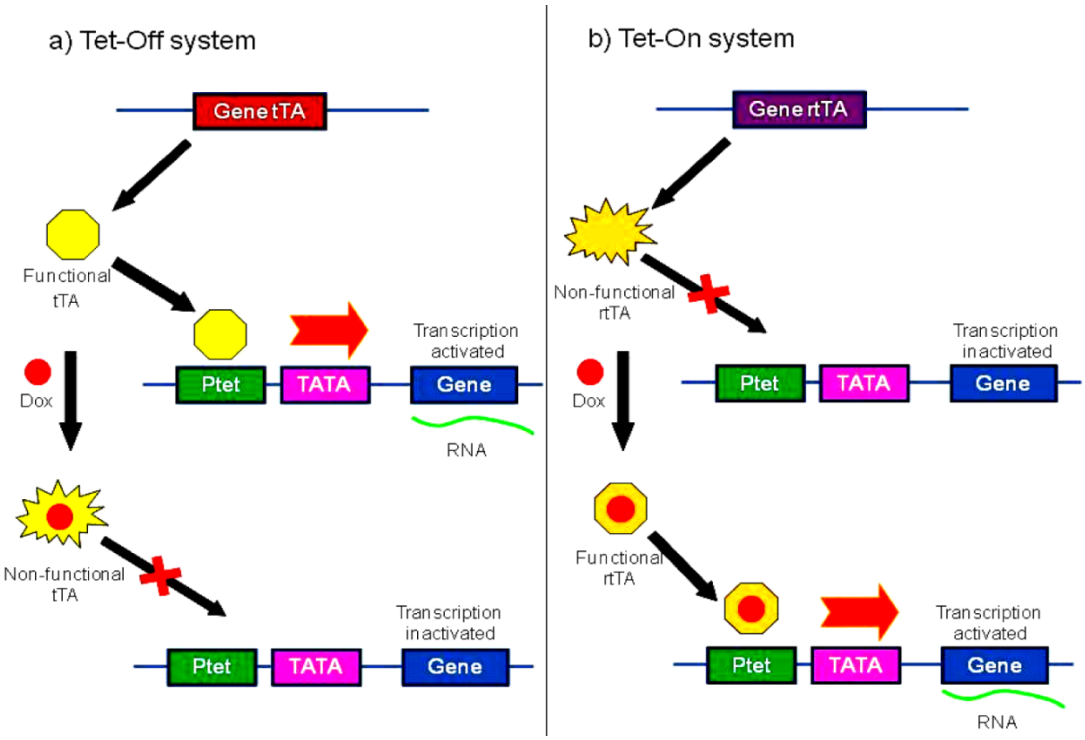

Figure 1.8 - Tetracycline-inducible system

(a) Tet-Off system. tTA is active without Dox (or tetracycline), and the gene of interest is expressed. With Dox (or tetracycline) treatment, tTA is inactivated, and the gene is no longer expressed. (b) Tet-On system. rtTA is inactive without Dox (or tetracycline), and the gene of interest is not expressed. With Dox (or tetracycline) treatment, rtTA is activated, and the gene is expressed. From (Zhang et al., 2012)

1.2.2.3 *Neuronal cell-type specificity*

Neuron-specific genetic manipulations can be produced in mice by assembling a DNA construct that contains neuron-specific promoter/enhancer elements. This DNA construct is then introduced into the host species by a conventional transgenic method like pronuclear microinjection. This is in contrast to gene targeting, where a transgenic construct is introduced by homologous recombination to a neuron-specific gene of interest (Rotolo et al., 2008). In theory, it could be possible to express a transgene in any desired cell-type by simply identifying a unique gene or enhancer in that cell population (Miyoshi and Fishell, 2006). In practice, however, robust and unique promoters are not abundant (Miyoshi and Fishell, 2006). Even so, some promoters have been used extensively, for example Thy1.2 (Caroni, 1997, Feng et al., 2000), CamKIIα (Tsien et al., 1996) and Nestin (Zimmerman et al., 1994, Tronche et al., 1999, Cheng et al., 2004). Additionally, several large-scale approaches set out to identify and characterize promising neuronal promoters (Gong et al., 2003, Madisen et al., 2010, Portales-Casamar et al., 2010).

The *Thy1* gene is expressed in pyramidal cells in both neuronal and non-neuronal tissue. Removal of one of its introns, however, eliminates expression in non-neuronal cell-types (Caroni, 1997). Using this modified Thy1.2 promoter, a transgene can be expressed throughout the central and peripheral nervous system without expression in non-neuronal tissue (Feng et al., 2000, Young et al., 2008, Heimer-McGinn and Young, 2011). Similarly, although the *Nestin* gene is expressed in several tissue types, one of its introns is neuron-specific so, in combination with a minimal promoter sequence, it can be used to attain transgene expression almost exclusively in neural progenitor cells (Zimmerman et al., 1994, Burns et al., 2007). Finally, the CamKIIα (α-calcium-calmodulin-dependent kinase II) enhancer promotes activity in the forebrain region only (Mayford et al., 1995, Erdmann et al., 2007).

Since transgene insertion is random, different lines produced from the same transgenic construct can display great variety of heritable expression patterns (Wilkie et al., 1986) Although position-effect variegation may lead to transcriptional silencing, the mosaicism it produces can also be beneficial if expression happens to be limited to a particular subset or area of interest. For instance, the SLICK lines (described in section 1.2.2.4.3) make use of the Thy1.2 promoter and display a wide range of mosaicism from less than 1% transgene expression in specific areas to over 95% neuronal expression in other lines (Young et al.,

2008, Heimer-McGinn and Young, 2011). Transgenic lines using the CamKIIα promoter tend to have strong widespread expression in the cortex and hippocampus and more scattered expression in the rest of the forebrain (Tsien et al., 1996, Erdmann et al., 2007, Madisen et al., 2010).

As illustrated by these examples, tissue-specific transgene expression can be combined with conditional gene manipulation strategies like SSR. Such binary systems use a "driver" transgenic line, in which recombinase expression (e.g. $CreER^{T2}$ or Flpe) is controlled by a cell-type specific promoter and a "reporter" line, in which gene deletion or transgene expression is achieved using recombinase recognition sites (e.g. *lox*P or FRT). The flexibility of binary systems allows for endless combinations that render precise spatial and temporal control in many different varieties of cell-types and subpopulations. Moreover, some of these lines utilize combinatorial control of gene expression or deletion by using more than one promoter/enhancer elements. Genetic manipulation in this case occurs only when the expression patterns of both promoters intersect (Zong et al., 2005, Farago et al., 2006, Kim et al., 2009). Some techniques that combine the use of cell-type specific genetic manipulation and cell labeling in sparse populations of cells are described in the following section.

1.2.2.4 *Novel techniques that combine genetic manipulation and cell labeling*

1.2.2.4.1 MARCM

Developed by Luo and colleagues, MARCM (Mosaic Analysis with a Repressible Cell Marker) provides a way to introduce genetic manipulation in fluorescently labeled *Drosophila melanogaster* cells. As described by Lee and Luo (1999, 2001) this is achieved by placing a GFP marker under the control of a repressible promoter. The GAL4/UAS inducible system is used, where transcription of the ubiquitously-expressed promoter GAL4 is activated by UAS (upstream activation sequence)(Brand and Perrimon, 1993) and blocked by the antagonist GAL80 (O'Donnell et al., 1994). A single FRT site is placed on identical locations in homologous chromosome arms; one arm contains the GAL80 repressor distal to the FRT site and the other arm contains GAL4, GFP and a mutation of interest, all distal to the FRT site. Following Flp-mediated interchromosomal recombination during mitosis, only cells that are homozygous for the mutation will express GFP. MARCM was a significant improvement over earlier methods that relied on negative labeling (GFP on one arm and a mutation on the other)(Xu and Rubin, 1993). With MARCM, the neuronal morphology of a homozygous

mutant cell can be visualized and studied *in vivo*. This technique is still widely used in fruit flies (e.g. Kuert et al. (2012)) and has also been extended for use in mammalian systems (Zong et al., 2005), as described below.

1.2.2.4.2 MADM Strategy

Also developed by Luo and colleagues, MADM (Mosaic Analysis with Double Markers) is a method of generating mice with genetic manipulations in fluorescently labeled cells. As described in Zong et al. (2005) and Tasic et al. (2012), two reciprocally chimeric markers are knocked in at identical loci on homologous chromosomes in separate mice. The chimeras, referred to as GR and RG, each contain part of the GFP coding sequence and part of an RFP coding sequence (DsRed2 or tdTomato). The N-terminus of one fluorescent marker and the C-terminus of the other are split by a *lox*P-containing intron. A mutation of interest is placed distal to the GR knock-in site, creating a heterozygous mutation. The two chimeric mice are crossed to each other and then to a Cre-expressing driver line. The resulting triple transgenic mice can undergo Cre-mediated interchromosomal recombination in mitotic and post-mitotic cells. Chromosomal crossover restores functional GFP and RFP expression cassettes. After mitosis, daughter cells are either (a) homozygous mutant expressing GFP, (b) homozygous wildtype expressing RFP, or (c) heterozygous expressing both GFP and RFP. In this way, the MADM strategy can introduce a genetic mutation, with fluorescent markers indicating cellular genotype. These mice can simultaneously be used to trigger genetic manipulation, analyze cellular lineage and visualize neuronal wiring patterns.

MADM-generated mouse lines can be mated to any Cre-expressing line in order to induce recombinase-mediated interchromosomal exchange. Several Cre-expressing lines have been crossed to MADM lines and characterized, including β-actin-, Nestin- and Wnt1-expressing lines (Zong et al., 2005). As described in this publication, labeling efficiency depends on the driver line used. When crossed to conditional Cre-expressing lines like β-actinCreER, double heterozygous mice show tight control in the absence of tamoxifen induction. In all cases GFP is strongly expressed without the need for further immunostaining. RFP fluorescence is strong for dtTomato but not for DsRed2 (so a Myc tag is generally used to enhance labeling). As discussed in Zong et al. (2005), a single copy of the knocked-in fluorescent marker gene has proven sufficient to label all neuronal processes including dendritic spines and long-distance axons. Since the strategy does not require a particular gene to be floxed/flirted, MADM can also provide markers for spontaneous or chemically induced mutations. Moreover, labeling of homozygous wildtype cells offers a built-in negative control.

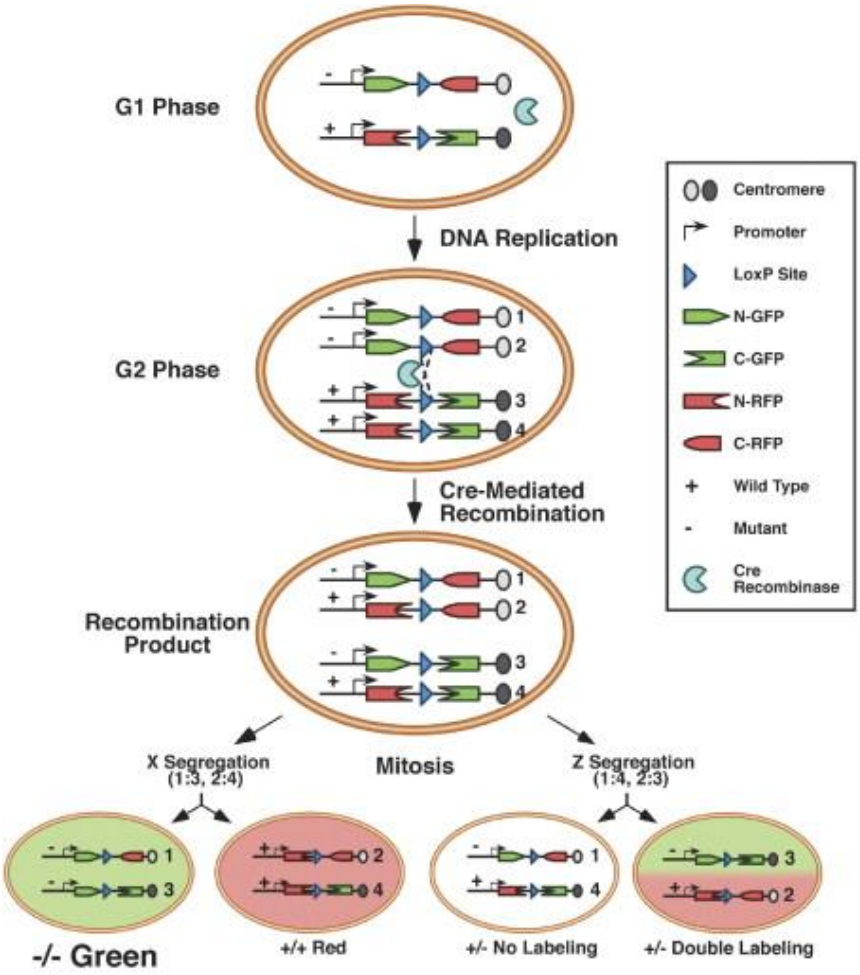

Figure 1.9 – Schematic of the MADM Strategy

G2 recombination followed by X segregation generates singly labeled cells that alter genotype if the original cell is heterozygous for a mutation of interest. G2 recombination followed by Z segregation generates either colorless or double-colored cells without altering genotype. From Zong et al. (2005)

MADM provides a method for introducing genetic mutations that is compatible with any Cre-expressing driver line. The approach is limited, however, by the fact that it can only be applied to introduce mutations distal to the MADM cassette (from the centromere) on a given chromosome. Currently, MADM cassettes are available for *Rosa26* on chromosome 6, *Miya1* on chromosome 1, *Miya10* on chromosome 10, and *Hipp11* on chromosome 11 (Tasic et al., 2012). Although there are efforts underway to find and characterize efficient loci on other chromosomes, this restriction limits the number of genes that can be manipulated using MADM. Additionally, this method is quite laborious as it involves the generation of two mice by gene targeting (or at least one that harbors the desired modification if it is compatible with an available mutually chimeric line) and requires mating of three lines to obtain triple heterozygosity.

1.2.2.4.3 SLICK Mice

Developed by Feng and colleagues, SLICK (Single-neuron Labeling with Inducible Cre-mediated Knockout) is another recently developed technique that allows for inducible genetic manipulation in fluorescently labeled single cells. As described by Young et al. (2008), this is achieved by simultaneous expression of CreER^{T2} and YFP (yellow fluorescent protein), driven by two back-to-back copies of the Thy1.2 promoter (Fig 1.10). SLICK mice can be crossed to any *lox*P-based transgenic mouse to achieve efficient genetic manipulations in YFP-labeled cells. Due to position-effect variegation, expression of the SLICK transgene varies over 30 different lines (Fig 1.11) including SLICK-V, where genetic manipulation is spatially restricted to small subpopulations of projection neurons, and SLICK-H, where expression is widespread in most populations of projection neurons in the brain. In both of these models, YFP fluorescence is bright and easily visualized in all cellular processes, including dendritic spines and long-distance axons. SLICK-V and SLICK-H, which have been characterized using the ROSA26 reporter line, display tight temporal control of induction in the absence of tamoxifen (Young et al., 2008, Heimer-McGinn and Young, 2011).

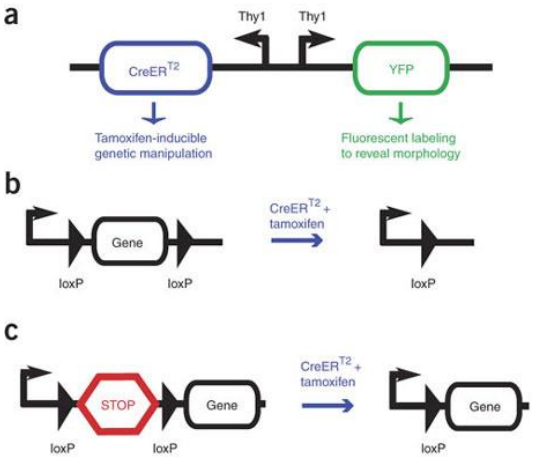

Figure 1.10 - Strategy for coexpression of YFP and Cre in SLICK transgenic mice.
(a) Schematic representation of the DNA construct used to generate SLICK transgenic mice. Two copies of the Thy1 promoter drive expression of YFP and the inducible form of Cre recombinase, CreER^{T2}. CreER^{T2} can be activated by the synthetic ligand tamoxifen, but not by endogenous estrogens. Tamoxifen administration can thus be used to control the timing of recombination. From Young et al. (2008)

The two components of the SLICK transgene, YFP fluorescent reporting and Cre/*lox*P compatibility, endow this method with several advantages. In SLICK-V, where expression is limited to less than 10% of cells in a given population, strong fluorescent labeling facilitates precise morphological analysis and examination of synaptic connectivity in individual mutant neurons. Because YFP fluorescence is expressed in the absence of Cre-mediated recombination, individual cells can be imaged before and after induction of a genetic manipulation, making it possible to analyze changes in neuronal properties. Dynamic processes like synaptic plasticity and spine morphology can also be visualized *in vivo* before and after gene activation or knockout. Another important feature of YFP expression before CreER^{T2} drug activation is that fluorescent cells in un-treated SLICK mice can be used as controls for mutant cells in treated mice.

As discussed in Young et al. (2008) and Heimer-McGinn and Young (2011) the CreER^{T2} component renders SLICK lines compatible with any *lox*P-based genetically modified mouse model, which makes it widely applicable in the field of mouse genetics. Since YFP is not easily distinguished from GFP, however, GFP cannot be used as a reporter to characterize gene expression. This does not hinder SLICK recombination efficiency, which is >90% in many areas of the brain, but does diminish the convenience of GFP-expressing *lox*P mice. The inducible nature of this system permits genetic modifications to be analyzed in the stable adult brain without early developmental defects arising. Studies can also be performed in younger mice although recombination efficiency is reduced due to the developmental nature of the Thy1.2 promoter (Caroni, 1997). In SLICK-V, the sparse expression pattern enables the study of competitive processes in the long term and prevents the disruption of general function, thus reducing crossover between cell-autonomous effects and those caused by more widespread dysfunction (Young et al., 2008). As for SLICK-H, it is currently one of the most efficient Cre-expressing lines available for pan-neuronal genetic manipulation (Heimer-McGinn and Young, 2011).

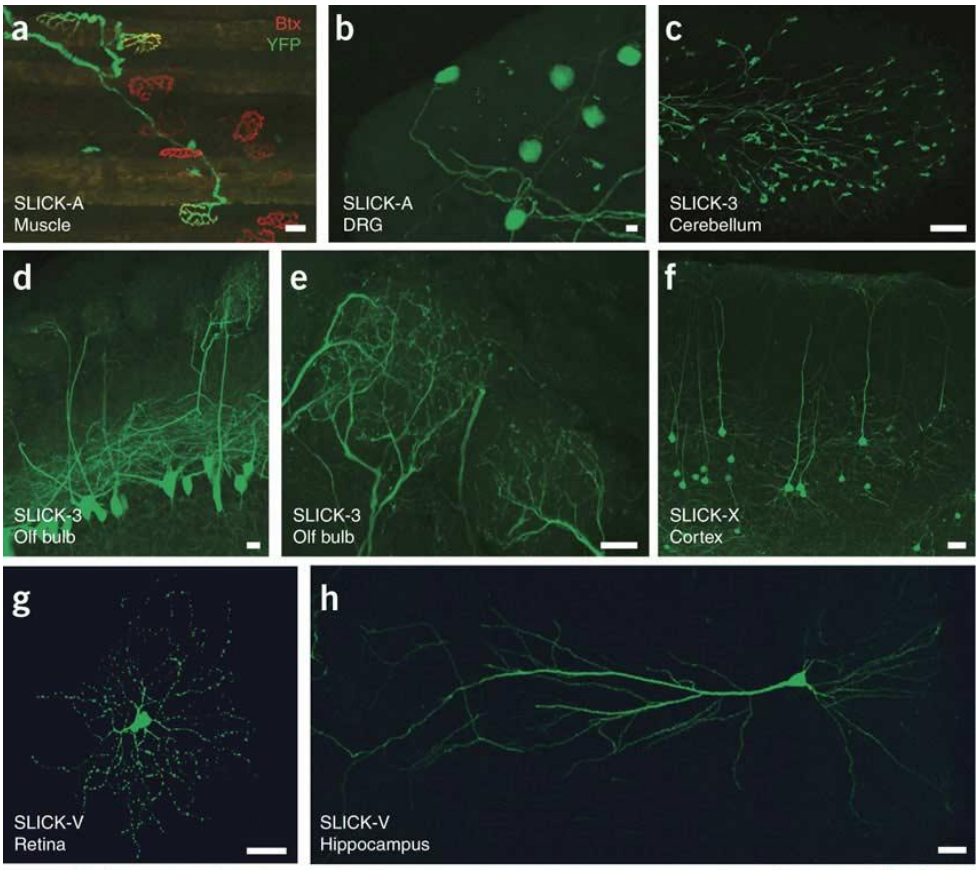

Figure 1.11– YFP labeling of distinct neuronal populations in SLICK transgenic lines
From Young et al. (2008)

1.2.3 Altering neuronal activity

The ability to modulate neuronal activity is essential to the study of neuronal circuits. Classical studies in the field of systems neuroscience used pharmacological agents like kainic acid or glutamate receptor antagonists to lesion, ablate or inhibit cell populations or brain regions (Wulff and Wisden, 2005). More recently, pharmacological agents like tetrodotoxin and bicuculline have been used to respectively inhibit or enhance global neuronal activity in cell cultures or brain slices (Khawaled et al., 1999, Narahashi, 2008). Although many important observations can be made using these methods, they do not provide cell-type specificity and are limited by compensatory mechanisms that complicate data analysis.

The recent merging of genetics and pharmacology, as well as the application of light-sensitive ion channels/pumps, provides a wealth of tools that offer precise spatial and temporal control. Select populations of cells can be activated or inhibited by either altering membrane potential or by regulating neurotransmitter release. These instruments greatly facilitate the study of neuronal circuit dynamics *in vivo*. (Wulff and Wisden, 2005, Miyoshi and Fishell, 2006, Dymecki and Kim, 2007, Havekes and Abel, 2009, Rogan and Roth, 2011).

1.2.3.1 *Alteration of ion gradients across the cell membrane*

Neuronal activity can be modulated by altering ion gradients across the cell membrane. Ion channels and pumps can be altered genetically by overexpression or mutation, pharmacologically by ligand-induced activation or inhibition, and optically using light-sensitive ion channels and pumps. Several approaches employ a combination of these methods. In this way, the modulated influx or efflux of certain ions can selectively alter neuronal excitability and therefore inhibit or activate Ca^{2+}-dependent synaptic transmission (Wulff and Wisden, 2005, Havekes and Abel, 2009). In this thesis we aimed to inhibit neuronal activity by overexpression of the Kir2.1 inward rectifying potassium channel, which is discussed in the following section.

1.2.3.1.1 Kir2.1 inward rectifying channel

Inward rectifying potassium (Kir) channels are transmembrane proteins that create an inward K^+ current and are critically involved in maintaining resting membrane potential following hyperpolarization (Hibino et al., 2010). Unlike conventional voltage-gated K^+ channels, Kir channels are insensitive to membrane voltage and instead respond to the

electrochemical gradient for K^+ (Hibino et al., 2010). At membrane potentials below potassium's reversal potential of -86 mV (i.e. when the cell is hyperpolarized), K^+ influx through Kir channels restores K^+ equilibrium and returns the membrane to its resting potential (Alger and Nicoll, 1980, Nichols and Lopatin, 1997). This serves to counteract the hyperpolarizing effect of excessive outward K^+ flux through voltage-gated channels following repolarization (Nichols and Lopatin, 1997). Inward rectification results from intracellular molecules like Mg^{2+} (Matsuda et al., 1987) and polyamines (Lopatin et al., 1994) that bind to Kir at several sites in order to block outward K^+ flux (Lu et al., 1999). Kir channel function and localization are further modulated by a variety of factors including (a) extracellular K^+ concentration, (b) intra- and extracellular pH, (c) phosphatidylinositol 4,5-bisphosphate (PtdIns-4,5-P2), (d) phosphorylation, (e) protein interactions, with PSD-95for example, and (f) internalization mediated by small GTPases.

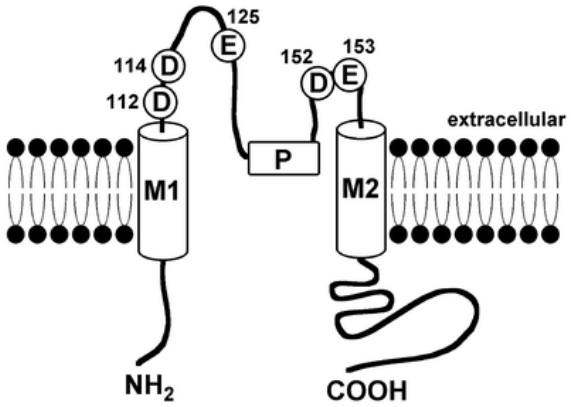

Figure 1.12 - Schematic representation of the structure of the Kir2.1 subunit
The Kir2.1 channel is composed of four subunits, each containing two transmembrane domains (M1 and M2) linked by a highly conserved pore region (P). The extracellular loops contains five negatively charged amino acid residues (D-Asp and E-Glu) that act as binding sites for Mg^{2+} or polyamides. These molecules block the outward flow of potassium and therefore enable inward rectification. From Hayashi and Matsuda (2007)

Kir2.1, from the Kir2.X subfamily (Fig 1.12), is considered to be critically involved in regulating neuronal excitability and has been used as a tool to inhibit neuronal activity (Kubo et al., 1993, Hibino et al., 2010). It is expressed diffusely and weakly throughout the brain and is restricted to neuronal somata and dendrites (Pruss et al., 2005). This classical Kir channel (as opposed to G protein-gated, ATP-sensitive or K+ transport Kir channels) displays a strong inward rectifying conductance that can be further modulated by neurotransmitter activity (Hibino et al., 2010). Kir2.1 knockout mice display symptoms similar to Andersen's syndrome (Zaritsky et al., 2000), which is caused by a mutation in the gene that encodes for Kir2.1 (Plaster et al., 2001).

For the study of activity-dependent competition in neuronal circuits, over-expression of the Kir2.1 channel has been widely used as a method to hyperpolarize individual neurons and therefore prevent them from firing action potentials (Burrone et al., 2002, Yu et al., 2004, Hua et al., 2005, Hartman et al., 2006). It was first overexpressed in mammalian cells by viral delivery in order to hyperpolarize cultured cervical ganglion cells (Johns et al., 1999, Holt et al., 1999). Transgenic delivery by microinjection has also been achieved in mice, where overexpression in a sparse population of olfactory neurons is regulated by tetracycline induction (Yu et al., 2004). Kir2.1 overexpression is a useful tool for the study of the activity-dependent effects of prolonged neuronal silencing in sparse populations of cells.

1.2.3.1.2 Other methods that alter ion gradients across the cell membrane

Pharmacogenetic methods provide the ability to reversibly and selectively suppress neuronal activity. G-protein-gated inward rectifying K^+ channels, for instance, can be used in combination with the allatostatin receptor, a *D. melanogaster* GPCR that is insensitive to mammalian peptide ligands (Lechner et al., 2002, Ehrengruber et al., 1997). When bound to its ligand, allatostatin receptors indirectly couple with GIRK channels to promote K^+ efflux. Thus, administration of allatostatin peptide transiently induces membrane hyperpolarization and consequently inhibits action potentials (Lechner et al., 2002, Tan et al., 2006, Gosgnach et al., 2006). Glutamate-gated Cl^- channels (GluCls), derived from *C. elegans*, can also be used in a similar fashion (Raymond and Sattelle, 2002). Administration of ivermectin , a GluCl agonist, promotes Cl^- influx and subsequent neuronal silencing. This has been done successfully in mice that are transgenically engineered to express GluCl in select cell types (Slimko et al., 2002, Raymond and Sattelle, 2002, Lerchner et al., 2007). Similarly, the $GABA_A$ receptor is positively modulated by the drug zoldipem: drug administration facilitates $GABA_A$-mediated transmission and thus inhibits excitatory activity (Rudolph and Mohler, 2004). Wuff and colleagues generated zoldipem-insensitive mice by genetically mutating all $GABA_A$ receptors and then used Cre-mediated recombination to restore sensitivity in select populations of cells (Wulff et al., 2007).

Reversible neuronal suppression can also be achieved using engineered GPCRs that are sensitive only to synthetic ligands (receptor activated solely by a synthetic ligand, RASSL) (Redfern et al., 1999, Scearce-Levie et al., 2001, Srinivasan et al., 2003). This method is advantageous because (a) there is an immense availability of natural GPCRs that can be targeted, (b) the relatively small size of GPCR cDNA constructs makes them easy to transfer, and because (c) they are commonly targeted for drug discovery, therefore many agonists

and antagonists have already been developed (Conklin et al., 2008). Several transgenic mice have been successfully developed that express RASSLs, including the modified κ-opiod receptor called Ro1 and the modified 5-HT_4 serotonin receptor called Rs1 (Sweger et al., 2007, Hsiao et al., 2011).

The previously mentioned strategies allow the study of neuronal activity on the timescale of minutes to hours, or longer. Synaptic processes, however, occur on the scale of milliseconds, so these methods are insufficient for the study of fast-acting circuit dynamics. A decade ago, several labs began exploring the use of light stimulation to modulate neurons (Zemelman et al., 2002, Banghart et al., 2004, Volgraf et al., 2006, Chambers et al., 2006). In 2005 it was shown that channelrhodopsin-2 (ChR2), a light-gated cation channel from the algae *C. reinhardtii (Nagel et al., 2003)*, can instantly prompt neuronal spiking by creating a cation influx in response to pulses of blue light (Boyden et al., 2005, Li et al., 2005, Deisseroth et al., 2006). The field of optogenetics, as it is coined, has since grown rapidly and vastly. Many new opsins, with differing light and ion sensitivities, have been found or engineered (Bernstein and Boyden, 2011). Because they respond to different wavelengths of light, they can be used simultaneously to selectively activate and/or inhibit cells *in vivo*. For example, halorhodopsins, from archaea, inhibit neuronal activity by allowing an influx of Cl^- in response to yellow/green light (Bamberg et al., 1993, Gradinaru et al., 2008), whereas light-driven proton pumps derived from archaea, bacteria or fungi pump protons out of the cell to hyperpolarize it (Chow et al., 2010).

Delivery of these microbial opsins to the neuronal cell membrane can be achieved by any gene-delivery method such as lentiviral transfer or transgenic delivery (Bernstein and Boyden, 2011). This has been done in a range of cell types, tissues, circuits and organisms (Zhao et al., 2011a, Goold and Nicoll, 2010, Portugues et al., 2013, Honjo et al., 2012, de Vries and Clandinin, 2013, Xu and Kim, 2011). Additionally, engineered step function opsins can be switched “on” or “off” in response to different wavelengths of light. These optical switches have an extended open-state conformation and can therefore operate on longer timescales (Berndt et al., 2009). Finally, chimeric light-activated GPCRs can be engineered by fusing the intracellular domain of a GPCR of interest to the transmembrane domain of rhodopsin (Airan et al., 2009). This approach facilitates the study of GPCR-mediated signaling pathways in behaving animals.

1.2.3.2 *Inhibition of neurotransmitter release*

As described in the previous section, neurons can be inhibited by hyperpolarizing the cell in order to prevent action potentials and inhibit synaptic activity. Another way to inhibit neuronal activity is to impede synaptic vesicle function and therefore block neurotransmission. Manipulations that affect synaptic transmission include neurotoxin-mediated cleavage or genetic manipulation of core SNARE proteins, and in *Drosophila*, temperature-sensitive paralysis induced by the shibire mutation (Schiavo et al., 2000, Karpova et al., 2005, Kitamoto, 2002). In this thesis we show that long-term inhibition of neurotransmission in a small population of cells by the tetanus toxin light chain can be used in the study of activity-dependent competition.

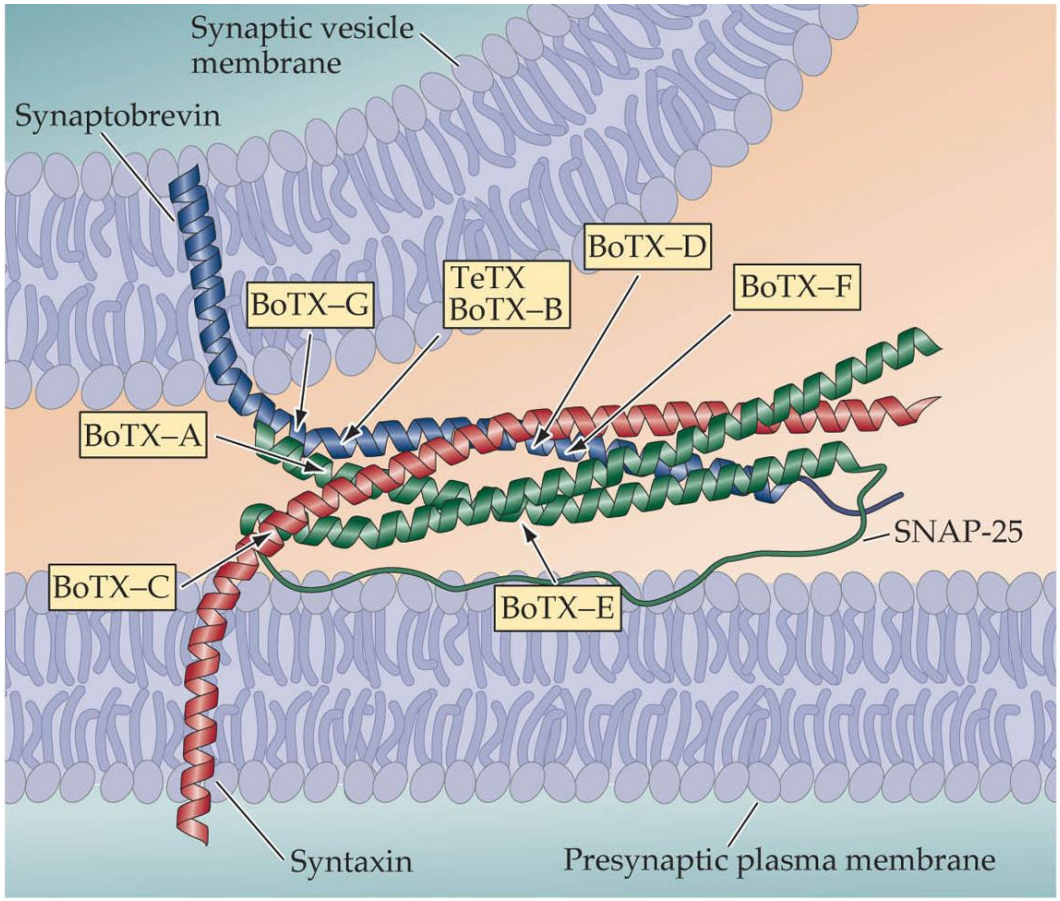

Figure 1.13 – SNARE-mediated synaptic vesicle fusion to the plasma membrane
From Purves et al. (2001)

In neurotransmission, the SNARE complex mediates synaptic vesicle fusion to the presynaptic membrane (Fig 1.13). The complex, composed of syntaxin-1, SNAP-25 and VAMP2/synaptobrevin, assembles reversibly into a tight and highly stable bundle of four α-helices (Fig 1.13) (Poirier et al., 1998). Syntaxin-1 and VAMP2 are transmembrane proteins

anchored to the synaptic membrane and synaptic vesicle, respectively and each contributes one α-helix to the SNARE complex (Bennett and Scheller, 1994, Sudhof, 1995). SNAP-25, which contributes two helices to the complex, is a cytosolic protein tethered to the plasma membrane by palmitoyl chains (Wilson et al., 1996). It is believed that the energy released during complex formation serves to overcome repulsive forces between the two membranes (Rizo and Sudhof, 1998, Li et al., 2007).

The clostridial neurotoxins, tetanus toxin (TeNT) and seven serotypically distinct botulinum neurotoxins (BoNT, A through G), are endowed with metalloprotease activity and can catalyze the degradation of the core SNARE proteins mentioned above (Schiavo et al., 2000). Despite their sequence similarity, each toxin has a very particular target and peptide bond specificity (Schiavo et al., 2000). Syntaxin is cleaved by BoNT/C, VAMP2 is cleaved by TeNT, BoNT/B, D, F, and G, and SNAP-25 is cleaved by BoNT/A, C, and E (Fig 1.13) (Schiavo et al., 2000, Ramakrishnan et al., 2012). It is well established that neurotoxin-mediated cleavage of SNARE proteins, particularly VAMP2, is responsible for blocking neurotransmission (Ramakrishnan et al., 2012). For this reason they are widely used for the purpose of neuronal silencing.

1.2.3.2.1 Tetanus toxin light chain (TetoxLC)

Tetanus neurotoxin (TeNT) is one of eight clostridial neurotoxins that act by directly interfering with neuroexocytosis. With a median lethal dose of 0.1 ng toxin/kg body weight, TeNT is one of the most toxic substances known. The protein is composed of three domains, (1) the NH_2-terminal domain, called the light (L) chain, is a zinc-dependent endopeptidase, (2) the central domain (H_N) is responsible for membrane translocation of the light chain, and (3) the COOH-terminal domain, is divided into two subdomains involved in protein-protein interactions at the synaptic membrane (Fig 1.14). The metalloprotease activity of the L-chain is responsible for cleaving the vesicle-associated membrane protein (VAMP)-2/synaptobrevin, an essential component of the SNARE complex which mediates synaptic vesicle fusion to the synaptic membrane. Intoxicated synapses display severe inhibition of synaptic vesicle release, which blocks neurotransmission, with no effect on action potential propagation or on Ca^{2+} homeostasis.

The TeNT light chain (TetoxLC), which is sufficient to inhibit neuroexocytosis (Bittner et al., 1989), cleaves VAMP2 by proteolyzing the peptide bond between residues 76-Gln and 77-Phe (Schiavo et al., 2000). An upstream remote cluster of amino acids initiates substrate

recognition and several additional residues close to the cleavage site are critical for catalytic activity (Sikorra et al., 2008). Several transgenic mice have been developed that conditionally express TetoxLC, both reversibly and irreversibly (Yamamoto et al., 2003, Yu et al., 2004, Nakashiba et al., 2008, Kim et al., 2009, Kobayashi et al., 2008). When induced, TetoxLC-mediated cleavage of VAMP2 blocks neurotransmission in select populations of cells of these transgenic models.

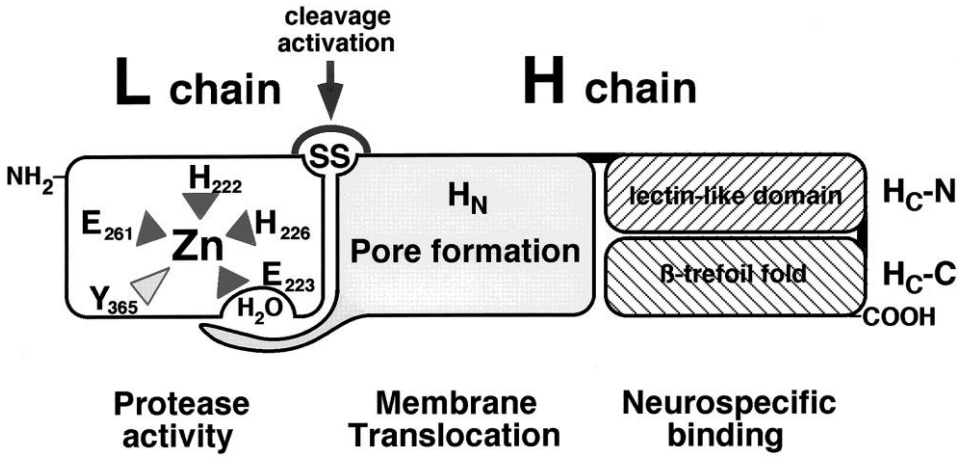

Figure 1.14 – Schematic representation of the tetanus toxin protein domain structure.
TeNT consist of 3 domains of similar size (50 kDa). NH2-terminal domain (left) is a zinc endopeptidase, and the active site zinc atom is coordinated by 2 histidine residues, a water molecule bound to a conserved glutamate residue and by the carboxylate group of another glutamate. H_N, the central domain, is responsible for the membrane translocation of the L chain into the neuronal cytosol. The COOH-terminal H_C domain (right) consists of two equally sized subdomains. The NH2-terminal subdomain has a structure similar to that of sugar binding proteins. The COOH-terminal subdomain folds similarly to proteins known to be involved in protein-protein binding functions such as the K1 channel specific dendrotoxin. Such structure is consistent with the toxin binding to the presynaptic membrane via a double interaction, most likely with two different molecules of the nerve terminal. From Schiavo et al (2000)

Some VAMP isoforms are insensitive to tetanus-mediated cleavage (VAMP4, 7 & 8), while others are sensitive to tetanus-mediated cleavage but absent from neurons (VAMP3/cellubrevin & VAMP5) (Proux-Gillardeaux et al., 2005). In the rat, VAMP1 is tetanus-insensitive due to a variation at residue 76 (Schiavo et al., 2000), although this substitution does not occur in the mouse and human VAMP1 (Fig 1.15). To our knowledge this has not been experimentally tested but it is possible that VAMP1 in the mouse is also cleaved by TetoxLC.

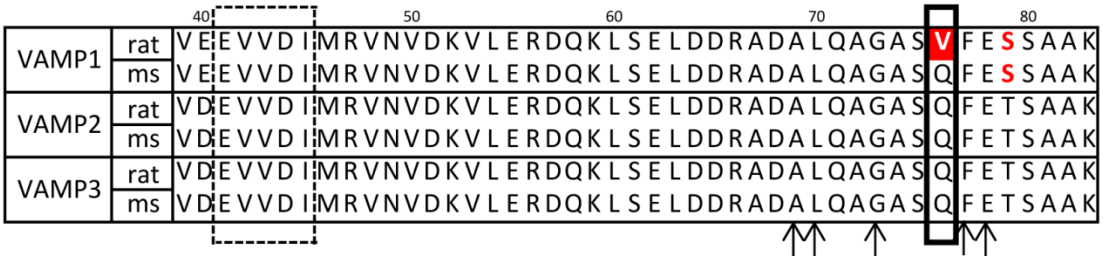

Figure 1.15 - Sequence alignment for the TetoxLC cleavage site in mouse and rat VAMP1/2/3
Sequence alignment of VAMP1/2/3 in mouse and rat shows the cleavage site for TetoxLC between Gln-76 and Phe-77 (box with solid lines). Rat VAMP1 is insensitive to TetoxLC-mediated cleavage because it has an amino acid substitution at position 76 (red box). The remote cluster where Tetox initiates substrate recognition is boxed with dotted lines and arrows indicate sites where mutagenesis results in a loss of cleavability.

1.2.3.2.2 Other methods that inhibit neurotransmitter release

Alternatively, molecules for inactivation of synaptic transmission (MIST) have been developed and characterized in cells and mice. In this technique, presynaptic proteins like VAMP2 and synaptophysin, a SNARE complex regulator, are crosslinked to small molecule "dimerizers" that interfere with protein function and consequently inhibit neurotransmission (Karpova et al., 2005). In *Drosophila*, a mutation in the shibire gene, a dynamin homolog, causes temperature-sensitive paralysis (van der Bliek and Meyerowitz, 1991). Because shibire is involved in vesicle endocytosis (De Camilli et al., 1995), a heterozygous mutation of this gene restricts vesicle reuptake and consequently inhibits synaptic transmission (Kitamoto, 2001, Kasuya et al., 2009). All of the tools mentioned in this section have been helpful in the study of activity-dependent processes in the brain.

1.3 Concluding remarks

It is fairly well established now that the processes of axonal and dendritic development and refinement occur in an activity-dependent manner and in response to competition between neurites and/or neurons. The precise mechanisms responsible for these alterations however, remain to be fully elucidated. Moreover, the field of neuroscience has evolved from studying the role of individual neurons, to trying to understand how cells within an entire circuit develop, interact and synchronize with each other. We are now interested, not only in synaptic plasticity, but also in the plasticity of whole circuits.

This higher-order plasticity, whereby the plasticity of individual synapses and cells is somehow synchronized throughout an entire network, is crucial to normal brain function. The development of the visual system, for example, relies on waves of spontaneous spiking activity that sweep across the retina, LGN and visual cortex in order to synchronize nearby cells to fire and group together (Huberman et al., 2008). Furthermore, Hebbian forms of synaptic plasticity like LTP and LTD are complimented by several forms of homeostatic plasticity, which ensure that the underlying circuits that drive behavior remain stable yet flexible (Turrigiano, 2012). The importance of higher-order plasticity is underscored by the fact that changes in normal activity patterns cause circuit-level alterations that can lead, for example, to intellectual disorders like Autism spectrum disorders and Fragile X syndrome (Goncalves et al., 2013).

The tools mentioned in this Introduction make it now feasible to study individual neurons more closely and investigate how their activity relates to other cells within a circuit. A common approach in studying activity-dependent competition is to alter the neuronal activity of a single cell or a sparse population of cells and observe the effect of an increased or decreased ability to compete in a wildtype environment. Previously, the effects of activity-dependent competition on dendritic and axonal arbors have been studied in the *Xenopus* and zebrafish visual systems as well as in mammalian hippocampal cell cultures and in the mouse olfactory system (Burrone et al., 2002, Ruthazer et al., 2003, Yu et al., 2004, Hua et al., 2005). The techniques used in these studies, however, are not broadly applicable to other structures in the mammalian brain. The hippocampus and cortex, for example, are of particular interest in the study of excitatory neurotransmission at dendritic spines.

In this thesis we aimed to develop two transgenic models that allow long-term inhibition of neuronal activity in a small subset of pyramidal cells; overexpression of the inward rectifying potassium channel Kir2.1 and expression of the tetanus toxin light chain (described in Chapter 3). We also apply the TetoxLC approach to study dendritic morphology in response to neuronal silencing in a small population of pyramidal CA1 cells (Chapter 5). The results from extreme manipulations such as these give insight into how normal circuit function may lead to disease and/or how these diseases might progress.

Chapter 2 Efficient inducible Pan-neuronal Cre-mediated recombination in SLICK-H transgenic mice

2.1 Abstract

Large-scale functional genomics in mice is becoming feasible through projects to develop conditional knockout alleles for every gene. Inducible neuron-specific gene knockout in such mice will permit the analysis of neuronal phenotypes while circumventing developmental defects or embryonic lethality. Here we describe a transgenic line, termed SLICK-H, that facilitates widespread inducible conditional genetic manipulation within most populations of projection neurons. In SLICK-H mice, the Thy1 promoter drives robust and relatively uniform expression of a drug-inducible form of Cre recombinase throughout the peripheral and central nervous system. This permits efficient induction of Cre-mediated genetic manipulation upon tamoxifen administration in adult mice. Importantly, Cre activity in the absence of tamoxifen is minimal, permitting tight control of recombination. In the present study, we catalog in detail the transgene expression patterns and recombination efficiencies in SLICK-H mice. Our results highlight the utility of SLICK-H mice for functional genomics in the nervous system.

2.2 Results

2.2.1 Background

The utility of the Cre recombinase system is such that large scale projects are currently underway to generate Cre/*Lox*P-compatible conditional knockout alleles of almost every mouse gene (http://www.knockoutmouse.org/). In concert with these efforts, improved ''Cre driver'' lines are being developed to facilitate gene knockout in any tissue or cell-type of interest. The temporal control afforded by the ligand-inducible CreER^{T2} recombinase is especially desirable, but the generation of such lines with optimal expression patterns and efficient induction of Cre activity is not trivial. The expression patterns of an endogenous promoter can be hard to reproduce in a transgenic construct either because some promoter elements are missing or due to positional effects upon insertion of the transgene into the genome. Achieving appropriate expression levels of CreER^{T2} is also crucial. Weak promoters may yield inefficient recombination, while strong promoters that drive very high levels of transgene expression will result in ''leaky'' recombination in the absence of tamoxifen administration. The efficient application of CreER^{T2} technology in the central nervous system, though highly desirable, is particularly challenging due to the diversity of cell types and complex anatomy of the brain.

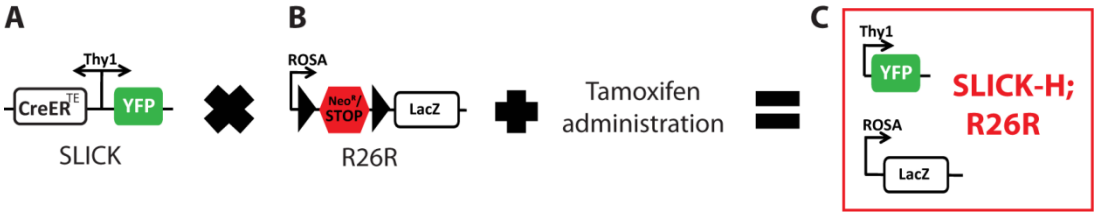

Figure 2.1 - Strategy for conditional transgenic co-expression of SLICK and ROSA26
(A) Schematic representation of the SLICK transgene. Two back-to-back copies of the Thy1 promoter drive expression of YFP and CreER^{T2}. (B) Schematic representation of R26R reporter strain used to assess Cre-mediated recombination. A neomycin resistance gene and transcriptional stop sequence are removed upon Cre-mediated recombination to allow expression of the LacZ reporter gene coding for β-galactosidase. The black triangles represent loxP sites. From Heimer-McGinn and Young (2011)

A recently developed a technique termed SLICK (single-neuron labeling with inducible Cre-mediated knockout) allows for inducible genetic manipulation of fluorescently labeled, single neurons in mice (Young et al., 2008). This is achieved by using two copies of the Thy1.2 promoter cassette to coexpress CreER^{T2} and yellow fluorescent protein (YFP) within the same small subsets of neurons (Fig 2.1*A*). The Thy1.2 promoter has been widely used to drive robust transgene expression in projection neurons and was the first promoter to yield bright labeling of neurons in mice through expression of fluorescent proteins (Caroni, 1997, Feng et al., 2000, Oddo et al., 2003). The primary objective in developing the SLICK method

was to identify transgenic lines that exhibit sparse labeling due to position-effect variegation, thus enabling high resolution imaging of single neurons (Young and Feng, 2004). In the process, however, many lines with broader transgene expression were also generated. These are not suitable for single neuron imaging purposes, but are valuable tools for wide-spread neuronal manipulation. In this chapter we describe one such line, called SLICK-H, which has expression properties that are optimal for efficient, inducible neuron-specific genetic manipulation in adult mice.

2.2.2 Transgene expression in adult SLICK-H mice

2.2.2.1 *Transgene expression pattern shown by YFP fluorescence*

We first set out to determine the patterns of SLICK transgene expression in the SLICK-H line. Examining YFP fluorescence in adult SLICK-H mice, we observed that transgene expression is widespread and relatively uniform in many brain regions (Fig 2.2*A*,*B*). Areas with extensive YFP labeling in cell somas include the visual, parietal, somatosensory, motor, insular, piriform and entorhinal cortical areas, the major hippocampal fields except CA2, the amygdala, the inferior and superior colliculi, many thalamic and brainstem nuclei, the anterior olfactory nucleus, granule and Purkinje cells of the cerebellum, and mitral cells in the olfactory bulb. Notable regions with dim or no YFP fluorescence in cell somas are the caudate-putamen, ventral striatum, hypothalamus, basal forebrain, and substantia nigra, although brightly labeled axons and nerve terminals are observed in some of these areas. SLICK-H also has strong YFP labeling in both sensory and motor neurons in the spinal cord, photoreceptors, and retinal ganglion cells in the retina and dorsal root ganglion (DRG) neurons (shown in Fig 2.7*D*).

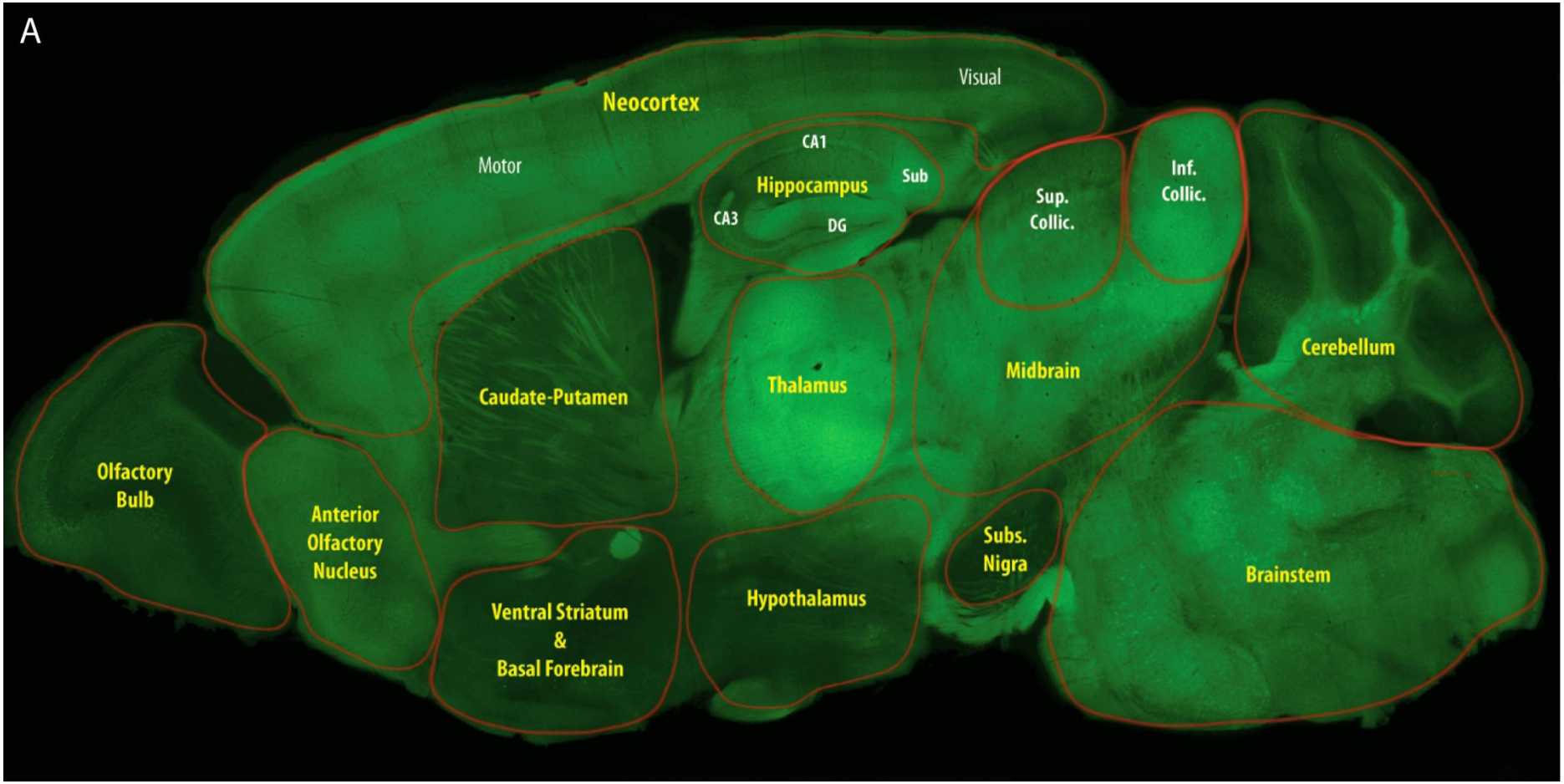
A
Neocortex
Visual
Motor
CA1
Hippocampus
Sub
CA3
DG
Sup.
Collic.
Inf.
Collic.
Cerebellum
Caudate-Putamen
Thalamus
Midbrain
Olfactory
Bulb
Anterior
Olfactory
Nucleus
Subs.
Nigra
Brainstem
Ventral Striatum
&
Basal Forebrain
Hypothalamus

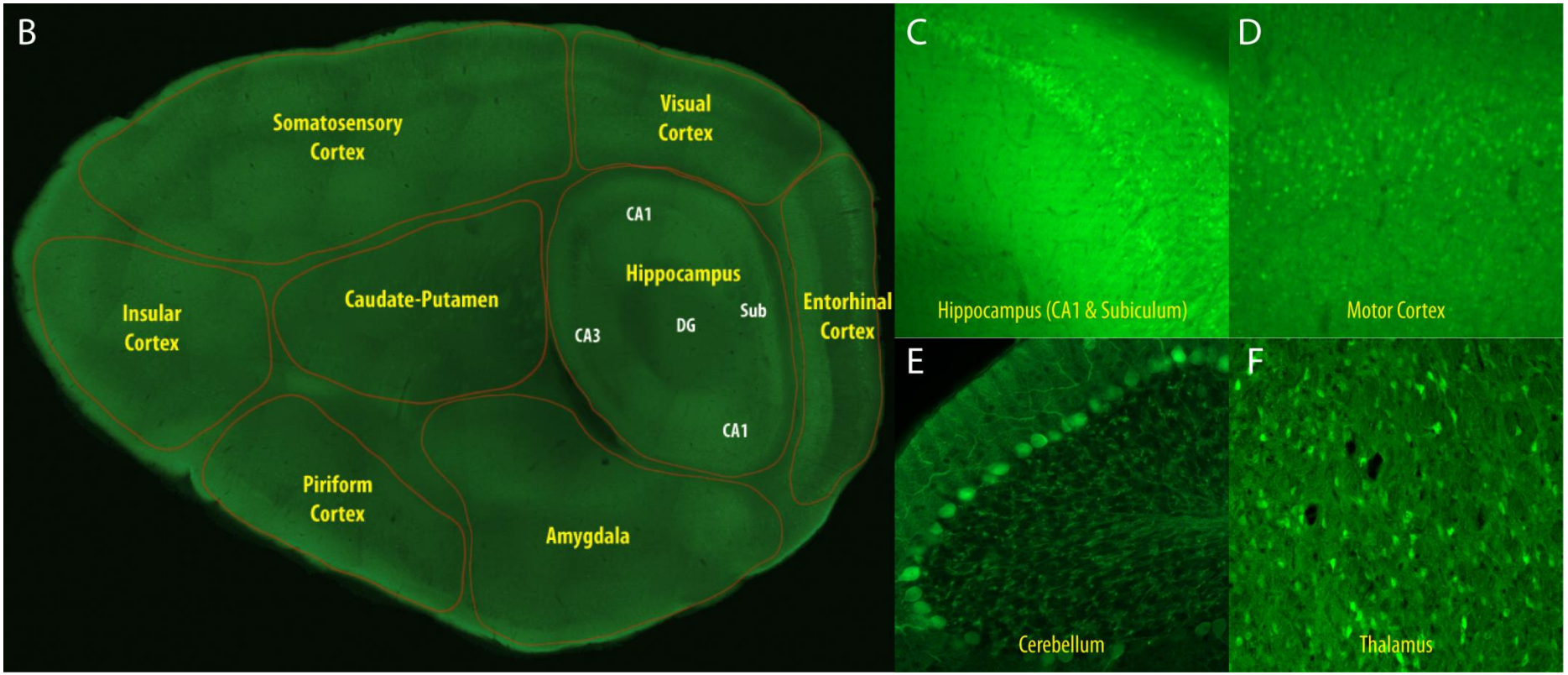

Figure 2.2 - Transgene expression in SLICK-H transgenic line.

Transgene expression as indicated by YFP labeling in a medial (A) and lateral (B) sagittal brain section from adult SLICK-H mice. Major anatomical brain regions are indicated. The CA1/subiculum (C), motor cortex (D), cerebellum (E), and thalamus (F) are shown at a magnification of 10X. FromHeimer-McGinn and Young (2011)

2.2.2.2 *Transgene expression is neuron-specific as shown by immunohistochemistry*

In order to ensure that transgene expression is restricted to neurons, we performed immunostaining using an α-GFAP antibody (Fig 2.3*A*) that recognizes GFAP (glial fibrillary acidic protein) and is commonly used as an astrocytic marker (Methods, Table 7.1). We also stained for an α-Olig2 antibody (Fig 2.3*B*) that recognizes Olig2 (oligodendrocyte transcription factor 2) and is commonly used as a marker for oligodendrocytes (Methods, Table 7.1). We carefully examined all brain regions and determined that YFP fluorescence or β-gal staining (described in section 2.2.3.1) does not colocalize with either glial cell-type in any brain region. We also carefully examined non-neuronal tissue for the presence of YFP fluorescence. Similarly, we observed no SLICK expression in these tissues (Fig 2.3*C-F*). SLICK--H therefore appears to be expressed specifically in neuronal populations of only the central and peripheral nervous systems.

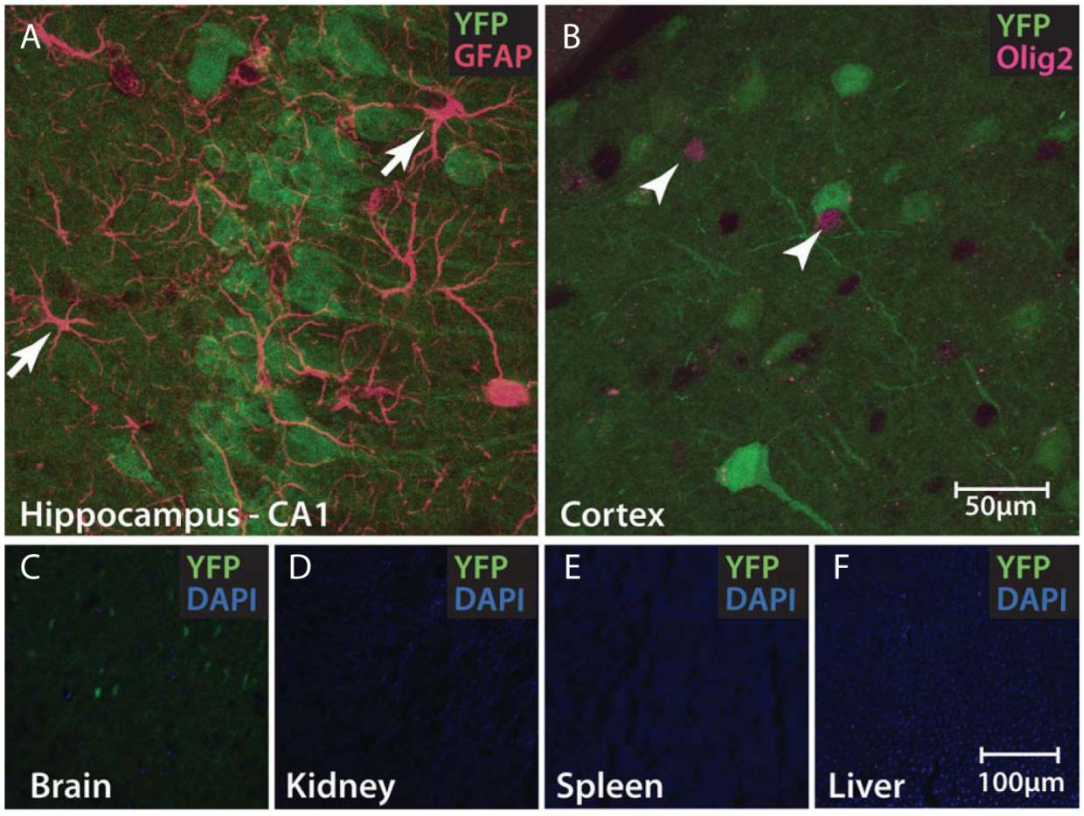

Figure 2.3 - Neuron-specific transgene expression in SLICK-H mice.
(A,B) YFP fluorescence (green) in brain sections from SLICK-H mice that were co-stained for the astrocyte marker GFAP (A; red) or the oligodendrocyte marker Olig2 (B; red). No YFP fluorescence is observed in either astrocytes (arrows) or oligodendrocytes (arrowheads). (C-F) YFP fluorescence (green) imaged in various tissues from SLICK-H mice. No YFP fluorescence is observed in non-neural tissues. Fom Heimer-McGinn and Young (2011)

2.2.3 Induction of Cre-mediated recombination in SLICK-H;ROSA26 mice

2.2.3.1 *Recombination pattern shown by X-gal staining*

To examine the full extent and efficiency of recombination afforded by the SLICK-H Cre-recombinase system, we crossed SLICK-H mice to the ROSA26 (R26R) Cre-reporter line that expresses β-galactosidase (β-gal) upon Cre activation (Soriano, 1999). β-gal cleaves the organic compound X-gal (5-bromo-4-chloro-indolyl-β-galactopyranoside) and results in an insoluble blue stain that is clearly visible under bright field microscopy (Kiernan, 2007). Double heterozygous mice for SLICK-H and R26R were treated with tamoxifen for ten days by oral gavage, rested for two weeks and then taken for analysis. Sections were stained for X-gal in order to detect the presence of β-gal and compared to age-matched untreated SLICK-H;R26R controls. We observed prevalent and efficient induction of reporter gene expression in the brain, retina, spinal cord, and DRG of tamoxifen-treated mice (Fig 2.4*A*). The recombination pattern in SLICK-H;R26R reflects the transgene expression pattern displayed by YFP fluorescence. Moreover, recombination in the absence of tamoxifen induction is minimal and occurs in less than 1% of cells in most brain regions (Fig 2.4*B*, Table2.2).

2.2.3.2 *Quantification of recombination efficiency measured by LacZ immunostaining*

To quantify the recombination efficiency in tamoxifen-induced SLICK-H;R26R mice we performed immunostaining for the β-gal reporter using the rabbit polyclonal antibody α-LacZ, a gift from Dr. Joshua Sanes at Harvard University (Methods, Table 7.2). We compared β-gal staining to the neuronal marker NeuN (Methods, Table 7.1) to calculate the percent of total neurons that expresses the reporter gene (Fig 2.5*A*-*D*, Table 2.1). We did not calculate β-gal abundance compared to SLICK transgene expression because YFP labeling is so ubiquitous that proper demarcation of cells is difficult to observe. We did, however, compare β-gal staining to YFP in some regions where α-NeuN was problematic (Fig 2.5*E*). Quantification was performed for the hippocampus (CA1, CA3, dentate gyrus and subiculum), the cortex (motor, visual, somatosensory and entorhinal), the cerebellum, amygdala, olfactory bulb, thalamus, superior and inferior colliculi, brainstem and spinal cord (Table 2.1).

Recombination efficiencies of 90% or more of NeuN positive cells were achieved in many regions including the hippocampus, thalamus, brainstem, superior and inferior colliculi, and

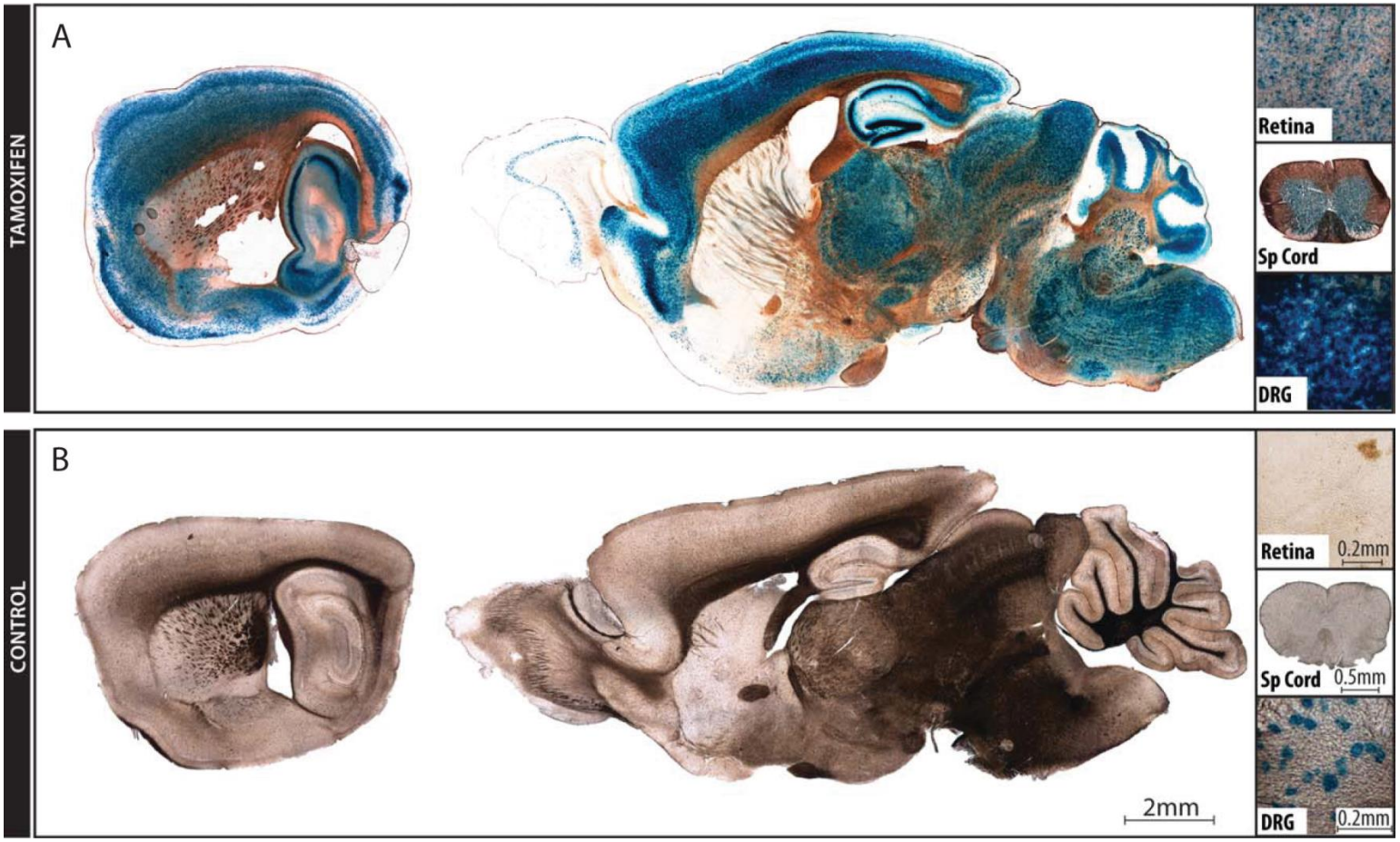

Figure 2.4 - Induction of Cre-mediated recombination in the central and peripheral nervous system of SLICK-H mice
Cre-mediated recombination in tamoxifen treated (a) or untreated control (b) SLICK-H/R26R mice was assessed by X-gal staining. Recombination with minimal leaky recombinase activity can be seen in both lateral and medial sagittal brain sections. Recombination is observed in most brain regions with some exceptions, such as the striatum. Likewise, efficient induction of Cre activity can be seen in the retina, spinal cord, and dorsal root ganglia (DRG) with just a small amount of leaky recombination in the DRG of control animals.

various neocortical regions (Table 2.1). Since some β-gal$^-$ cells are probably NeuN$^+$ interneurons, the actual efficiency in projection neurons probably approaches 100% in these areas. A few neuronal populations in SLICK-H mice, such as Purkinje cells of the cerebellum and mitral cells of the olfactory bulb show low recombination efficiency. Pyramidal cells of the visual cortex and motor and sensory neurons of the spinal cord also display lower levels of recombination compared to other areas. These cells exhibit bright YFP fluorescence and presumably co-express high levels of CreER^{T2}, so the reasons for inefficient recombination are not apparent.

Neuronal Population	Recombination efficiency	
Adult Mice		
Hippocampus		
CA1 - pyramidal cells	92%	(n=122)
CA3 - pyramidal cells	93%	(n=67)
Subiculum - pyramidal cells	99%	(n=82)
Dentate gyrus - granule cells	95%	(n=401)
Neocortex		
Motor cortex - layers II, III & V	92%	(n=61)
Sensory cortex - layers II, III & V	97%	(n=78)
Visual cortex - layers II, III & V	71%	(n=138)
Entorhinal cortex	94%	(n=121)
Cerebellum - purkinje cells	35%	(n=57)
Amygdala - basal nucleaus	83%	(n=97)
Olfactory bulb - mitral cells	77%	(n=31)
Thalamus	89%	(n=79)
Superior Colliculus	90%	(n=124)
Inferior Colliculus	88%	(n=141)
Brain Stem	97%	(n=67)
Spinal Cord	77%	(n=123)
Two-week-old mice		
Hippocampus (CA1 and subiculum)	59%	(n=218)
Somatosensory Cortex	51%	(n=367)

Table 2.1 – Quantification of Recombination Efficiency in SLICK-H Mice

Recombination efficiencies were calculated by quantification of the number of β-gal$^+$ cells relative to either NeuN$^+$ or YFP$^+$ cells using immunostained images as shown in Figure 2.5. Data are derived from multiple brain sections from at least two tamoxifen-treated SLICK-H;R26R mice. n = number of cells counted.

Neuronal Population	Recombination rate	
Neocortex (All areas)	0.3%	(n>3x104)
Hippocampus:		
CA1 - pyramidal cells	0.0%	(n= 806)
CA3 - pyramidal cells	0.7%	(n= 301)
Subiculum - pyramidal cells	3.5%	(n= 400)
Dentate gyrus - granule cells	3.0%	(n>1000)
Thalamus	1.3%	(n>1000)
Inferior Colliculus	0.4%	(n>2000)
Superior Colliculus	0.5%	(n>4000)
Cerebellum – Purkinje cells	0.0%	(n>100)
Brain Stem	1.0%	(n>9000)
DRG	0.5%	(n=211)

Table 2.2 – Quantification of leaky recombination in SLICK-H mice

Leaky recombination per area was calculated by counting the number of β-gal$^+$ cells in un-treated SLICK-H;R26R mice. This number was compared to the total of NeuN$^+$ cells in immuno-stained sections. Data are derived from multiple brain sections from at least two untreated SLICK-H;R26R mice. n = number of cells counted.

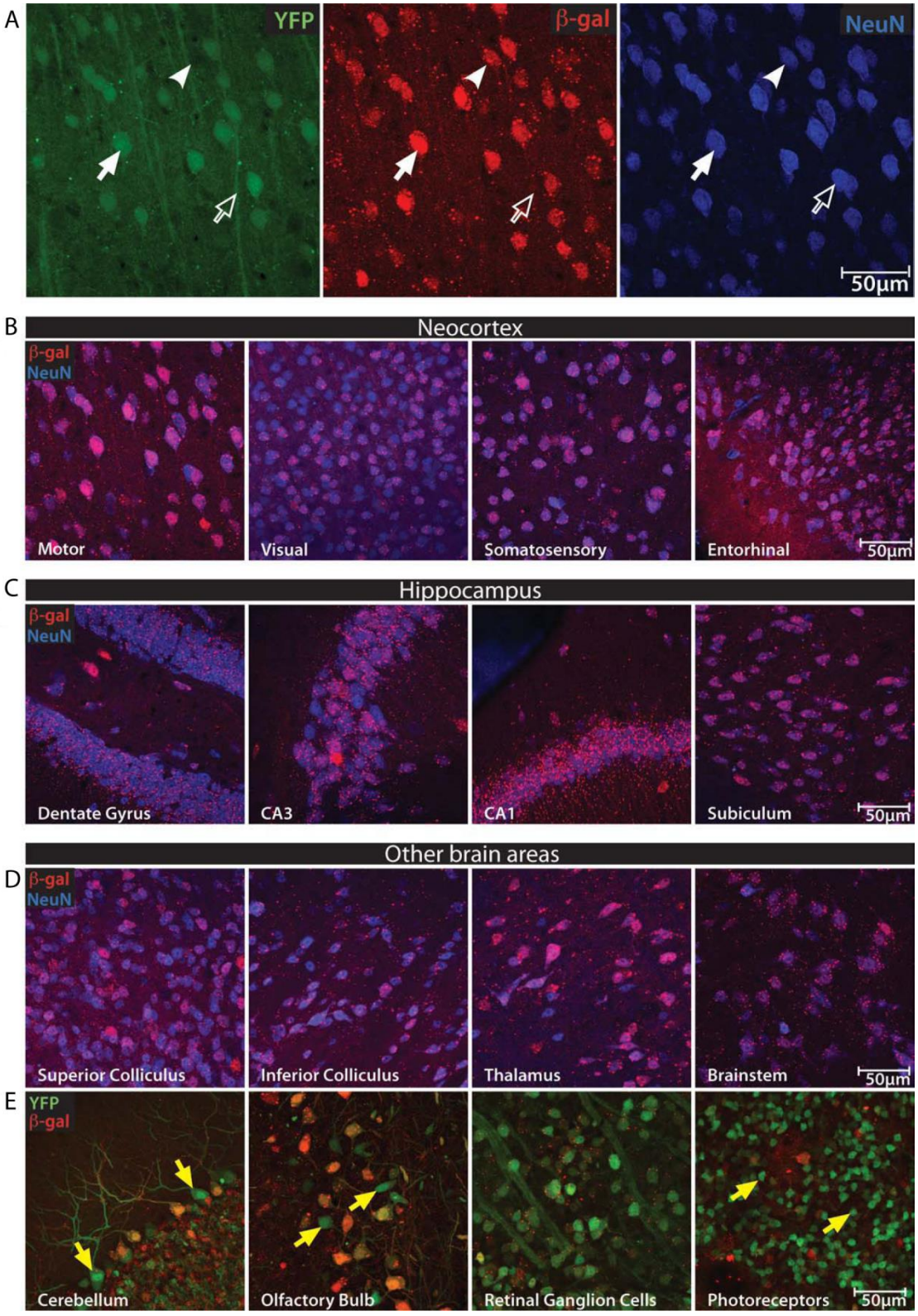

Figure 2.5 - Efficient tamoxifen-inducible recombination in many neuronal populations in SLICK-H mice. The efficiency of Cre-mediated recombination was assessed by immunofluorescent staining and confocal microscopy. Brain sections from tamoxifen-treated SLICK-H;R26R were costained for the neuronal marker NeuN (blue) and the Cre reporter β-galactosidase (β-gal; red). YFP fluorescence is shown in green. Colocalization of the punctate β-gal staining within NeuN or YFP-positive cell bodies was used to quantify recombination efficiencies. (A) Individual fluorescence channels are shown for the motor cortex for illustrative purposes. Most cells are YFP^+, $NeuN^+$, $\beta\text{-gal}^+$ (solid arrow), though

there are some YFP$^-$, NeuN$^+$, β-gal$^+$ cells in which recombination has occurred but YFP is absent or below the limit of detection (arrowhead). There are also a few NeuN$^+$, β-gal$^-$ cells that are YFP$^-$ and may represent NeuN$^+$ interneurons (open arrow). (B-D) Two-color merged images for NeuN and β-gal are shown for the indicated brain regions, with NeuN$^+$, β-gal$^+$ cells appearing pink, or blue with pink puncta. In most of these regions, 90% or more of NeuN$^+$ neurons are β-gal$^+$ positive. (E) In neuronal populations that are not stained by NeuN, recombination was assessed relative to YFP$^+$ cells. In cerebellar Purkinje cells, mitral cells of the olfactory bulb and especially photoreceptor cells in the retina, recombination efficiency is poor and there is a significant proportion of YFP$^+$, β-gal$^-$ cells (arrows in E). Supplemental high-resolution images of the individual fluorescence channels and two-color merges are provided for all neuronal populations in Figure 2.7.

2.2.4 Comparison of SLICK-H and SLICK-A lines

In order to emphasize the usefulness of the SLICK-H line as a tool for pan-neuronal Cre-dependent manipulations, we compared it to another SLICK line called SLICK-A. The SLICK-H and SLICK-A lines both show strong YFP labeling in projection neurons across many brain regions as expected for the Thy1.2 promoter (Fig 2.6*A,D*). YFP fluorescence is brighter in SLICK-A but is less uniform, with very bright labeling in some hippocampal regions and in cortical layer V. However, in other regions, such as the cerebellum, midbrain and brainstem, labeling is sparse and dim (Fig 2.6*D*). In comparison to SLICK-A, YFP fluorescence in SLICK-H is moderately bright but there is a much more widespread and uniform pattern of transgene expression (Fig 2.6*A*).

To examine the utility of these two lines for widespread neuron-specific induction of recombination, they were crossed to the R26R reporter line and assayed using X-gal staining for β-gal. Tamoxifen-treated SLICK-H;R26R and similarly treated SLICK-A;R262R mice were compared to their respective untreated controls. X-gal staining revealed that SLICK-A;R26R mice exhibit somewhat restricted reporter gene expression after induction compared to SLICK-H;R26R, with notably inefficient recombination in hippocampal CA3 region and cortical layers 2 and 3 (Fig 2.6*F*). Moreover, they exhibit significant recombination in the absence of tamoxifen induction, with leaky recombination being most prominent in areas that have bright YFP labeling such as hippocampal CA1 region and cortical layer V (Fig 2.6*E*). This suggests that YFP and CreER^{T2} expression levels are tightly coupled and that excessive levels of CreER^{T2} must be avoided to achieve tight control of recombinase activity. This is contrast to the SLICK-H line, which shows efficient induction of reporter gene expression upon tamoxifen administration (Fig 2.6*C*) with minimal leaky Cre activity upon induction (Fig 2.6*B*). SLICK-H thus appears to have an optimal level of CreER^{T2} expression.

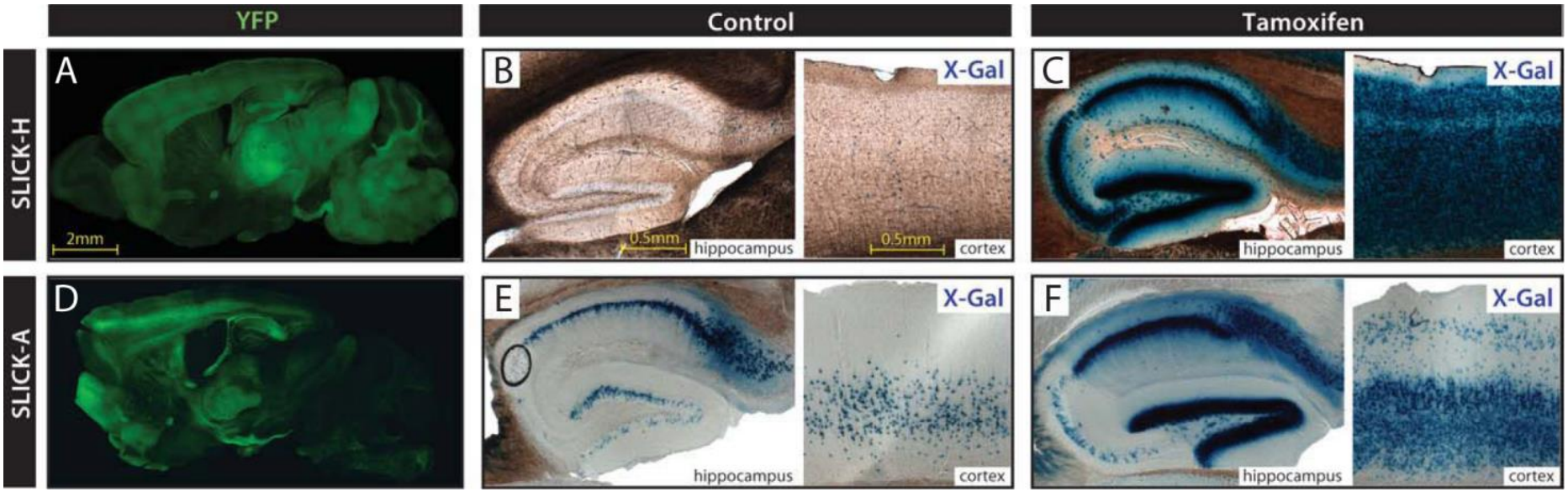

Figure 2.6 – Comparison of transgene expression and induction of recombination in two SLICK transgenic lines.

(A, D) YFP labeling in sagittal brain sections from SLICK-H and SLICK-A mice. Widespread fluorescence is seen in both lines with the hippocampus and neocortex being especially bright in SLICK-A. (B, C, E, F) Recombination assessed by X-gal staining of the hippocampus and neocortex from SLICK-H;R26R (B, C) and SLICK-A/R26R (E, F) mice. Efficient recombination upon tamoxifen treatment is seen in both lines (C, F), but significant recombination in untreated control animals is observed for the SLICK-A line (E). From Heimer-McGinn and Young (2011)

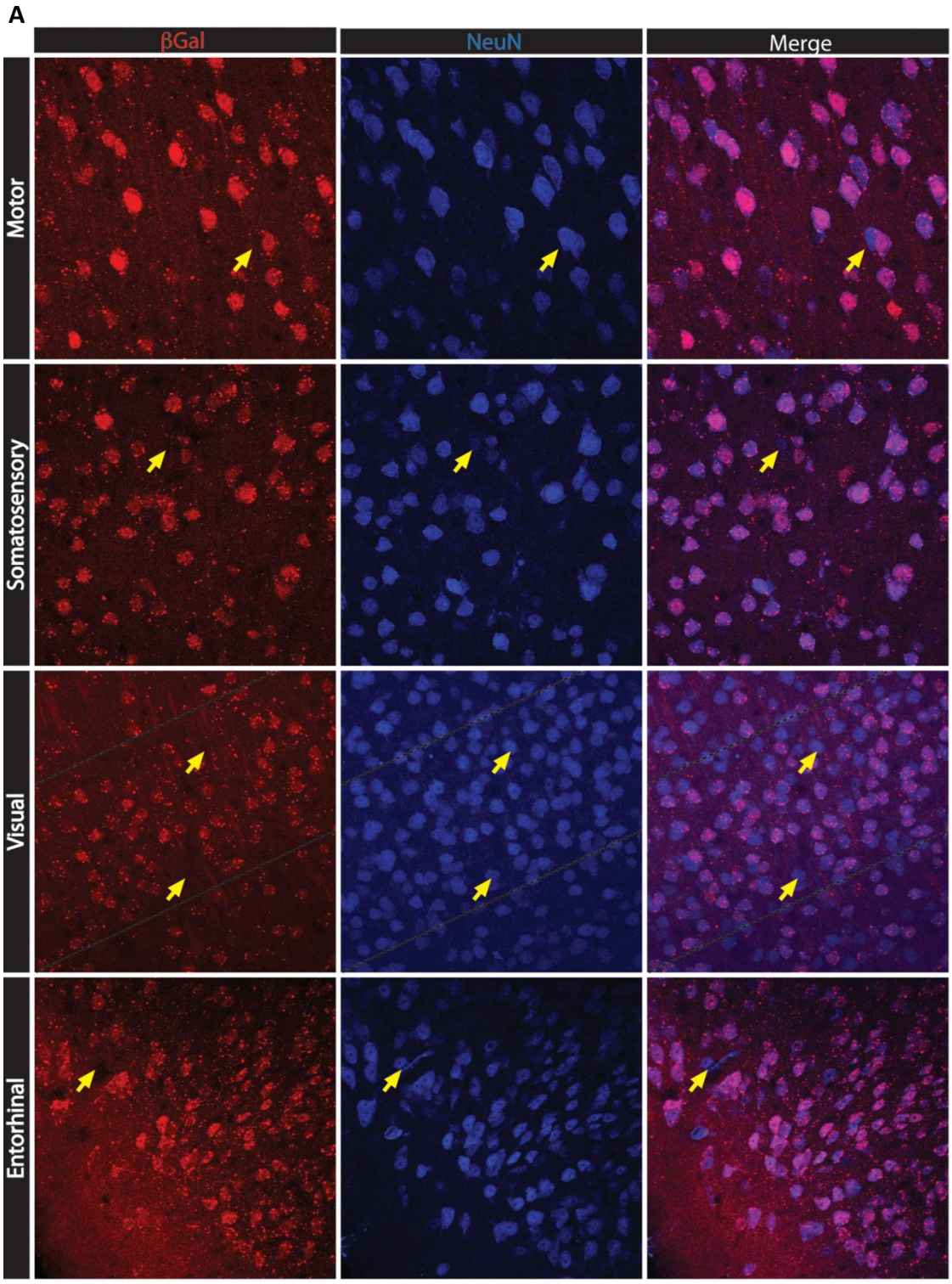

Figure 2.7 *A* – Efficient tamoxifen-inducible recombination in many neuronal populations in SLICK-H mice, Supplement to Figure 2.5. The efficiency of Cre-mediated recombination in the indicated brain regions was assessed by immunofluorescent staining and confocal microscopy. Individual channels for β-gal (red) and NeuN (blue) and two-color merges are shown for several cortical areas (motor, somatosensory, visual and entorhinal cortices). To demonstrate that β-gal staining is specific, β-gal negative cells are highlighted by yellow arrows.

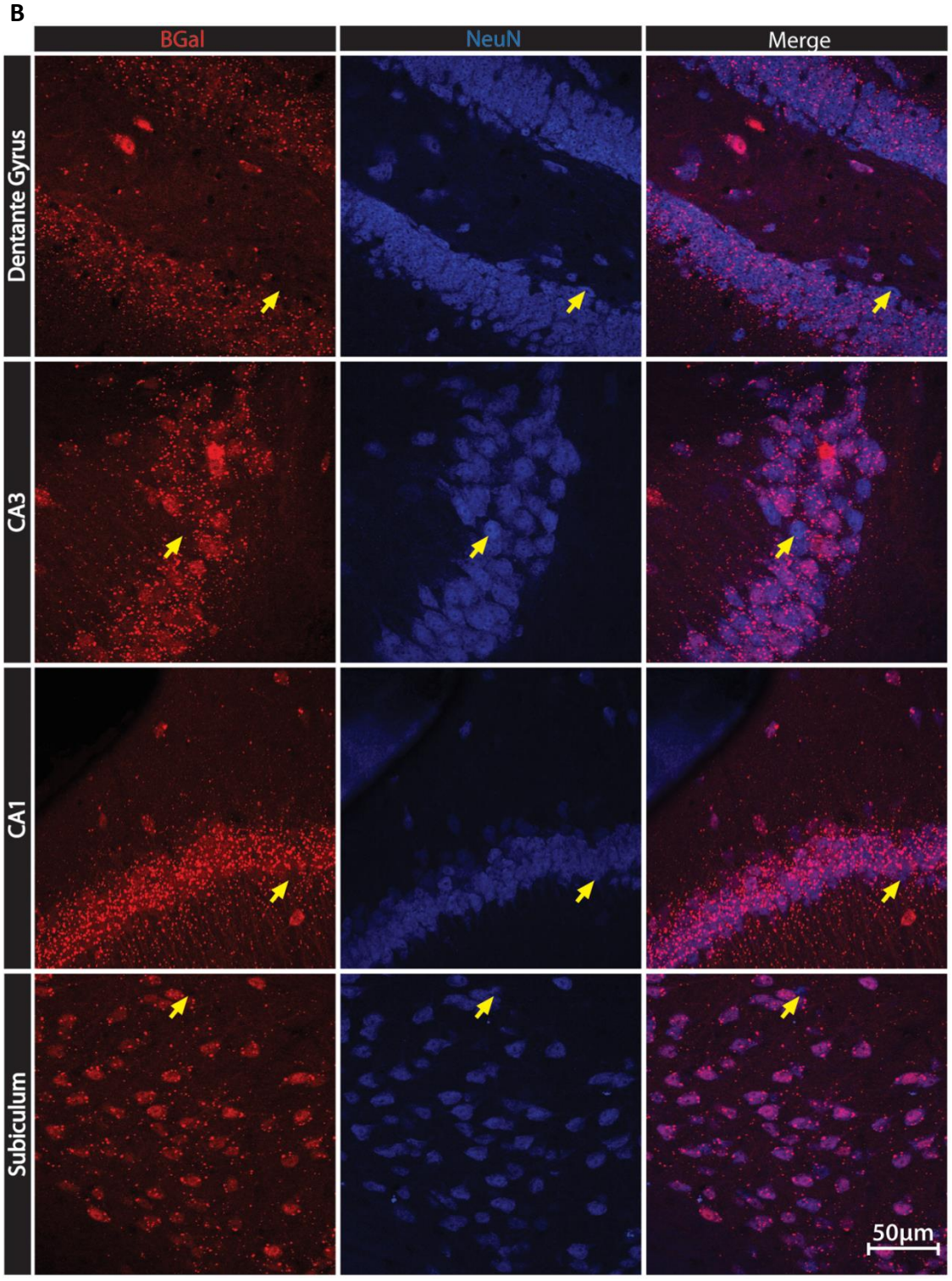

Figure 2.7 *B* – Efficient tamoxifen-inducible recombination in many neuronal populations in SLICK-H mice, Supplement to Figure 2.5. The efficiency of Cre-mediated recombination in the indicated brain regions was assessed by immunofluorescent staining and confocal microscopy. Individual channels for β-gal (red) and NeuN (blue) and two-color merges are shown for several hippocampal areas (dentate gyrus, CA3, CA1 and subiculum). To demonstrate that β-gal staining is specific, β-gal negative cells are highlighted by yellow arrows.

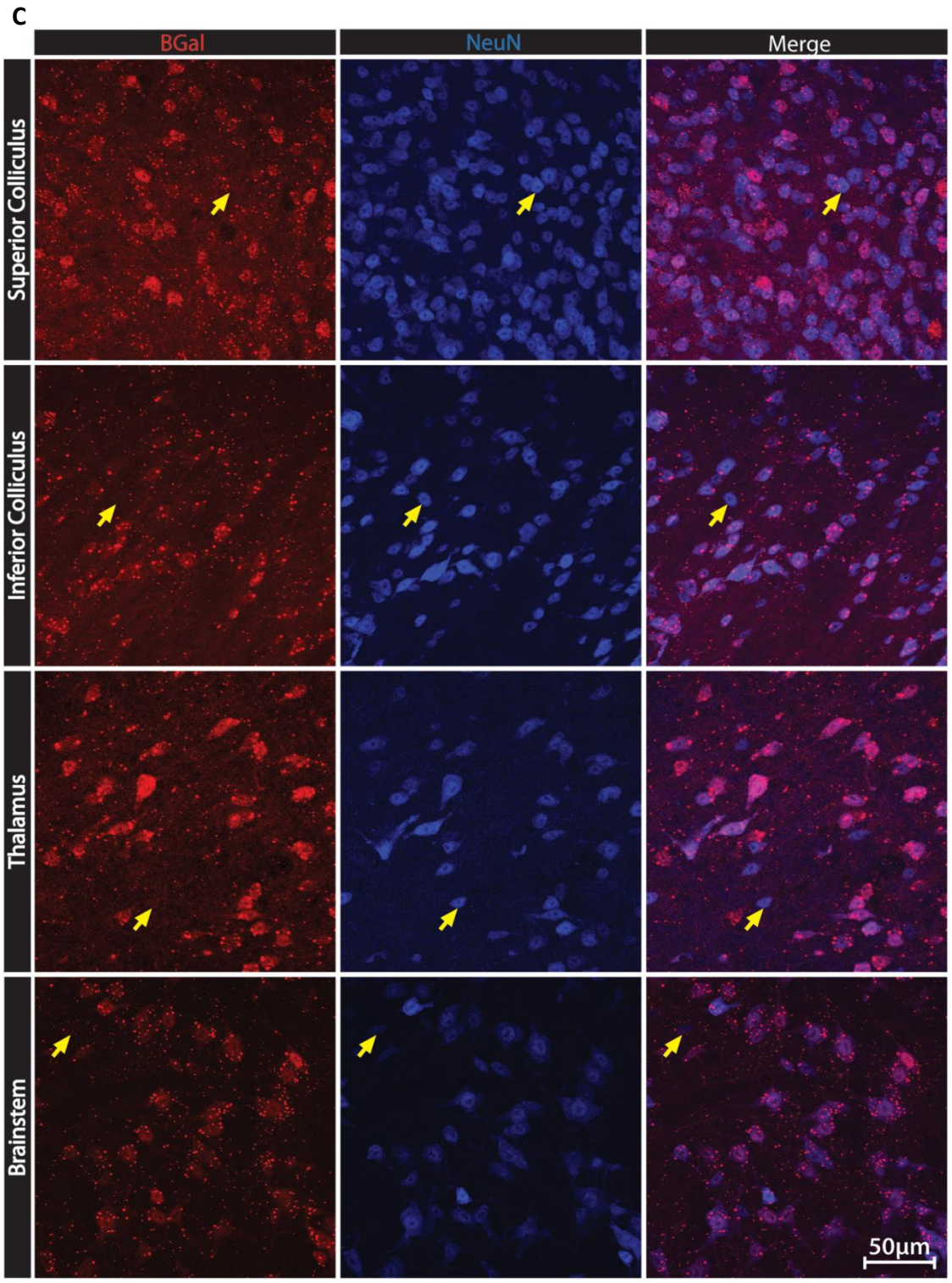

Figure 2.7 *C* – Efficient tamoxifen-inducible recombination in many neuronal populations in SLICK-H mice, Supplement to Figure 2.5. The efficiency of Cre-mediated recombination in the indicated brain regions was assessed by immunofluorescent staining and confocal microscopy. Individual channels for β-gal (red) and NeuN (blue) and two-color merges are shown for the superior and inferior colliculi, thalamus and brain stem. To demonstrate that β-gal staining is specific, β-gal negative cells are highlighted by yellow arrows.

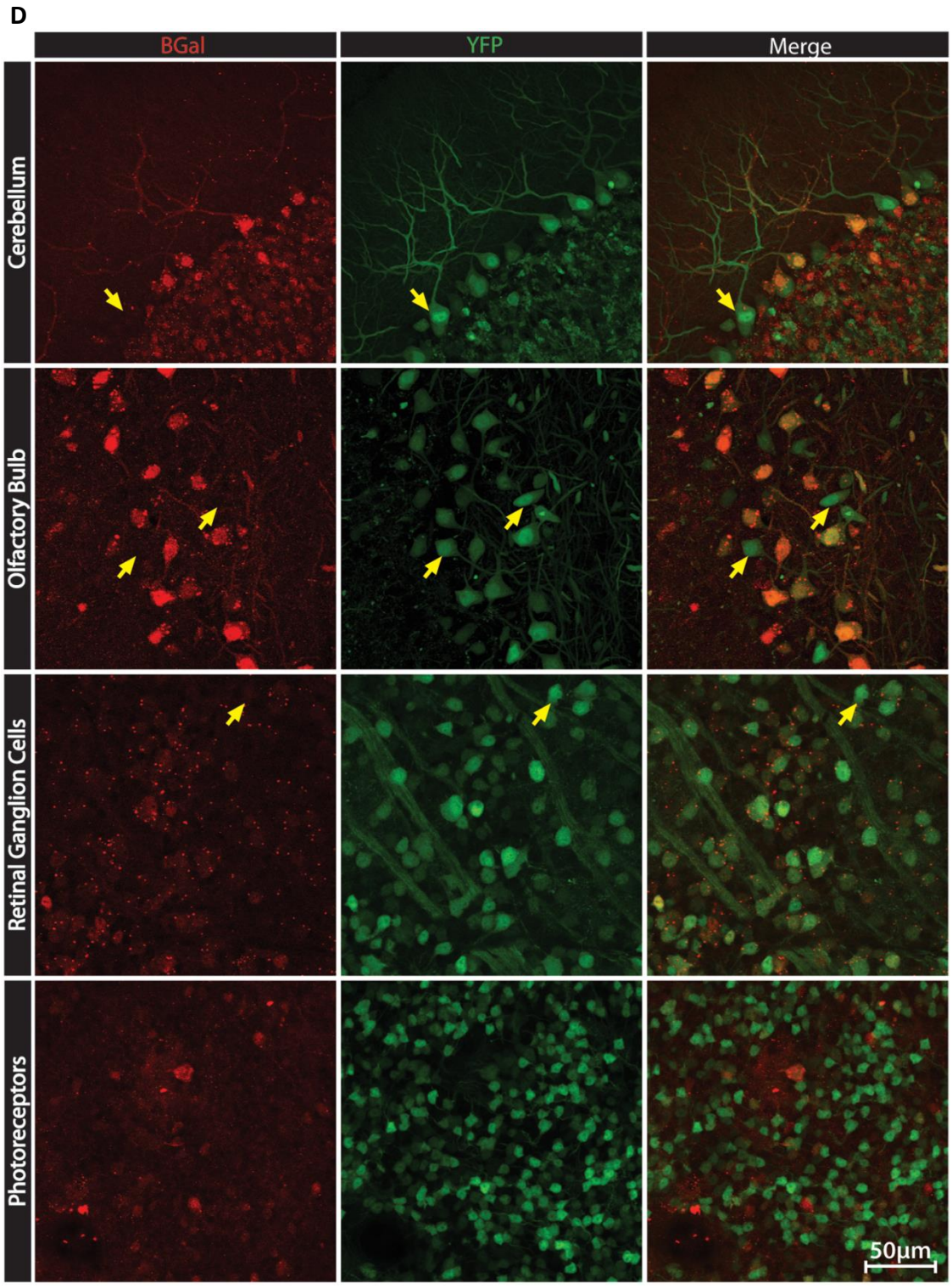

Figure 2.7 *D* – Efficient tamoxifen-inducible recombination in many neuronal populations in SLICK-H mice, Supplement to Figure 2.5. The efficiency of Cre-mediated recombination in the indicated brain regions was assessed by immunofluorescent staining and confocal microscopy. Individual channels for β-gal (red) and NeuN (blue) and two-color merges are shown for the cerebellum, olfactory bulb, retinal ganglion cells and photoreceptors. To demonstrate that β-gal staining is specific, β-gal negative cells are highlighted by yellow arrows.

2.2.5 Characterization of two-week-old SLICK-H mice

To further characterize the SLICK-H line, we examined transgene expression and recombination efficiencies in two-week-old mice. At embryonic and early developmental stages, transgene expression in SLICK-H is limited due to the late onset of Thy1 promoter activity (Caroni, 1997). Although not as widespread and intense as in adult mice (Fig 2.2), significant YFP fluorescence is observed in young mice (Fig 2.8).

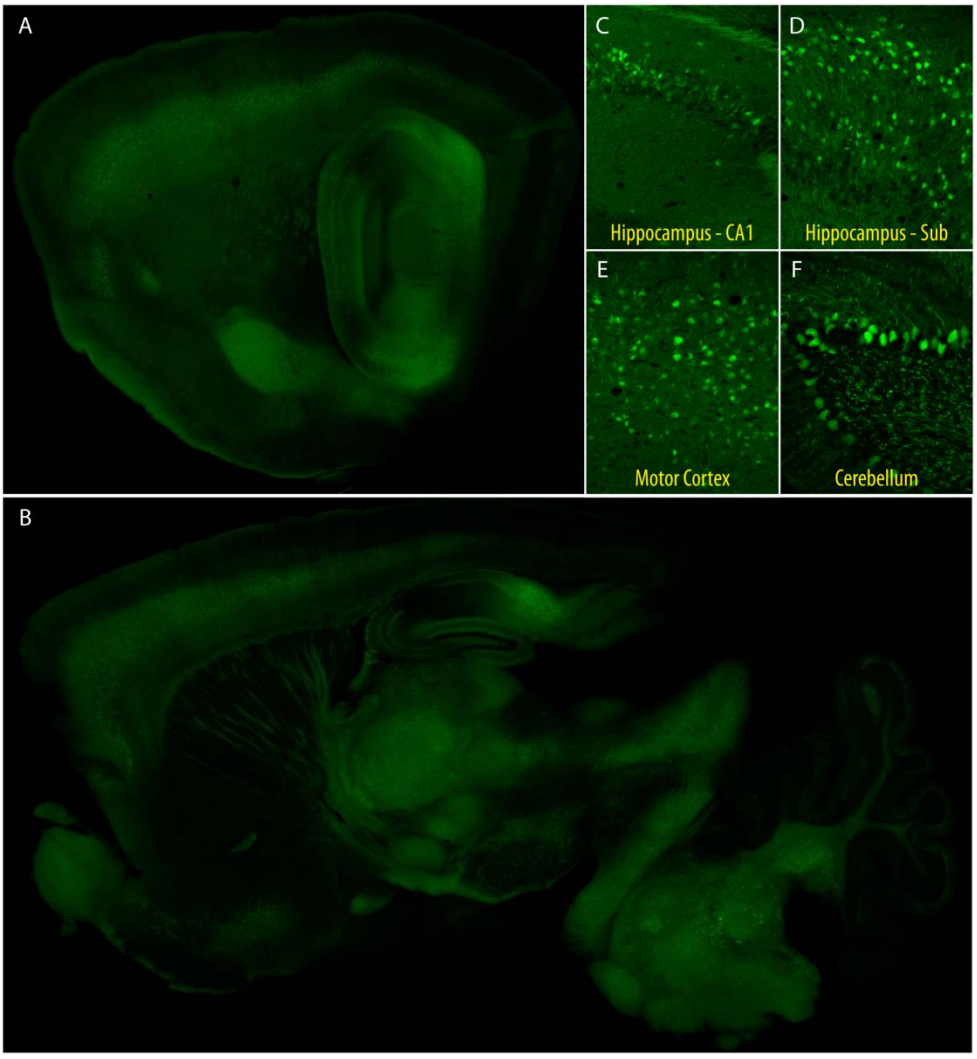

Figure 2.8 - Transgene expression in young SLICK-H transgenic line. Transgene expression as indicated by YFP labeling in a medial (A) and lateral (B) sagittal brain section from young SLICK-H mice. The CA1 (C), subiculum (D), motor cortex (E), and cerebellum (F) are shown at a magnification of 10X.

To assess recombination pattern and efficiencies in young SLICK-H mice, 2-week-old SLICK-H;R26R pups were treated with tamoxifen and then assayed by X-gal staining. Tight control of recombination in the absence of tamoxifen is observed in these younger mice (Fig 2.9). Recombination efficiencies were calculated by comparing β-gal staining to YFP labeling,

which in these younger mice provides a more clear definition of cell bodies (Fig 2.8, C-F). Recombination efficiencies in two-week-old mice that were administered tamoxifen for two days via intraperitoneal injection ranged from 50%-60% (Table 2.1). Mice of this age do not respond well to oral gavage, so tamoxifen delivery was performed either directly by intraperitoneal injection or indirectly by oral gavaging the nursing mother. Indirect delivery through nursing produced some activation of CreER^{T2} but to a much lesser extent than direct intraperitoneal delivery.

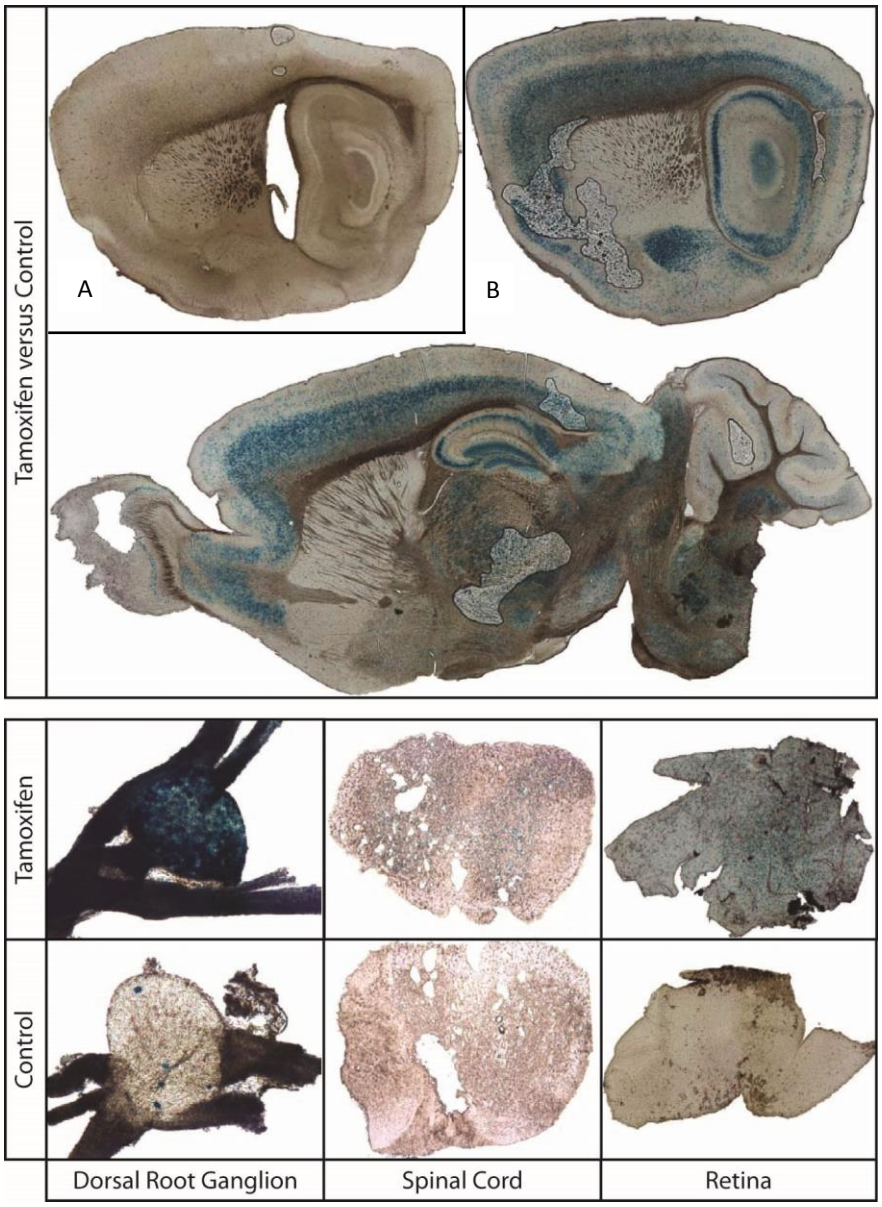

Figure 2.9 - Induction of Cre-mediated recombination in the central and peripheral nervous system of young SLICK-H mice. Cre-mediated recombination in (A) tamoxifen treated or (B) untreated control SLICK-H/R26R mice was assessed by X-gal staining. Recombination with minimal leaky recombinase activity can be seen in both lateral and medial sagittal brain sections. Recombination is observed in most brain regions with some exceptions, such as the striatum. Likewise, efficient induction of Cre activity can be seen in the retina, spinal cord, and dorsal root ganglia (DRG) with just a small amount of leaky recombination in the DRG of control animals

2.3 Discussion

2.3.1 SLICK-H as a technique for pan-neuronal conditional transgenic expression

Our SLICK-A data demonstrate the challenges of generating transgenic lines that express CreER^{T2} and facilitate efficient Cre-mediated gene knockout. Achieving optimal levels of transgene expression is crucial. Robust expression is required for efficient recombination, but a strong promoter like Thy1.2 can produce excessive CreER^{T2} causing leaky recombinase activity as observed in the SLICK-A line. This is probably a consequence of overwhelming the cellular factors that sequester inactive CreER^{T2} in the cytoplasm. The SLICK-H line was 1 of 30 SLICK transgenic lines generated and was selected for further characterization on the basis of widespread and uniform transgene expression. This expression pattern permits efficient non-leaky recombination. The fusion of two copies of the estrogen receptor ligand binding domain to Cre-recombinase (ER^{T2}-Cre-ER^{T2}) has been reported to reduce leaky recombination associated with Cre-ER^{T2} in *in vivo* electroporation studies (Casanova et al., 2002, Matsuda and Cepko, 2007). Although ER^{T2}-Cre-ER^{T2} may be advantageous in this regard, our results indicate that Cre-ER^{T2} is adequate to achieve tight control of recombination, provided expression levels are not excessive. YFP labeling in SLICK-H is too dense for imaging of individual neurons. It does, however, highlight the cell populations and anatomic nuclei in which CreER^{T2}-mediated recombination should be achievable. Since transgene expression is not excessively high, we do not anticipate any cytotoxic effects of either YFP or CreER^{T2} expression. The only drawback of strong YFP fluorescence in SLICK-H is that it would mask GFP in loxP lines that use GFP either as a reporter or as a component of a fusion protein. The utility of SLICK-H in developmental studies is reduced due to the postnatal onset of Thy1-driven transgene expression and poor tolerance of repeated tamoxifen administration in these animals.

2.3.2 Alternatives to the SLICK-H technique or pan-neuronal conditional expression

2.3.2.1 *Methods using Thy1.2 variant of the Thy1 promoter*

The Thy1.2 variant of the Thy1 promoter has been widely used as a neuron-specific promoter in transgenic mice including various disease models (Caroni, 1997, Feng et al., 2000, Oddo et al., 2003). Several Thy1-Cre lines have been generated that exhibit neuronal Cre recombinase activity as expected (Campsall et al., 2002, Dewachter et al., 2002) (http://www.credrivermice.org/). However, at least two and perhaps all of these lines also

show recombination in non-neuronal tissues, most likely due to nonspecific promoter activity at early embryonic stages (Campsall et al., 2002) (http://cre.jax. org/Thy1/Thy1-cre.html). By using CreER^{T2} we avoid this problem since the recombinase is not active in the absence of tamoxifen, even if it is expressed at embryonic stages. Transgenic mice in which Thy1 drives expression of an inducible Cre-progesterone receptor fusion protein have been generated (Kellendonk et al., 1999). However, the pattern of recombination in this line would not appear to be as widespread or uniform as in SLICK-H. To our knowledge, no other Thy1-CreER^{T2} lines have been generated.

2.3.2.2 *Other promoters and techniques*

A variety of other promoters have been used for neuron-specific expression of CreER^{T2}, and several large-scale approaches have characterized neuronal promoters for this purpose (Gong et al., 2003, Madisen et al., 2010, Portales-Casamar et al., 2010) (2003; http:// www.credrivermice.org/). However, most of these lines have either a region-specific expression pattern or drive expression in neurons with a particular neurotransmitter phenotype and do not exhibit such widespread expression as SLICK-H. Pan-neuronal expression of CreER^{T2} has been achieved using a knock-in approach that targets the vesicle associate membrane protein 2 and neurofilament light chain loci (Rotolo et al., 2008). However, the goal in this study was to achieve low recombination efficiency and sparse neuronal labeling. The CaMKIIα promoter has also been used to drive expression of Cre-recombinase and other transgenes in projection neurons in a pattern that overlaps with Thy1 in the forebrain (Tsien et al., 1996). CaMKIIα-CreER^{T2} mice have also been generated; however, recombination in these mice is restricted to the forebrain and thus is not as broad as in SLICK-H (Erdmann et al., 2007, Madisen et al., 2010). The widespread expression and tight control of CreER^{T2} activity in SLICK-H thus offer significant advantages over currently available inducible Cre recombinase lines, and make the SLICK-H line highly suitable for functional genomic analysis of behavioral and other neuronal phenotypes in adult mice.

Chapter 3 Generating Cre-compatible mouse lines that conditionally inhibit neuronal connectivity

3.1 Results

Our aim in the work described in this chapter was to develop efficient and simple-to-use transgenic methods that would allow neuronal activity-dependent processes to be studied *in vivo* throughout the mammalian brain. The SLICK-V line of mice is well suited for this purpose as it expresses CreER^{T2} and YFP in a small subset of pyramidal neurons throughout the central and peripheral nervous systems (Fig 3.1*A*). YFP fluorescence is strong in these mice and Cre-mediated recombination occurs efficiently with tight temporal control of induction. In combination with a Cre/*lox*P-compatible line that inhibits neuronal function, this model could be used to suppress neuronal activity in a small subset of cells and then observe how these cells behave in a competitive, wildtype environment.

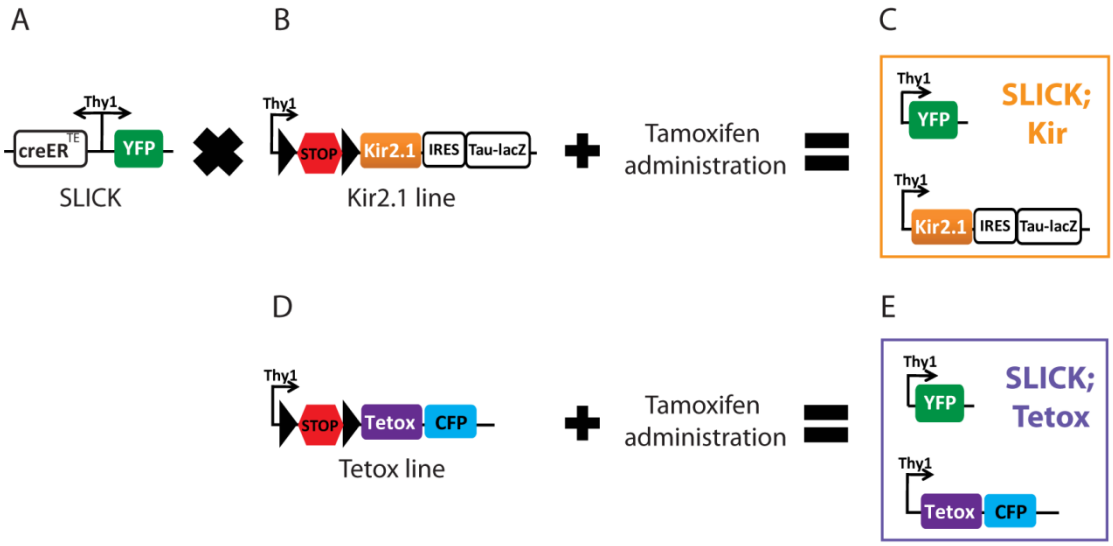

Figure 3.1 – Strategy for conditional transgenic co-expression of SLICK and either Kir2.1 potassium channel or tetanus toxin light chain, a schematic representation

(A) In SLICK mice, two copies of the Thy1 promoter drive expression of both YFP and CreER^{T2} in projection neurons. (B) In the Kir2.1 construct, the Thy1 promoter drives conditional expression of a floxed STOP cassette, Kir2.1, an IRES sequence and a TauLacZ reporter gene. (C) Double transgenic mice (SLICK;Kir) treated with the drug tamoxifen will coexpress YFP, Kir2.1 and TauLacZ in projection neurons. (D) In the TetoxLC line, the Thy1 promoter drives conditional expression of a floxed STOP sequence, TetoxLC, and CFP (E) Double transgenic animals treated with the drug tamoxifen will coexpress YFP, TetoxLC and CFP in projection neurons. Black triangles represent *lox*P sites.

The Kir2.1 transgenic construct (Fig 3.1*B*) includes a LacZ reporter that encodes for β-galactosidase, which cleaves the organic compound X-gal (5-bromo-4-chloro-indolyl-β-galactopyranoside) and results in an insoluble blue stain that is clearly visible using bright

field microscopy (Kiernan, 2007). Fusion to the protein tau localizes LacZ expression to axonal microtubules (Weingarten et al., 1975) and an upstream IRES sequence allows translation initiation of the TauLacZ reporter without requiring 5' cap recognition (Pelletier and Sonenberg, 1988). The TetoxLC construct (Fig 3.1*D*) includes a cyan fluorescent protein (CFP) reporter that is spectrally distinct from the SLICK-derived YFP. Both constructs are driven by the Thy1 neuronal promoter and include a floxed transcriptional STOP cassette to prevent transgene expression in the absence of Cre-mediated recombination. Administration of the drug tamoxifen to double transgenic mice induces CreER^{T2}-mediated recombination allowing the STOP cassette to be removed and the transgenic sequences to be expressed (Fig 3.1*C,E*). The inhibitory mechanisms of these two approaches are discussed below.

3.1.1 Cre recombinase-compatible transgenic mouse for the conditional expression of the Kir2.1 potassium channel in projection neurons

3.1.1.1 *Construction of a transgene for conditional expression of Kir2.1 under control of the Thy1 promoter*

We received a DNA plasmid from C. Ron Yu containing the Kir2.1 sequence followed by an internal ribosomal entry site (IRES) and a TauLacZ reporter gene (Yu et al., 2004). This Kir2.1-IRES-tauLacZ sequence was then cloned into a customized pBlueScriptII SK+ plasmid that includes the neuronal promoter Thy1 and a transcriptional STOP cassette flanked by two loxP sites in the same orientation (Fig 3.2*A*). This aspect of the work was done prior to my joining the project. Once I commenced my work I tested the construct by digesting it with the restriction enzyme HindIII, which produced DNA bands of the expected sizes (Fig 3.2*B*). We will henceforth refer to the Thy1-STOP-Kir2.1-IRES-tauLacZ transgene simply as Kir.

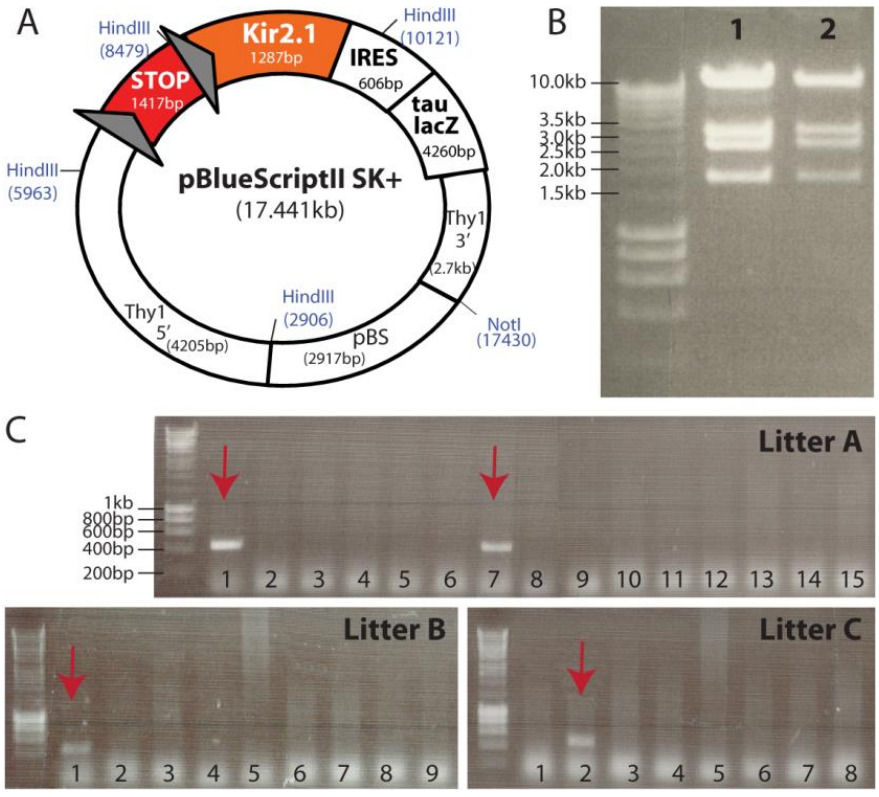

Figure 3.2 – Production of Cre recombinase-compatible transgenic mice for the conditional expression of Kir2.1 inward-rectifying potassium channel

(A) Schematic representation of the Kir2.1 DNA construct that we used to generate potential Kir transgenic mice. LoxP sites are shown as grey triangles and restriction enzymes used to linearize and verify the construct are shown in blue. The construct includes the pBlueScriptII-SK^{+} plasmid DNA and the Thy1 neuronal promoter sequence. (B) Restriction digest of the Kir construct by HindIII produces expected band sizes. Lanes 1 and 2 represent two clones of the same construct. (C) Genotyping PCR identified four founders produced by pronuclear microinjection of the Kir construct (red arrows).

3.1.1.2 *Generation and genotyping Kir transgenic mice*

The Kir construct was linearized by digestion with the restriction enzyme NotI and purified from a 1% agarose gel. Pronuclear microinjection was then carried out in collaboration with Drs Tom Moore and Melanie Ball at University College Cork (Richa, 2000). The DNA construct was injected into the pronuclei of fertilized oocytes, which were then implanted into pseudo-pregnant CD1 female mice. Three rounds of injections produced litters of 15, 9, and 8 pups respectively. Transgene presence was detected by PCR using two different primer combinations (Methods Table 7.2). Out of a total of 32 pups, 2 females and 2 males tested positive for both primer sets (Fig 3.2*C*). These founders are hereafter referred to as Kir-1A, Kir-7, Kir-1B and Kir-2.

3.1.1.3 *Establishing Kir transgenic lines*

All four founders were crossed to wildtype CD1 and C57 mice in order to establish the lines. Breeding patterns differed among founders. Founder Kir-1B, a male, was fertile but failed to produce any Kir-positive progeny. He was mated with various females over the course of nine months but produced only two litters with a total of 21 pups, none of which genotyped positive for Kir. Founder Kir-2, also a male, produced a total of 67 pups, out of which 5 pups (7%) were positive for the Kir transgene. From the entire Kir-2 line, 29 out of 137 (21%) pups were Kir-positive. Founder Kir-7, a female, produced two Kir-positive pups out of a total of 18 born (11%). From the entire Kir-7 line, 15 out of 70 pups (21%) were positive for the Kir transgene. Founder Kir-1A, a female, was a poor breeder. She lost three litters before beginning to produce viable litters, four months after initial mating. She then produced 4 of 18 (22%) Kir-positive pups. First and second generation Kir-1A mice were equally poor breeders, having many litter losses and long periods between litters compared to the Kir-7 and Kir-2 lines. Once the Kir-1A line was established, 17 out of 82 pups were Kir-positive (21%). Distribution of males and females throughout the Kir-2, Kir-7, and Kir-1A lines was equal, as expected. In summary, from four Kir founders, two lines were easily established, one was not established at all and another was difficult to breed but was eventually established.

3.1.1.4 *Characterization of potential transgene transcription in Kir lines*

The Kir lines were first characterized at the RNA level to determine whether the transgene had inserted into a transcriptionally active locus of the genome. We tested this by *in situ* hybridization, using a probe designed to detect the STOP cassette. This gave us an indication of expression prior to crossing the Kir lines to Cre recombinase-expressing lines. The Kir-2 line showed ample RNA expression in the brain, notably in the cortex and hippocampus (Fig

3.3). The caudate putamen, thalamus and hypothalamus did not exhibit any RNA expression in the Kir-2 line. The Kir-7 line presented some expression in the brainstem and midbrain but not in the cortex and hippocampus. As a negative control we used wildtype mice that did not show any staining, as expected (Fig 3.3*C*). Kir-1A was not included in this study as the line was not yet well established.

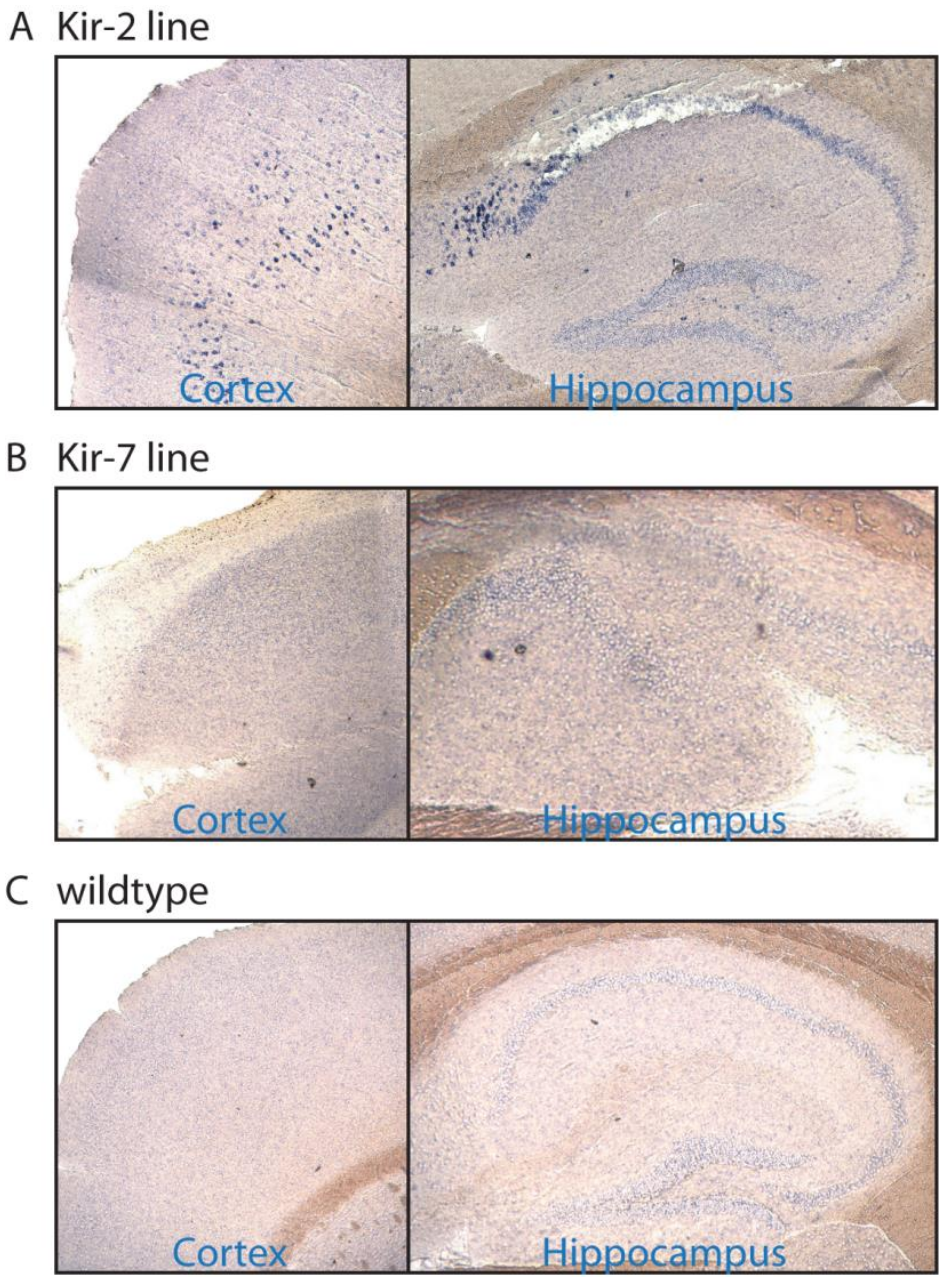

Figure 3.3 – RNA Expression of the Kir transgene

In situ hybridization (ISH) was used to examine RNA expression of the STOP cassette (contained in the transgenic Kir sequence) throughout the brain, with particular interest in the cortex and hippocampus. (A) The Kir-2 line reveals moderate expression in both the cortex and hippocampus (mainly in the subiculum). (B) The Kir-7 line does not express Kir RNA in the cortex or hippocampus. (C) Wildtype mice acted as a negative control and do not exhibit any staining in either structure.

3.1.1.5 *Characterization of tauLacZ reporter gene expression in Kir lines*

For characterization purposes, the Kir lines were crossed to the SLICK-H line, which, as described in the previous chapter, exhibits conditional pan-neuronal expression of Cre recombinase and YFP upon drug activation. SLICK-H;Kir double transgenic mice were administered the drug tamoxifen in order to activate Cre recombinase. Cre should excise the STOP cassette and lead to the expression of Kir and tauLacZ (Fig 3.1). As a negative control, we used untreated transgenic mice. X-gal staining was not detected in any of our lines compared to untreated controls, revealing that our lines do not actually express the Kir transgene (Fig 3.4). SLICK-H;Kir-2 (n=3) and SLICK-H;Kir-7 (n=2) consistently lacked the LacZ reporter gene. SLICK-H;Kir-1A exhibited the LacZ reporter gene in only one of four animals tested so we concluded that it does not truly exhibit Kir expression either. Since consistent expression of the reporter gene could not be detected following recombination, we did not proceed with these lines and all three lines were terminated.

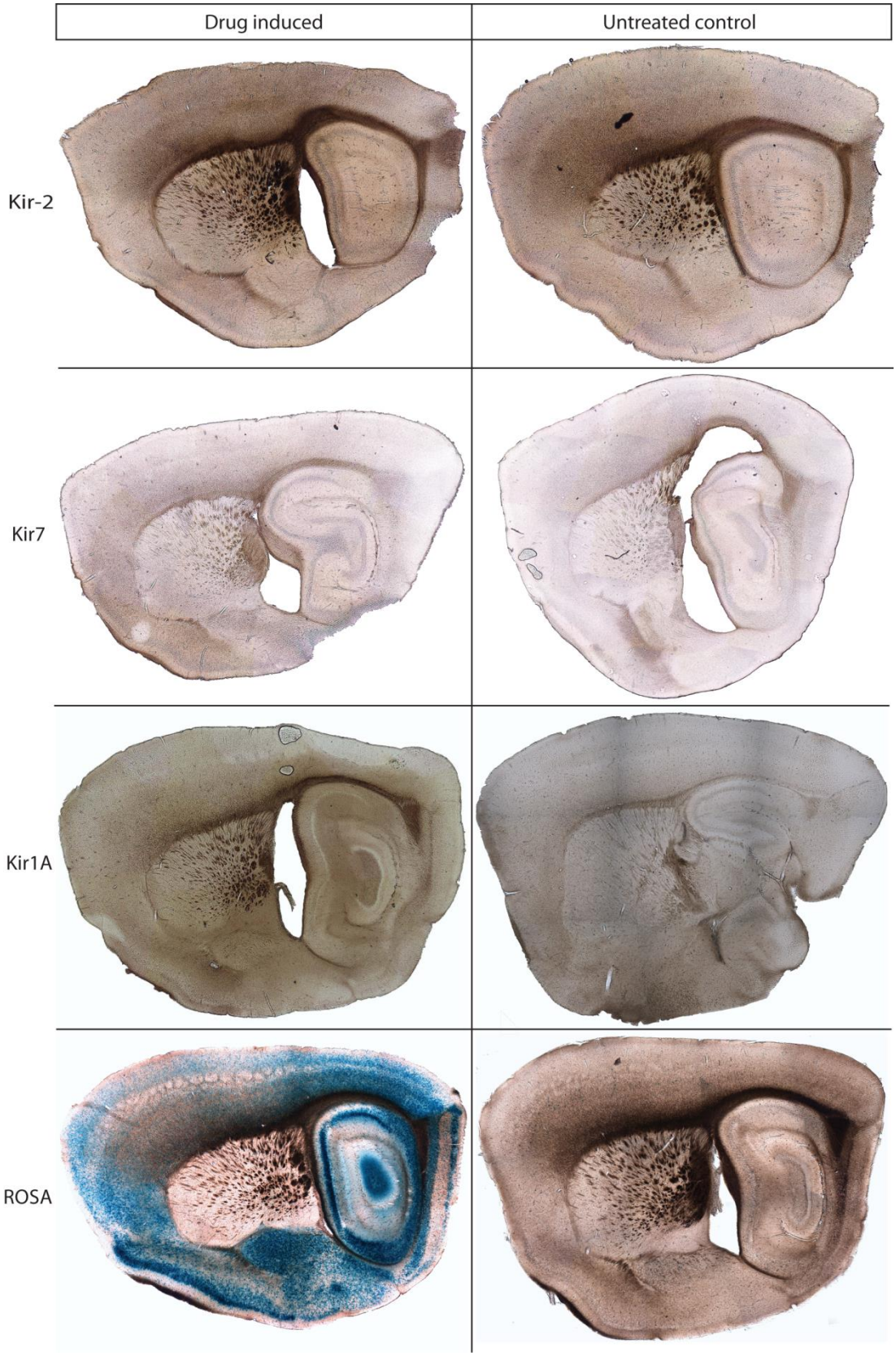

Figure 3.4 – LacZ reporter gene expression in the Kir lines

SLICK-H;Kir double transgenic mice were tested for the presence of LacZ reporter using the X-Gal staining method. Drug-induced mice were compared to untreated transgenic controls. None of the potential Kir lines express the LacZ reporter gene. SLICK-H;ROSA26R mice served as positive controls and show ample LacZ expression in drug-induced mice but not in untreated controls.

3.1.2 Cre recombinase-compatible transgenic mouse for the conditional expression of the tetanus toxin light chain in projection neurons

3.1.2.1 *Construction of a transgene for conditional expression of TetoxLC under control of the Thy1 promoter*

We obtained the TetoxLC sequence in the pGEMT7-EZ vector as a gift from Dr. C. Ron Yu (Yu et al., 2004). Initially we attempted to ligate the TetoxLC sequence with an IRES-tau-LacZ sequence, as had been done for Kir. This, however, proved unsuccessful. Instead we fused TetoxLC to cyan fluorescent protein (CFP), which is spectrally distinct from the YFP that is expressed in the SLICK lines. The CFP sequence was obtained by PCR amplification using primers that contain restriction sites and then ligated to TetoxLC (for further details see Chapter 7, Section 7.1.2.2). The fusion of tetanus toxin light chain and CFP is known to express stably in neuronal cultures (Harms et al., 2005).

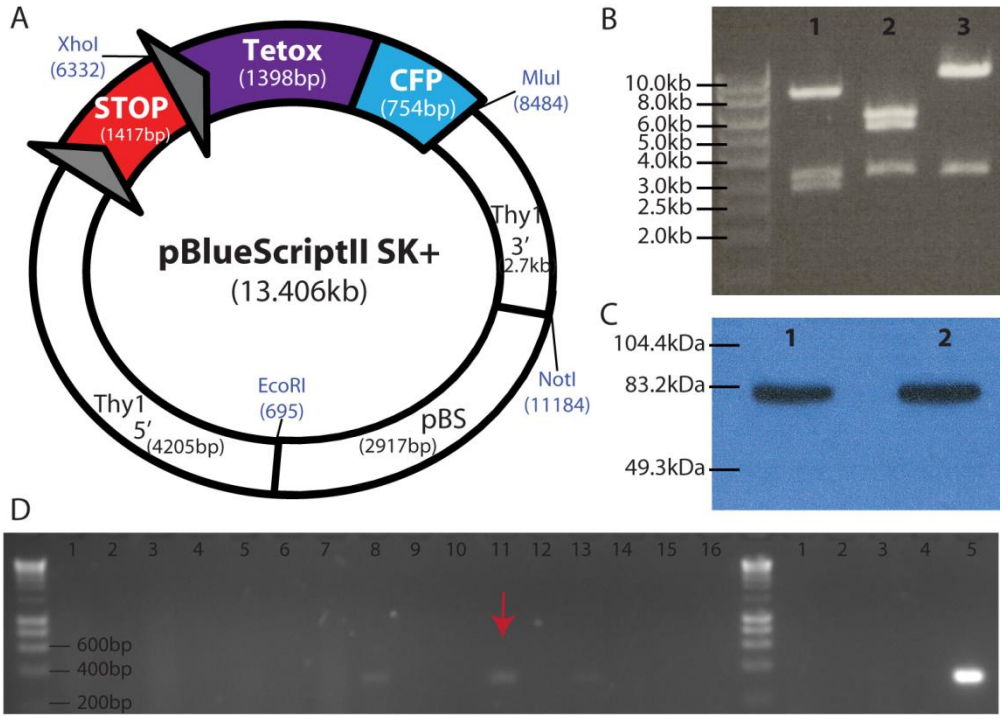

Figure 3.5 –Production of Cre recombinase-compatible transgenic mice for the conditional expression of tetanus toxin light chain

(A) Schematic representation of the tetanus toxin DNA construct that we used to generate potential TetoxLC transgenic mice. LoxP sites are shown as grey triangles and restriction enzymes used to linearize and verify the construct are shown in blue. The construct includes the pBlueScriptII-SK^{+} plasmid DNA and the Thy1 neuronal promoter sequence. (B) Restriction digests of the TetoxLC construct with EcoRI/NotI/MluI (lane 1), EcoRI/NotI/XhoI (lane 2), and EcoRI/Not (lane 3) produced bands of the expected sizes. (C) A western blot of transfected cell lysate probed with a rabbit-anti-GFP antibody shows a strong band for TetoxLC with no degradation product. Lanes 1 and 2 represent lysates from two different transformations. (D) Genotyping PCR identified one founder produced by pronuclear microinjection of the TetoxLC construct (red arrow). TetoxLC-CFP construct DNA was used as a positive control, shown in the last lane.

It is worth noting that tetanus-related cloning was problematic. When XL1Blue *E.coli* cells were transformed and plated onto selective antibiotic agar plates, normal-sized colonies were consistently obtained from cells transformed with either an empty vector or a TetoxLC-containing vector. Small colonies, which we originally mistook for background, were only present in TetoxLC-transformed plates and not in control plates. After performing colony PCR on a variety of colonies from several plates we concluded that these smaller colonies did in fact contain the TetoxLC insert, whereas the conventional colonies did not. We also observed that E. coli cells harboring a tetanus plasmid grew very slowly.

As with the Kir construct, we cloned TetoxLC-CFP into a modified pBlueScriptII SK+ vector that contains the neuronal promoter Thy1 and a STOP cassette flanked by loxP sites with parallel orientation (Fig 3.5*A*, for more detail refer to Chapter 7, Section 7.1.2.2). Once we successfully cloned our TetoxLC construct, we carried out several restriction digestions using different combinations of restriction enzymes to ensure the accuracy of our final construct. Expected bands were produced upon digestion with EcoRI, NotI and MluI (Fig 3.5*B*, lane 1), with EcoRI, NotI and XhoI (Fig 3.5*B*, lane 2), and withEcoRI and NotI (Fig 3.5*B*, lane 3). The finalized TetoxLC construct was then linearized with the restriction enzymes NotI and EcoRI, which removed the pBlueScript portion of the vector. This linearized DNA construct was then purified from a 1% agarose gel in preparation for pronuclear injection.

To check the expression and stability of the TetoxLC-CFP fusion protein we cloned the TetoxLC-CFP sequence into pCMV, a eukaryotic expression vector and transfected this into COS7 cells. We then performed a western blot on the cell lysates from these cultures. Blots probed with a rabbit-anti-GFP antibody (Methods Table 7.1) resulted in a single band with no degradation product, signifying that TetoxLC-CFP was successfully expressed in cells (Fig 3.5*C*). Cell cultures were also inspected under a fluorescent microscope where we confirmed that CFP staining was visible in transfected cells. Judging by morphology and rate of cell growth, we detected no obvious toxicity.

3.1.2.2 *Pronuclear injections of the TetoxLC construct*

Two rounds of pronuclear injections were performed at UCC in collaboration with Dr. Tom Moore's laboratory. Only one litter of 3 pups was produced. Tail samples were genotyped using two primer sets that recognized TetoxLC but no Tetox-positives were detected. After several lost litters, and/or small litter sizes, we decided to send the TetoxLC-CFP construct to the Transgenic Production Facility at the University of Cardiff in Wales, England, for

microinjection. Two rounds of injections there yielded 6 litters. Out of a total of 53 mice, several sporadically showed positive for the TetoxLC genotyping PCR but only one was consistent after several repetitions (Fig 3.5*D*). Tail samples were often received in a degraded state from the Cardiff transgenic facility as judged by failure to produce PCR products using primers that identify wildtype genes such as choline acetyltransferase. It is therefore possible that we overlooked other founders. Moreover, by the time we identified the only TetoxLC-CFP founder, she was 9-12 months old and did not produce any litters upon mating.

3.2 Discussion

Our objective was to create a mouse model for Cre recombinase-dependent over-expression of Kir and another for Cre recombinase-dependent expression of tetanus toxin light chain. We successfully created DNA constructs for both of these models and performed pronuclear injections. Kir injections produced four transgenic founders but one did not breed, and the other three did not express the LacZ reporter gene. Of these three, two expressed the transgene at the RNA level. Microinjections of the TetoxLC-CFP construct produced one founder from whom we were not able to establish a colony.

3.2.1 Transgenic delivery and germline transmission of the Kir construct

Genome integration typically occurs in only 10-30% of mice produced by microinjection (Wilkie et al., 1986). Our injections for Kir DNA yielded 4 founders out of 32 pups (12.5%), which is low but still within the established range. Our founders Kir-1B, Kir-2, Kir-7 and Kir-1A in turn yielded a germline transmission of 0%, 7%, 11% and 22% respectively. These numbers suggest a high level of mosaicism in germline cells of these founders, which is common in transgenic founders (Wilkie et al., 1986, Palmiter and Brinster, 1986). This is probably a consequence of injecting the transgenic DNA after more than one round of mitosis or of delayed DNA integration. Pronuclear injections were not regularly practiced by Dr. Tom Moore's lab at the time, so it is likely that the timing of delivery was not optimal, resulting in a high level of mosaicism. In the case of Kir-1B (0%) and Kir-2 (7%), which were males, it is also possible that the heterozygous transgenic sperm was less efficient at fertilizing ova than non-transgenic sperm (Ellison et al., 2000). The high level of mosaicism made the Kir lines more difficult than usual to establish but it did not affect the final outcome regarding protein expression.

3.2.2 RNA expression and reporter gene characterization of the Kir lines

Two of our lines, Kir-2 and Kir-7, showed transgenic RNA expression when probed for the STOP cassette by *in situ* hybridization. We know therefore, that in these lines the transgene was inserted into a transcriptionally active locus and that transcription was possible. Further characterization by X-gal staining, however, revealed no expression of the reporter gene LacZ. This could indicate either (1) transgene silencing, (2) absence of recombination or (3) that the IRES strategy was ineffective or insufficient.

Since insertion site and copy number are random following pronuclear microinjection, it is possible that our transgene was silenced due to position effect variegation (Graubert et al., 1998, Feng et al., 2000). Insertion of the construct into heterochromatin regions, for example, can cause site-dependent silencing, while in other regions, endogenous enhancers could alter transgene expression levels (Gama Sosa et al., 2010). It is likely that our lines Kir-2 and Kir-7 suffered from these position-site-dependent effects. We assume that recombination in SLICK-H;Kir mice did occur, based on known efficiency levels of recombination in SLICK-H;ROSA26 mice upon tamoxifen administration (Heimer-McGinn and Young, 2011). However, it is possible that recombination is less efficient for the Kir transgene if Cre cannot easily access the locus where it was randomly inserted. If recombination did not occur, then the floxed STOP cassette would not be excised and Kir would not have been transcribed. Finally, it is possible that recombination occurred and that the Kir sequence was translated, but that the IRES sequence did not properly initiate the translation of tau-LacZ. Although the IRES sequence has previously been shown to function in projection neurons (Dahlhaus et al., 2008), other studies have found that sequences following IRES are not always well expressed in these cells (Young et al., 2008). We are ultimately interested in applying this model to single-cell studies, so a malfunctioning reporter gene would pose a great inconvenience in distinguishing between endogenous and transgenic Kir at the single-cell level. Since convenience was one of the major benefits of this model, we did not think that any further characterizations were worthwhile.

3.2.3 Transgenic delivery of the TetoxLC construct

Pronuclear injections of the TetoxLC construct that were carried out at UCC yielded very few mice. Considering a typical genome integration rate of 10%-30% (Wilkie et al., 1986), it is not surprising that we did not obtain any founders from these injections. The low birth rate could be due to either toxicity of the construct, which we will discuss, or to technical problems. It is important to note that pronuclear microinjections in Dr. Moore's lab were not performed on a regular basis at the time. The injections that were carried out at the University of Cardiff did yield larger litter sizes but produced only one founder out of 53 (2%). This can again be an effect of either toxicity or technical problems. It is also important to point out that we had various difficulties with the Transgenic Production Facility at Cardiff University. More than once we received tail samples for genotyping that appeared to be degraded due to extended time in transit at room temperature. The only founder for TetoxLC was discovered past her optimal breeding age and did not produce any litters upon

being mated. Moreover, it is possible that more founders were in fact produced but overlooked due to the quality of the samples received.

It is possible that TetoxLC toxicity may have contributed to reduced litter sizes at UCC and reduced frequency of founders at the commercial facility, although we consider this to be unlikely. Our construct contains only the light chain domain of the toxin, which is the proteolytic domain responsible for cleaving the vSNARE protein VAMP2 (Schiavo et al., 2000). Without the heavy chain domain, which is responsible for membrane trafficking, tetanus should be unable to cross membranes and therefore attack the host at other locations (Schiavo et al., 2000). Moreover, the transcriptional STOP cassette upstream of the tetanus sequence should only be removed if these mice are crossed to a Cre recombinase-expressing line and, in the case of conditional Cre lines like SLICK, after administration of the drug tamoxifen. Also, the fact that cell cultures transfected with TetoxLC were stable provides some indication that this construct should not be toxic to its host. Alternatively, toxicity could arise from impurities in the actual DNA sample. Although possible, this does not seem likely since each injection was performed using a newly-made lot of purified DNA and yet the same difficulties arose for each injection. Judging by the relative success of Kir transgene delivery, we do not think we were experiencing a systemic problem of impure DNA.

As far as we understand, we were not able to produce enough TetoxLC-CFP founders either because (a) the DNA construct was toxic (due to DNA impurity or inherent toxicity of the gene), (b) because the DNA construct was not delivered effectively or (c) because we were not able to identify founders due to poor quality of tissue samples. In either case, considering we had already received and begun to characterize a tetanus-expressing line from Dr. Susan Dymecki's laboratory at Harvard University (discussed in the next chapter), we decided not to pursue the TetoxLC-CFP mouse model.

3.2.4 Alternative delivery methods

Although production of transgenic mice by pronuclear injection is beneficial because it is less expensive, time consuming and less technically challenging than other alternatives, it does have some shortcomings (Gama Sosa et al., 2010). Since copy number and insertion site of the DNA are random in this type of procedure, our transgene might have been silenced due to site-dependent effects or due to excessive copy number (Gama Sosa et al., 2010). In the

future we might consider either (a) modifying our construct so as to increase our likelihood of success or (b) attempting an alternative strategy of DNA delivery.

As far as the actual construct is concerned, we might consider adding insulator sequences that can protect the DNA from the effects of neighboring sequences (Bushey et al., 2008). Introducing an intron either up or downstream from the gene of interest may also result in more stable mRNA and more efficient translocation of RNA from the nucleus (Haruyama et al., 2009). We do not believe that the size of our fragment has negatively impacted our efficiency rate. These modifications would require careful planning and design but would ultimately be a reasonable approach.

We might also attempt to design a bacterial artificial construct (BAC) because they contain many of the regulatory elements required for expression and regulation of the gene of interest, some of which may also serve as insulator sequences (Montoliu et al., 1993). Also, a more widespread expression pattern that is independent of the Thy1 promoter may increase the likelihood of high transgene expression levels. BAC's, however, are more difficult to design, produce and deliver (because it is much larger) and may contain genes that affect phenotype in a manner independent of the gene of interest (Gama Sosa et al., 2010).

Other delivery methods we might consider are intracytoplasmic sperm injection, which is also random but produces a higher frequency of founders than pronuclear injection (Kaneko et al., 2005), or gene targeting by homologous recombination. Gene targeting would be a more controlled way of delivering DNA; we could prevent silencing of our gene and also disruption of normal endogenous gene function (Joyner, 2000, Notarianni and Evans, 2006). We would also have more consistent expression levels from generation to generation (Joyner, 2000). Gene targeting, however, is more laborious and expensive and requires a much longer timeframe. It is interesting to note that the tetanus-expressing mice we received from Dr. Dymecki's lab are knock-ins rather than transgenics. Although we do not know why they chose gene targeting over pronuclear injection, it is possible that this approach works best for this particular protein.

Chapter 4 Characterization of inducible TetoxLC expression in RC::Ptox mice

4.1 Results

4.1.1 General Strategy

While attempting to generate Cre recombinase-compatible mouse models for Kir2.1 and TetoxLC, we learned that Dr Susan Dymecki's laboratory (Harvard University, USA) recently created a line with Cre-compatible TetoxLC expression, albeit using a different approach of gene reporting (Kim et al., 2009). As an alternative strategy we requested access to Dymecki's RC::Ptox line (distinct from RC::PFtox described in Kim *et al* 2009). The RC::Ptox mice we received express a transgene (Fig 4.1*A*) that is knocked-in to the ROSA26 locus (Zambrowicz et al., 1997) and contains a CAG promoter (Niwa et al., 1991), a floxed STOP cassette and GFPtox, which is a fusion of enhanced green fluorescent protein (EGFP) and tetanus toxin light chain (Yamamoto et al., 2003).

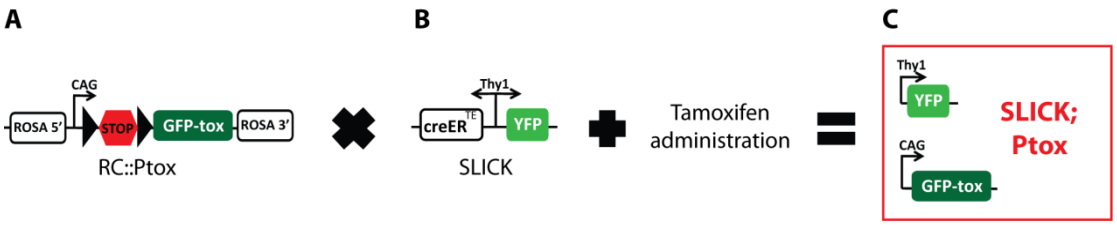

Figure 4.1 – Strategy to conditionally coexpress SLICK and GFPtox in pyramidal neurons
(A) The RC::Ptox construct contains a STOP cassette flanked by *lox*P sites (triangles), followed by GFPtox, a fusion protein between eGFP (enhanced green fluorescent protein) and the tetanus toxin light chain. The transgene is targeted to the ROSA26 locus and also contains a CAG promoter. (B) The SLICK transgene contains two copies of the Thy1 neuronal promoter that drive simultaneous expression of YFP (yellow fluorescent protein) and the Cre recombinase CreER^{T2}. The drug tamoxifen activates Cre-mediated recombination in double transgenic mice (SLICK;Ptox). (C) Drug-induced SLICK;Ptox mice coexpress YFP and GFPtox in pyramidal neurons. Since YFP and GFP are spectrally very similar, GFP is not a useful reporter as it will not distinguish between cells that are SLICK^{+}/Ptox^{-} and cells that are SLICK^{+}/Ptox^{+}.

Although RC::Ptox transgene expression has been previously characterized (unpublished data from Dr. Dymecki's lab), we wanted to ensure compatibility with our SLICK lines as well as efficient levels of recombination upon administration of the drug tamoxifen. For this purpose we crossed the RC::Ptox and SLICK lines. As described in Chapter 2, the SLICK transgene (Fig 4.1*B*) contains the Cre recombinase CreER^{T2} as well as yellow fluorescent protein (YFP), both under the control of the Thy1 promoter. Upon drug activation, cells in

double transgenic SLICK-H;Ptox mice will express both YFP and GFP (Fig 4.1*C*). YFP and GFP, however, are spectrally very similar (unlike YFP and CFP). Moreover, since YFP is expressed strongly in SLICK mice (refer to Chapter 2), whereas GFPtox produces weak expression (unpublished data; Dymecki), cells that express GFPtox will be difficult to distinguish from cells that only contain the SLICK transgene but no recombined GFPtox. Since our future studies with SLICK-V;Ptox require single-cell detection of tetanus expression, we were eager to either (a) detect a high recombination efficiency and GFPtox expression and/or (b) establish a reliable method for direct tetanus detection.

4.1.2 Does recombination occur in tamoxifen-treated SLICK-H;Ptox mice?

For the purpose of characterization, the Cre-compatible RC::Ptox transgenic mouse line received from Susan Dymecki's laboratory was crossed to our SLICK-H line that exhibits conditional widespread neuronal expression of CreER^{T2} and YFP (Fig 4.1*B*). SLICK-H;Ptox double transgenic mice were treated with tamoxifen in order to activate CreER^{T2} and induce expression of GFPtox. Untreated SLICK-H;Ptox mice served as controls.

4.1.2.1 *Characterization of recombination by polymerase chain reaction*

We tested several PCR primer combinations intended to ensure that recombination occurs only upon tamoxifen-induced CreER^{T2} activation. The first primer set is designed to produce a band of 372 bp in the presence of drug-induced recombination and a 3040 bp band in the absence of treatment (Fig 4.2*A*, in blue). As shown in figure 4.2*B*, top panel, tamoxifen-induced SLICK-H;Ptox mice display a strong band at the expected size signifying that recombination has occurred (lanes 1-3), whereas un-induced SLICK-H;Ptox samples do not (lanes 4-6). In two of three un-induced samples, the 3040 bp band representing the un-recombined transgene is weakly visible. Another primer set detects only the un-recombined transgene and produces a band of 381 bp (Fig 4.2*A*, in pink). As seen in figure 4.2*B*, middle panel, all three un-induced SLICK-H;Ptox samples (lanes 4-6) produced strong bands at the appropriate size. Two of the three tamoxifen-induced SLICK-H;Ptox samples also show bands signifying the presence of un-recombined transgene (lanes 1,3). Finally, a wildtype PCR primer pair detecting the presence of choline acetyltransferase (ChAT) assured us that all samples of the purified DNA were of good quality (Fig 4.2*B*, bottom panel).

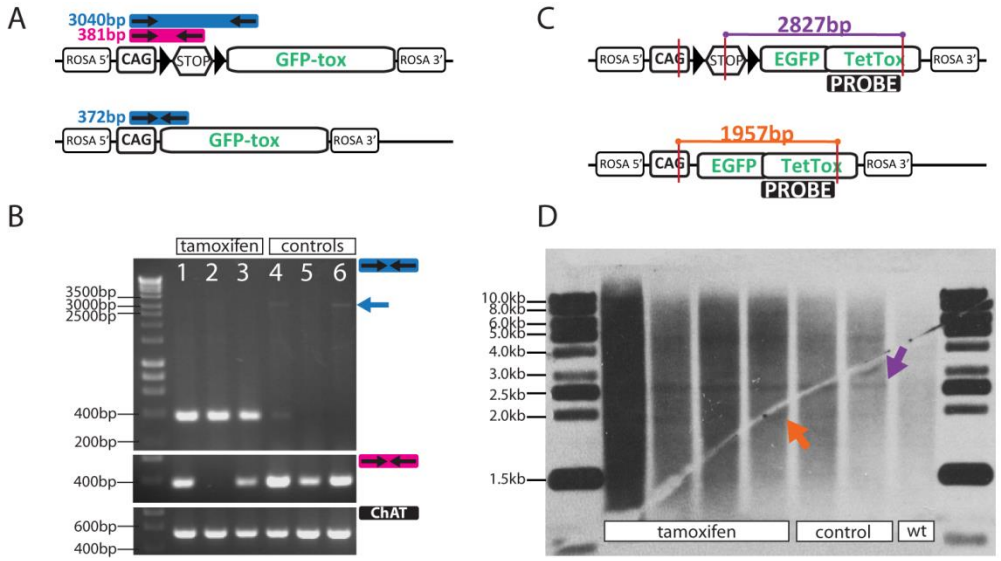

Figure 4.2 – Characterization of Cre-mediated recombination in SLICK;Ptox mice by PCR and by Southern blot

(A) Schematic representation of two PCR primer sets used to identify Cre-mediated excision of the STOP cassette in the RC::Ptox construct. The GPFtox1 (blue) primer combination recognizes both recombined and non-recombined DNA, whereas the GPFtox2 (pink) primer combination identifies only un-recombined DNA. Because GPFtox2 amplifies a smaller DNA sample than GPFtox1 in the presence of the STOP cassette, it is more useful in consistently recognizing the widespread presence of the RC::Ptox construct (SLICK$^-$/Ptox$^+$ cells will contain un-recombined DNA). (B) PCR amplification. Lanes 1-3 contain samples extracted from tamoxifen-treated SLICK-H;Ptox mice, lanes 4-6 contain control samples extracted from un-treated SLICK-H;Ptox mice. Amplification was performed using GPFtox1 (top panel, blue), GPFtox2 (middle panel, pink) and a combination of wildtype ChAT primers that verify the quality of the samples (bottom panel, green). A blue arrow in the top panel points out a weak band identifying un-recombined DNA. (C) Schematic representation of the probes used to identify Cre-mediated recombination of the RC::Ptox construct by Southern blot. Vertical red lines represent the sites where DNA samples were digested using restriction enzymes. Horizontal purple and orange lines represent the probes that recognize the un-recombined and the recombined DNA, respectively. (D) Southern blot. Lanes 1-4 contain samples extracted from tamoxifen-treated SLICK-H;Ptox mice, lanes 5-6 from untreated SLICK-H;Ptox control mice, and lane 7 from untreated wildtype mice. A purple arrow points to a band that represents the un-recombined construct and an orange arrow points to a band that represents the recombined construct.

4.1.2.2 *Characterization of recombination by Southern blot analysis*

Once we knew that Cre-recombinase is properly activated in the presence of tamoxifen, we attempted to quantify the levels of recombination by Southern blot (SB) analysis. Our approach was to compare the amount of recombination in SLICK-H;Ptox versus SLICK-H;ROSA26 mice, whose recombination efficiency is known to be high (see Chapter 2). We administered three doses of tamoxifen to SLICK-H;Ptox mice and purified DNA from brain tissue. As negative controls for recombination, we used untreated SLICK-H;Ptox mice as well as a wildtype mouse. Purified DNA from these mice was digested using EcoRV and EcoRI and then tested with a probe that we designed to recognize the full TetoxLC sequence (Fig 4.2*C*). Recombination should be marked by a band at 1957bp (Fig 4.2*C*, in orange), the un-recombined transgene should produce a band at 2827bp (Fig 4.2*C*, in purple), and the

wildtype control lacking the transgene should exhibit no bands. To test recombination of SLICK-H;ROSA26, we treated age-matched SLICK-H;ROSA26mice with three doses of tamoxifen and compared them to untreated ROSA26 mice, and to a wildtype mouse. We designed a probe that recognizes the LacZ sequence and digested the purified DNA using EcoRV.

As expected, the tamoxifen-induced SLICK-H;Ptox and the untreated controls exhibit the 2827bp band signifying the un-recombined transgene, whereas the wildtype control does not. The band at 1957bp is faintly observed in the tamoxifen-induced samples but is not strong enough to draw any conclusions. Furthermore, the band may also be faintly observed in the untreated control samples, although not in the wildtype control. Detection of LacZ by Southern blot produced bands for both the recombined and un-recombined transgene but these bands were present in both the tamoxifen-induced and the untreated samples. No bands were produced in the wildtype control.

To summarize, our Tetox probe is not sensitive enough to confidently detect the recombined transgene in SLICK-H;Ptox at the administered dose of tamoxifen. Both the Tetox and the LacZ probe seem to pick up a band in untreated controls that should signify the presence of recombined transgene. Considering this unspecific band, we did not use these data to quantify recombination in SLICK-H;Ptox relative to SLICK-H;ROSA26 tissue.

4.1.3 Do tamoxifen-treated SLICK;Ptox mice express RC::Ptox mRNA?

4.1.3.1 *Characterization of transgene mRNA expression by ISH in SLICK-H;Ptox mice*

In order to characterize the mRNA expression of GFPtox we designed a single-stranded RNA probe for *in situ* hybridization (ISH) that detects the full tetanus toxin light chain sequence (1398 bp). We also carried out staining with a probe for proteolipid protein (PLP) as a positive control to assess tissue sample quality; all tissue included in our analysis displayed widespread PLP staining in oligodendrocytes, as expected. SLICK-H;Ptox mice were treated with three doses of tamoxifen and compared to age-matched untreated SLICK-H;Ptox or untreated Ptox mice (Fig 4.3). ISH labeling can be observed in the cortex (Fig 4.3*a,f*), hippocampus (Fig 4.3*b,d,e*), cerebellum (Fig 4.3*c*), brainstem (Fig 4.3*g*), and thalamus (Fig 4.3*h*). In the hippocampus, staining is most abundant in the subiculum (Fig 4.3*e*), followed by the CA1 (Fig 4.3*d*). Occasional staining is observed in the dentate gyrus and CA3 and no staining is seen in the CA2 area. Taking into account the fact that recombination the

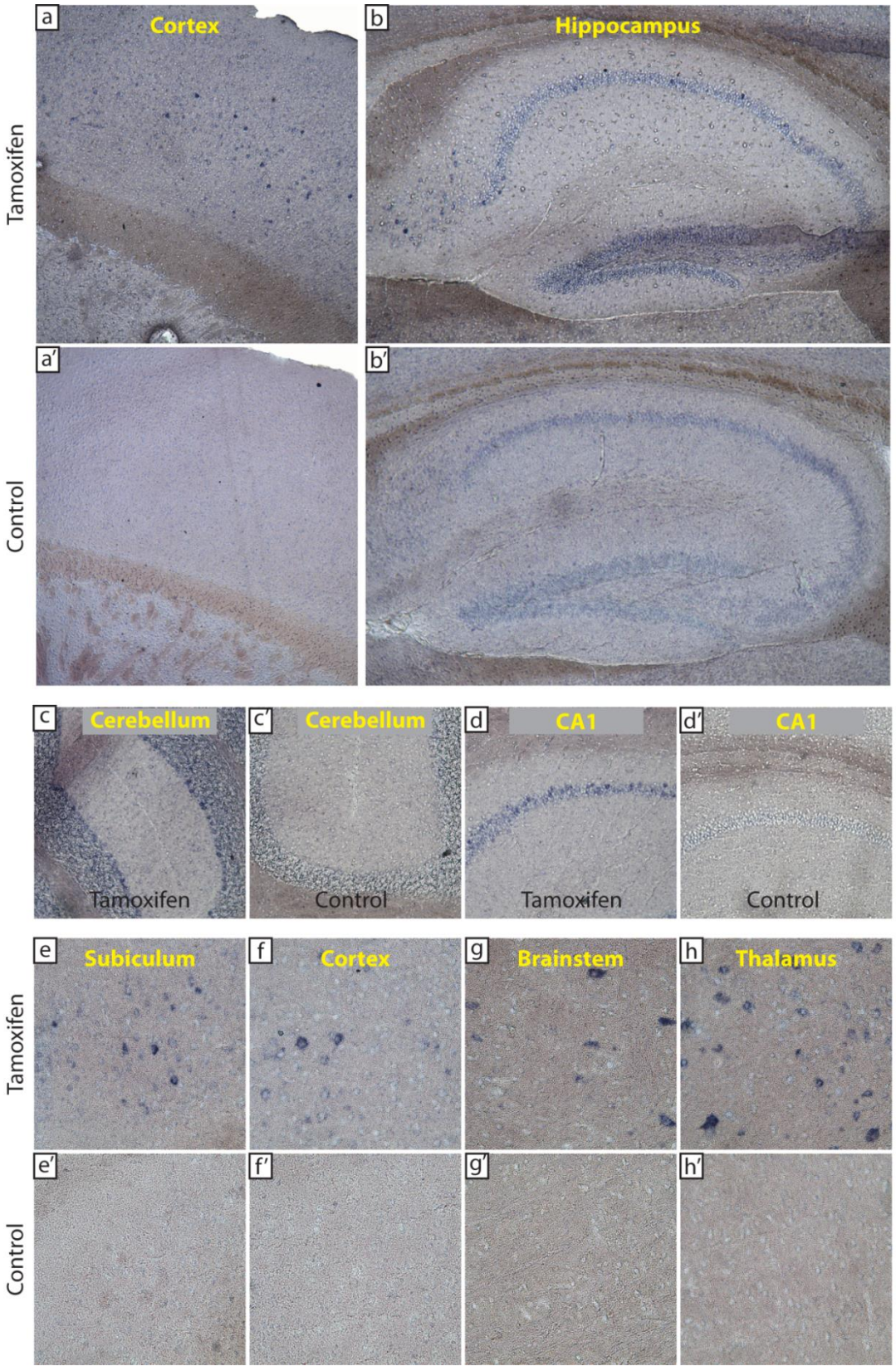

Figure 4.3 – Widespread mRNA expression of TetoxLC in SLICK-H;Ptox double transgenic mice

In situ hybridization (ISH) was used to examine RNA expression levels of the RC::Ptox construct in Ptox mice crossed with the SLICK-H line of mice, which expresses $CreER^{T2}$ in almost all pyramidal neurons. Tamoxifen-treated SLICK-H;Ptox double transgenic mice (a-h) were compared to untreated double transgenic controls (a'-h'). The cortex and hippocampus are shown at a magnification of 4X (a-b, a'-b'). The cerebellum and CA1 are shown at 10X (c-d, c'-d'). Individual cells that express TetoxLC mRNA in the subiculum (e), cortex (f), brainstem (g) and thalamus (h) are magnified at 20X, along with their corresponding controls (e'-h').

efficiency for SLICK-H;R26R in the cerebellum was found to be low compared to other areas (Chapter 2), cerebellar staining in SLICK-H;Ptox is relatively abundant. In general however, ISH staining for tetanus shows labeling throughout the brain in a pattern similar to SLICK-H;R26R albeit less abundantly (Chapter 2).

Multiple optimizations, including higher hybridization temperature, shorter wash steps, use of proteinase K, and use of polyvinyl alcohol (PVA) did not increase the degree of labeling in our treated samples compared to background levels in the untreated controls. To obtain better tissue penetration, we also designed three smaller probes to be used simultaneously, each of which should detect roughly one third of the full tetanus sequence. These probes, however, produced excessive background even in the untreated control. We also compared staining in mice treated with either three or six doses of tamoxifen and saw no significant increase in staining. In general, we were able to detect of GFPtox mRNA expression in SLICK-H;Ptox mice although not with the abundance that we expected based on our SLICK-H;ROSA26 characterization in Chapter 2.

4.1.3.2 *Characterization of transgene mRNA expression by ISH in SLICK-V;Ptox mice*

Once we established the optimal conditions for testing GFPtox mRNA expression through ISH, we decided to look at expression in SLICK-V;Ptox mice as well. SLICK-V exhibits extremely sparse labeling in the hippocampus and cortex (Young et al., 2008) where we are interested in studying activity-dependent processes in single cells.

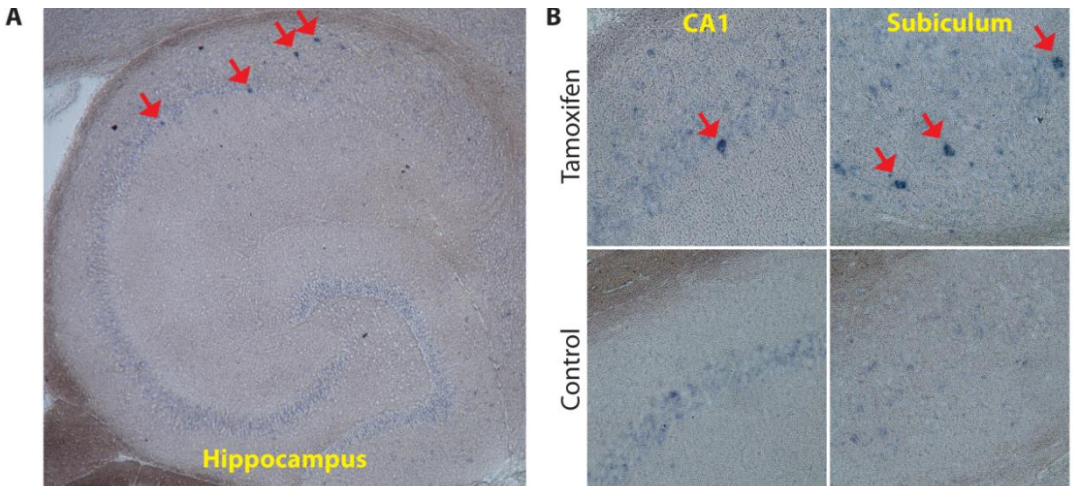

Figure 4.4 – Sparse mRNA expression of TetoxLC in SLICK-V;Ptox double transgenic mice
In situ hybridization (ISH) was used to examine RNA expression levels of the RC::Ptox construct in Ptox mice crossed with SLICK-V, which expresses $CreER^{T2}$ in a sparse number of pyramidal neurons. (A) The hippocampus of a tamoxifen-treated SLICK-V;Ptox mouse is shown at a magnification of 4X. (B) Stained cells in the CA1 and subiculum of tamoxifen-treated SLICK-V;Ptox mice are magnified to 20X and compared to untreated SLICK-V;Ptox controls. In both panels, red arrows point to individual cells that express the RC::Ptox mRNA.

SLICK-V;Ptox mice treated with ten doses of tamoxifen were compared to age-matched untreated SLICK-V;Ptox mice. ISH staining using the same full-length tetanus probe described above revealed several single cells that show GFPtox expression. Hippocampal staining (Fig 4.4*A*) is most common in the subiculum (Fig 4.4*B*), followed by the CA1 (Fig 4.4*B*) and least common in the dentate gyrus (Fig 4.4*A*). We did not detect any labeled cells in the CA3 or cortex. Labeled cells were also observed in the brainstem and midbrain but not in the thalamus, cerebellum or amygdala.

4.1.4 Do tamoxifen-treated SLICK-H;Ptox mice express the GFPtox protein?

4.1.4.1 *Characterization of TetoxLC antibodies by western blot analysis*

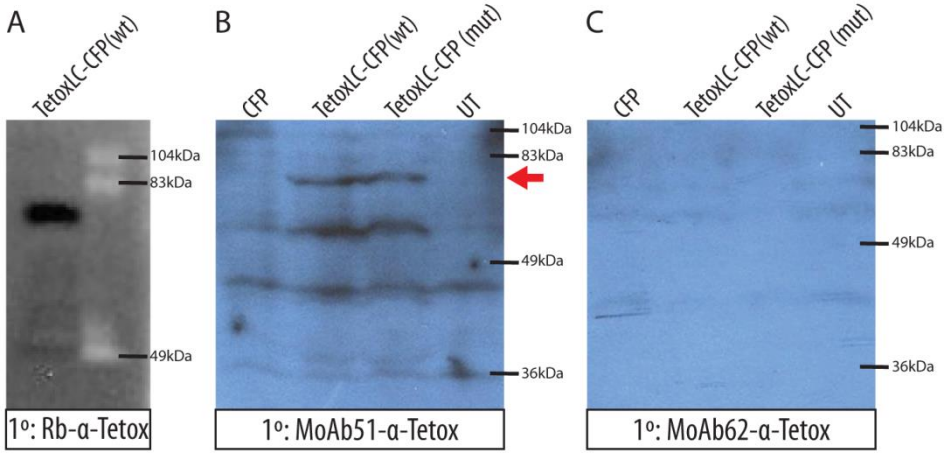

Figure 4.5 – Western blot characterization of TetoxLC antibodies using transfected cell lysates
(A) A western blot using Rb-α-Tetox (1:2000) as the primary antibody. A clear band at 75kDa represents the TetoxLC-CFP fusion protein. (B) A western blot using MoAb51-α-Tetox (1:100) as the primary antibody. The 1st lane contains control cell lysate derived from CFP-transfected cells, the 2nd and 3rd lanes contain lysate from TetoxLC-CFP transfected cells and the 4th lane contains control lysate from untransfected cells. A red arrow identifies the 75kDa band that represents TetoxLC-CFP. (C) A western blot using MoAb62-α-Tetox (1:100) as the primary antibody. Cell lysates are the same as in the previous blot.

We characterized three antibodies that recognize the 50kDa light chain of tetanus toxin (TetoxLC), one polyclonal unpurified serum raised in rabbit (Rb) and two purified monoclonal antibodies received as gifts from Dr. Vladimir Petrusic (Chapter 7, Table 7.1). In order to do this we transfected COS-7 cells with a TetoxLC-CFP fusion protein (as described in Fig 3.5*C*) and probed total cell lysates by western blot (WB) analysis. As negative controls in some trials we used un-transfected cells and cells transfected with only CFP. Rb-α-Tetox, which we tested at 1:100, 1:500, 1:2000 and 1:5000, recognizes the protein robustly at all but 1:5000 (Fig 4.5*A*) and does not pick up any other background bands. MoAb51-α-Tetox recognizes Tetox-CFP at 1:100 (Fig 4.5*B*) and more weakly at 1:500. It also picks up several other

background bands. MoAb62-α-Tetox does not recognize the fusion protein at 1:100 (Fig 4.5*C*). As expected, the CFP-transfected lysates and the un-transfected lysates did not exhibit the 75kDa band that represents TetoxLC-CFP. We therefore have one polyclonal unpurified serum that recognizes TetoxLC robustly with no background and one purified monoclonal (MoAb51) that recognizes the protein less intensely and with some background.

4.1.4.2 *Characterization of GFPtox protein expression by western blot analysis*

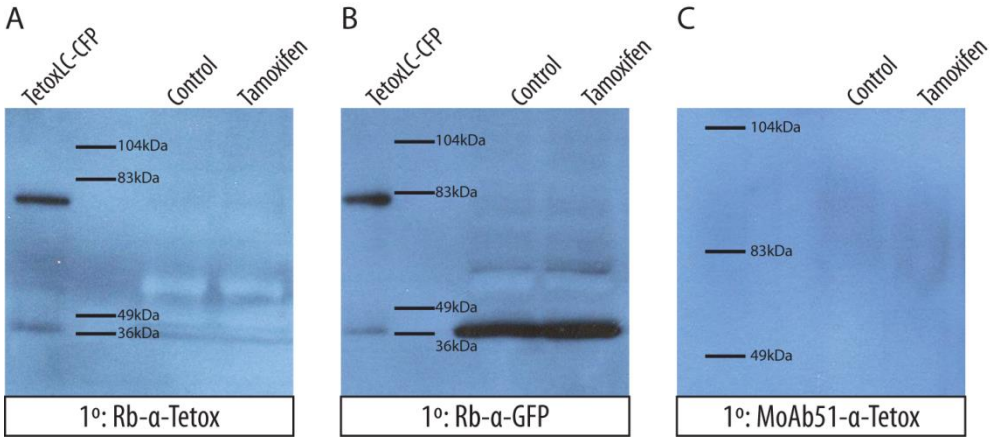

Figure 4.6 – Western blot analysis of TetoxLC protein in brain samples extracted from tamoxifen-treated SLICK-H;Ptox mice

(A) A western blot using Rb-α-Tetox as the primary antibody. The 1st lane contains TetoxLC-CFP transfected cell lysate as a positive control. The 75kDa band represents the TetoxLC-CFP construct. The 2nd lane contains a marker, the 3rd lane contains brain homogenate from untreated SLICK-H;Ptox mice and the 4th lane from SLICK-H;Ptox mice treated with 3 doses of tamoxifen. (B) A western blot using Rb-α-GFP as the primary antibody. Sample setup is identical to the previous blot. The strong lower band in the 3rd and 4th lanes represents YFP (27 kDa) from the SLICK transgene. (C) A western blot using MoAb51-α-Tetox (1:100) as the primary antibody. The lanes labeled "control" and "tamoxifen" refer respectively to brain homogenate from untreated SLICK-H;Ptox mice and from SLICK-H;Ptox mice treated with 8 doses of tamoxifen.

We then attempted to use these antibodies to detect GFPtox expression in tamoxifen-treated SLICK-H;Ptox mice. We homogenized whole-brain samples of tamoxifen-treated (3 doses) versus untreated SLICK-H;Ptox mice and used these lysates to probe by western blot analysis. As primary antibodies we used either Rb-α-Tetox, MoAb51-α-Tetox or a rabbit polyclonal GFP antibody (since Ptox mice contain the GFPtox fusion construct) (Methods, Table 7.1). As a positive control we included the TetoxLC-CFP-transfected lysate used in Figure 4.5. Rb-α-Tetox recognized TetoxLC-CFP in the transfected lysate but did not pick up any GFPtox in the tamoxifen-treated SLICK-H;Ptox (Fig 4.6*A*). Rb-α-GFP was equally ineffective at recognizing any GFPtox protein (Fig 4.6*B*) although it did detect the transfected positive control as well as the YFP derived from the SLICK-H transgene (Fig 4.1*B*). Similarly, MoAb51-α-Tetox did not recognize any expressed GFPtox (Fig 4.6*C*) although it did recognize

the positive control. In summary, neither of the three antibodies we used for western blot was able to successfully recognize GFPtox protein in cell lysates from SLICK-H;Ptox mice treated with three doses of tamoxifen.

4.1.4.3 *Characterization of GFPtox protein expression by immunoprecipitation*

We next performed an immunoprecipitation (IP) assay in order to concentrate GFPtox protein levels and increase our chances of detecting low levels of the tetanus toxin. We first tested the Tetox antibodies for their ability to precipitate the desired protein (Fig 4.7*A*). We used COS7 cell lysates transfected with TetoxLC-CFP and precipitated the protein by incubation with either Rb-α-Tetox, MoAb51-α-Tetox or MoAb62-α-Tetox. We then performed three western blots of the immunoprecipitated samples, and each blot was probed using one of the three Tetox antibodies.

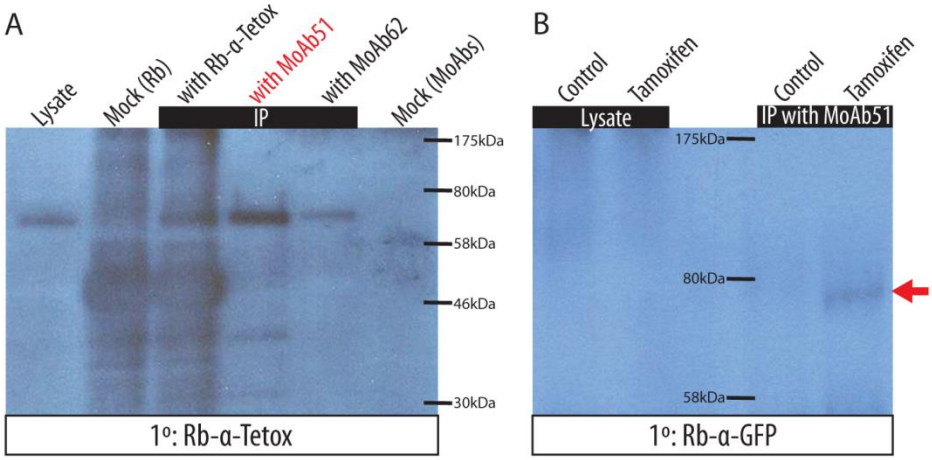

Figure 4.7 – Western blot of TetoxLC immunoprecipitation in cell lysates and in brain samples derived from tamoxifen-treated SLICK-H;Ptox mice

(A) A western blot probed with Rb-α-Tetox. Blot shows the immunoprecipitation of TetoxLC protein from cell lysates transfected with TetoxLC-CFP. The 1st lane contains crude lysate used as a positive control. The 2nd and last lanes contain mock precipitations using the polyclonal and monoclonal antibodies, respectively. The 3rd, 4th and 5th lanes, labeled "IP", show immuno-precipitation by incubation with Rb-α-Tetox, MoAb51-α-Tetox or MoAb62-α-Tetox respectively. The strongest and clearest staining is obtained by incubation with MoAb51-α-Tetox (in red). (B) A western blot probed with Rb-α-GFP. Blot shows the immunoprecipitation of GFPtox protein by incubation with MoAb51-α-Tetox in brain homogenates derived from treated and untreated SLICK-H;Ptox mice. The first two lanes contain un-precipitated brain homogenate samples. The 1st lane is derived from the combined brain homogenates of three untreated SLICK-H;Ptox control mice. The 2nd lane is derived from the combined brain homogenates of three SLICK-H;Ptox mice treated with 8 doses of tamoxifen. The last two lanes contain control and tamoxifen-treated brain homogenates incubated with MoAb51-α-Tetox. A yellow arrow points to the 75kDa band that represents the GFPtox transgenic protein.

Immunoprecipitation with MoAb51 presented the strongest and clearest staining (Fig 4.7A) compared to Rb -α-Tetox (Fig 4.7A, lane 3) and MoAb62 (Fig 4.7A, lane 5). This was true

when the samples were probed by western with any of the three antibodies (only Rb-α-Tetox used as a primary antibody is shown) but as expected, Rb-α-Tetox proved to be the most effective as a primary antibody for western blotting (Fig 4.7*A*). The monoclonal antibodies displayed a great deal of background when used as primary antibodies for the western blot. As expected, the transfected lysate displayed the TetoxLC-CFP band, whereas the two mock precipitations did not. In conclusion, after testing several combinations of antibodies with which to precipitate and probe, we concluded that precipitation by MoAb51 α-Tetox, followed by western analysis using Rb-α-Tetox as a primary antibody provides the clearest data.

Once we established the optimal combination of antibodies to precipitate and probe Tetox, we treated three SLICK-H;Ptox mice with eight doses of tamoxifen and pooled their whole-brain lysates. These were compared to three whole-brain lysates for untreated SLICK-H;Ptox mice. We used MoAb51-α-Tetox to immunoprecipitate the samples, and then performed a western blot analysis using either Rb-α-Tetox or Rb-α-GFP as the primary antibody (Fig 4.7*B*). Rb-α-Tetox did not pick up any protein expression, whereas Rb-α-GFP successfully detected the precipitated GFPtox protein in tamoxifen-treated SLICK-H;Ptox mice compared to untreated controls. Neither antibody was sensitive enough to detect protein expression in the crude lysates consisting of three brain homogenates pooled (for either control or tamoxifen-treated). Although GFPtox protein concentration appears to be quite low even in SLICK-H;Ptox mice treated with a higher dose of tamoxifen (8 doses), we were able to detect it after pooling three whole-brain samples and then concentrating the protein by immunoprecipitation.

Judging by the low levels of GFPtox detected by immunoprecipitation, we suspected that the antibodies would not be sensitive enough to detect the protein by immunofluorescence. We did, however, test them by immunocytochemistry (ICC) in transfected cells and by immunohistochemistry (IHC) in SLICK-H;Ptox and SLICK-V;Ptox mice treated with tamoxifen. In both assays, staining proved to be non-specific, showing equal levels of background in transfected versus un-transfected cells, and in treated versus untreated tissue. Optimizations such as pre-absorption of antibody using wildtype brain extract or purification of the polyclonal antibody by proteinG did not increase the sensitivity of the antibodies.

4.1.5 Behavioral observations of SLICK-H;Ptox mice treated with elevated doses of tamoxifen

When treating SLICK-H;Ptox mice, we generally administered a reduced dosage of tamoxifen because we reasoned that if recombination efficiency was a high as in SLICK-H;ROSA26 (Chapter 2), a full ten-day course of tamoxifen administration might be lethal. In SLICK-H;R26R this "reduced dose" produces detectable levels of recombination. After performing several assays that showed that GFPtox expression in SLICK-H;Ptox mice was low compared to SLICK-H;R26R, we decided to increase the tamoxifen dosage. Mice were closely examined daily upon tamoxifen administration to ensure that the animals did not show any signs of distress. Using age-matched pairs of treated versus untreated SLICK-H;Ptox mice, we observed that 8-9 doses of tamoxifen produces an ataxic phenotype in treated mice only. Additional wildtype mice treated in tandem served as controls to rule out any effect that the tamoxifen delivery itself might inflict. Ten tamoxifen-treated mice displayed the ataxic phenotype compared to ten untreated controls and compared to treated wildtype controls.

Figure 4.8 – Still frames from video footage of tamoxifen-treated SLICK-H;Ptox mice showing a slightly ataxic phenotype. SLICK-H;Ptox mice treated with 8-9 doses of tamoxifen display reduced coordination resulting in repeated falls or slips. These still images show two affected mice attempting to recover after a fall. Full videos include comparison with control mice. These are available in digital format upon request.

SLICK-H;Ptox mice treated with 8-9 doses of tamoxifen display reduced coordination, repeated loss of balance resulting in falls or slips and lateral deviations when attempting to walk. They display mild tremors when standing still and their backs appear slightly arched in comparison to controls. Their movements are slower in general than those of the control mice and they seem less inclined to explore their environment. We are not currently equipped to quantify these behavioral observations but they are apparent upon casual observation and were observed consistently in treated animals versus controls (n=10). These

observations indicate that at least in SLICK-H;Ptox mice, 8-9 doses of tamoxifen results in enough TetoxLC expression to produce an observable behavioral phenotype.

4.1.6 Do tamoxifen-treated SLICK-H;Ptox mice exhibit reduced expression levels of VAMP2?

Having observed a phenotype in SLICK-H;Ptox mice treated with eight doses of tamoxifen, we decided to look at expression of the vesicle-associated membrane protein 2 (VAMP2) in these mice. VAMP2, also known as synaptobrevin-2, resides in the synaptic vesicle membrane and assembles to form part of the SNARE complex responsible for vesicle fusion to the presynaptic membrane (Sutton et al., 1998). Tetanus toxin light chain acts by cleaving this protein between residues 76-77, which prevents synaptic vesicle exocytosis and therefore inhibits neurotransmitter release (Schiavo et al., 1992, 2000). If GFPtox is functional in tamoxifen-treated SLICK-H;Ptox mice, we should see a reduction in the amount of full-length VAMP2 protein compared to untreated controls.

4.1.6.1 *Characterization of VAMP2 expression by western blot analysis*

In order to characterize VAMP2 expression in SLICK;Ptox mice, we obtained two commercially available antibodies that recognize synaptobrevin-2 (Methods, Table 7.1). Monoclonal mouse α-VAMP2 recognizes residues 2-17 from the rat VAMP2 sequence and has no cross-reactivity with the other two isoforms, VAMP1 or VAMP3. Although the epitope for this antibody is present in the tetanus-cleaved form of VAMP2, the supplier Synaptic Systems states that the cleaved VAMP2 is not recognized. Moreover, this antibody is widely used for verifying VAMP2 cleavage (Yu et al., 2004, Kim et al., 2009). Polyclonal rabbit α-VAMP1/2/3 is raised against residues 1-81 of VAMP3, also known as cellubrevin, and recognizes all three isoforms VAMP1, 2 and 3. The antibody also weakly recognizes the cleaved product of VAMP2.

We compared SLICK-H;Ptox mice treated with eight doses of tamoxifen to age-matched untreated SLICK-H;Ptox controls by western blot analysis using both antibodies α-VAMP2 and α-VAMP1/2/3. We also used α-GAPDH as a loading control (Methods, Table 7.1). Considering that ataxic behavior in these mice could implicate cerebellar dysfunction (Schmahmann, 2004), we analyzed cerebellum tissue lysates separately from forebrain tissue lysates. As shown in Figure 4.6*A*, α-VAMP2 (in green) detects the protein strongly (only 15ug of total protein was loaded) and is very specific (no other bands displayed even

when 60ug of total protein was loaded). α-VAMP1/2/3 (Fig 4.6*B*) robustly and specifically recognizes VAMP1 (top band), VAMP2 (middle band) and VAMP3 (bottom band) but does not seem to pick up the cleavage product of VAMP2 in our samples. Both antibodies seemed suitable for comparing levels of VAMP2 expression.

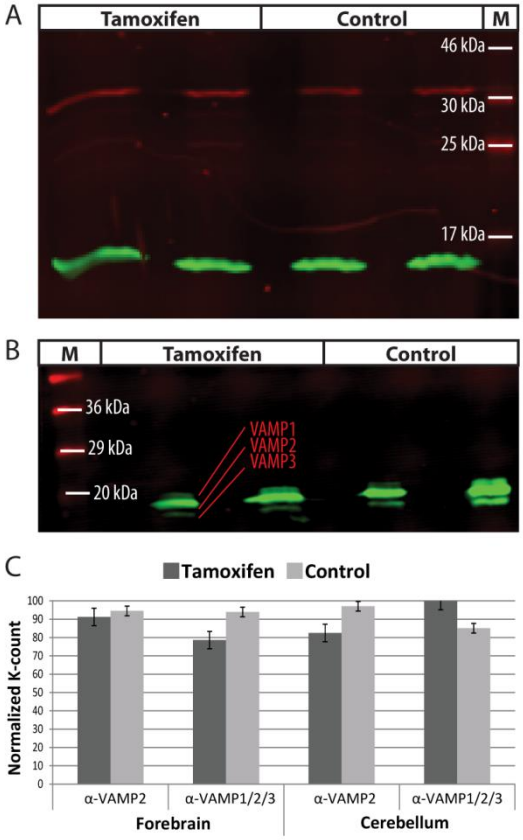

Fig 4.9 – Western blot analysis of VAMP2 expression levels in SLICK-H;Ptox mice

(A) A western blot comparing forebrain homogenates from tamoxifen-treated SLICK-H;Ptox mice (1st and 2nd lanes) and untreated SLICK-H;Ptox mice (3rd and 4th lanes). Anti-VAMP2 is shown in green and α-GAPDH is shown in red. (B) A western blot comparing forebrain homogenates from tamoxifen-treated SLICK-H;Ptox mice (2nd and 3rd lanes) and untreated SLICK-H;Ptox mice (4th and 5th lanes). Anti-VAMP1/2/3 is shown in green. (C) Graph of normalized K-counts comparing five age-matched pairs of tamoxifen-treated SLICK-H;Ptox versus untreated SLICK-H;Ptox mice. Forebrain and cerebellum samples were repeatedly probed using either α-VAMP2 or α-VAMP1/2/3. Mean normalized k-counts for each pair were averaged and graphed as shown. Error bars represent standard error.

In order to quantify VAMP2 expression levels, we repeated the assay using five age-matched pairs of tamoxifen-treated versus untreated SLICK-H;Ptox mice. Each pair was analyzed over several blots, using both antibodies, for both forebrain and cerebellar lysates. We observed average reductions in protein expression in treated versus untreated controls but none of the relationships were significant ($p>0.05$) (Fig 4.6*C*). Moreover, different blots using the exact same samples showed different relationships; sometimes averages showed a reduction in VAMP2 in treated samples, sometimes an increase and sometimes no difference at all. Loading controls usually showed equal levels of protein loading; blots that did not fulfill this requirement were excluded from calculations. In general, we did not detect any significant reduction in VAMP2 expression levels in tamoxifen-treated SLICK-H;Ptox mice versus untreated controls. The same was true in forebrain tissue and cerebellar tissue probed with either α-VAMP2 or α-VAMP1/2/3.

4.1.6.2 *Characterization of VAMP2 expression by immunohistochemistry*

Along with performing western blot analysis, we also used α-VAMP2 to stain SLICK;Ptox brain tissue. Immunohistochemistry (IHC) was performed on vibratome sections of tamoxifen-treated versus untreated SLICK-H;Ptox mice. We did not observe a global reduction in VAMP2 fluorescence, as we would have expected from the behavioral observations in these mice. Moreover, the staining was indistinct and did not resemble the clear punctate staining previously observed in rats (Johnson et al., 2005). The staining also did not colocalize well with SLICK-labeled cells. We wondered whether the punctate staining might be more clearly visible in SLICK-V;Ptox where Cre-mediated recombination is more sparse. We compared treated versus untreated SLICK-V;Ptox staining, and looked for staining in areas like the entorhinal cortex, where projection neurons synapse onto cortical cells (Andersen, 2007) and in the cerebellum where SLICK^{+} mossy fibers synapse onto granule cells (Shepherd, 2004). We observed some VAMP2 staining in the cerebellum but could not detect any obvious reduction in treated versus untreated animals. It is worth noting that staining is so sparse in SLICK-V that this approach might not be the most efficient in finding individual terminals. In summary, we were not able to detect a reduction in VAMP2 in tamoxifen-treated double transgenics compared to untreated controls.

4.2 Discussion

SLICK mice were crossed to RC::Ptox mice and administered the drug tamoxifen in order to induce coexpression of (a) YFP and CreER^{T2} and (b) the fusion protein GFPtox that consists of GFP and the tetanus toxin light chain (TetoxLC). Since the bright YFP labeling in the SLICK system precludes the detection of GFP fluorescence as an indication of GFPtox expression, we instead characterized the mice using several other methods (Table 4.1). We first confirmed by PCR that Cre-mediated recombination occurs in tamoxifen-treated but not untreated SLICK-V;Ptox mice. Next, induction of GFPtox mRNA expression was observed by *in situ* hybridization in several brain regions including the CA1 region of the hippocampus. The sparse GFPtox expression observed was in line with the sparse labeling of neurons in the SLICK-V line. Furthermore, although the available antibodies directed against TetoxLC do not work well for immunohistochemistry, induction of GFPtox protein could be observed by western blotting following immunoprecipitation from brain lysates of tamoxifen-treated SLICK-H;Ptox mice. We could not detect a reduction in VAMP2 expression in tamoxifen-treated mice versus untreated controls. Importantly, however, we observed that SLICK-H;Ptox mice treated with 8-9 doses of tamoxifen show a behavioral phenotype. Taken together, these observations validate SLICK;Ptox as a model in which inducible expression of GFPtox can be achieved in CA1 pyramidal cells of the hippocampus, as well as other brain regions.

Table 4.1 – Characterization summary for SLICK;Ptox mice

RECOMBINATION (confirmed)		
✔	PCR	Clearly shows recombination
	SB	Inconclusive, shows recombination in untreated control
GFPtox EXPRESSION (confirmed)		
✔	ISH	Clearly shows mRNA expression
	WB	Protein levels insufficient for western detection
✔	IP/WB	Shows low levels of GFPtox protein expression
	IHC	Antibodies are not sufficiently sensitive
VAMP2 CLEAVAGE		
	IHC	Antibody staining is blurry
	WB	Shows inconsistent levels in treated vs controls
NT RELEASE		
	FM dye	Problematic to set up
	Electrophysiology	Attempted by our collaborators
PHENOTYPE (confirmed)		
✔	Behavior	Motor defects displayed with high tamoxifen dose

The levels of GFPtox expression in tamoxifen-induced cells of *SLICK-V;RC::Ptox* mice appear to be quite low, although this should not be a hindrance considering that tetanus toxin is a potent synaptic inhibitor that is lethal even at very low doses (Schiavo et al., 2000). In *Aplysia,* for example, 4-10 molecules of tetanus toxin are sufficient to inhibit 50% of neurotransmission within 20 minutes (Schiavo et al., 2000). Accordingly, although we cannot directly detect GFPtox expression within individual cells, expression levels are nonetheless sufficient to elicit behavioral affects in SLICK-H;Ptox mice. In RC::PFtox mice, which are similar to the RC::Ptox mice used in this study, GFPtox cannot be directly detected by GFP fluorescence but is nonetheless sufficient to cleave a significant fraction of VAMP2 and elicit behavioral and electrophysiological effects (Kim et al., 2009). The inability to detect GFPtox in individual cell does, however, poses an inconvenience as we are unable to distinguish between $SLICK^{+}/Ptox^{-}$ and $SLICK^{+}/Ptox^{+}$ neurons.

4.2.1 Recombination in SLICK-H;Ptox

We carried out polymerase chain reaction (PCR) and Southern blot to assess whether or not recombination is possible in tamoxifen-induced SLICK-H;Ptox mice. PCR results clearly indicate that recombination does take place in treated versus untreated mice (n=4), as shown by two primers sets that detect the presence of the recombined transgene in drug-induced mice and one primer set that detects the presence of the un-recombined transgene in all un-induced mice. One tamoxifen-induced mouse did not test positive for the un-recombined transgene. This could be an indication that recombination was higher in this mouse than in the others and that non-recombined DNA was below detection level.

Southern blot was performed with the intention to quantify the relative levels of recombination in SLICK-H;Ptox mice compared to SLICK-H;R26R mice. Results are inconclusive for two reasons: (1) the sensitivity of our assay was very weak and (2) a band that should represent the recombined transgene was observed very faintly in untreated controls. The sensitivity issue could arise from the probe and perhaps designing another could increase detection of the recombined transgene. Alternatively, lack of sensitivity could have resulted from poor sample quality. The recombination band observed in untreated controls could be a sign of (a) contamination in our samples, (b) background produced by our probe, or (c) leaky recombination in untreated controls. Judging by the fact that the wild-type sample did not show any trace of this band, it seems more likely that our untreated samples were either contaminated or that the band indicates leaky recombination

in these mice, although this is not expected based on the data in Chapter 2 showing tight control of recombination in the SLICK-H line.

4.2.2 GFPtox mRNA expression in SLICK-H;Ptox and SLICK-V;Ptox

We used *in situ* hybridization (ISH) to evaluate mRNA expression of the GFPtox transgene. SLICK-H;Ptox mice, which exhibit widespread SLICK expression, showed clear widespread staining in treated versus untreated controls. The pattern of mRNA expression we detected is similar that of SLICK-H crossed to the reporter line ROSA26, although staining is not as abundant. The pattern and abundance of mRNA staining is even more similar to the immunostaining of GFPtox protein observed by Dr. Jun Chul Kim in RC::Ptox mice crossed to the CamKIIα -Cre line (Fig 4.10, unpublished data provided by Dr. Jun Chol Kim)

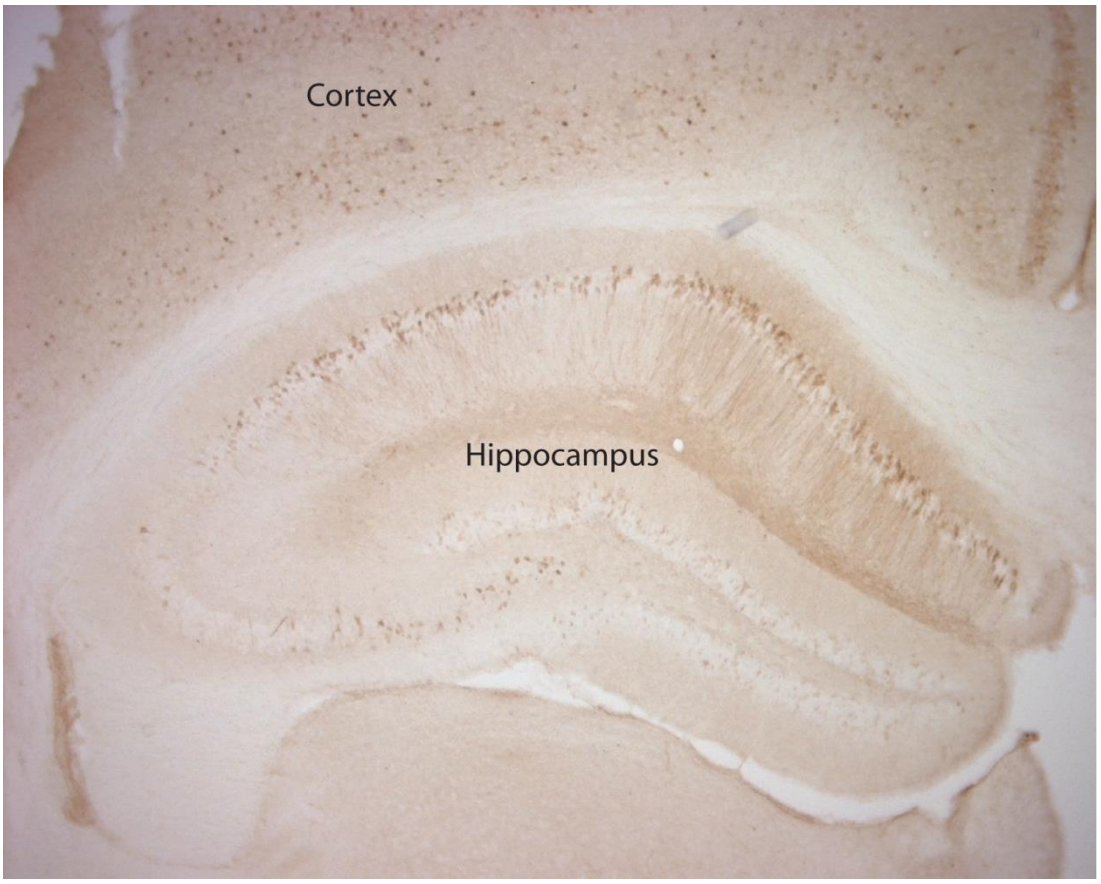

Figure 4.10 – GFPtox detection in tamoxifen-treated CaMKIIα;Ptox mice
Unpublished data provided by Dr. Jun Chol Kim, Harvard University
Since GFP fluorescence was not readily detectable in these mice, 3,3'-diaminobenzidine (DAB)-staining was instead used to detect GFPtox expression. Expression levels in the hippocampus and cortex of tamoxifen-treated double transgenic mice are shown.

In SLICK-V;Ptox, which has sparse SLICK expression, we observed a very small number of cells labeled in the hippocampus, brainstem and midbrain, but not in the cortex, thalamus, cerebellum or amygdala. Although the number of GFPtox^{+} cells that we found in these treated double-transgenic mice is far fewer that the number of YFP cells labeled in SLICK-V mice, we suspect that we are only detecting cells with the most robust GFPtox expression.

We do not know why SLICK-H;Ptox and SLICK-V;Ptox show reduced expression of GFPtox compared to the amount of cells that express the SLICK transgene itself. Since GFPtox is targeted to the ROSA locus, we should expect recombination to occur with the same frequency as in SLICK;R26R. Technical problems, although possible, do not seem likely in light of the many optimizations that we attempted, including new probe designs and higher tamoxifen doses. It seems more likely that the ISH is not sensitive enough to detect neurons with very low levels of tetanus which, as mentioned already, would be sufficient to inhibit neurotransmitter release in these cells. We suspect that we have only detected cells with very robust expression of GFPtox and these are only a small proportion of the total number of cells that actually express the protein.

4.2.3 GFPtox protein expression in SLICK-H;Ptox

We examined GFPtox protein expression by western blot, by immunoprecipitation followed by western blot, and by immunohistochemistry (IHC). We used three antibodies raised against the light chain of tetanus toxin, as well as an antibody against GFP. Western blotting was not sensitive enough to detect any expression, whereas IHC showed excessive unspecific labeling. We were able to detect GFPtox expression only by pooling together three whole-brain lysates of treated SLICK-H;Ptox mice (administered with an elevated dosage of tamoxifen) and then immunoprecipitating them to concentrate the protein. These data indicate that toxin levels in tamoxifen-induced SLICK;Ptox mice are quite low. Considering the previously described efficiency of tetanus toxin at low levels, however, this should not hinder the efficiency of the model (Schiavo et al., 2000). Moreover, since very low levels of GFPtox in a cell would be difficult to detect, there are probably many cells expressing GFPtox at levels below the detection threshold of our assays, particularly immunohistochemistry.

Further studies to concentrate tetanus-expressing cells could include isolation of YFP-labeled cells in SLICK-V;Ptox by fluorescence activated cell sorting (FACS) or laser capture

microdissection. These isolated cells could then be used for quantitative assays like real-time polymerase chain reaction (qPCR), to determine what proportion of SLICK^{+} cells express GFPtox. Since we currently cannot detect GFPtox directly in individual cells, this information would at least allow us to determine what percentage of cells express TetoxLC.

4.2.4 Behavioral observations in SLICK-H;Ptox

We observed a behavioral phenotype in SLICK-H;Ptox mice administered with 8-9 doses of tamoxifen (n=10). The defects in motor coordination are similar, although less pronounced, than those observed by Kim et al in RC::PFtox mice crossed to the Math1-Cre line (Matei et al., 2005). The reduced prominence of motor coordination defects in our double transgenics is likely due to the fact that SLICK-H exhibits low recombination rates in the cerebellum (refer to Chapter 2) whereas Math1-Cre has robust recombination efficiency in this area (Matei et al., 2005). Since expression of TetoxLC in the cerebellum, which exhibits low recombination rates in SLICK-H mice, is sufficient to produce a phenotype, we assume that TetoxLC expression is even higher in other areas of the brain like the cortex and hippocampus. In any case, the observed phenotype suggests that despite our difficulty detecting the GFPtox protein, TetoxLC expression is sufficient to inhibit neurotransmission in a significant proportion of cells.

4.2.5 VAMP2 expression in SLICK-H;Ptox

Having detected minute levels of GFPtox protein, as well as a behavioral phenotype in SLICK-H;Ptox mice, we examined VAMP2 protein expression using western blot and immunohistochemistry. Reduced expression of VAMP2 in tamoxifen-induced mice would indicate successful GFPtox expression and translocation from the cell body to the presynaptic terminal and subsequent proteolysis of the SNARE complex.

Using two different antibodies for the western blot, we were not able to detect any consistent VAMP2 reduction in tamoxifen-treated SLICK-H;Ptox (n=5). One of these antibodies, α-VAMP2, is widely used for confirming tetanus-mediated cleavage of the protein, and should therefore be adequate for our study (Yu et al., 2004, Kim et al., 2009). Considering that our samples resulted in inconsistent relative expression levels across several blots, we suspect that we are faced with a systematic technical problem rather than a true indication of uniform expression in treated versus untreated mice.

We were likewise not able to detect a loss of VAMP2 fluorescence through immunohistochemistry (n=3). In the case of IHC, however, α-VAMP2 has not been characterized or used as widely in mouse tissue. Although staining in rat tissue produces clear punctate staining of VAMP2 in pre-synaptic terminals (Johnson et al., 2005), staining in our mouse tissue appears more diffuse. This would render the approach inadequate for looking at specific terminals in SLICK-V;Ptox mice. As for SLICK-H;Ptox mice, however, it should have been possible to detect a global loss of VAMP2 in treated transgenics. This reduction should be similar in proportion to the amount of GFPtox labeling observed with *in situ* hybridization.

We are not sure why we were not able to detect a decrease in VAMP2 levels in tamoxifen-induced SLICK-H;Ptox mice. We suspect that technical complications are a likely factor influencing our results for both assays. Also, although the SLICK lines have been shown to display tight control of recombination in the absence of tamoxifen administration, it is possible that SLICK;Ptox do experience leaky recombination. This could result in irregular data considering our small sample sizes. Southern blot data showing "recombination" in untreated controls could support this suggestion. Finally, it is possible that a small amount of cleaved VAMP2 is exerting a dominant negative effect on uncleaved VAMP2. Considering (a) the successful reduction of VAMP2 in RC::PFtox mice when crossed to several other Cre-expressing lines (Kim et al., 2009), (b) the efficiency of recombination in the SLICK lines, and (c) our detection of GFPtox expression and behavioral observations, it seems unlikely that VAMP2 expression is genuinely not reduced in treated SLICK-H;Ptox mice.

4.2.6 Further studies

Our data present reassuring evidence that the GFPtox protein is expressed in SLICK;Ptox mice, although we have not yet been able to confirm an effect on VAMP2 expression levels. We attempted to clarify our results by using FM stryryl dyes to study exocytosis but found the technique problematic and were not able to obtain clear staining of vesicles. We were able to visualize the dye in cell cultures treated with AM-65 but not in wild-type tissue.

We are now collaborating with Dr. Mark Rea of the Physiology Department at UCC to carry out electrophysiological studies in SLICK-V;Ptox mice. His laboratory will, among other studies mentioned in Chapter 5, measure synaptic input to muscle fibers innervated by $SLICK^{+}$ axons (labeled brightly with YFP) in treated versus untreated SLICK-V;Ptox mice. He

will also compare these measurements to wildtype terminals in SLICK-V single transgenic mice to determine whether there is in fact leaky recombination in untreated double transgenics. Muscle fibers in treated SLICK-V;Ptox mice should suffer reduced synaptic input compared to cells in untreated and wild-type controls. If successful, these studies will determine conclusively whether GFPtox expression in SLICK;Ptox mice leads to effective inhibition of neurotransmission.

Chapter 5 Analysis of dendritic spines in single-neurons inhibited with tetanus toxin

5.1 Results

We conditionally suppressed neurotransmission in a small subset of neurons and investigated the effect that this has on synaptic inputs to individual cells. Burrone and colleagues had shown that cultured hippocampal neurons whose activity has been suppressed by Kir2.1 overexpression exhibit a competition-dependent reduction in dendritic spine density and mEPSC frequency (Burrone et al., 2002). Based on these and other results, we examined dendritic spine density and morphology in a small subset of CA1 hippocampal neurons.

5.1.1 Experimental Design

In order to suppress neuronal activity in a small subset of cell, we crossed the $CreER^{T2}$-expressing SLICK-V line to the *RC::Ptox* line, which conditionally expresses TetoxLC (characterized in Chapter 4). Double transgenic mice treated with tamoxifen should exhibit YFP labeling in small subsets of pyramidal neurons that simultaneously express the tetanus toxin light chain and therefore display reduced ability to release neurotransmitter signals. Since the Thy1 promoter used in SLICK is developmentally expressed and generally produces optimal expression after 6 weeks postnatal, this study is of the adult mouse brain, ages 4-7 months.

Male SLICK-V;Ptox mice aged 6-10 weeks were administered ten doses of tamoxifen and then rested for two months or more. We used two control groups for this study; the first is untreated SLICK-V;Ptox mice used to compare induced versus un-induced transgenic cells, and the second is tamoxifen-treated $Ptox^{-}$/SLICK-V^{+} mice that will control for any effects caused by drug delivery. Tamoxifen is a modulator of estrogen receptors and has been shown to alter dendritic spine density in CA1 pyramidal neurons of male rats (Gonzalez-Burgos et al., 2012). Both controls are sex and age matched in most cases (Table 5.1*B*). For clarity, the three treatment groups, (1) tamoxifen-treated SLICK-V;Ptox, (2) untreated SLICK-V;Ptox, and (3) tamoxifen-treated SLICK-V, are color coded and referred to in this chapter as VP-tmx (in red), VP-ctrl (in blue) and V-tmx (in green) respectively. We performed eight

trials, each of which includes one mouse from each treatment group. Imaging, data analysis and quantification were performed under blinded conditions.

5.1.2 Strategy for cell and dendritic segment selection

Since we do not know the rate of recombination in treated SLICK-V;Ptox, nor the extent of leaky recombination (if any) in untreated SLICK-V;Ptox controls, we decided to analyze multiple cells per animal. CA1 hippocampal neurons were chosen based on overall brightness of the cell body and preference was given to cells whose dendritic branches ran parallel to the surface of the section (filaments will then lie in the x/y plane of the z-stack and therefore exhibit better resolution). Where possible, we avoided cells that were very close to the subiculum or to the CA2.

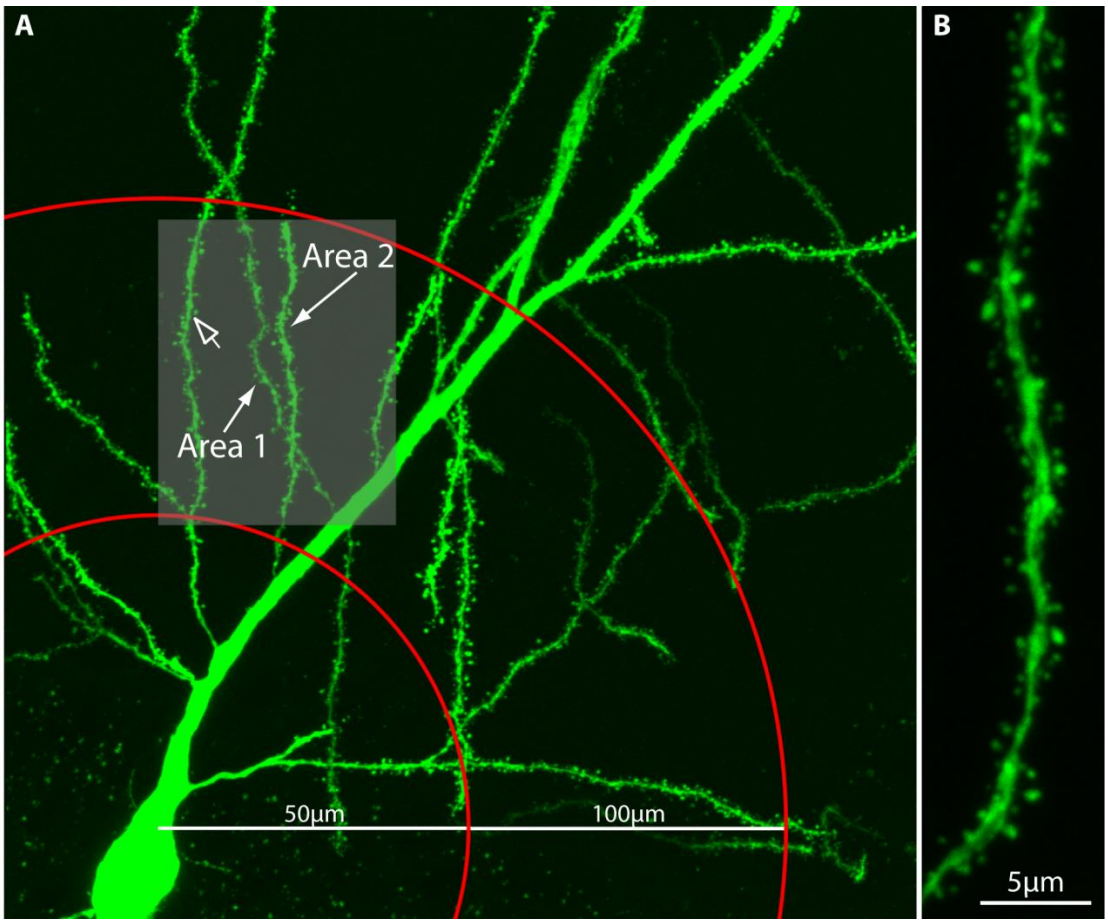

Figure 5.1 – Strategy for selecting dendritic branch segments of CA1 pyramidal cells
(A) Using the cell body as the center, we drew two circles with radii of 50 and 100 µm using the Zen Imaging Software (Zeiss, UK). For each cell we chose two primary branch segments that fell between the two circles (shown as "Area 1" and "Area 2" with arrow). We did not select bifurcated branches (open arrow). Once selected, a 3.5X optical zoom was applied for imaging (shaded box, to scale). (B) Example of a dendritic segment z-stack of ~8 µm in thickness.

Within each cell, we only analyzed primary branches of the main apical dendrite; higher order branches were avoided for consistency (Fig 5.1*A*). These were always approximately 50-100 µm from the pyramidal cell layer. Two to three different branch segments per cell were imaged at 63X with an additional 3.5X optical zoom (Fig 5.1*B*). In total, we documented approximately 70-120 µm of dendrite length per cell, averaging out to about 450 µm per animal (Table 5.1). These images were then analyzed using the Filament Tracer module in Bitpane Imaris software. We focused on spine number and spine length. Including all three treatments groups, we counted a total of 21,391 spines over a total dendritic length of 11,188 µm.

5.1.3 Dendritic spine density and length in tamoxifen-treated SLICK-V;Ptox

Since we do not know whether recombination is high in VP-tmx or whether VP-ctrl experiences any leaky recombination, a nested statistical approach most appropriately fits our experimental design because it takes into account variation between cells of a single animal. In order to obtain mean spine densities using a nested design, we grouped all of the cells for each treatment group and directly calculated an average (as opposed to averaging cells within each mouse and then averaging the mice within a treatment group). Using the nested approach we obtained mean spine densities for VP-tmx, VP-ctrl and V-tmx of 1.696 (n=39 cells), 1.990 (n=40 cells), and 2.088 (n=42 cells), respectively (in spines/µm) (Table 5.1). Mean spine lengths for VP-tmx, VP-ctrl and V-tmx were 0.800 µm (n=39 cells), 0.756 µm (n=40 cells), and 0.807 µm (n=42 cells), respectively (Table 5.1). Further information for each trial, including age and mean spine density and length for each mouse, is provided in Table 5.1.

For spine density, general significance between the three treatment groups was obtained using a mixed-model nested ANOVA ($p<0.05$). This was followed by three post-hoc tests that revealed that the observed reduction in spine density in VP-tmx mice is significant compared to both controls ($p<0.05$) (Table 5.2). A nested analysis of our data produces a more conservative p-value than a one-way ANOVA or individual Student T-tests (see section 5.2.2 for further discussion). Differences in spine length were not significant according to both a mixed model nested ANOVA and a one-way ANOVA.

Table 5.1 – Additional information for each treatment group and animal analyzed

GRAND TOTAL Nested and organized by treatment group	Total Cells Analyzed	Total Dendrite Length Analyzed (µm)	Mean Spine Density (spines/µm)	Mean Spine Length (µm)
Tamoxifen treated SLICK-V;Ptox	39	3607	1.696	0.800
Untreated SLICK-V;Ptox	40	3782	1.990	0.756
Tamoxifen treated SLICK-V	42	3799	2.088	0.807

Animal	Gender	Age Dosed (weeks)	Weeks rested	Age Killed (mo)	Total Cells Analyzed	Total Dendrite Length Analyzed (µm)	Mean Spine Density (spines/µm)	Mean Spine Length (µm)
Trial 1								
VP-tmx	♂	7	11	5	6	488	1.616	0.839
VP-ctrl	♂	/	/	5	6	602	1.566	0.810
V-tmx	♂	9	6	4	7	556	2.317	0.812
Trial 2								
VP-tmx	♂	7	12	5	5	484	1.794	0.928
VP-ctrl	♂	/	/	5	7	490	2.057	0.781
V-tmx	♂	10	7	5	5	407	2.310	0.919
Trial 3								
VP-tmx	♂	6	15	6	5	452	1.770	0.779
VP-ctrl	♂	/	/	5	5	592	1.636	0.642
V-tmx	♂	10	8	5	5	490	2.050	0.714
Trial 4								
VP-tmx	♂	7	14	6	7	605	1.574	0.779
VP-ctrl	♂	/	/	4	5	505	2.540	0.812
V-tmx	♂	6	9	4	6	468	2.021	0.825
Trial 5								
VP-tmx	♂	10	15	7	5	515	1.347	0.706
VP-ctrl	♂	/	/	6	6	429	1.591	0.756
V-tmx	♂	10	15	7	5	419	1.589	0.807
Trial 6								
VP-tmx	♂	10	17	7	5	490	2.119	0.876
VP-ctrl	♂	/	/	7	5	497	2.491	0.808
V-tmx	♂	9	17	7	6	583	1.973	0.770
Trial 7								
VP-tmx	♂	6	18	6	3	311	1.656	0.728
VP-ctrl	♂	/	/	7	3	376	2.113	0.585
V-tmx	♂	6	18	6	3	292	2.193	0.715
Trial 8								
VP-tmx	♀	9	20	7	3	262	1.773	0.696
VP-ctrl	♀	/	/	7	3	290	2.201	0.768
V-tmx	♂	6	9	4	5	585	2.203	0.850

Overall, VP-tmx mice show a 15% and 19% decrease in spine density compared to VP-ctrl and V-tmx, respectively (Fig 5.2*A*), whereas spine length appears to be unaffected (Fig 5.2*B*). VP-tmx compared to V-tmx is more significant than VP-tmx compared to VP-ctrl. A closer look at individual measurements also revealed that VP-ctrl mice exhibit greater variation than VP-tmx or V-tmx at the level of cells (Fig 5.3*B*) and of animals (Fig 5.3*A*). This is demonstrated by a larger 95% confidence interval for both nested (Fig 5.3*B*) and non-nested (Fig 5.3*A*) datasets, as well as by uneven variance components calculated by the mixed-model nested ANOVA.

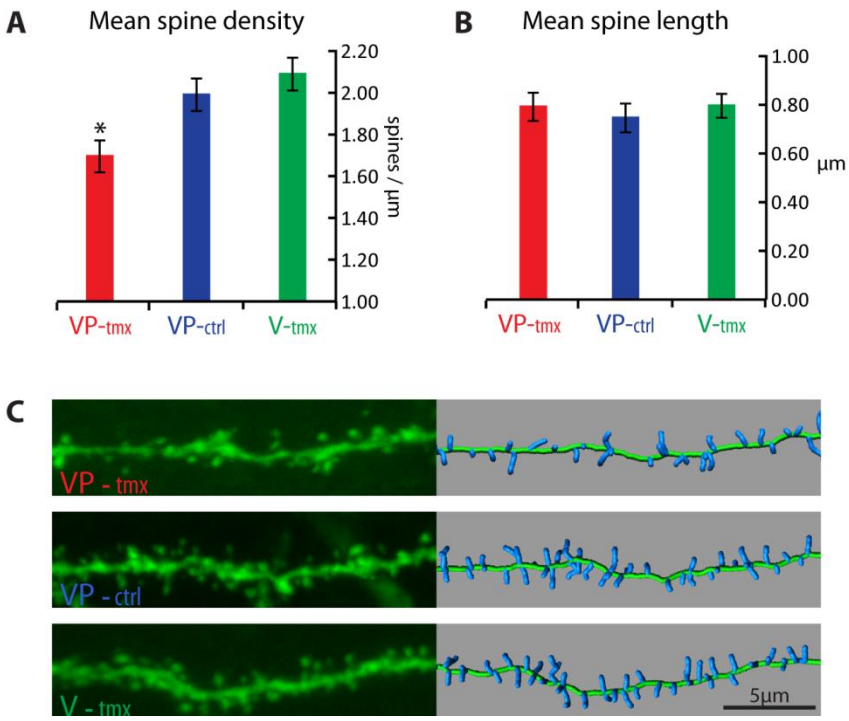

Figure 5.2 –Mean spine density and mean spine length

(A) Graph of mean spine densities. Error bars represent Gabriel's confidence intervals, a statistical test that indicates significance ($p<0.05$) when intervals do not overlap. An asterisk shows the treatment group that is significantly reduced. (B) Graph of mean spine length. Error bars represent 95% confidence intervals. (C) Representative dendritic segments for the three treatment groups. The left panel shows confocal projections and the right panel shows the 3D representations used for quantification. Spine densities of the segments shown are 1.6919, 1.990, and 2.0973 spines/µm, respectively for VP-tmx, VP-ctrl and V-tmx.

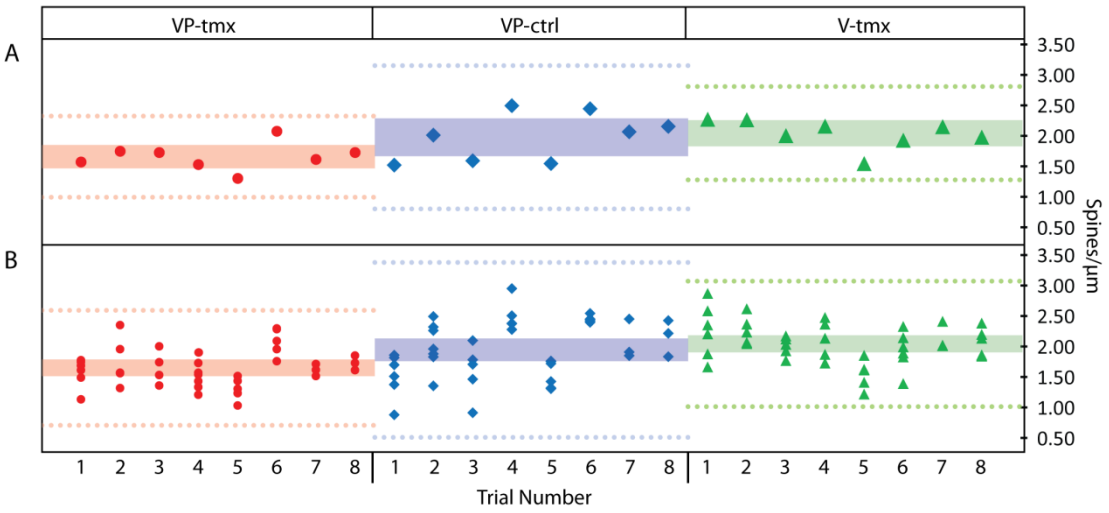

Figure 5.3 – Mean spine densities for animals and for cells; organized by trial number

(A) Scatter plot of mean spine densities obtained by averaging cell means for each animal. Shaded area represents 95% confidence interval (CI) and dotted line represents one standard deviation. Red dots, blue diamonds and green triangles indicate VP-tmx, VP-ctrl and V-tmx mice respectively. This un-nested approach is misleading as it does not acknowledge the possibility of differential expression of TetoxLC in each cell (B) Scatter plot of mean spine densities for each cell analyzed. Clustered dots, diamonds or triangles indicate the cells analyzed for each animal within each corresponding treatment group.

Thus, as demonstrated by a nested ANOVA and three post-hoc tests of mean comparisons, our results clearly show a reduction in spine density in tamoxifen-treated SLICK-V;Ptox compared to untreated SLICK-V;Ptox (15%) and compared to treated SLICK-V (19%). Representative dendritic segments for each treatment group show that this reduction is visually apparent (Fig 5.2 *C*-*E* and *C'*-*E'*). Our results also show that average spine length is not affected in tamoxifen-treated SLICK-V;Ptox compared to controls.

5.2 Discussion

Using a technique that conditionally inhibits neurotransmission in a small subset of YFP-labeled CA1 pyramidal neurons we found that apical spine density is decreased by 15%-19% in cells that express the tetanus toxin light chain. This reduction is apparent in adult VP-tmx mice, double transgenics that have been treated with the drug tamoxifen in order to induce recombination of the GFPtox transgene. The reduction is statistically significant ($p<0.05$, $n=8$) when compared to VP-ctrl mice (un-induced double transgenics), as well as to V-tmx mice (tamoxifen-treated $Ptox^{-}$/SLICK-V^{+}). Significance is obtained using both a nested approach (mixed-model nested ANOVA and three post-hoc tests) and a non-nested approach (one way ANOVA or two tailed t-tests). Spine length does not appear to be altered in tamoxifen-treated SLICK-V;Ptox mice compared to either control. The observed reduction in apical spine density of single tetanus-expressing cells is further discussed in Chapter 6, General Discussion.

5.2.1 Spine length stability in tamoxifen-induced SLICK-V;Ptox mice

Spine length in the apical dendrites of CA1 pyramidal neurons does not appear to be altered in response to neuronal silencing. We investigated this property because it is one possible way in which a cell could compensate for a reduction in the total number of spines at its disposal. Since longer/thinner spines can undergo LTP more readily (Matsuzaki et al., 2004), this homeostatic change would allow the remaining synapses to become more plastic. Further studies should include an investigation of spine shape; since spine morphology is closely related to synaptic function (Lee et al., 2012), knowing whether a certain type of spine shape is preferentially eliminated or maintained could provide insight into the mechanisms for spine density reduction. In terms of molecular parameters, synaptic scaling of AMPARs (Gainey et al., 2009) or NMDARs (Rao and Craig, 1997) in remaining spines should also be investigated as they could point to homeostatic compensatory mechanisms (Turrigiano, 2011).

5.2.2 Statistical Analysis

5.2.2.1 *Mixed-model nested ANOVA*

Because we do not know the recombination rate for VP-tmx, or the extent of leaky recombination in VP-ctrl, variation in our data could occur on three levels: across treatment groups, across animals within a group, or across cells within an animal. A nested ANOVA, which takes into consideration such variation, is therefore the most appropriate statistical test for our design. This test gives a p-value indicating significance between treatment groups and also provides a variance component indicating which level produces the most variation (MacDonald, 2009, Picquelle and Mier, 2011). "Mixed-model" indicates that the difference between treatment groups is inherently interesting as opposed to a design where first-level groups represent samples within a population (MacDonald, 2009). A nested analysis of our data produces a more conservative p-value than a single ANOVA or individual Student T-tests, reassuring us that significance is genuine. Values were adjusted for uneven sample sizes (n=39, 40, and 42 cells for VP-tmx, VP-ctrl and V-tmx respectively).

5.2.2.2 *Post-Hoc tests comparing group means*

Following a significant result from the nested ANOVA, we performed three post-hoc tests to determine which groups are significantly different from each other. Using Dunnett's T-test, Tukey's standardized range and Gabriel's comparison intervals, we compared the means of VP-tmx versus VP-ctrl and of VP-tmx versus V-tmx. All three algorithms are similar to a Student's T-test, except that they are more conservative because they adjust for the fact that increasing the number of comparisons also increases the probability of falsely rejecting the null hypothesis (Sokal and Rohlf, 1995, Zar, 1999, MacDonald, 2009).

Dunnett's T-test, which is designed to compare one reference group against all others, is the test most appropriate for our experimental setup (Ludbrook, 1998). A typical example of this design is a single placebo being compared to several new drugs. In our case, a single experimental condition is being compared to two controls in a two-tailed fashion. Tukey's T-test is similar except that it allows for multiple comparisons to be made without the need for a particular reference group (Ludbrook, 1998). When sample sizes are unequal, this test is especially conservative (Ludbrook, 1998). Gabriel's comparison intervals is similar to Tukey's test except that significance is displayed by comparison limits (similar to a confidence interval) (Gabriel, 1978). When the intervals for two group means do not overlap, the relationship is considered significant (Gabriel, 1978). We used this method because it is

practical for presenting significance in graphical form (Fig 5.2*A*). In summary, Dunnett's T-test is the most relevant to our experimental design, whereas Tukey's T-test is the most conservative. Both of these, along with a third test that plots significance on a graph, show that the spine density reduction in VP-tmx is significant compared to both controls.

5.2.2.3 *Unequal distribution of variance could indicate leaky expression in SLICK;Ptox mice*

The nested ANOVA comparing the three treatment groups revealed that variation at the level of cells and animals is greater than at the level of treatment groups. Individual nested ANOVAS (comparing VP-tmx to each control separately), revealed that this unequal distribution of variance occurs when VP-tmx is compared to VP-ctrl but not when it is compared to V-tmx. This suggests that a greater variation occurs among cells of untreated SLICK-V;Ptox mice. This is consistent with the fact that this group, when averaged using either a nested or non-nested approach, has a higher standard deviation and confidence interval than the other two. This variation is evident at the level of animals (Fig 5.3*A*) and at the level of cells (Fig 5.3*B*).

Variation among the cells from the same animal could be due to some percentage of leaky recombination in untreated SLICK-V;Ptox mice. Although this is not fully substantiated by our data in Chapter 4 (we did not, for instance observe leaky recombination in the *in situ* assays; Figs 4.3 & 4.4), it could partially account for the results of the Southern blot, where a band for recombined DNA appears weakly in un-treated controls (Fig 4.2). Our difficulty detecting a reduction in VAMP2 expression through western blotting (Fig 4.9) could also have been partially confounded by leaky expression in VP-ctrl considering our small sample size. Finally, the fact that variation does not seem to be significant among cells of tamoxifen-treated SLICK-V;Ptox suggests that these mice exhibit a high rate of recombination.

Chapter 6 General Discussion

In this thesis we have characterized in detail two transgenic mouse lines that facilitate the study of neuronal circuits by allowing conditional genetic manipulations to be triggered in fluorescently labeled pyramidal neurons throughout the central and peripheral nervous system. SLICK-H (Chapter 2 & Section 6.1.1) can be crossed to any Cre-*loxP* driven mouse line to induce widespread conditional neuron-specific genetic manipulation. SLICK-V::Ptox (Chapters 4 - 5 & Sections 6.1.2 - 6.2) conditionally inhibits neurotransmission in a small subset (<1%) of YFP-labeled pyramidal cells due to the inducible expression of TetoxLC (the tetanus toxin light chain). In Chapter 3 we also describe the attempt to create two additional Cre-driven mouse lines that would allow conditional expression of either the potassium channel Kir2.1 or of TetoxLC. Finally, in Chapter 5 we use SLICK-V::Ptox mice to show that single neurons whose neurotransmission is disrupted by TetoxLC experience a 15% - 19% decrease in apical spine density compared to wildtype neurons (Section 6.2).

The tools presented in this thesis directly address the outstanding biological questions in the field of neuroscience today. SLICK-V::Ptox in particular, which allows single cells to be conditionally inhibited in an otherwise wildtype environment, greatly facilitates the study of activity-dependent competition. Extreme manipulations of this sort are instrumental in deciphering the mechanisms by which the normal brain synchronizes activity within and among circuits and how a disruption in this activity can lead to disease.

6.1 Novel mouse models for the study of neuronal circuits

6.1.1 SLICK-H mice for pan-neuronal Cre-mediated inducible recombination

We have cataloged in detail the transgene expression patterns and recombination efficiencies in SLICK-H mice, a transgenic line that facilitates widespread inducible conditional genetic manipulation within most populations of projection neurons. Using two back-to back copies of the Thy1.2 promoter cassette, SLICK-H mice co-express robust and relatively uniform levels of $CreER^{T2}$ (a drug-inducible form of Cre recombinase) and YFP throughout the peripheral and central nervous system. This allows for efficient induction of Cre-mediated genetic manipulation upon tamoxifen administration in fluorescently labeled neuronal populations in adult mice. Importantly, Cre activity in the absence of tamoxifen is minimal, permitting tight control of recombination.

Compared to other available neuron-specific "Cre driver" lines, SLICK-H displays a more widespread transgene distribution, superior control of recombination in the absence of tamoxifen, higher recombination efficiency upon drug administration and higher tissue and cell-type specificity. SLICK-H mice thus offer significant advantages over currently available inducible Cre recombinase lines (discussed in Section 2.3.2), and make the SLICK-H line highly suitable for functional genomic analysis of behavioral and other neuronal phenotypes in adult mice. SLICK-H transgenic mice are available from The Jackson Laboratory.

6.1.2 SLICK-V/Ptox mice for single-cell silencing

We crossed the SLICK-V line, which expresses robust levels of $CreER^{T2}$ and YFP in very sparse populations of projection neurons (<1%) throughout the nervous system, to the RC::Ptox line, which conditionally expresses TetoxLC (Young et al., 2008, Kim et al., 2009). Double transgenic mice thus contain single fluorescent projection neurons in which pre-synaptic neurotransmitter release (and possibly post-synaptic dendritic exocytosis) is inhibited. Detailed characterization of this model confirmed that Cre-mediated recombination takes place, and that TetoxLC mRNA and protein are expressed. Importantly, we observed an ataxic behavioral phenotype similar to that seen when RC::PFtox mice are crossed to other Cre-expressing lines. Although we were not able to detect a reduction in VAMP2, whose TetoxLC-mediated cleavage causes inhibition of neurotransmitter release, we suspect that this is either due to inaccurate detection of VAMP2 levels, or to a dominant negative effect

caused by a small amount of cleaved VAMP2 (discussed in Section 4.2.5). In any case, all other lines of evidence suggest that this model is fully functional.

This model is a useful tool for studying cellular processes that are shaped by activity-dependent competition. As an initial application, for example, we used these mice to observe *in vivo* whether dendritic spine density is reduced in single-suppressed cells, as is observed in cultured hippocampal cells (Burrone et al., 2002), discussed below. This model could also be widely applicable, for example, to the study of guidance molecules that govern axonal and dendritic growth and refinement.

6.2 Spine density reduction in tamoxifen-expressing projection neurons

Our results in Chapter 5 show that when tetanus toxin is expressed in a small subset (<1%) of CA1 neurons in the adult mouse hippocampus, these cells have difficulty maintaining excitatory post-synaptic connections. This is evidenced by a 15%-19% spine density reduction on apical dendrites. Since the tetanus toxin light chain cleaves v-SNARE proteins, it inhibits neurotransmitter release pre-synaptically and possibly inhibits activity-dependent dendritic exocytosis. This raises the question as to which of these is responsible for the observed loss of synaptic connectivity. Both possibilities are discussed in the next two sections.

6.2.1 Reduced spine density as a result of inhibiting dendritic exocytosis

The most straightforward explanation for the observed reduction in dendritic spine density is that TetoxLC cleaves a v-SNARE protein present in dendrites and thereby inhibits Ca^{2+}-dependent dendritic exocytosis. While not as extensively studied as presynaptic vesicle fusion, the ability of clostridial neurotoxins to block regulated dendritic exocytosis implicates SNARE proteins in some forms of synaptic plasticity. SNAP-25 and syntaxin-4, for example, are known to be involved in calcium-dependent dendritic exocytosis (Lau et al., 2010, Kennedy et al., 2010). Regulated dendritic exocytosis is essential for the secretion of retrograde signaling molecules, dendritic neurotransmitter release and the delivery of neurotransmitter receptors to synapses during synaptic plasticity (Kennedy and Ehlers, 2011).

The evidence for VAMP2 involvement in dendritic exocytosis is promising but not entirely clear. VAMP2 is localized in the somatodendritic compartment of spiny dopaminergic neurons of the substantia nigra (Witkovsky et al., 2009) and botulinum toxin B, which cleaves VAMP2, reduces somatodendritic dopamine release in cultured dopaminergic neurons (Fortin et al., 2006). Dopamine release, however, is not inhibited *in vivo* by tetanus neurotoxin in the substantia nigra or the striatum (Bergquist et al., 2002). Importantly, TetoxLC has been shown to inhibit calcium-dependent dendritic exocytosis in cultured hippocampal neurons (Maletic-Savatic and Malinow, 1998) and to block LTP-associated membrane insertion of AMPA-type glutamate receptors (Lu et al., 2001). A study conducted in cultured hippocampal neurons found that VAMP2 is trafficked to both the axon and

dendrites but is endocytosed from the dendritic membrane and subsequently transported back to the axon (Sampo et al., 2003). This roundabout delivery to the axon may allow VAMP2 to be transiently active in the dendrite (Kennedy and Ehlers, 2011).

If VAMP2 is indeed present and active in dendrites, TetoxLC could inhibit Ca^{2+}-dependent dendritic exocytosis that is required for LTP (Lledo et al., 1998). Over time, the blockade of LTP-associated exocytosis of AMPA-type glutamate receptors to the synaptic membrane (and possibly other synaptic components) could lead to structural changes and ultimately the loss of dendritic spines. For example, perturbation of LTP induction through genetic deletion of NMDA-type glutamate receptor subunits decreases spine density (Brigman et al., 2010). Our observations would suggest that blocking exocytosis – a much later step in the LTP pathway – is sufficient to lead to spine loss *in vivo*. This would agree with findings that exocytosis of AMPA receptors is required for the maintenance of LTP-associated spine growth in hippocampal slice preparations (Kopec et al., 2007, Yang et al., 2008).

6.2.2 Reduced spine density as a result of inhibiting neurotransmitter release

Although less direct, it is also possible that presynaptic inhibition alone is somehow responsible for shaping postsynaptic connectivity within the same cell. Do the axons and dendrites of an individual cell act in response to each other? Is there a mechanism, either permissive or instructive, by which presynaptic partners avoid postsynaptic partners whose axons cannot efficiently relay information? Thinking in terms of a whole circuit, synapsing onto a "silent" cell seems like a waste of resources and it does not seem far-fetched that neurons are equipped with ways to prevent this. In a three-cell chain, as shown in Figure 6.1, one could hypothesize that a postsynaptic retrograde messenger from cell C affects the ability of dendrites from cell B to form or maintain synapses with cell A. For example, (1) a retrograde messenger such as a neurotrophin is secreted by the postsynaptic membrane of cell C and (2) travels retrogradely via the axon to the nucleus of cell B where it (3) regulates gene transcription for postsynaptic proteins required in synapse formation or maintenance. If presynaptic activity is inhibited in cell B, and retrograde messengers from cell C are not received, transcription of essential postsynaptic proteins in cell B could be downregulated. This would reduce the ability of dendritic spines on cell B to maintain synapses or to form new ones. Such hypothetical molecular circuits could help to ensure optimal wiring of the brain.

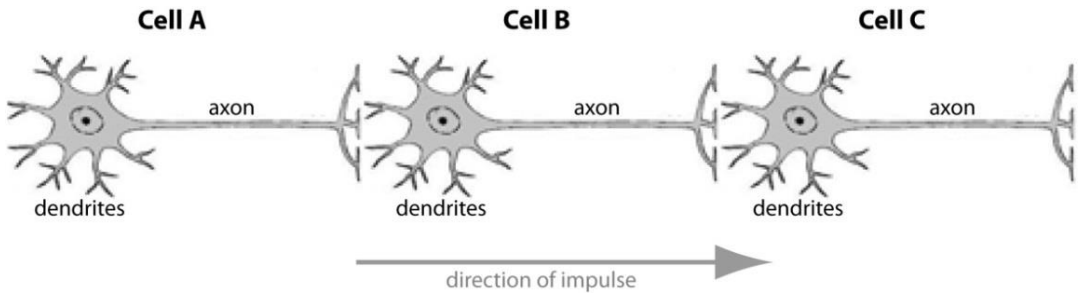

Figure 6.1 – Schematic diagram of three interconnected cells

6.2.3 Relevance to dendritic activity-dependent competition

In terms of activity-dependent competition, our results relate to previous work in two ways. Firstly, they complement studies showing that long-term inhibition of synaptic release in small subsets of cells produces activity-dependent reductions in synaptic inputs, as well as axonal misguidance and reduced axonal arborization (Burrone et al., 2002, Buffelli et al., 2003, Yu et al., 2004, Hua et al., 2005, Yasuda et al., 2011). This is in contrast to global inhibition of synaptic release, where cells do not experience such alterations. A study by Burrone et al (2002) showed that small subsets of cultured hippocampal neurons whose activity is inhibited by Kir2.1 overexpression display reduced spine density and reduced frequency of miniature excitatory post-synaptic currents (mEPSCs). By showing that synaptic input reduction does not occur in cells treated globally with tetrodotoxin (TTX), they also demonstrate that these alterations in synaptic connectivity arise from a relative inhibition of activity, rather than from non-specific effects on cell viability or function. Our results expand on this study by showing that the same effect is evident *in vivo*, where mammalian neuronal circuits are kept intact. Our work should be expanded to investigate whether the same effect is seen when CA1 neurons are suppressed globally.

Our results differ substantially, however, when developmental time-points are taken into consideration. While Burrone and colleagues find a substantial reduction in dendritic spine density (35%) and mEPSC frequency (50%) when hippocampal cultures are transfected with Kir2.1 *before* synapse formation, they find no such effects when transfection is performed *after* synapse maturation. In fact, they find that neurons in mature cultures experience a homeostatic increase in spine density (12%) and mEPSC frequency (46%) when silenced by Kir2.1 overexpression (Burrone et al., 2002). By contrast, our results provide evidence that competitive synaptic input reduction may also occur in the adult brain, albeit less

dramatically than in the developing brain. This difference could arise from the use of TetoxLC versus Kir2.1 and/or from the behavior of cultured hippocampal cells compared to cells in an intact circuit. The use of Kir2.1 versus TetoxLC, for example, has been shown to differentially affect axonal arborization during topographic map formation and maintenance in the mouse olfactory system (Yu et al., 2004).

Finally, a study performed in the rat somatosensory barrel cortex found that suppressing somatodendritic spiking in a small subset of cells by siRNA knockdown of Na^+ channels results in a 16% *increase* in dendritic spine density (Komai et al., 2006). This increase, observed in young developing synapses, is attributed by the authors to the cell's inability to prune immature and synaptically silent filopodia. The sharp contrast between the results of this study and ours could be due to the fact that Na^+ channel knockdown was shown to affect only somatodendritic and not axosomatic spiking (Komai et al., 2006), whereas TetoxLC expression in our study affects axonal and potentially dendritic exocytosis. Another consideration is the fact that their study was performed at a much earlier developmental timepoint than our own, although this is also in contrast to the hippocampal culture studies that found reduced spine density in neurons transfected with Kir2.1 before synapse formation (Burrone et al., 2002). The effects of single-cell inhibition on dendritic spine morphology/density have not been extensively studied, so a variety of factors, such as brain region specificity, temporal specificity throughout development or pre- versus postsynaptic inhibition, could be at play.

6.2.4 Pathological relevance of spine density reduction

The magnitude of the reduction in spine density that we observed (15%-19%) can be considered biologically relevant when compared to human case studies of neuropsychiatric diseases. Synaptic anomalies are prominent, for example, in diseases like schizophrenia (SZ) and Alzheimer's disease (AD) (Glantz and Lewis, 2000, Garey et al., 1998, Selkoe, 2002, Penzes et al., 2011). In postmortem brains of schizophrenia patients, for example, cortical neurons exhibit spine density reductions that range from 23% to 66%. Furthermore, even minor synaptic loss may have a drastic effect on the onset and/or progression of disease. In AD for example, spine loss has been shown to occur very early (Arendt, 2009) and to show stronger correlation to cognitive decline than do neurofibrillary tangles, amyloid beta oligomers or neuronal death itself (DeKosky and Scheff, 1990, Terry et al., 1991). Since

synaptic connectivity plays such an important role in the brain – as evidenced by the diverse clinical manifestations of spine pathologies – we assume that a 15%-19% loss of dendritic spine density observed in the adult mouse hippocampus is biologically relevant to the study of neuropsychiatric disease.

Chapter 7 Materials and Methods

7.1 Molecular Biology, Biochemistry and Immunostaining Techniques

7.1.1 General Cloning Procedures

7.1.1.1 *DNA digestion and purification*

DNA sequences (0.5 µg) intended for general restriction analysis or for ligation into a cut vector were digested in 1X NEB buffer, 1X BSA, and 0.5 µl of each required enzyme in a 20 µl reaction volume. Reaction was incubated at 37°C for 2 hours. DNA vectors (1 µg) to be opened were digested in 1X NEB buffer, 1X BSA, and 0.7 µl of each required enzyme in a 50 µl reaction volume. This reaction was incubated at 37°C for 4 hours. Plasmids linearized in preparation for microinjection (8-10 µg) were digested in 10X NEB buffer, 10X BSA, and 2 µl of each required enzyme in a 100 µl reaction volume. Digested DNA was run on an agarose gel and purified from the gel using Quiagen II Gel Extraction Kit standard protocol.

7.1.1.2 *Ligation and transformation*

3 µl of DNA were ligated into 1 µl of cut vector using 0.3 µl of T4 DNA Ligase and 10X T4 ligation buffer in a 20 µl reaction volume. Reactions were incubated at room temperature (RT) for 2 hours. Half of the ligation reaction (10 µl) was incubated with 50-100 µl of competent cells (XL1Blue or DH5α) on ice for 20 minutes, transformed by heat shock (at 42°C) for 1 minute, and then incubated at 37°C in SOB medium. Transformed cells were pelleted in a tabletop centrifuge at 3,000 rpm for 3 minutes, resuspended in 100 µl SOB, plated onto selective LB agar medium and incubated overnight at 37°C. Kanamycin and ampicillin agar plates were made by adding 50 µg/ml of antibiotic into the agar before setting.

7.1.1.3 *Plasmid Preparation*

In some instances, colony PCR was used to select transfected colonies that express the desired construct. This was done using one primer from the vector and one from the insert, using a small amount of bacterial colony as the template. A single colony was picked and grown overnight in 5 ml of selective LB liquid medium in a 37°C shaker. Plasmid purifications were performed using QIAprep Miniprep or QIAGEN Plasmid Midi standard protocols. Antibiotics used for selective LB media were ampicillin and kanamycin, both at 50 µg/ml.

7.1.1.4 *Competent cell preparation*

DH5α E. coli cells, which are stored at -80°C in a glycerol stock, were streaked on an LB-agar plate containing no antibiotics and allowed to grow overnight at 37°C. A single colony was picked and grown overnight at 37°C in 5 ml of liquid LB medium. 1 ml of the overnight-grown DH5α culture was inoculated into 50 ml of SOB medium and grown at room temperature in a shaker until cell density reading gave an O.D. 600 value in the range of 0.4 - 0.6 . The bacterial culture was kept on ice for 10 minutes and then centrifuged at 3,000 rpm for 6 minutes at 4°C. The bacterial pellet was then processed using a Z-Competent E. coli Transformation Kit & Buffer Set (Zymo Research, Irvine, CA, USA) as per manufacturer's instructions. 50, 100, and 200 µl aliquots of Z-competent cells were snap-frozen in liquid nitrogen and stored at -80°C for further use in transformations.

7.1.2 Cloning strategies for transgenic constructs

7.1.2.1 *Kir2.1-IRES-tauLacZ DNA construct*

The pBlueScriptII SK^+ vector (pBS II-SK^+) was previously modified to contain the Thy1 promoter and a floxed transcriptional STOP cassette (Caroni, 1997), and is hereafter referred to as pBThy1. The Kir2.1-IRES-tauLacZ sequence was received as a gift from Dr. C. Ron Yun and then ligated into pBThy1. In preparation for pronuclear injection, 6-8 µg of plasmid DNA was linearized using 2 µl of NotI in a 100 µl reaction volume. The reactions was incubated at 37^{o}C for 6 hours and then heat-inactivated at 65^{o}C for 20 minutes. The linearized product was run on a 1% agarose gel under sterile conditions and purified from the gel using Roche High Pure PCR Product Purification Kit standard protocol. Purified product was quantified by comparing it HyperLadderI on a 1% agarose gel.

7.1.2.2 *TetoxLC-CFP DNA construct*

We obtained the tetanus toxin light chain sequence (TetoxLC) from Dr. C. Ron Yu in the pGEMT7-EZ vector (Yu et al., 2004). For the CFP sequence, we designed a 3' primer containing an HA tag, as well as the restriction sites MluI and XbaI. The CFP sequence was amplified (Methods Table 7.2), digested with EcoRI and XbaI and ligated into the pBSII-SK^+ multiple cloning site (MCS). The TetoxLC sequence was digested with XhoI and XmaI and ligated directly upstream of CFP-HA in the pBSII-SK^+ MCS. The TetoxLC-CFP-HA sequence was then digested with XhoI and MluI and ligated into the pBThy1 vector described above (Section 7.1.2.1). In all transformation reactions involving TetoxLC, colony PCR was

performed (Methods Table 7.2) to assess expression in the *E. coli* cells. In preparation for pronuclear injection, 6-8 µg of plasmid DNA were linearized using 2 µl of NotI and 2 µl of EcoRI in a 100 µl reaction volume. The reactions was incubated at 37°C for 6 hours and then heat-inactivated at 65°C for 20 minutes. The digested product, containing Thy1-TetoxLC-CFP was run on a 1% agarose gel under sterile conditions and purified from the gel using Roche High Pure PCR Product Purification Kit, standard protocol. Purified product was quantified by comparing it to HyperLadder I on a 1% agarose gel.

7.1.3 Polymerase Chain Reaction (PCR)

Mice genotypes were determined by PCR using the primer combinations described in Methods Table 7.2. Genomic DNA was obtained by digesting 5mm of mouse tail overnight at55°C in 100µl tail digestion buffer (50 mM Tris-HCl pH8.0, 1 mM $CaCl_2$, 1% Tween-20) plus 10µl proteinaseK (10 mg/ml) (Roche, Indianapolis, IN).Digested tails were boiled for 10 minutes to inactivate proteinase K. PCR reactions mixture included 10X Taq buffer, 0.25 µM of each primer, 0.25 mM of each dNTP, 0.25 µl of TAQ, and 2 µl of genomic DNA in a 25 µl reaction volume. Conditions were: 96°C – 3min, 40 cycles of [96°C – 40 sec, 60°C – 40 sec, 68°C – 1.5min], 68°C – 10min, hold at 4°C. Similar conditions were used to asses recombination in *SLICK;Ptox* mice (annealing temperature of 62°C) and to amplify probes for Southern blotting (annealing temperature of 56°C) (Methods Table 7.2).

7.1.3.1 *Colony PCR*

Colony polymerase chain reaction (PCR) was performed in some cases to select for colonies containing plasmids with the desired insert. Reaction mixture per colony included 10X buffer with 15 mM $MgCl_2$, 0.25 µM of each primer, 0.25 mM of each dNTP and .025 µl of TAQ polymerase (homemade) in a 20 µl reaction volume. Conditions were: 94°C – 3min, 35 cycles of [94°C – 30 sec, 60°C – 40 sec, 70°C – 1min], 70°C – 7min, hold at 4°C. For primer information see Methods Table 7.2.

7.1.4 *Insitu* hybridization (ISH)

7.1.4.1 *Designing antisense probes for TetoxLC*

In preparation for probe production, 7 µg of DNA sequence was linearized using 3 µl of restriction enzyme in a 100 µl reaction volume. Linearized DNA was digested with proteinase K at 55°C for 30 minutes, extracted with phenol/chloroform, re-purified with sodium acetate

and resuspended in 30 µl of diethylpyrocarbonate (DEPC)-treated water. Digoxygenin (DIG)-labeled probes were produced by *in vitro* transcription using 1 µg of template DNA, and 2 µl of either T3 or T7 RNA polymerase (DIG RNA Labeling Kit, Roche) and then purified with sodium acetate. RNA probes were stored at -80^{o}C. Immediately before using, probes were diluted in hybridization solution (Section 7.1.4.3) and denatured at 80^{o}C for 5-10 min.

Specifically, the full-length TetoxLC antisense probe used in Chapter 4 (Fig4.3, Fig4.4) was linearized with BamHI from the pGEMT7-EZ vector (obtained from C. Ron Yu) and transcribed with T7 RNA polymerase. To generate three smaller TetoxLC probes (432bp, 515bp and 496bp), we designed primers to amplify different sections of the full sequence. Forward primers included an XhoI restriction site and reverse primers included an EcoRI site. These tetox "bits" were amplified by PCR, purified by gel extraction, digested with XhoI and EcoRI, and ligated into the pBSII-SK^{+} multiple cloning site. Antisense probes were linearized with XhoI and transcribed with T3 RNA polymerase.

7.1.4.2 *ISH procedure*

Tissue sections were prepared as described in Section 7.3.4.3, post- fixed for 10 minutes in 4% PFA/PBS, washed 3 times in DEPC-PBS, acetylated for 10 min at room temperature in acetylation solution and washed again in DECP-PBS. Processed slides were pre-hybridized in hybridization solution for 1-3 hours at room temperate and then hybridized with a DIG-labeled probe overnight at 68^{o}C in a sealed chamber humidified with 50% formamide/2XSSC. Slides were washed in 0.2XSSC for 3 hours with 4 changes of solution and then washed twice for 5 min in TBS. For color development with NBT/BCIP slides were blocked for 1 hour in blocking solution and incubated overnight at 4^{o}C in alkaline-phosphatase-conjugated sheep anti-DIG antibody, Fab fragments (Roche) at 1:2000 in blocking solution. Slides were then washed four times 10 minutes with TBST and once with detection buffer, and then incubated with NBT/BCIP solution overnight at 37^{o}C in a dark humidified chamber. Stained sections were imaged under bright field using a Leica DMI 3000 microscope.

7.1.4.3 *Solutions for ISH*

Acetylation solution

49 ml	H_2O
666 µl	triethanolamine (Sigma 90278)
87.5 µl	concentrated HCl
125 µl	acetic anhydride (Sigma A6404)

Detection buffer

0.1 M	Tris-HCl (pH9.5)
0.1 M	NaCl
50 mM	MgCl2
0.24 mg/ml	levamisole
	in dH2O
	add 0.05% Tween 20

Hybridization solution

50%	Formamide (Sigma F9037)
5X	SSC
5X	Denhart's solution (Sigma D2532)
250 µg/ml	yeast tRNA (Roche 10109495001)
500 µg/ml	salmon sperm DNA (Sigma D7656)
50 µg/ml	heparin (Sigma H9399)
	in DEPC-dH2O

NBT/BCIP solution

0.35 mg/ml	NBT (Sigma N 6639)
0.175 mg/ml	BCIP (Sigma B8503)
	in detection buffer with Tween

Blocking solution

10%	normal sheep serum
0.2%	Blocking Solution (Roche 1096176)
	in TBS

7.1.5 Southern blotting

Digoxigenin (DIG)-labeled probes were amplified using the DIG High Prime DNA Labeling and Detection Starter Kit II (RocheDiagnostics, West Sussex, UK) following standard protocol. PCR conditions are described in Section 7.1.3 and primers are outlined in Methods Table 7.2. Probe concentration was measured using a standard dot blot method with reagents from the same kit. Following quantification, the remainder of the synthesized probe was purified using the High Pure PCR Product Purification Kit (Roche Diagnostics, West Sussex, UK).

Genomic DNA was isolated from brain tissue as described in Section 7.3.4.2. Purified DNA (20 µg) was digested overnight at 37^{o}C in total reaction volume of 500 µl. Samples to be tested with the TetoxLC probe were digested with 10 µl of EcoRV-HF and 10 µl of EcoRI-HF, and samples to be tested with the ROSA26 probe were digested with 10 µl of EcoRV-HF. Digested DNA was precipitated with isopropanol (500 µl DNA, 100 µl NaCl, 400 µl isopropanol, 1 µl glycogen) at room temperature for 30 minutes, centrifuged for 30 minutes, washed with 75% ethanol and resuspended in double distilled water.

DNA was loaded onto a 0.9% agarose gel and separated by electrophoresis at 60V for 2 hours; 0.1 M TAE buffer was replaced once after 1 hour. Southern blot was performed according to standard protocol as detailed in several sources, including Sambrook and Russell (2006). A general outline of the protocol is: (1) gel is denatured and neutralized, (2) DNA is transferred onto an uncharged nylon membrane by capillary transfer, (3) membrane is UV-crosslinked, (4) immobilized DNA is hybridized using the DIG-labeled probes described above, (5)membrane is incubated with horseradish peroxidase-conjugated anti-DIG antibody, (6) probe is detected using ECL substrate (Thermo Scientific Pierce, Rockford, IL, USA), and (7) chemiluminescent signal is developed onto X-ray film (Thermo Scientific Pierce) using an Agfa CP 1000 film developer.

7.1.6 Western blotting

Protein concentration from cell or tissue lysates was measured using a BCA assay kit (Thermo Scientific Pierce) and a microplate reader (Tecan Group Ltd., Männedorf, Switzerland). In preparation for immunoblotting, protein samples were combined with 2X SDS gel loading buffer, boiled for 10 minutes and centrifuged briefly. Samples were then loaded onto SDS-polyacrylamide gels of varying percentages and resolved at 100V in running buffer (1X TRIS/glycine/SDS). Proteins were transferred by electroblotting to an Immobilon membrane (Millipore, Carrigtwohill, Ireland) at 100V in cold transfer buffer (25 mM TRIS, 192 mM glycine, 10% methanol). PonceauS staining was applied to verify protein content and then washed off using distilled water. Protein-containing membranes were washed briefly (2-3 min) in TBST (TBS plus 0.1% Tween-20) and then blocked for 1 hour at room temperature in 4% non-fat dried milk diluted in TBST. Primary antibody incubation was performed overnight at 4^{o}C in a humidified chamber. The membrane was then washed three times for 5 minutes at room temperature in TBST on a rocker. Secondary antibody incubation was performed at room temperature in a dark container while rocking. The membrane was then washed three times in TBST and once in TBS. Both primary and secondary antibodies were diluted in blocking solution (4% milk/TBST). Proteins tagged with peroxidase secondary antibodies were detected using ECL substrate (Thermo Scientific Pierce) and developed onto X-ray film using a table top film processor (Agfa CP 1000). Proteins tagged with fluorescent secondary antibodies were detected using the Odyssey Infrared Imaging System (LI-COR Biosciences, Cambridge, UK). Signal intensities were analyzed quantitatively using the Odyssey V3.0 software.

7.1.7 Immunoprecipitation (IP)

Tissue lysates were prepared as described in Section 7.3.4.1 and then pre-cleared for 1 hour at 4°C using 25 µl of Protein G Sepharose beads (Thermo Fisher Scientific, Dublin, Ireland). Pre-cleared lysates were immunoprecipitated for 2 – 4 hours at 4°C by incubation with 8 µl of MoAB51 antibody (Methods Table 7.1). Pre-clearing and immunoprecipitation were performed under constant mixing using a nutator mixer. The protein beads (~25 µl) were then washed with 1X PBS, blocked with 1% BSA for 30 minutes at 4°C (with mixing), washed again, and then spun down. Wash buffer (50 ml of cell lysis buffer) was added to the blocked beads in a 1:1 ratio. Part of this mixture (25 µl) was added to each of the pre-cleared protein lysates and incubated with constant mixing for 1 – 4 hours at 4°C. Following immunoprecipitation, the samples were centrifuged at 1,000g for 2 minutes at 4°C, interspersed with washing the agarose beads with wash buffer every 5 minutes. The wash and spin down steps were repeated at least 5 times so as to ensure removal of any non-specific protein interactions occurring with the beads. Following the final wash and spin down step, most of the wash buffer was removed except the last 25 µl (containing the beads) and 25 µl 2X gel loading buffer was added 50 µl of 2X gel loading buffer was added to protein lysates kept aside as input protein samples. All samples were boiled for 5 minutes, spun down briefly and resolved by SDS-polyacrylamide electrophoresis. Western blotting of both lysate and immunoprecipitates was performed using an anti-GFP antibody (Method Table 7.1) coupled with enhanced chemiluminescence detection.

7.1.8 Immunohistochemistry (IHC)

Tissue was dissected, sectioned, and post-fixed as described in Section 7.3.4.4. Floating sections were blocked for 4 hours at room temperature (RT) in a 24-well plate. They were then incubated overnight at 4^{o}C in primary antibody dilution, washed 3 times for 20 minutes in PBS, incubated for 4 hours at RT in secondary antibody dilution (in the dark) and washed again. Stained sections were mounted with Fluoromount (Sigma), sealed with nail varnish and stored at -20^{o}C. Primary and secondary antibodies were incubated in separate wells to prevent carryover. Cryosections were encircled with a PAP pen, blocked for 1 hour, incubated in primary antibody dilution for 4 hours, washed 4 times for 5 minutes in 1X PBS, incubated in secondary antibody for 1 hour, washed again, and mounted with Fluoromount, all at RT.

Blocking solution for both types of sections contained 5% normal goat serum (NGS), 3% bovine serum albumin (BSA) and 0.2% triton X-100 in PBS (blocking solution for LacZ staining had 1% triton X-100). Primary and secondary antibodies, outlined in Methods Table 7.1 were diluted in blocking solution without triton X-100.

7.1.8.1 *Sections used for dendritic spine analysis*

The brain was extracted, separated into hemispheres, post-fixed in 4% PFA/PBS for 2 hours and then transferred to 1X PBS for 1-2 hours. Vibratome sections (50-66 µm) were cut and stained on the same day as the tissue was harvested. Sections were blocked at RT for 2-3 hours in a 24-well plate (5% NGS, 3% BSA and 0.2% Triton-X in PBS), incubated in Att-488-GFP Booster (Chromotek, Somewhere. Germany) overnight at 4^{o}C (1:200 in blocking solution without triton), washed 4 times for 40 minutes in 1X PBS and mounted with Fluoromount. Slides were sealed with nail varnish and stored overnight at 4^{o}C to avoid freeze-thawing and preserve morphology. Confocal images were taken over the next two days.

7.1.9 X-Gal Staining

X-gal staining for β-galactosidase was performed by incubating sections in X-gal staining solution (2 Mm Xgal, 5 mM potassium ferrocyanide, 5 mM potassium ferricyanide, 2 mM $MgCl_2$) at room temperature for 16 hours. Sections were then washed in 1X PBS, mounted using Fluoromount and viewed under bright field using a Leica DMI 3000 microscope. Thick X-gal-stained vibratome sections show some nonspecific brown staining that is apparent in Chapter 2 (Fig 2.4, Fig2.6, and Fig2.8) and Chapter 3 (Fig3.3, Fig3.4).

7.2 Tissue Culture Techniques

COS-7 cells were cultured in Dulbecco's Modified Eagle Media (Sigma-Aldrich, catalog # D6429), 10% fetal bovine serum (FBS), 1% penicillin/streptomycin and 1% L-glutamine. Cells were maintained routinely at 37°C at 100% humidity and 5% CO_2 saturation.

7.2.1 Calcium phosphatase transfection and cell extract preparation

COS-7 cell cultures were transfected when subconfluent (2.5 x 106 cells for a 10 cm dish) using the calcium phosphate precipitation method described by Schenborn and Goiffon (2000). For each transfection, 4 µg of DNA was the set upper limit of DNA transfected per 10 cm dish or per well of a 6-well dish to prevent cytotoxicity. Media was changed 12 hours post-transfection and cells were allowed to grow for another 24 hours before being harvested.

7.3 Animal Procedures

All animal experiments at University College Cork were approved by the University Ethics Committee and conducted under a license from the Irish Department of Health and Children. Mice were housed at the Biological Services Unit of University College Cork, Cork.

7.3.1 Transgenic mice generation at UCC

Injections of gel-purified DNA into fertilized oocytes were carried out by Dr. Melanie Ball using standard techniques (Richa, 2000). Embryos were introduced into pseudo-pregnant CD1 females. Transgenic founders were backcrossed to C57 mice for initial analysis of mRNA expression patterns and then to SLICK-H mice (Jackson Labs stock #012708) for analysis of reporter gene expression.

7.3.2 Tamoxifen Administration

Tamoxifen (Sigma, Arklow, Ireland; catalog numberT5648) was dissolved in corn oil (Dunnes Stores, Cork, Ireland) at a concentration of 20 mg/ml by rocking overnight at room temperature. This was stored at room temperature for immediate use. Adult mice (2 to 3 months-old) were administered 0.25 mg of tamoxifen per gram of body weight by oral gavage. Mice were dosed once daily for one, three, or five consecutive days and rested for at least 10 days before analyzing. Untreated control mice were housed in separate cages to avoid carryover of tamoxifen.

7.3.3 Animal sacrifice

Mice were anesthetized by isofluorane inhalation and perfused through the left ventricle of the heart using a peristaltic pump. Ice-cold 0.1 M PBS (pH =7.4) was used to flush out blood from all vessels and tissues. Animals whose tissue was intended for immunohistochemistry or X-Gal staining were further perfused with 4% paraformaldehyde dissolved in PBS. For *in situ* hybridization, mice were perfused manually using a syringe with 10ml of DEPC-treated PBS.

7.3.4 Tissue processing

7.3.4.1 *Tissue homogenization for western blot an immunoprecipitation*

Whole brains were harvested and then either processed immediately or stored at -20^{o}C for several days to weeks. A glass homogenizer placed in ice was used to grind tissue in 500 µl of ice-cold solution (20mM Tris pH7.5, 100mM NaCl, 1% NP40, 0.1% deoxycholate, 1mM EDTA,

protease inhibitors). Tissue lysate was left on ice for 30 minutes and then spun down (13,000 rpm) at 4°C for 20 minutes. Supernatant was collected, measured for total protein concentration using a BCA assay kit, and stored at -20°C for future use. For immunoprecipitation, 3 brains per treatment group were homogenized together in a 9X volume of lysis buffer.

7.3.4.2 *DNA extraction used for Southern blot and PCR*

For PCR, the hippocampus or brainstem were dissected on ice and immediately processed. Tissue was lysed on ice using a glass homogenizer with 500 µl of lysis buffer (100 mM Tris-HCl pH 8.5, 5 mM EDTA pH 8.0, 0.2% SDS, 200 mM NaCl), rested on ice for 20 minutes, spun down for 15 minutes at 4°C in a tabletop centrifuge (13,000 rpm), and the supernatant collected. DNA was extracted using phenol/chloroform/isoamyl alcohol (25:24:1), then 100% ethanol, washed with 75% ethanol, airdried for 20 minutes and resuspended in 100 µl of TE buffer at 65°C. Exceptional care was taken not to sheer the DNA; gentle rocking was used instead of vortexing, P1000 tips were cut to allow a wider opening and pipetting was done gently in all instances.

For Southern blot, whole brains were extracted, halved into hemispheres and stored at -20°C for several weeks until required for further processing (being careful to maintain the shape of the hemispheres). When needed, a medial sagittal slice weighing approximately 60 g was cut from the frozen tissue, then diced finely with a blade and aliquoted into two different tubes. Isolation of genomic DNA was performed using the QIAamp DNA Mini Kit according to manufacturer's protocol. Great care was again taken not to sheer the DNA; gentle rocking was used instead of vortexing (except during tissue lysis), P1000 tips were cut to allow a wider opening and pipetting was done gently in all instances.

7.3.4.3 *Tissue sectioned for in situ hybridization*

Brain tissue was removed, embedded in cryomatrix resin and snap-frozen in liquid nitrogen-cooled isopentane or in dry ice-cooled ethanol. Tissue blocks were immediately sectioned (20 µm) using a Leica CM 1850 cryostat, placed onto sterile SuperFrost Plus slides (VWR International, Dublin, Ireland), air dried for 10 minutes, placed at 65°C for 10 minutes, and then air dried again for 10 minutes. Slides were processed immediately as described in Section 7.1.4.

7.3.4.4 *Tissue sectioned for immunohistochemistry and X-Gal stain*

Tissue was extracted, post-fixed in 4% PFA/PBS (30 min for X-Gal stain, overnight for IHC), and then transferred to PBS for either 1 hour or overnight. Brains were sectioned (50-100 µm thick) using a Lancer Vibratome Sectioning System Series 1000 (Technical Products International Inc., Saint Louis, MO, USA). Spinal cord, dorsal root ganglia (DRG) and retina were embedded in cryomatrix, snap-frozen in liquid nitrogen-cooled isopentane, and sectioned (20 µm) using a Leica CM 1850 cryostat. Some DRG and retina were mounted whole onto slides.

7.4 Microscopy

7.4.1 Fluorescent imaging

The following filters from the Leica DMI 3000 fluorescent microscope were used:

(1)	A	excitation filter BP 340-380	suppression filter LP 425
(2)	CFP	excitation filter BP 436/20	suppression filter BP 480/40
(3)	GFP	excitation filter BP 470/40	suppression filter BP 525/50
(4)	YFP	excitation filter BP 500/20	suppression filter BP 535/30
(5)	Y3	excitation filter BP 545/30	suppression filter BP 610/75

7.4.2 Confocal imaging

The Zeiss LSM 510 confocal microscope, which belongs to Mary McCaffrey in the Department of Biochemistry, University College Cork, Ireland, has the following four lasers:

(1) 405 diode, 25-30mW
(2) argon 458, 477, 488, 514
(3) HeNe 543
(4) HeNe 633

Confocal images shown in Chapter 2 were obtained using 40X or 63X objectives (Fig7.1*A*). YFP was excited using the 488 nm laser line and fluorescence emission collected between 505 and 550 nm. Cy3 was excited at 543 nm and fluorescence collected between 555 and 627 nm. DAPI was excited using the 405 nm laser and fluorescence collected between 420 and 480. Dylight 649 was excited using the 633 nm laser line. Confocal images presented in Chapter 5 were taken using a 63X objective. YFP/GFP Booster was excited using the 488 nm laser line and fluorescence emission collected between 505 and 530 nm (Fig7.1*B*).

Figure 7.1 – Confocal settings for images presented in Chapter 2 (A) and Chapter 5 (B)

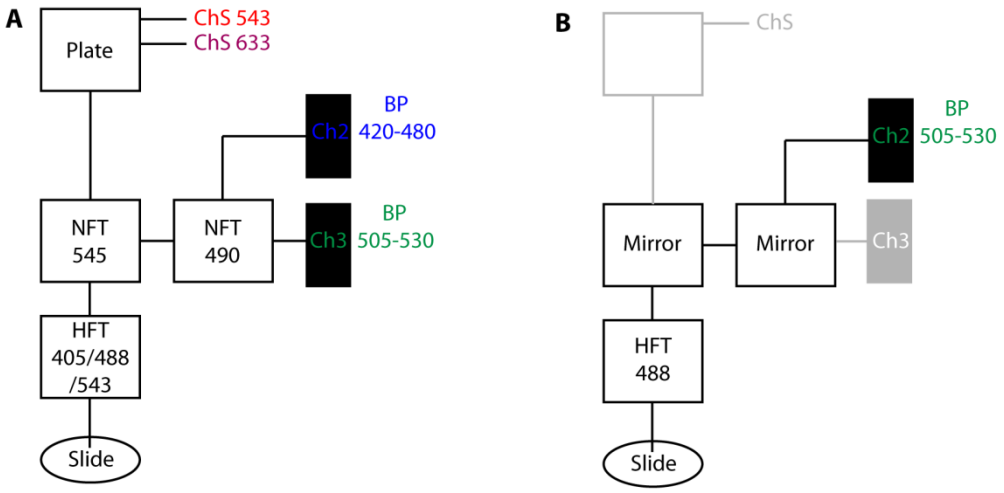

7.5 Data Analysis

In Chapter 2, confocal images of β-galactosidase, NeuN, DAPI and YFP were merged using Adobe Photoshop software, and ImageJ Cell Counter was used to count cells manually. Cells were scored as β-gal positive only when one or more large puncta or numerous small puncta were present within a cell body. Very weak staining for NeuN and YFP was excluded from the total number of cells.

In Chapter 4, western blot signal intensities were determined with the Odyssey V3.0 software (LI-COR Biosciences, Cambridge, UK) using GAPDH as loading control. The sum of K-counts for each pair of tamoxifen-treated versus untreated control samples was normalized to 100. When the same sample pair was analyzed on more than one blot, the normalized K-counts were averaged. Five forebrain sample pairs were probed for VAMP2, four forebrain sample pairs were probed for VAMP1/2/3, four cerebellum sample pairs were probed for VAMP2 and two cerebellum sample pairs were probed for VAMP1/2/3. Differences between tamoxifen-treated and untreated control sample pairs were statistically evaluated using Student's t-test. These results were graphed with an error bar representing standard error (Fig4.9*C*).

In Chapter 5, confocal images were analyzed under continued blinded conditions using the Filament Tracer module in BitpLane Imaris software (Bitplane AG, Zurich, Switzerland). Initial identification of dendritic spine was performed automatically but this was inspected and corrected manually. Spine density and spine length parameters were obtained from the Imaris software. In order to account for possible variation between cells in the treatment groups, we analyzed our data using a mixed-model nested ANOVA test. This test returned a p-value of 0.04714, indicating that one or more relationships between experimental groups are statistically significant with a confidence level of 0.05. In order to determine which relationship(s) are statistically significant, we ran three post-hoc tests comparing the means of either tamoxifen-treated versus untreated *SLICK-V;Ptox* or tamoxifen-treated *SLICK-V;Ptox* versus tamoxifen-treated SLICK-V mice. These tests were: Dunnett's T-test, Tukey's Standardized Student Range, and Gabriel's Comparison Intervals. All three tests revealed that the observed reduction in spine density in tamoxifen-treated *SLICK-V;Ptox* mice is significant compared to both controls ($p<0.05$).

7.6 Materials

7.6.1 Materials and reagents

All reagents used in these studies were purchased from Sigma-Aldrich (Arklow, Ireland) unless otherwise stated. Restriction enzymes, T4 DNA ligase, and pre-stained molecular weight protein markers were purchased from New England Biolabs (Hitchin, UK). Bicinchoninic acid (BCA) protein assay kit was obtained from Thermo Scientific Pierce (Rockford, IL, USA) through Medical Supply Company (Dublin, Ireland). Immobilon Transfer PVDF (polyvinylidene difluoride) membranes, western blotting filter papers, and bacterial plating beads were obtained from Merck Millipore Ltd. (Cork, Ireland). DNA ladder - HyperLadder 1kb was obtained from Bioline Reagents Ltd. (London, UK). Taq polymerase used routinely for PCR amplifications was prepared in-house following a protocol obtained from Charles Spillane, NUI Galway, Ireland. Primers and oligonucleotides designed by us for this study were purchased from Integrated DNA Technologies, Inc. (Leuven, Belgium).

7.6.2 Antibodies

Table 7.1 - List of antibodies used in this thesis; with dilutions and sources

	Antibody	Dilution	Catalogue #	Source
Chapter 2	LacZ	1:500 IHC	/	Dr. Joshua Sanes (Harvard University, USA)
	GFAP	1:500 IHC	MAB3402	Merck Millipore (Carrigtwohill, Ireland)
	Olig2	1:500 IHC	AB9610	Merck Millipore (Carrigtwohill, Ireland)
	NeuN	1:500 IHC	MAB377	Merck Millipore (Carrigtwohill, Ireland)
	GAD67	1:1,000 IHC	MAB5406	Merck Millipore MAB5406 (Carrigtwohill, Ireland)
	CaMKII	1:500 IHC	05-532	Upstate Cell Signaling Solutions (Lake Placid, NY)
Chapter 4	TeNT	1:500 WB	POL016	Statens Serum Institut (Copengagen, Denmark)
	MoAb 51	1:100 WB	/	Dr. Vladimir Petrusic (Seatovic et al. 2004)
	MoAb T-62	/	/	Dr. Vladimir Petrusic (Petrusic et al. 2011)
	GFP	1:500 IHC 1:1,000 WB	AB290	Abcam AB290 (Cambridge, UK)
	VAMP2	1:500 IHC 1:10,000 WB	104 211	Synaptic Systems (Gottingen, Germany)
	VAMP1/2/3	1:1,000 WB	104 203	Synaptic Systems (Gottingen, Germany)
	GAPDH	1:5,000 WB	G8795	Sigma-Aldrich (Arklow, Ireland)
Ch 5	GFP Booster Atto 488	1:200 IHC	GBA488	ChromoTek (Munich, Germany)
Secondaries	CY3	1:1,000 IHC	711-165-152 711-165-150	Jackson ImmunoResearch Laboratories (West Grove, PA, USA)
	Dylight 649	1:200 IHC	715-495-150	Jackson ImmunoResearch Laboratories (West Grove, PA, USA)
	Dylight 405	1:100 IHC	715-475-150	Jackson ImmunoResearch Laboratories (West Grove, PA, USA)
	Dylight 488	1:400 IHC	706-485-148	Jackson ImmunoResearch Laboratories (West Grove, PA, USA)
	DIG	1:2,000 ISH	11093274910	Roche Applied Sciences (Burgess Hill, UK)
	HRP	1:10,000 WB	18-8817	eBioscience, Ltd. (Hatfield, UK)
	IRDYE 800CW	1:10,000 WB	926-32210	Rockland (Gilbertsville, USA)
	IRDYE 700DX	1:10,000 WB	610-130-121	Rockland (Gilbertsville, USA)

7.6.3 Primers

Table 7.2 – List of primers and oligonucleotides used in this thesis; with sequence and location information

	Amplifies	Primer name	Sequence (5'-3')	Location
Cloning	CFP-HA	CerFus-F	TCTGAATTCCCGGGGAATGGTGAGCAAGGGCGAGGA	5' end of CFP
		CFP-R-HA	AGTTCTAGAACGCGTTTAGGCATAGTCTGGTACATCATAGGGATACTTGTACAGCTCGTCCATGCC	3' end of CFP
	TetoxLC colony PCR	T7	GTAATACGACTCACTATAGGGCG	5' end of MCS in pBSII-SK+
		Tetox-R2	GTACGCAGGTAGTTCGGGTCG	5' end of TetoxLC
	TetoxLC in pETd-Nhis	Tetox-F-XhoI	AGCTCGAGTCCGATCACCATCAACAACTTC	5' end of TetoxLC
		Tetox-R-EcoRI	GGTGAATTCTTAAGCGGTACGGTTGTACAG (incl STOP codon)	3' end of TetoxLC
Genotyping	Genomic	ChAT-F4	CAACCGCCTGGCCCTGCCAGT	Choline acetyltransferase
		ChAT-R13	GAGGATGAAATCCTGACAGAT	Choline acetyltransferase
	Genomic	R26R_0883	AAAGTCGCTCTGAGTTGTTAT	ROSA26 locus
		R26R_Wtnew	CACACACCAGGTTAGCCTTTAAGCC	ROSA26 locus
	Kir2.1	Thy1-F1	TCTGAGTGGCAAAGGACCTTAGG	before STOP cassette in Thy1
		STOP-R1	GGCAGCTTCTTTAGCAACAACCG	5' end of STOP cassette
	Kir2.1	STOP-F1	CTGACATGGTAAGTAAGCTTGGG	3' end of STOP cassette
		KirAAA-R	CGTCTGTCACACACCTGAATGCTGCGGCAATGGTTG	about 400bp into Kir2.1
	GFPtox	Ptox-F	GCCGATCACCATCAACAACTT	5' end of TetoxLC
		Ptox-R	GCAGAGCTTCACCAGCAACG	about 300bp into TetoxLC
	ROSA26	4xpolyA-F-bp2600	TCAGCCATACCACATTTGTAGAGG	3' end of STOP cassette
		LacZ-R2	TTCAGGCTGCGCAACTGTTGGG	5' end of LacZ
	SLICK	cre-F1	CGGTCGATGCAACGAGTGATG	5' end of creER
		cre-R1	ACGAACCTGGTCGAAATCAGT	3' end of creER
	TetoxLC	Thy1-F1	TCTGAGTGGCAAAGGACCTTAGG	before STOP cassette in Thy1
		Tetox-R2	GTACGCAGGTAGTTCGGGTCG	5' end of TetoxLC
	TetoxLC	STOP-F1	CTGACATGGTAAGTAAGCTTGGG	3' end of STOP cassette
		Tetox-R2	GTACGCAGGTAGTTCGGGTCG	5' end of TetoxLC
Recombination	GFPtox1	CAG-F1	GGGCACGTGCTGGTTATTGTGC	within the CAG promoter
		PGKp-rev	CCAGAGGCCACTTGTGTAGCG	5' end of STOP cassette
	GFPtox2	oIMR0315reversed-F	CGGTTGAGGACAAACTCTTCGC	after CAG promoter; before LoxP site
		PGKp-rev	CCAGAGGCCACTTGTGTAGCG	5' end of STOP cassette
	GFPtox3	CAG-F1	GGGCACGTGCTGGTTATTGTGC	within the CAG promoter
		YFP-R1	CGCTGAACTTGTGGCCGTTTACG	5' end of EGFP
	GFPtox4	oIMR0315reversed-F	CGGTTGAGGACAAACTCTTCGC	after CAG promoter; before LoxP site
		YFP-R1	CGCTGAACTTGTGGCCGTTTACG	5' end of EGFP
Souther	TetoxLC	TetTox-F-XhoI	AGCTCGAGTCCGATCACCATCAACAACTTC	5' end of TetoxLC
		TetoxBitsR3	TAGGAATTCTCGACTGCAGAATAGCGG	3' end of TetoxLC
	ROSA26	LacZ-F5	CGTTTTACAACGTCGTGACTGGG	5' end of LacZ
		LacZ-R5-EcoRV	GGATATCCTGCACCATCGTCTGC	within LacZ
In situ	TetoxLC	TetTox-F-XhoI	AGCTCGAGTCCGATCACCATCAACAACTTC	5' end of TetoxLC
		TetoxBits-R1	TACGAATTCGAAGGAAACGGAGTTGG	within TetoxLC
	TetoxLC	TetoxBits-F2	TGACTCGAGCCAACTCCGTTTCCTTC	within TetoxLC
		TetoxBits-R2	GTAGAATTCGCGATAGCTTTGTAGTCG	within TetoxLC
	TetoxLC	TetoxBits-F3	ATGCTCGAGCGACTACAAAGCTATCGC	within TetoxLC
		TetoxBits-R3	TAGGAATTCTCGACTGCAGAATAGCGG	3' end of TetoxLC

III. References

ABREMSKI, K. & HOESS, R. 1984. Bacteriophage P1 site-specific recombination. Purification and properties of the Cre recombinase protein. *J Biol Chem,* 259**,** 1509-14.

AIRAN, R. D., THOMPSON, K. R., FENNO, L. E., BERNSTEIN, H. & DEISSEROTH, K. 2009. Temporally precise in vivo control of intracellular signalling. *Nature,* 458**,** 1025-9.

AKEMANN, W., MUTOH, H., PERRON, A., ROSSIER, J. & KNOPFEL, T. 2010. Imaging brain electric signals with genetically targeted voltage-sensitive fluorescent proteins. *Nat Methods,* 7**,** 643-9.

ALEXANDER, M., SELMAN, G., SEETHARAMAN, A., CHAN, K. K., D'SOUZA, S. A., BYRNE, A. B. & ROY, P. J. 2010. MADD-2, a homolog of the Opitz syndrome protein MID1, regulates guidance to the midline through UNC-40 in Caenorhabditis elegans. *Dev Cell,* 18**,** 961-72.

ALGER, B. E. & NICOLL, R. A. 1980. Epileptiform burst afterhyperolarization: calcium-dependent potassium potential in hippocampal CA1 pyramidal cells. *Science,* 210**,** 1122-1124.

ANDERSEN, P. 2007. *The hippocampus book,* Oxford ; New York, Oxford University Press.

ARAYA, R., JIANG, J., EISENTHAL, K. B. & YUSTE, R. 2006. The spine neck filters membrane potentials. *Proceedings of the National Academy of Sciences of the United States of America,* 103**,** 17961-6.

ARENDT, T. 2009. Synaptic degeneration in Alzheimer's disease. *Acta Neuropathol,* 118**,** 167-79.

ASHBY, M. C., MAIER, S. R., NISHIMUNE, A. & HENLEY, J. M. 2006. Lateral diffusion drives constitutive exchange of AMPA receptors at dendritic spines and is regulated by spine morphology. *The Journal of neuroscience : the official journal of the Society for Neuroscience,* 26**,** 7046-55.

AZEVEDO, F. A., CARVALHO, L. R., GRINBERG, L. T., FARFEL, J. M., FERRETTI, R. E., LEITE, R. E., JACOB FILHO, W., LENT, R. & HERCULANO-HOUZEL, S. 2009. Equal numbers of neuronal and nonneuronal cells make the human brain an isometrically scaled-up primate brain. *J Comp Neurol,* 513**,** 532-41.

BAIRD, G. S., ZACHARIAS, D. A. & TSIEN, R. Y. 2000. Biochemistry, mutagenesis, and oligomerization of DsRed, a red fluorescent protein from coral. *Proc Natl Acad Sci U S A,* 97**,** 11984-9.

BALOYANNIS, S. J. 2011. Mitochondria are related to synaptic pathology in Alzheimer's disease. *Int J Alzheimers Dis,* 2011**,** 305395.

BALOYANNIS, S. J., COSTA, V. & MICHMIZOS, D. 2004. Mitochondrial alterations in Alzheimer's disease. *Am J Alzheimers Dis Other Demen,* 19**,** 89-93.

BAMBERG, E., TITTOR, J. & OESTERHELT, D. 1993. Light-driven proton or chloride pumping by halorhodopsin. *Proceedings of the National Academy of Sciences of the United States of America,* 90**,** 639-43.

BANGHART, M., BORGES, K., ISACOFF, E., TRAUNER, D. & KRAMER, R. H. 2004. Light-activated ion channels for remote control of neuronal firing. *Nat Neurosci,* 7**,** 1381-6.

BARRIA, A. & MALINOW, R. 2005. NMDA receptor subunit composition controls synaptic plasticity by regulating binding to CaMKII. *Neuron,* 48**,** 289-301.

BEN FREDJ, N., HAMMOND, S., OTSUNA, H., CHIEN, C. B., BURRONE, J. & MEYER, M. P. 2010. Synaptic activity and activity-dependent competition regulates axon arbor maturation, growth arrest, and territory in the retinotectal projection. *The Journal of neuroscience : the official journal of the Society for Neuroscience,* 30**,** 10939-51.

BENNETT, M. K. & SCHELLER, R. H. 1994. A molecular description of synaptic vesicle membrane trafficking. *Annu Rev Biochem,* 63**,** 63-100.

BENTIVOGLIO, M., KUYPERS, H. G., CATSMAN-BERREVOETS, C. E., LOEWE, H. & DANN, O. 1980. Two new fluorescent retrograde neuronal tracers which are transported over long distances. *Neurosci Lett,* 18**,** 25-30.

BERGQUIST, F., NIAZI, H. S. & NISSBRANDT, H. 2002. Evidence for different exocytosis pathways in dendritic and terminal dopamine release in vivo. *Brain Res,* 950**,** 245-53.

BERNDT, A., YIZHAR, O., GUNAYDIN, L. A., HEGEMANN, P. & DEISSEROTH, K. 2009. Bi-stable neural state switches. *Nat Neurosci,* 12**,** 229-34.

BERNSTEIN, J. G. & BOYDEN, E. S. 2011. Optogenetic tools for analyzing the neural circuits of behavior. *Trends Cogn Sci,* 15**,** 592-600.

BIANCHI, S., STIMPSON, C. D., BAUERNFEIND, A. L., SCHAPIRO, S. J., BAZE, W. B., MCARTHUR, M. J., BRONSON, E., HOPKINS, W. D., SEMENDEFERI, K., JACOBS, B., HOF, P. R. & SHERWOOD, C. C. 2012. Dendritic Morphology of Pyramidal Neurons in the Chimpanzee Neocortex: Regional Specializations and Comparison to Humans. *Cereb Cortex*.

BITTNER, M. A., HABIG, W. H. & HOLZ, R. W. 1989. Isolated light chain of tetanus toxin inhibits exocytosis: studies in digitonin-permeabilized cells. *J Neurochem,* 53**,** 966-8.

BLANPIED, T. A., SCOTT, D. B. & EHLERS, M. D. 2002. Dynamics and regulation of clathrin coats at specialized endocytic zones of dendrites and spines. *Neuron,* 36**,** 435-49.

BLOODGOOD, B. L. & SABATINI, B. L. 2005. Neuronal activity regulates diffusion across the neck of dendritic spines. *Science,* 310**,** 866-9.

BOSCH, M. & HAYASHI, Y. 2012. Structural plasticity of dendritic spines. *Curr Opin Neurobiol,* 22**,** 383-8.

BOURGEOIS, J. P., GOLDMAN-RAKIC, P. S. & RAKIC, P. 1994. Synaptogenesis in the prefrontal cortex of rhesus monkeys. *Cereb Cortex,* 4**,** 78-96.

BOYDEN, E. S., ZHANG, F., BAMBERG, E., NAGEL, G. & DEISSEROTH, K. 2005. Millisecond-timescale, genetically targeted optical control of neural activity. *Nat Neurosci,* 8**,** 1263-8.

BRAND, A. H. & PERRIMON, N. 1993. Targeted gene expression as a means of altering cell fates and generating dominant phenotypes. *Development,* 118**,** 401-15.

BRANDA, C. S. & DYMECKI, S. M. 2004. Talking about a revolution: The impact of site-specific recombinases on genetic analyses in mice. *Dev Cell,* 6**,** 7-28.

BRIGMAN, J. L., WRIGHT, T., TALANI, G., PRASAD-MULCARE, S., JINDE, S., SEABOLD, G. K., MATHUR, P., DAVIS, M. I., BOCK, R., GUSTIN, R. M., COLBRAN, R. J., ALVAREZ, V. A., NAKAZAWA, K., DELPIRE, E., LOVINGER, D. M. & HOLMES, A. 2010. Loss of GluN2B-containing NMDA receptors in CA1 hippocampus and cortex impairs long-term depression, reduces dendritic spine density, and disrupts learning. *J Neurosci,* 30**,** 4590-600.

BROWN, T. C., TRAN, I. C., BACKOS, D. S. & ESTEBAN, J. A. 2005. NMDA receptor-dependent activation of the small GTPase Rab5 drives the removal of synaptic AMPA receptors during hippocampal LTD. *Neuron,* 45**,** 81-94.

BUCHHOLZ, F., ANGRAND, P. O. & STEWART, A. F. 1998. Improved properties of FLP recombinase evolved by cycling mutagenesis. *Nat Biotechnol,* 16**,** 657-62.

BUCHHOLZ, F. & STEWART, A. F. 2001. Alteration of Cre recombinase site specificity by substrate-linked protein evolution. *Nat Biotechnol,* 19**,** 1047-52.

BUFFELLI, M., BURGESS, R. W., FENG, G., LOBE, C. G., LICHTMAN, J. W. & SANES, J. R. 2003. Genetic evidence that relative synaptic efficacy biases the outcome of synaptic competition. *Nature,* 424**,** 430-4.

BURNS, K. A., AYOUB, A. E., BREUNIG, J. J., ADHAMI, F., WENG, W. L., COLBERT, M. C., RAKIC, P. & KUAN, C. Y. 2007. Nestin-CreER mice reveal DNA synthesis by nonapoptotic neurons following cerebral ischemia hypoxia. *Cereb Cortex,* 17**,** 2585-92.

BURRONE, J., O'BYRNE, M. & MURTHY, V. N. 2002. Multiple forms of synaptic plasticity triggered by selective suppression of activity in individual neurons. *Nature,* 420**,** 414-8.

BUSHEY, A. M., DORMAN, E. R. & CORCES, V. G. 2008. Chromatin insulators: regulatory mechanisms and epigenetic inheritance. *Mol Cell,* 32**,** 1-9.

BUTLER, S. J. & TEAR, G. 2007. Getting axons onto the right path: the role of transcription factors in axon guidance. *Development,* 134**,** 439-48.

CAMPBELL, R. E., TOUR, O., PALMER, A. E., STEINBACH, P. A., BAIRD, G. S., ZACHARIAS, D. A. & TSIEN, R. Y. 2002. A monomeric red fluorescent protein. *Proc Natl Acad Sci U S A,* 99**,** 7877-82.

CAMPSALL, K. D., MAZEROLLE, C. J., DE REPENTINGY, Y., KOTHARY, R. & WALLACE, V. A. 2002. Characterization of transgene expression and Cre recombinase activity in a panel of Thy-1 promoter-Cre transgenic mice. *Dev Dyn,* 224**,** 135-43.

CARONI, P. 1997. Overexpression of growth-associated proteins in the neurons of adult transgenic mice. *J Neurosci Methods,* 71**,** 3-9.

CARONI, P., DONATO, F. & MULLER, D. 2012. Structural plasticity upon learning: regulation and functions. *Nat Rev Neurosci,* 13**,** 478-90.

CASANOVA, E., FEHSENFELD, S., LEMBERGER, T., SHIMSHEK, D. R., SPRENGEL, R. & MANTAMADIOTIS, T. 2002. ER-based double iCre fusion protein allows partial recombination in forebrain. *Genesis,* 34**,** 208-14.

CHALFIE, M. 1995. Green fluorescent protein. *Photochem Photobiol,* 62**,** 651-6.

CHALFIE, M., TU, Y., EUSKIRCHEN, G., WARD, W. W. & PRASHER, D. C. 1994. Green fluorescent protein as a marker for gene expression. *Science,* 263**,** 802-5.

CHAMBERS, J. J., BANGHART, M. R., TRAUNER, D. & KRAMER, R. H. 2006. Light-induced depolarization of neurons using a modified Shaker K(+) channel and a molecular photoswitch. *J Neurophysiol,* 96**,** 2792-6.

CHAN, D. C. 2006. Mitochondria: dynamic organelles in disease, aging, and development. *Cell,* 125**,** 1241-52.

CHENG, D., HOOGENRAAD, C. C., RUSH, J., RAMM, E., SCHLAGER, M. A., DUONG, D. M., XU, P., WIJAYAWARDANA, S. R., HANFELT, J., NAKAGAWA, T., SHENG, M. & PENG, J. 2006. Relative and absolute quantification of postsynaptic density proteome isolated from rat forebrain and cerebellum. *Mol Cell Proteomics,* 5**,** 1158-70.

CHENG, L., JIN, Z., LIU, L., YAN, Y., LI, T., ZHU, X. & JING, N. 2004. Characterization and promoter analysis of the mouse nestin gene. *FEBS Lett,* 565**,** 195-202.

CHILTON, J. K. 2006. Molecular mechanisms of axon guidance. *Developmental biology,* 292**,** 13-24.

CHOQUET, D. 2010. Fast AMPAR trafficking for a high-frequency synaptic transmission. *Eur J Neurosci,* 32**,** 250-60.

CHOW, B. Y., HAN, X., DOBRY, A. S., QIAN, X., CHUONG, A. S., LI, M., HENNINGER, M. A., BELFORT, G. M., LIN, Y., MONAHAN, P. E. & BOYDEN, E. S. 2010. High-performance genetically targetable optical neural silencing by light-driven proton pumps. *Nature,* 463**,** 98-102.

CHUNG, W. S. & BARRES, B. A. 2012. The role of glial cells in synapse elimination. *Curr Opin Neurobiol,* 22**,** 438-45.

CLINE, H. & HAAS, K. 2008. The regulation of dendritic arbor development and plasticity by glutamatergic synaptic input: a review of the synaptotrophic hypothesis. *J Physiol,* 586**,** 1509-17.

CLINE, H. T. 2001. Dendritic arbor development and synaptogenesis. *Curr Opin Neurobiol,* 11**,** 118-26.

CONKLIN, B. R., HSIAO, E. C., CLAEYSEN, S., DUMUIS, A., SRINIVASAN, S., FORSAYETH, J. R., GUETTIER, J. M., CHANG, W. C., PEI, Y., MCCARTHY, K. D., NISSENSON, R. A., WESS,

J., BOCKAERT, J. & ROTH, B. L. 2008. Engineering GPCR signaling pathways with RASSLs. *Nat Methods,* 5**,** 673-8.

CORDELL, J. L., FALINI, B., ERBER, W. N., GHOSH, A. K., ABDULAZIZ, Z., MACDONALD, S., PULFORD, K. A., STEIN, H. & MASON, D. Y. 1984. Immunoenzymatic labeling of monoclonal antibodies using immune complexes of alkaline phosphatase and monoclonal anti-alkaline phosphatase (APAAP complexes). *J Histochem Cytochem,* 32**,** 219-29.

COX, M. M. 1983. The FLP protein of the yeast 2-microns plasmid: expression of a eukaryotic genetic recombination system in Escherichia coli. *Proc Natl Acad Sci U S A,* 80**,** 4223-7.

DAGNINO-SUBIABRE, A., PEREZ, M. A., TERREROS, G., CHENG, M. Y., HOUSE, P. & SAPOLSKY, R. 2012. Corticosterone treatment impairs auditory fear learning and the dendritic morphology of the rat inferior colliculus. *Hear Res,* 294**,** 104-13.

DAHLHAUS, M., HERMANS, J. M., VAN WOERDEN, L. H., SAIEPOUR, M. H., NAKAZAWA, K., MANSVELDER, H. D., HEIMEL, J. A. & LEVELT, C. N. 2008. Notch1 signaling in pyramidal neurons regulates synaptic connectivity and experience-dependent modifications of acuity in the visual cortex. *The Journal of neuroscience : the official journal of the Society for Neuroscience,* 28**,** 10794-802.

DAILEY, M. E. & SMITH, S. J. 1996. The dynamics of dendritic structure in developing hippocampal slices. *The Journal of neuroscience : the official journal of the Society for Neuroscience,* 16**,** 2983-94.

DALVA, M. B., TAKASU, M. A., LIN, M. Z., SHAMAH, S. M., HU, L., GALE, N. W. & GREENBERG, M. E. 2000. EphB receptors interact with NMDA receptors and regulate excitatory synapse formation. *Cell,* 103**,** 945-56.

DAVIES, C. A., MANN, D. M., SUMPTER, P. Q. & YATES, P. O. 1987. A quantitative morphometric analysis of the neuronal and synaptic content of the frontal and temporal cortex in patients with Alzheimer's disease. *J Neurol Sci,* 78**,** 151-64.

DAY, R. N. & DAVIDSON, M. W. 2009. The fluorescent protein palette: tools for cellular imaging. *Chem Soc Rev,* 38**,** 2887-921.

DE CAMILLI, P., TAKEI, K. & MCPHERSON, P. S. 1995. The function of dynamin in endocytosis. *Curr Opin Neurobiol,* 5**,** 559-65.

DE VRIES, S. E. & CLANDININ, T. 2013. Optogenetic Stimulation of Escape Behavior in Drosophila melanogaster. *J Vis Exp*.

DEAN, C., SCHOLL, F. G., CHOIH, J., DEMARIA, S., BERGER, J., ISACOFF, E. & SCHEIFFELE, P. 2003. Neurexin mediates the assembly of presynaptic terminals. *Nat Neurosci,* 6**,** 708-16.

DEISSEROTH, K., FENG, G., MAJEWSKA, A. K., MIESENBOCK, G., TING, A. & SCHNITZER, M. J. 2006. Next-generation optical technologies for illuminating genetically targeted brain circuits. *The Journal of neuroscience : the official journal of the Society for Neuroscience,* 26**,** 10380-6.

DEKOSKY, S. T. & SCHEFF, S. W. 1990. Synapse loss in frontal cortex biopsies in Alzheimer's disease: correlation with cognitive severity. *Annals of neurology,* 27**,** 457-64.

DENT, E. W. & GERTLER, F. B. 2003. Cytoskeletal dynamics and transport in growth cone motility and axon guidance. *Neuron,* 40**,** 209-27.

DEWACHTER, I., REVERSE, D., CALUWAERTS, N., RIS, L., KUIPERI, C., VAN DEN HAUTE, C., SPITTAELS, K., UMANS, L., SERNEELS, L., THIRY, E., MOECHARS, D., MERCKEN, M., GODAUX, E. & VAN LEUVEN, F. 2002. Neuronal deficiency of presenilin 1 inhibits amyloid plaque formation and corrects hippocampal long-term potentiation but not a cognitive defect of amyloid precursor protein [V717I] transgenic mice. *The Journal of neuroscience : the official journal of the Society for Neuroscience,* 22**,** 3445-53.

DICKSON, R. M., CUBITT, A. B., TSIEN, R. Y. & MOERNER, W. E. 1997. On/off blinking and switching behaviour of single molecules of green fluorescent protein. *Nature,* 388**,** 355-8.

DONG, W. & AIZENMAN, C. D. 2012. A competition-based mechanism mediates developmental refinement of tectal neuron receptive fields. *The Journal of neuroscience : the official journal of the Society for Neuroscience,* 32**,** 16872-9.

DYMECKI, S. M. & KIM, J. C. 2007. Molecular neuroanatomy's "Three Gs": a primer. *Neuron,* 54**,** 17-34.

DYNES, J. L. & NGAI, J. 1998. Pathfinding of olfactory neuron axons to stereotyped glomerular targets revealed by dynamic imaging in living zebrafish embryos. *Neuron,* 20**,** 1081-91.

EHRENGRUBER, M. U., DOUPNIK, C. A., XU, Y., GARVEY, J., JASEK, M. C., LESTER, H. A. & DAVIDSON, N. 1997. Activation of heteromeric G protein-gated inward rectifier K+ channels overexpressed by adenovirus gene transfer inhibits the excitability of hippocampal neurons. *Proceedings of the National Academy of Sciences of the United States of America,* 94**,** 7070-5.

EL HACHIMI, K. H. & FONCIN, J. F. 1990. [Loss of dendritic spines in Alzheimer's disease]. *C R Acad Sci III,* 311**,** 397-402.

ELLISON, A. R., WEST, J. D., SPEARS, N., MURRAY, A., EVERETT, C. A. & BISHOP, J. O. 2000. Failure of founder transgenic male mice to transmit an attenuated HSV thymidine kinase transgene results from mosaicism and sperm competition. *Mol Reprod Dev,* 55**,** 249-55.

ERDMANN, G., SCHUTZ, G. & BERGER, S. 2007. Inducible gene inactivation in neurons of the adult mouse forebrain. *BMC Neurosci,* 8**,** 63.

EVANS, A. R., EUTENEUER, S., CHAVEZ, E., MULLEN, L. M., HUI, E. E., BHATIA, S. N. & RYAN, A. F. 2007. Laminin and fibronectin modulate inner ear spiral ganglion neurite outgrowth in an in vitro alternate choice assay. *Dev Neurobiol,* 67**,** 1721-30.

FARAGO, A. F., AWATRAMANI, R. B. & DYMECKI, S. M. 2006. Assembly of the brainstem cochlear nuclear complex is revealed by intersectional and subtractive genetic fate maps. *Neuron,* 50**,** 205-18.

FARRUGGIO, A. P., CHAVEZ, C. L., MIKELL, C. L. & CALOS, M. P. 2012. Efficient reversal of phiC31 integrase recombination in mammalian cells. *Biotechnol J,* 7**,** 1332-6.

FEIL, R., BROCARD, J., MASCREZ, B., LEMEUR, M., METZGER, D. & CHAMBON, P. 1996. Ligand-activated site-specific recombination in mice. *Proc Natl Acad Sci U S A,* 93**,** 10887-90.

FEIL, R., WAGNER, J., METZGER, D. & CHAMBON, P. 1997. Regulation of Cre recombinase activity by mutated estrogen receptor ligand-binding domains. *Biochem Biophys Res Commun,* 237**,** 752-7.

FEIL, S., VALTCHEVA, N. & FEIL, R. 2009. Inducible Cre mice. *Methods Mol Biol,* 530**,** 343-63.

FENG, G., MELLOR, R. H., BERNSTEIN, M., KELLER-PECK, C., NGUYEN, Q. T., WALLACE, M., NERBONNE, J. M., LICHTMAN, J. W. & SANES, J. R. 2000. Imaging neuronal subsets in transgenic mice expressing multiple spectral variants of GFP. *Neuron,* 28**,** 41-51.

FERRER, I. & GULLOTTA, F. 1990. Down's syndrome and Alzheimer's disease: dendritic spine counts in the hippocampus. *Acta Neuropathol,* 79**,** 680-5.

FORTIN, G. D., DESROSIERS, C. C., YAMAGUCHI, N. & TRUDEAU, L. E. 2006. Basal somatodendritic dopamine release requires snare proteins. *J Neurochem,* 96**,** 1740-9.

FROST, N. A., SHROFF, H., KONG, H., BETZIG, E. & BLANPIED, T. A. 2010. Single-molecule discrimination of discrete perisynaptic and distributed sites of actin filament assembly within dendritic spines. *Neuron,* 67**,** 86-99.

FUERST, P. G., BRUCE, F., TIAN, M., WEI, W., ELSTROTT, J., FELLER, M. B., ERSKINE, L., SINGER, J. H. & BURGESS, R. W. 2009. DSCAM and DSCAML1 function in self-avoidance in multiple cell types in the developing mouse retina. *Neuron,* 64**,** 484-97.

FUERST, P. G., KOIZUMI, A., MASLAND, R. H. & BURGESS, R. W. 2008. Neurite arborization and mosaic spacing in the mouse retina require DSCAM. *Nature,* 451**,** 470-4.

GABRIEL, K. R. 1978. A simple method of multiple comparison of means. *J. Amer. Stat. Assoc,* 73**,** 724-729.

GAINEY, M. A., HURVITZ-WOLFF, J. R., LAMBO, M. E. & TURRIGIANO, G. G. 2009. Synaptic scaling requires the GluR2 subunit of the AMPA receptor. *The Journal of neuroscience : the official journal of the Society for Neuroscience,* 29**,** 6479-89.

GAMA SOSA, M. A., DE GASPERI, R. & ELDER, G. A. 2010. Animal transgenesis: an overview. *Brain Struct Funct,* 214**,** 91-109.

GAN, W.-B., GRUTZENDLER, J., WONG, W. T., WONG, R. O. L. & LICHTMAN, J. W. 2000. Multicolor "DiOlistic" Labeling of the Nervous System Using Lipophilic Dye Combinations. *Neuron,* 27**,** 219-225.

GARDIOL, A., RACCA, C. & TRILLER, A. 1999. Dendritic and postsynaptic protein synthetic machinery. *The Journal of neuroscience : the official journal of the Society for Neuroscience,* 19**,** 168-79.

GAREY, L. J., ONG, W. Y., PATEL, T. S., KANANI, M., DAVIS, A., MORTIMER, A. M., BARNES, T. R. & HIRSCH, S. R. 1998. Reduced dendritic spine density on cerebral cortical pyramidal neurons in schizophrenia. *J Neurol Neurosurg Psychiatry,* 65**,** 446-53.

GERROW, K. & EL-HUSSEINI, A. 2006. Cell adhesion molecules at the synapse. *Front Biosci,* 11**,** 2400-19.

GERROW, K., ROMORINI, S., NABI, S. M., COLICOS, M. A., SALA, C. & EL-HUSSEINI, A. 2006. A preformed complex of postsynaptic proteins is involved in excitatory synapse development. *Neuron,* 49**,** 547-62.

GIBSON, D. A. & MA, L. 2011. Developmental regulation of axon branching in the vertebrate nervous system. *Development,* 138**,** 183-95.

GIGER, R. J., HOLLIS, E. R., 2ND & TUSZYNSKI, M. H. 2010. Guidance molecules in axon regeneration. *Cold Spring Harb Perspect Biol,* 2**,** a001867.

GLANTZ, L. A. & LEWIS, D. A. 2000. Decreased dendritic spine density on prefrontal cortical pyramidal neurons in schizophrenia. *Arch Gen Psychiatry,* 57**,** 65-73.

GLAUSIER, J. R. & LEWIS, D. A. 2012. Dendritic spine pathology in schizophrenia. *Neuroscience*.

GOLD, M. G. 2012. A frontier in the understanding of synaptic plasticity: solving the structure of the postsynaptic density. *Bioessays,* 34**,** 599-608.

GOLDBERG, D. J. & BURMEISTER, D. W. 1986. Stages in axon formation: observations of growth of Aplysia axons in culture using video-enhanced contrast-differential interference contrast microscopy. *J Cell Biol,* 103**,** 1921-31.

GOLIC, K. G. & LINDQUIST, S. 1989. The FLP recombinase of yeast catalyzes site-specific recombination in the Drosophila genome. *Cell,* 59**,** 499-509.

GONCALVES, J. T., ANSTEY, J. E., GOLSHANI, P. & PORTERA-CAILLIAU, C. 2013. Circuit level defects in the developing neocortex of Fragile X mice. *Nat Neurosci,* 16**,** 903-9.

GONG, S., ZHENG, C., DOUGHTY, M. L., LOSOS, K., DIDKOVSKY, N., SCHAMBRA, U. B., NOWAK, N. J., JOYNER, A., LEBLANC, G., HATTEN, M. E. & HEINTZ, N. 2003. A gene expression atlas of the central nervous system based on bacterial artificial chromosomes. *Nature,* 425**,** 917-25.

GONZALEZ-BURGOS, I., RIVERA-CERVANTES, M. C., VELAZQUEZ-ZAMORA, D. A., FERIA-VELASCO, A. & GARCIA-SEGURA, L. M. 2012. Selective estrogen receptor modulators regulate dendritic spine plasticity in the hippocampus of male rats. *Neural Plast,* 2012**,** 309494.

GOOLD, C. P. & NICOLL, R. A. 2010. Single-cell optogenetic excitation drives homeostatic synaptic depression. *Neuron,* 68**,** 512-28.

GOSGNACH, S., LANUZA, G. M., BUTT, S. J., SAUERESSIG, H., ZHANG, Y., VELASQUEZ, T., RIETHMACHER, D., CALLAWAY, E. M., KIEHN, O. & GOULDING, M. 2006. V1 spinal neurons regulate the speed of vertebrate locomotor outputs. *Nature,* 440**,** 215-9.

GOSSE, N. J., NEVIN, L. M. & BAIER, H. 2008. Retinotopic order in the absence of axon competition. *Nature,* 452**,** 892-5.

GOSSEN, M. & BUJARD, H. 1992. Tight control of gene expression in mammalian cells by tetracycline-responsive promoters. *Proc Natl Acad Sci U S A,* 89**,** 5547-51.

GOSSEN, M., FREUNDLIEB, S., BENDER, G., MULLER, G., HILLEN, W. & BUJARD, H. 1995. Transcriptional activation by tetracyclines in mammalian cells. *Science,* 268**,** 1766-9.

GRADINARU, V., THOMPSON, K. R. & DEISSEROTH, K. 2008. eNpHR: a Natronomonas halorhodopsin enhanced for optogenetic applications. *Brain Cell Biol,* 36**,** 129-39.

GRAUBERT, T. A., HUG, B. A., WESSELSCHMIDT, R., HSIEH, C. L., RYAN, T. M., TOWNES, T. M. & LEY, T. J. 1998. Stochastic, stage-specific mechanisms account for the variegation of a human globin transgene. *Nucleic Acids Res,* 26**,** 2849-58.

GRAY, E. G. 1959. Axo-somatic and axo-dendritic synapses of the cerebral cortex: an electron microscope study. *J Anat,* 93**,** 420-33.

GRIMBERT, F. & CANG, J. 2012. New model of retinocollicular mapping predicts the mechanisms of axonal competition and explains the role of reverse molecular signaling during development. *The Journal of neuroscience : the official journal of the Society for Neuroscience,* 32**,** 9755-68.

GROTH, A. C., OLIVARES, E. C., THYAGARAJAN, B. & CALOS, M. P. 2000. A phage integrase directs efficient site-specific integration in human cells. *Proc Natl Acad Sci U S A,* 97**,** 5995-6000.

GRUEBER, W. B. & SAGASTI, A. 2010. Self-avoidance and tiling: Mechanisms of dendrite and axon spacing. *Cold Spring Harb Perspect Biol,* 2**,** a001750.

GRUTZENDLER, J., KASTHURI, N. & GAN, W. B. 2002. Long-term dendritic spine stability in the adult cortex. *Nature,* 420**,** 812-6.

GULLEDGE, A. T., CARNEVALE, N. T. & STUART, G. J. 2012. Electrical advantages of dendritic spines. *Plos One,* 7**,** e36007.

HAAS, K., LI, J. & CLINE, H. T. 2006. AMPA receptors regulate experience-dependent dendritic arbor growth in vivo. *Proceedings of the National Academy of Sciences of the United States of America,* 103**,** 12127-31.

HALL, A. C., LUCAS, F. R. & SALINAS, P. C. 2000. Axonal remodeling and synaptic differentiation in the cerebellum is regulated by WNT-7a signaling. *Cell,* 100**,** 525-35.

HAMILTON, D. L. & ABREMSKI, K. 1984. Site-specific recombination by the bacteriophage P1 lox-Cre system. Cre-mediated synapsis of two lox sites. *J Mol Biol,* 178**,** 481-6.

HAO, J. C., ADLER, C. E., MEBANE, L., GERTLER, F. B., BARGMANN, C. I. & TESSIER-LAVIGNE, M. 2010. The tripartite motif protein MADD-2 functions with the receptor UNC-40 (DCC) in Netrin-mediated axon attraction and branching. *Dev Cell,* 18**,** 950-60.

HARMS, K. J., TOVAR, K. R. & CRAIG, A. M. 2005. Synapse-specific regulation of AMPA receptor subunit composition by activity. *The Journal of neuroscience : the official journal of the Society for Neuroscience,* 25**,** 6379-88.

HARNETT, M. T., MAKARA, J. K., SPRUSTON, N., KATH, W. L. & MAGEE, J. C. 2012. Synaptic amplification by dendritic spines enhances input cooperativity. *Nature,* 491**,** 599-602.

HARTMAN, K. N., PAL, S. K., BURRONE, J. & MURTHY, V. N. 2006. Activity-dependent regulation of inhibitory synaptic transmission in hippocampal neurons. *Nat Neurosci,* 9**,** 642-9.

HARUYAMA, N., CHO, A. & KULKARNI, A. B. 2009. Overview: engineering transgenic constructs and mice. *Curr Protoc Cell Biol,* Chapter 19**,** Unit 19 10.

HARVEY, C. D., YASUDA, R., ZHONG, H. & SVOBODA, K. 2008. The spread of Ras activity triggered by activation of a single dendritic spine. *Science,* 321**,** 136-40.

HASAN, M. T., SCHONIG, K., BERGER, S., GRAEWE, W. & BUJARD, H. 2001. Long-term, noninvasive imaging of regulated gene expression in living mice. *Genesis,* 29**,** 116-22.

HASHIMOTO, K. & KANO, M. 2005. Postnatal development and synapse elimination of climbing fiber to Purkinje cell projection in the cerebellum. *Neurosci Res,* 53**,** 221-8.

HAVEKES, R. & ABEL, T. 2009. Genetic dissection of neural circuits and behavior in Mus musculus. *Adv Genet,* 65**,** 1-38.

HAYASHI, M. & MATSUDA, H. 2007. Negatively charged residues located near the external entrance are required for the Kir2.1 channel to function. *Pflugers Arch,* 455**,** 455-64.

HAYASHI, Y. & MAJEWSKA, A. K. 2005. Dendritic spine geometry: functional implication and regulation. *Neuron,* 46**,** 529-32.

HE, C. X. & PORTERA-CAILLIAU, C. 2012. The trouble with spines in fragile X syndrome: density, maturity and plasticity. *Neuroscience*.

HEIMER-MCGINN, V. & YOUNG, P. 2011. Efficient inducible Pan-neuronal cre-mediated recombination in SLICK-H transgenic mice. *Genesis,* 49**,** 942-9.

HEIMER, L. 2003. The legacy of the silver methods and the new anatomy of the basal forebrain: implications for neuropsychiatry and drug abuse. *Scand J Psychol,* 44**,** 189-201.

HIBINO, H., INANOBE, A., FURUTANI, K., MURAKAMI, S., FINDLAY, I. & KURACHI, Y. 2010. Inwardly rectifying potassium channels: their structure, function, and physiological roles. *Physiol Rev,* 90**,** 291-366.

HOESS, R. H., WIERZBICKI, A. & ABREMSKI, K. 1986. The role of the loxP spacer region in P1 site-specific recombination. *Nucleic Acids Res,* 14**,** 2287-300.

HOESS, R. H., ZIESE, M. & STERNBERG, N. 1982. P1 site-specific recombination: nucleotide sequence of the recombining sites. *Proc Natl Acad Sci U S A,* 79**,** 3398-402.

HOLT, J. R., JOHNS, D. C., WANG, S., CHEN, Z. Y., DUNN, R. J., MARBAN, E. & COREY, D. P. 1999. Functional expression of exogenous proteins in mammalian sensory hair cells infected with adenoviral vectors. *J Neurophysiol,* 81**,** 1881-8.

HOLTMAAT, A. J., TRACHTENBERG, J. T., WILBRECHT, L., SHEPHERD, G. M., ZHANG, X., KNOTT, G. W. & SVOBODA, K. 2005. Transient and persistent dendritic spines in the neocortex in vivo. *Neuron,* 45**,** 279-91.

HONIG, M. G. & HUME, R. I. 1989. DiI and diO: versatile fluorescent dyes for neuronal labelling and pathway tracing. *Trends Neurosci,* 12**,** 333-5, 340-1.

HONJO, K., HWANG, R. Y. & TRACEY, W. D., JR. 2012. Optogenetic manipulation of neural circuits and behavior in Drosophila larvae. *Nat Protoc,* 7**,** 1470-8.

HONKURA, N., MATSUZAKI, M., NOGUCHI, J., ELLIS-DAVIES, G. C. & KASAI, H. 2008. The subspine organization of actin fibers regulates the structure and plasticity of dendritic spines. *Neuron,* 57**,** 719-29.

HORTON, A. C. & EHLERS, M. D. 2004. Secretory trafficking in neuronal dendrites. *Nat Cell Biol,* 6**,** 585-91.

HSIAO, E. C., NGUYEN, T. D., NG, J. K., SCOTT, M. J., CHANG, W. C., ZAHED, H. & CONKLIN, B. R. 2011. Constitutive Gs activation using a single-construct tetracycline-inducible expression system in embryonic stem cells and mice. *Stem Cell Res Ther,* 2**,** 11.

HUA, J. Y., SMEAR, M. C., BAIER, H. & SMITH, S. J. 2005. Regulation of axon growth in vivo by activity-based competition. *Nature,* 434**,** 1022-6.

HUA, J. Y. & SMITH, S. J. 2004. Neural activity and the dynamics of central nervous system development. *Nat Neurosci,* 7**,** 327-32.

HUBERMAN, A. D., FELLER, M. B. & CHAPMAN, B. 2008. Mechanisms underlying development of visual maps and receptive fields. *Annu Rev Neurosci,* 31**,** 479-509.

HUNTER, N. L., AWATRAMANI, R. B., FARLEY, F. W. & DYMECKI, S. M. 2005. Ligand-activated Flpe for temporally regulated gene modifications. *Genesis,* 41**,** 99-109.

HUSI, H., WARD, M. A., CHOUDHARY, J. S., BLACKSTOCK, W. P. & GRANT, S. G. 2000. Proteomic analysis of NMDA receptor-adhesion protein signaling complexes. *Nat Neurosci,* 3**,** 661-9.

HUTSLER, J. J. & ZHANG, H. 2010. Increased dendritic spine densities on cortical projection neurons in autism spectrum disorders. *Brain Res,* 1309**,** 83-94.

HUTTENLOCHER, P. R. 1979. Synaptic density in human frontal cortex - developmental changes and effects of aging. *Brain Res,* 163**,** 195-205.

INDRA, A. K., WAROT, X., BROCARD, J., BORNERT, J. M., XIAO, J. H., CHAMBON, P. & METZGER, D. 1999. Temporally-controlled site-specific mutagenesis in the basal layer of the epidermis: comparison of the recombinase activity of the tamoxifen-inducible Cre-ER(T) and Cre-ER(T2) recombinases. *Nucleic Acids Res,* 27**,** 4324-7.

IRWIN, S. A., PATEL, B., IDUPULAPATI, M., HARRIS, J. B., CRISOSTOMO, R. A., LARSEN, B. P., KOOY, F., WILLEMS, P. J., CRAS, P., KOZLOWSKI, P. B., SWAIN, R. A., WEILER, I. J. & GREENOUGH, W. T. 2001. Abnormal dendritic spine characteristics in the temporal and visual cortices of patients with fragile-X syndrome: a quantitative examination. *Am J Med Genet,* 98**,** 161-7.

JAN, Y. N. & JAN, L. Y. 2010. Branching out: mechanisms of dendritic arborization. *Nat Rev Neurosci,* 11**,** 316-28.

JAWORSKI, J., KAPITEIN, L. C., GOUVEIA, S. M., DORTLAND, B. R., WULF, P. S., GRIGORIEV, I., CAMERA, P., SPANGLER, S. A., DI STEFANO, P., DEMMERS, J., KRUGERS, H., DEFILIPPI, P., AKHMANOVA, A. & HOOGENRAAD, C. C. 2009. Dynamic microtubules regulate dendritic spine morphology and synaptic plasticity. *Neuron,* 61**,** 85-100.

JE, H. S., YANG, F., JI, Y., NAGAPPAN, G., HEMPSTEAD, B. L. & LU, B. 2012. Role of pro-brain-derived neurotrophic factor (proBDNF) to mature BDNF conversion in activity-dependent competition at developing neuromuscular synapses. *Proceedings of the National Academy of Sciences of the United States of America,* 109**,** 15924-9.

JOHNS, D. C., MARX, R., MAINS, R. E., O'ROURKE, B. & MARBAN, E. 1999. Inducible genetic suppression of neuronal excitability. *The Journal of neuroscience : the official journal of the Society for Neuroscience,* 19**,** 1691-7.

JOHNSON, P. T., BROWN, M. N., PULLIAM, B. C., ANDERSON, D. H. & JOHNSON, L. V. 2005. Synaptic pathology, altered gene expression, and degeneration in photoreceptors impacted by drusen. *Invest Ophthalmol Vis Sci,* 46**,** 4788-95.

JONES, E. G. 2007. Neuroanatomy: Cajal and after Cajal. *Brain Res Rev,* 55**,** 248-55.

JOYNER, A. L. 2000. *Gene targeting : a practical approach,* Oxford, Oxford University Press.

JU, W., MORISHITA, W., TSUI, J., GAIETTA, G., DEERINCK, T. J., ADAMS, S. R., GARNER, C. C., TSIEN, R. Y., ELLISMAN, M. H. & MALENKA, R. C. 2004. Activity-dependent regulation of dendritic synthesis and trafficking of AMPA receptors. *Nat Neurosci,* 7**,** 244-53.

JUNG, Y., MULHOLLAND, P. J., WISEMAN, S. L., JUDSON CHANDLER, L. & PICCIOTTO, M. R. 2013. Constitutive knockout of the membrane cytoskeleton protein beta adducin decreases mushroom spine density in the nucleus accumbens but does not prevent spine remodeling in response to cocaine. *Eur J Neurosci,* 37**,** 1-9.

KADAR, A., WITTMANN, G., LIPOSITS, Z. & FEKETE, C. 2009. Improved method for combination of immunocytochemistry and Nissl staining. *J Neurosci Methods,* 184**,** 115-8.

KANEKO, T., MOISYADI, S., SUGANUMA, R., HOHN, B., YANAGIMACHI, R. & PELCZAR, P. 2005. Recombinase-mediated mouse transgenesis by intracytoplasmic sperm injection. *Theriogenology,* 64**,** 1704-15.

KARPOVA, A. Y., TERVO, D. G., GRAY, N. W. & SVOBODA, K. 2005. Rapid and reversible chemical inactivation of synaptic transmission in genetically targeted neurons. *Neuron,* 48**,** 727-35.

KASAI, H., FUKUDA, M., WATANABE, S., HAYASHI-TAKAGI, A. & NOGUCHI, J. 2010. Structural dynamics of dendritic spines in memory and cognition. *Trends Neurosci,* 33**,** 121-9.

KASAI, H., MATSUZAKI, M., NOGUCHI, J., YASUMATSU, N. & NAKAHARA, H. 2003. Structure-stability-function relationships of dendritic spines. *Trends Neurosci,* 26**,** 360-8.

KASUYA, J., ISHIMOTO, H. & KITAMOTO, T. 2009. Neuronal mechanisms of learning and memory revealed by spatial and temporal suppression of neurotransmission using shibire, a temperature-sensitive dynamin mutant gene in Drosophila melanogaster. *Front Mol Neurosci,* 2**,** 11.

KATZ, L. C. & SHATZ, C. J. 1996. Synaptic activity and the construction of cortical circuits. *Science,* 274**,** 1133-8.

KAUFMANN, W. E. & MOSER, H. W. 2000. Dendritic anomalies in disorders associated with mental retardation. *Cereb Cortex,* 10**,** 981-91.

KAYSER, M. S., NOLT, M. J. & DALVA, M. B. 2008. EphB receptors couple dendritic filopodia motility to synapse formation. *Neuron,* 59**,** 56-69.

KELLENDONK, C., TRONCHE, F., CASANOVA, E., ANLAG, K., OPHERK, C. & SCHUTZ, G. 1999. Inducible site-specific recombination in the brain. *J Mol Biol,* 285**,** 175-82.

KELLENDONK, C., TRONCHE, F., MONAGHAN, A. P., ANGRAND, P. O., STEWART, F. & SCHUTZ, G. 1996. Regulation of Cre recombinase activity by the synthetic steroid RU 486. *Nucleic Acids Res,* 24**,** 1404-11.

KELLY, E. E., HORGAN, C. P., MCCAFFREY, M. W. & YOUNG, P. 2011. The role of endosomal-recycling in long-term potentiation. *Cell Mol Life Sci,* 68**,** 185-94.

KENNEDY, M. B., BEALE, H. C., CARLISLE, H. J. & WASHBURN, L. R. 2005. Integration of biochemical signalling in spines. *Nat Rev Neurosci,* 6**,** 423-34.

KENNEDY, M. J., DAVISON, I. G., ROBINSON, C. G. & EHLERS, M. D. 2010. Syntaxin-4 defines a domain for activity-dependent exocytosis in dendritic spines. *Cell,* 141**,** 524-35.

KENNEDY, M. J. & EHLERS, M. D. 2011. Mechanisms and function of dendritic exocytosis. *Neuron,* 69**,** 856-75.

KESSELS, H. W. & MALINOW, R. 2009. Synaptic AMPA receptor plasticity and behavior. *Neuron,* 61**,** 340-50.

KHAWALED, R., BRUENING-WRIGHT, A., ADELMAN, J. P. & MAYLIE, J. 1999. Bicuculline block of small-conductance calcium-activated potassium channels. *Pflugers Arch,* 438**,** 314-21.

KIERNAN, J. A. 2007. Indigogenic substrates for detection and localization of enzymes. *Biotech Histochem,* 82**,** 73-103.

KIM, J. C., COOK, M. N., CAREY, M. R., SHEN, C., REGEHR, W. G. & DYMECKI, S. M. 2009. Linking genetically defined neurons to behavior through a broadly applicable silencing allele. *Neuron,* 63**,** 305-15.

KIMURA, H., USUI, T., TSUBOUCHI, A. & UEMURA, T. 2006. Potential dual molecular interaction of the Drosophila 7-pass transmembrane cadherin Flamingo in dendritic morphogenesis. *J Cell Sci,* 119**,** 1118-29.

KISTNER, A., GOSSEN, M., ZIMMERMANN, F., JERECIC, J., ULLMER, C., LUBBERT, H. & BUJARD, H. 1996. Doxycycline-mediated quantitative and tissue-specific control of gene expression in transgenic mice. *Proc Natl Acad Sci U S A,* 93**,** 10933-8.

KITAMOTO, T. 2001. Conditional modification of behavior in Drosophila by targeted expression of a temperature-sensitive shibire allele in defined neurons. *J Neurobiol,* 47**,** 81-92.

KITAMOTO, T. 2002. Targeted expression of temperature-sensitive dynamin to study neural mechanisms of complex behavior in Drosophila. *J Neurogenet,* 16**,** 205-28.

KNOBEL, K. M., JORGENSEN, E. M. & BASTIANI, M. J. 1999. Growth cones stall and collapse during axon outgrowth in Caenorhabditis elegans. *Development,* 126**,** 4489-98.

KNOTT, G. W., HOLTMAAT, A., WILBRECHT, L., WELKER, E. & SVOBODA, K. 2006. Spine growth precedes synapse formation in the adult neocortex in vivo. *Nat Neurosci,* 9**,** 1117-24.

KOBAYASHI, T., KAI, N., KOBAYASHI, K., FUJIWARA, T., AKAGAWA, K., ONDA, M. & KOBAYASHI, K. 2008. Transient silencing of synaptic transmitter release from specific neuronal types by recombinant tetanus toxin light chain fused to antibody variable region. *J Neurosci Methods,* 175**,** 125-32.

KOCH, C. & ZADOR, A. 1993. The function of dendritic spines: devices subserving biochemical rather than electrical compartmentalization. *The Journal of neuroscience : the official journal of the Society for Neuroscience,* 13**,** 413-22.

KOLLURI, N., SUN, Z., SAMPSON, A. R. & LEWIS, D. A. 2005. Lamina-specific reductions in dendritic spine density in the prefrontal cortex of subjects with schizophrenia. *Am J Psychiatry,* 162**,** 1200-2.

KOLOMEETS, N. S., ORLOVSKAYA, D. D., RACHMANOVA, V. I. & URANOVA, N. A. 2005. Ultrastructural alterations in hippocampal mossy fiber synapses in schizophrenia: a postmortem morphometric study. *Synapse,* 57**,** 47-55.

KOLOMEETS, N. S., ORLOVSKAYA, D. D. & URANOVA, N. A. 2007. Decreased numerical density of CA3 hippocampal mossy fiber synapses in schizophrenia. *Synapse,* 61**,** 615-21.

KOMAI, S., LICZNERSKI, P., CETIN, A., WATERS, J., DENK, W., BRECHT, M. & OSTEN, P. 2006. Postsynaptic excitability is necessary for strengthening of cortical sensory responses during experience-dependent development. *Nat Neurosci,* 9**,** 1125-33.

KOPEC, C. D., REAL, E., KESSELS, H. W. & MALINOW, R. 2007. GluR1 links structural and functional plasticity at excitatory synapses. *J Neurosci,* 27**,** 13706-18.

KRISTENSEN, A. S., JENKINS, M. A., BANKE, T. G., SCHOUSBOE, A., MAKINO, Y., JOHNSON, R. C., HUGANIR, R. & TRAYNELIS, S. F. 2011. Mechanism of Ca2+/calmodulin-dependent kinase II regulation of AMPA receptor gating. *Nat Neurosci,* 14**,** 727-35.

KRISTENSSON, K. & OLSSON, Y. 1971. Retrograde axonal transport of protein. *Brain Res,* 29**,** 363-5.

KUBO, Y., BALDWIN, T. J., JAN, Y. N. & JAN, L. Y. 1993. Primary structure and functional expression of a mouse inward rectifier potassium channel. *Nature,* 362**,** 127-33.

KUERT, P. A., BELLO, B. C. & REICHERT, H. 2012. The labial gene is required to terminate proliferation of identified neuroblasts in postembryonic development of the Drosophila brain. *Biol Open,* 1**,** 1006-15.

KULKARNI, V. A. & FIRESTEIN, B. L. 2012. The dendritic tree and brain disorders. *Mol Cell Neurosci,* 50**,** 10-20.

LAI, C. S., FRANKE, T. F. & GAN, W. B. 2012. Opposite effects of fear conditioning and extinction on dendritic spine remodelling. *Nature,* 483**,** 87-91.

LANGER, S. J., GHAFOORI, A. P., BYRD, M. & LEINWAND, L. 2002. A genetic screen identifies novel non-compatible loxP sites. *Nucleic Acids Res,* 30**,** 3067-77.

LAU, C. G., TAKAYASU, Y., RODENAS-RUANO, A., PATERNAIN, A. V., LERMA, J., BENNETT, M. V. & ZUKIN, R. S. 2010. SNAP-25 is a target of protein kinase C phosphorylation critical to NMDA receptor trafficking. *The Journal of neuroscience : the official journal of the Society for Neuroscience,* 30**,** 242-54.

LECHNER, H. A., LEIN, E. S. & CALLAWAY, E. M. 2002. A genetic method for selective and quickly reversible silencing of Mammalian neurons. *J Neurosci,* 22**,** 5287-90.

LEE, G. & SAITO, I. 1998. Role of nucleotide sequences of loxP spacer region in Cre-mediated recombination. *Gene,* 216**,** 55-65.

LEE, K. F., SOARES, C. & BEIQUE, J. C. 2012. Examining form and function of dendritic spines. *Neural Plast,* 2012**,** 704103.

LEE, S. J., ESCOBEDO-LOZOYA, Y., SZATMARI, E. M. & YASUDA, R. 2009. Activation of CaMKII in single dendritic spines during long-term potentiation. *Nature,* 458**,** 299-304.

LEE, T. & LUO, L. 1999. Mosaic analysis with a repressible cell marker for studies of gene function in neuronal morphogenesis. *Neuron,* 22**,** 451-61.

LEE, T. & LUO, L. 2001. Mosaic analysis with a repressible cell marker (MARCM) for Drosophila neural development. *Trends Neurosci,* 24**,** 251-4.

LENTZ, S. I., KNUDSON, C. M., KORSMEYER, S. J. & SNIDER, W. D. 1999. Neurotrophins support the development of diverse sensory axon morphologies. *The Journal of neuroscience : the official journal of the Society for Neuroscience,* 19**,** 1038-48.

LERCHNER, W., XIAO, C., NASHMI, R., SLIMKO, E. M., VAN TRIGT, L., LESTER, H. A. & ANDERSON, D. J. 2007. Reversible silencing of neuronal excitability in behaving mice by a genetically targeted, ivermectin-gated Cl- channel. *Neuron,* 54**,** 35-49.

LEVENGA, J. & WILLEMSEN, R. 2012. Perturbation of dendritic protrusions in intellectual disability. *Prog Brain Res,* 197**,** 153-68.

LEWANDOSKI, M. 2001. Conditional control of gene expression in the mouse. *Nat Rev Genet,* 2**,** 743-55.

LI, F., PINCET, F., PEREZ, E., ENG, W. S., MELIA, T. J., ROTHMAN, J. E. & TARESTE, D. 2007. Energetics and dynamics of SNAREpin folding across lipid bilayers. *Nat Struct Mol Biol,* 14**,** 890-6.

LI, X., GUTIERREZ, D. V., HANSON, M. G., HAN, J., MARK, M. D., CHIEL, H., HEGEMANN, P., LANDMESSER, L. T. & HERLITZE, S. 2005. Fast noninvasive activation and inhibition of neural and network activity by vertebrate rhodopsin and green algae channelrhodopsin. *Proceedings of the National Academy of Sciences of the United States of America,* 102**,** 17816-21.

LI, Z., OKAMOTO, K., HAYASHI, Y. & SHENG, M. 2004. The importance of dendritic mitochondria in the morphogenesis and plasticity of spines and synapses. *Cell,* 119**,** 873-87.

LICHTMAN, J. W. & COLMAN, H. 2000. Synapse elimination and indelible memory. *Neuron,* 25**,** 269-78.

LIPPINCOTT-SCHWARTZ, J., ALTAN-BONNET, N. & PATTERSON, G. H. 2003. Photobleaching and photoactivation: following protein dynamics in living cells. *Nat Cell Biol,* Suppl**,** S7-14.

LISMAN, J., YASUDA, R. & RAGHAVACHARI, S. 2012. Mechanisms of CaMKII action in long-term potentiation. *Nat Rev Neurosci,* 13**,** 169-82.

LIU, X. B., LOW, L. K., JONES, E. G. & CHENG, H. J. 2005. Stereotyped axon pruning via plexin signaling is associated with synaptic complex elimination in the hippocampus. *The Journal of neuroscience : the official journal of the Society for Neuroscience,* 25**,** 9124-34.

LIVET, J., WEISSMAN, T. A., KANG, H., DRAFT, R. W., LU, J., BENNIS, R. A., SANES, J. R. & LICHTMAN, J. W. 2007. Transgenic strategies for combinatorial expression of fluorescent proteins in the nervous system. *Nature,* 450**,** 56-62.

LLEDO, P. M., ZHANG, X., SUDHOF, T. C., MALENKA, R. C. & NICOLL, R. A. 1998. Postsynaptic membrane fusion and long-term potentiation. *Science,* 279**,** 399-403.

LO, D. C., MCALLISTER, A. K. & KATZ, L. C. 1994. Neuronal transfection in brain slices using particle-mediated gene transfer. *Neuron,* 13**,** 1263-8.

LOGIE, C. & STEWART, A. F. 1995. Ligand-regulated site-specific recombination. *Proc Natl Acad Sci U S A,* 92**,** 5940-4.

LOPATIN, A. N., MAKHINA, E. N. & NICHOLS, C. G. 1994. Potassium channel block by cytoplasmic polyamines as the mechanism of intrinsic rectification. *Nature,* 372**,** 366-9.

LOWERY, L. A. & VAN VACTOR, D. 2009. The trip of the tip: understanding the growth cone machinery. *Nat Rev Mol Cell Biol,* 10**,** 332-43.

LU, T., NGUYEN, B., ZHANG, X. & YANG, J. 1999. Architecture of a K+ channel inner pore revealed by stoichiometric covalent modification. *Neuron,* 22**,** 571-80.

LU, W., MAN, H., JU, W., TRIMBLE, W. S., MACDONALD, J. F. & WANG, Y. T. 2001. Activation of synaptic NMDA receptors induces membrane insertion of new AMPA receptors and LTP in cultured hippocampal neurons. *Neuron,* 29**,** 243-54.

LUDBROOK, J. 1998. Multiple comparison procedures updated. *Clin Exp Pharmacol Physiol,* 25**,** 1032-7.

LUKYANOV, K. A., CHUDAKOV, D. M., LUKYANOV, S. & VERKHUSHA, V. V. 2005. Innovation: Photoactivatable fluorescent proteins. *Nat Rev Mol Cell Biol,* 6**,** 885-91.

LUO, L. & O'LEARY, D. D. 2005. Axon retraction and degeneration in development and disease. *Annu Rev Neurosci,* 28**,** 127-56.

MACDONALD, J. H. 2009. *Handbook of Biological Statistics,* Baltimore, Maryland, Sparky House Publishing.

MADISEN, L., ZWINGMAN, T. A., SUNKIN, S. M., OH, S. W., ZARIWALA, H. A., GU, H., NG, L. L., PALMITER, R. D., HAWRYLYCZ, M. J., JONES, A. R., LEIN, E. S. & ZENG, H. 2010. A robust and high-throughput Cre reporting and characterization system for the whole mouse brain. *Nat Neurosci,* 13**,** 133-40.

MAKINO, H. & MALINOW, R. 2009. AMPA receptor incorporation into synapses during LTP: the role of lateral movement and exocytosis. *Neuron,* 64**,** 381-90.

MALENKA, R. C. & BEAR, M. F. 2004. LTP and LTD: an embarrassment of riches. *Neuron,* 44**,** 5-21.

MALETIC-SAVATIC, M. & MALINOW, R. 1998. Calcium-evoked dendritic exocytosis in cultured hippocampal neurons. Part I: trans-Golgi network-derived organelles undergo regulated exocytosis. *J Neurosci,* 18**,** 6803-13.

MALINOW, R. & MALENKA, R. C. 2002. AMPA receptor trafficking and synaptic plasticity. *Annu Rev Neurosci,* 25**,** 103-26.

MANESS, P. F. & SCHACHNER, M. 2007. Neural recognition molecules of the immunoglobulin superfamily: signaling transducers of axon guidance and neuronal migration. *Nat Neurosci,* 10**,** 19-26.

MARANTO, A. R. 1982. Neuronal mapping: a photooxidation reaction makes Lucifer yellow useful for electron microscopy. *Science,* 217**,** 953-5.

MARIN-PADILLA, M. 1972. Structural abnormalities of the cerebral cortex in human chromosomal aberrations: a Golgi study. *Brain Res,* 44**,** 625-9.

MARIN-PADILLA, M. 1976. Pyramidal cell abnormalities in the motor cortex of a child with Down's syndrome. A Golgi study. *J Comp Neurol,* 167**,** 63-81.

MASKERY, S. & SHINBROT, T. 2005. Deterministic and stochastic elements of axonal guidance. *Annu Rev Biomed Eng,* 7**,** 187-221.

MASLAND, R. H. 2001. Neuronal diversity in the retina. *Curr Opin Neurobiol,* 11**,** 431-6.

MATEI, V., PAULEY, S., KAING, S., ROWITCH, D., BEISEL, K. W., MORRIS, K., FENG, F., JONES, K., LEE, J. & FRITZSCH, B. 2005. Smaller inner ear sensory epithelia in Neurog 1 null mice are related to earlier hair cell cycle exit. *Dev Dyn,* 234**,** 633-50.

MATSUDA, H., SAIGUSA, A. & IRISAWA, H. 1987. Ohmic conductance through the inwardly rectifying K channel and blocking by internal Mg2+. *Nature,* 325**,** 156-9.

MATSUDA, T. & CEPKO, C. L. 2007. Controlled expression of transgenes introduced by in vivo electroporation. *Proceedings of the National Academy of Sciences of the United States of America,* 104**,** 1027-32.

MATSUZAKI, M. 2007. Factors critical for the plasticity of dendritic spines and memory storage. *Neuroscience Research,* 57**,** 1-9.

MATSUZAKI, M., HONKURA, N., ELLIS-DAVIES, G. C. & KASAI, H. 2004. Structural basis of long-term potentiation in single dendritic spines. *Nature,* 429**,** 761-6.

MATTSON, M. P., DOU, P. & KATER, S. B. 1988. Outgrowth-regulating actions of glutamate in isolated hippocampal pyramidal neurons. *The Journal of neuroscience : the official journal of the Society for Neuroscience,* 8**,** 2087-100.

MAYFORD, M., WANG, J., KANDEL, E. R. & O'DELL, T. J. 1995. CaMKII regulates the frequency-response function of hippocampal synapses for the production of both LTD and LTP. *Cell,* 81**,** 891-904.

MCLEOD, M., CRAFT, S. & BROACH, J. R. 1986. Identification of the crossover site during FLP-mediated recombination in the Saccharomyces cerevisiae plasmid 2 microns circle. *Mol Cell Biol,* 6**,** 3357-67.

METZGER, D., CLIFFORD, J., CHIBA, H. & CHAMBON, P. 1995. Conditional site-specific recombination in mammalian cells using a ligand-dependent chimeric Cre recombinase. *Proc Natl Acad Sci U S A,* 92**,** 6991-5.

MEYER, M. P. & SMITH, S. J. 2006. Evidence from in vivo imaging that synaptogenesis guides the growth and branching of axonal arbors by two distinct mechanisms. *The Journal of neuroscience : the official journal of the Society for Neuroscience,* 26**,** 3604-14.

MISSLER, M., SUDHOF, T. C. & BIEDERER, T. 2012. Synaptic cell adhesion. *Cold Spring Harb Perspect Biol,* 4**,** a005694.

MIYAWAKI, A. 2004. Fluorescent proteins in a new light. *Nat Biotechnol,* 22**,** 1374-6.

MIYOSHI, G. & FISHELL, G. 2006. Directing neuron-specific transgene expression in the mouse CNS. *Curr Opin Neurobiol,* 16**,** 577-84.

MONTOLIU, L., SCHEDL, A., KELSEY, G., LICHTER, P., LARIN, Z., LEHRACH, H. & SCHUTZ, G. 1993. Generation of transgenic mice with yeast artificial chromosomes. *Cold Spring Harb Symp Quant Biol,* 58**,** 55-62.

MORRIS, A. C., SCHAUB, T. L. & JAMES, A. A. 1991. FLP-mediated recombination in the vector mosquito, Aedes aegypti. *Nucleic Acids Res,* 19**,** 5895-900.

MULLER, W. & CONNOR, J. A. 1992. Ca2+ signalling in postsynaptic dendrites and spines of mammalian neurons in brain slice. *J Physiol Paris,* 86**,** 57-66.

MURAKOSHI, H., WANG, H. & YASUDA, R. 2011. Local, persistent activation of Rho GTPases during plasticity of single dendritic spines. *Nature,* 472**,** 100-4.

MURAKOSHI, H. & YASUDA, R. 2012. Postsynaptic signaling during plasticity of dendritic spines. *Trends Neurosci,* 35**,** 135-43.

MURRAY, M. J., MERRITT, D. J., BRAND, A. H. & WHITINGTON, P. M. 1998. In vivo dynamics of axon pathfinding in the Drosophilia CNS: a time-lapse study of an identified motorneuron. *J Neurobiol,* 37**,** 607-21.

NAGEL, G., SZELLAS, T., HUHN, W., KATERIYA, S., ADEISHVILI, N., BERTHOLD, P., OLLIG, D., HEGEMANN, P. & BAMBERG, E. 2003. Channelrhodopsin-2, a directly light-gated cation-selective membrane channel. *Proceedings of the National Academy of Sciences of the United States of America,* 100**,** 13940-5.

NAKASHIBA, T., YOUNG, J. Z., MCHUGH, T. J., BUHL, D. L. & TONEGAWA, S. 2008. Transgenic inhibition of synaptic transmission reveals role of CA3 output in hippocampal learning. *Science,* 319**,** 1260-4.

NARAHASHI, T. 2008. Tetrodotoxin: a brief history. *Proc Jpn Acad Ser B Phys Biol Sci,* 84**,** 147-54.

NERN, A., PFEIFFER, B. D., SVOBODA, K. & RUBIN, G. M. 2011. Multiple new site-specific recombinases for use in manipulating animal genomes. *Proceedings of the National Academy of Sciences of the United States of America,* 108**,** 14198-203.

NICHOLS, C. G. & LOPATIN, A. N. 1997. Inward rectifier potassium channels. *Annu Rev Physiol,* 59**,** 171-91.

NICOLL, R. A. & MALENKA, R. C. 1995. Contrasting properties of two forms of long-term potentiation in the hippocampus. *Nature,* 377**,** 115-8.

NICOLL, R. A. & ROCHE, K. W. 2013. Long-term potentiation: peeling the onion. *Neuropharmacology*.

NIELL, C. M., MEYER, M. P. & SMITH, S. J. 2004. In vivo imaging of synapse formation on a growing dendritic arbor. *Nat Neurosci,* 7**,** 254-60.

NIWA, H., YAMAMURA, K. & MIYAZAKI, J. 1991. Efficient selection for high-expression transfectants with a novel eukaryotic vector. *Gene,* 108**,** 193-9.

NOGUCHI, J., MATSUZAKI, M., ELLIS-DAVIES, G. C. & KASAI, H. 2005. Spine-neck geometry determines NMDA receptor-dependent Ca2+ signaling in dendrites. *Neuron,* 46**,** 609-22.

NOTARIANNI, E. & EVANS, M. J. 2006. *Embryonic stem cells : a practical approach,* Oxford ; New York, Oxford University Press.

O'DONNELL, K. H., CHEN, C. T. & WENSINK, P. C. 1994. Insulating DNA directs ubiquitous transcription of the Drosophila melanogaster alpha 1-tubulin gene. *Mol Cell Biol,* 14**,** 6398-408.

ODDO, S., CACCAMO, A., SHEPHERD, J. D., MURPHY, M. P., GOLDE, T. E., KAYED, R., METHERATE, R., MATTSON, M. P., AKBARI, Y. & LAFERLA, F. M. 2003. Triple-transgenic model of Alzheimer's disease with plaques and tangles: intracellular Abeta and synaptic dysfunction. *Neuron,* 39**,** 409-21.

OKAMOTO, K., NAGAI, T., MIYAWAKI, A. & HAYASHI, Y. 2004. Rapid and persistent modulation of actin dynamics regulates postsynaptic reorganization underlying bidirectional plasticity. *Nat Neurosci,* 7**,** 1104-12.

OKAMOTO, K., NARAYANAN, R., LEE, S. H., MURATA, K. & HAYASHI, Y. 2007. The role of CaMKII as an F-actin-bundling protein crucial for maintenance of dendritic spine structure. *Proceedings of the National Academy of Sciences of the United States of America,* 104**,** 6418-23.

OSTROFF, L. E., FIALA, J. C., ALLWARDT, B. & HARRIS, K. M. 2002. Polyribosomes redistribute from dendritic shafts into spines with enlarged synapses during LTP in developing rat hippocampal slices. *Neuron,* 35**,** 535-45.

OTTERSEN, O. P. 2005. Neurobiology: sculpted by competition. *Nature,* 434**,** 969.

PALMITER, R. D. & BRINSTER, R. L. 1986. Germ-line transformation of mice. *Annu Rev Genet,* 20**,** 465-99.

PAN, F. & GAN, W. B. 2008. Two-photon imaging of dendritic spine development in the mouse cortex. *Dev Neurobiol,* 68**,** 771-8.

PARK, M., PENICK, E. C., EDWARDS, J. G., KAUER, J. A. & EHLERS, M. D. 2004. Recycling endosomes supply AMPA receptors for LTP. *Science,* 305**,** 1972-5.

PARK, M., SALGADO, J. M., OSTROFF, L., HELTON, T. D., ROBINSON, C. G., HARRIS, K. M. & EHLERS, M. D. 2006. Plasticity-induced growth of dendritic spines by exocytic trafficking from recycling endosomes. *Neuron,* 52**,** 817-30.

PARRISH, J. Z., EMOTO, K., KIM, M. D. & JAN, Y. N. 2007. Mechanisms that regulate establishment, maintenance, and remodeling of dendritic fields. *Annu Rev Neurosci,* 30**,** 399-423.

PARRISH, J. Z., KIM, M. D., JAN, L. Y. & JAN, Y. N. 2006. Genome-wide analyses identify transcription factors required for proper morphogenesis of Drosophila sensory neuron dendrites. *Genes Dev,* 20**,** 820-35.

PASSAFARO, M., NAKAGAWA, T., SALA, C. & SHENG, M. 2003. Induction of dendritic spines by an extracellular domain of AMPA receptor subunit GluR2. *Nature,* 424**,** 677-81.

PATEL, T. D., JACKMAN, A., RICE, F. L., KUCERA, J. & SNIDER, W. D. 2000. Development of sensory neurons in the absence of NGF/TrkA signaling in vivo. *Neuron,* 25**,** 345-57.

PATTERSON, M. A., SZATMARI, E. M. & YASUDA, R. 2010. AMPA receptors are exocytosed in stimulated spines and adjacent dendrites in a Ras-ERK-dependent manner during long-term potentiation. *Proceedings of the National Academy of Sciences of the United States of America,* 107**,** 15951-6.

PELLETIER, J. & SONENBERG, N. 1988. Internal initiation of translation of eukaryotic mRNA directed by a sequence derived from poliovirus RNA. *Nature,* 334**,** 320-5.

PENZES, P., CAHILL, M. E., JONES, K. A., VANLEEUWEN, J. E. & WOOLFREY, K. M. 2011. Dendritic spine pathology in neuropsychiatric disorders. *Nat Neurosci,* 14**,** 285-93.

PENZES, P. & RAFALOVICH, I. 2012. Regulation of the actin cytoskeleton in dendritic spines. *Adv Exp Med Biol,* 970**,** 81-95.

PETERS, A. & KAISERMAN-ABRAMOF, I. R. 1970. The small pyramidal neuron of the rat cerebral cortex. The perikaryon, dendrites and spines. *Am J Anat,* 127**,** 321-55.

PICQUELLE, S. J. & MIER, K. L. 2011. A practical guide to statistical methods for comparing means from two-stage sampling. *Fisheries Research,* 107**,** 1-13.

PLASTER, N. M., TAWIL, R., TRISTANI-FIROUZI, M., CANUN, S., BENDAHHOU, S., TSUNODA, A., DONALDSON, M. R., IANNACCONE, S. T., BRUNT, E., BAROHN, R., CLARK, J., DEYMEER, F., GEORGE, A. L., JR., FISH, F. A., HAHN, A., NITU, A., OZDEMIR, C., SERDAROGLU, P., SUBRAMONY, S. H., WOLFE, G., FU, Y. H. & PTACEK, L. J. 2001. Mutations in Kir2.1 cause the developmental and episodic electrical phenotypes of Andersen's syndrome. *Cell,* 105**,** 511-9.

PLAZAS, P. V., NICOL, X. & SPITZER, N. C. 2013. Activity-dependent competition regulates motor neuron axon pathfinding via PlexinA3. *Proceedings of the National Academy of Sciences of the United States of America,* 110**,** 1524-9.

POIRIER, M. A., XIAO, W., MACOSKO, J. C., CHAN, C., SHIN, Y. K. & BENNETT, M. K. 1998. The synaptic SNARE complex is a parallel four-stranded helical bundle. *Nat Struct Biol,* 5**,** 765-9.

PORTALES-CASAMAR, E., SWANSON, D. J., LIU, L., DE LEEUW, C. N., BANKS, K. G., HO SUI, S. J., FULTON, D. L., ALI, J., AMIRABBASI, M., ARENILLAS, D. J., BABYAK, N., BLACK, S. F., BONAGURO, R. J., BRAUER, E., CANDIDO, T. R., CASTELLARIN, M., CHEN, J., CHEN, Y., CHENG, J. C., CHOPRA, V., DOCKING, T. R., DREOLINI, L., D'SOUZA, C. A., FLYNN, E. K., GLENN, R., HATAKKA, K., HEARTY, T. G., IMANIAN, B., JIANG, S., KHORASAN-ZADEH, S., KOMLJENOVIC, I., LAPRISE, S., LIAO, N. Y., LIM, J. S., LITHWICK, S., LIU, F., LIU, J., LU, M., MCCONECHY, M., MCLEOD, A. J., MILISAVLJEVIC, M., MIS, J., O'CONNOR, K., PALMA, B., PALMQUIST, D. L., SCHMOUTH, J. F., SWANSON, M. I., TAM, B., TICOLL, A., TURNER, J. L., VARHOL, R., VERMEULEN, J., WATKINS, R. F., WILSON, G., WONG, B. K., WONG, S. H., WONG, T. Y., YANG, G. S., YPSILANTI, A. R., JONES, S. J., HOLT, R. A., GOLDOWITZ, D., WASSERMAN, W. W. & SIMPSON, E. M. 2010. A regulatory toolbox of MiniPromoters to drive selective expression in the brain. *Proceedings of the National Academy of Sciences of the United States of America,* 107**,** 16589-94.

PORTUGUES, R., SEVERI, K. E., WYART, C. & AHRENS, M. B. 2013. Optogenetics in a transparent animal: circuit function in the larval zebrafish. *Curr Opin Neurobiol,* 23**,** 119-26.

PROUX-GILLARDEAUX, V., RUDGE, R. & GALLI, T. 2005. The tetanus neurotoxin-sensitive and insensitive routes to and from the plasma membrane: fast and slow pathways? *Traffic,* 6**,** 366-73.

PRUSS, H., DERST, C., LOMMEL, R. & VEH, R. W. 2005. Differential distribution of individual subunits of strongly inwardly rectifying potassium channels (Kir2 family) in rat brain. *Brain Res Mol Brain Res,* 139**,** 63-79.

PURVES, D., AUGUSTINE, G. J., FITZPATRICK, D., KATZ, L. C., LAMANTIA, A., MCNAMARA, J. O. & WILLIAMS, M. S. 2001. *Neuroscience,* Sunderland (MA), Sinauer Associates.

RACZ, B., BLANPIED, T. A., EHLERS, M. D. & WEINBERG, R. J. 2004. Lateral organization of endocytic machinery in dendritic spines. *Nat Neurosci,* 7**,** 917-8.

RAMAKRISHNAN, N. A., DRESCHER, M. J. & DRESCHER, D. G. 2012. The SNARE complex in neuronal and sensory cells. *Mol Cell Neurosci,* 50**,** 58-69.

RAO, A. & CRAIG, A. M. 1997. Activity regulates the synaptic localization of the NMDA receptor in hippocampal neurons. *Neuron,* 19**,** 801-12.

RAYMOND, C. S. & SORIANO, P. 2007. High-efficiency FLP and PhiC31 site-specific recombination in mammalian cells. *PLoS One,* 2**,** e162.

RAYMOND, V. & SATTELLE, D. B. 2002. Novel animal-health drug targets from ligand-gated chloride channels. *Nat Rev Drug Discov,* 1**,** 427-36.

REDFERN, C. H., COWARD, P., DEGTYAREV, M. Y., LEE, E. K., KWA, A. T., HENNIGHAUSEN, L., BUJARD, H., FISHMAN, G. I. & CONKLIN, B. R. 1999. Conditional expression and signaling of a specifically designed Gi-coupled receptor in transgenic mice. *Nat Biotechnol,* 17**,** 165-9.

RICHA, J. 2000. Production of Transgenic Mice. *In:* TUAN, R. & LO, C. (eds.) *Developmental Biology Protocols: Volume II.* Humana Press.

RIZO, J. & SUDHOF, T. C. 1998. Mechanics of membrane fusion. *Nat Struct Biol,* 5**,** 839-42.

ROBERTS, R. C., CONLEY, R., KUNG, L., PERETTI, F. J. & CHUTE, D. J. 1996. Reduced striatal spine size in schizophrenia: a postmortem ultrastructural study. *Neuroreport,* 7**,** 1214-8.

ROBERTS, T. F., TSCHIDA, K. A., KLEIN, M. E. & MOONEY, R. 2010. Rapid spine stabilization and synaptic enhancement at the onset of behavioural learning. *Nature,* 463**,** 948-52.

RODRIGUEZ, I., FEINSTEIN, P. & MOMBAERTS, P. 1999. Variable patterns of axonal projections of sensory neurons in the mouse vomeronasal system. *Cell,* 97**,** 199-208.

ROGAN, S. C. & ROTH, B. L. 2011. Remote control of neuronal signaling. *Pharmacol Rev,* 63**,** 291-315.

ROTOLO, T., SMALLWOOD, P. M., WILLIAMS, J. & NATHANS, J. 2008. Genetically-directed, cell type-specific sparse labeling for the analysis of neuronal morphology. *Plos One,* 3**,** e4099.

RUDOLPH, U. & MOHLER, H. 2004. Analysis of GABAA receptor function and dissection of the pharmacology of benzodiazepines and general anesthetics through mouse genetics. *Annu Rev Pharmacol Toxicol,* 44**,** 475-98.

RUI, Y., GU, J., YU, K., HARTZELL, H. C. & ZHENG, J. Q. 2010. Inhibition of AMPA receptor trafficking at hippocampal synapses by beta-amyloid oligomers: the mitochondrial contribution. *Mol Brain,* 3**,** 10.

RUSSO, S. J., DIETZ, D. M., DUMITRIU, D., MORRISON, J. H., MALENKA, R. C. & NESTLER, E. J. 2010. The addicted synapse: mechanisms of synaptic and structural plasticity in nucleus accumbens. *Trends Neurosci,* 33**,** 267-76.

RUTHAZER, E. S., AKERMAN, C. J. & CLINE, H. T. 2003. Control of axon branch dynamics by correlated activity in vivo. *Science,* 301**,** 66-70.

RUTHAZER, E. S., LI, J. & CLINE, H. T. 2006. Stabilization of axon branch dynamics by synaptic maturation. *The Journal of neuroscience : the official journal of the Society for Neuroscience,* 26**,** 3594-603.

SAMBROOK, J. & RUSSELL, D. W. 2006. Southern blotting: capillary transfer of DNA to membranes. *CSH Protoc,* 2006.

SAMPO, B., KAECH, S., KUNZ, S. & BANKER, G. 2003. Two distinct mechanisms target membrane proteins to the axonal surface. *Neuron,* 37**,** 611-24.

SANES, J. R. & LICHTMAN, J. W. 1999. Development of the vertebrate neuromuscular junction. *Annu Rev Neurosci,* 22**,** 389-442.

SANEYOSHI, T., FORTIN, D. A. & SODERLING, T. R. 2010. Regulation of spine and synapse formation by activity-dependent intracellular signaling pathways. *Curr Opin Neurobiol,* 20**,** 108-15.

SANFORD, S. D., GATLIN, J. C., HOKFELT, T. & PFENNINGER, K. H. 2008. Growth cone responses to growth and chemotropic factors. *Eur J Neurosci,* 28**,** 268-78.

SAUNDERS, T. L. 2011. Inducible transgenic mouse models. *Methods Mol Biol,* 693**,** 103-15.

SCEARCE-LEVIE, K., COWARD, P., REDFERN, C. H. & CONKLIN, B. R. 2001. Engineering receptors activated solely by synthetic ligands (RASSLs). *Trends Pharmacol Sci,* 22**,** 414-20.

SCHAFER, D. P., LEHRMAN, E. K., KAUTZMAN, A. G., KOYAMA, R., MARDINLY, A. R., YAMASAKI, R., RANSOHOFF, R. M., GREENBERG, M. E., BARRES, B. A. & STEVENS, B. 2012. Microglia sculpt postnatal neural circuits in an activity and complement-dependent manner. *Neuron,* 74**,** 691-705.

SCHENBORN, E. T. & GOIFFON, V. 2000. Calcium phosphate transfection of mammalian cultured cells. *Methods Mol Biol,* 130**,** 135-45.

SCHIAVO, G., MATTEOLI, M. & MONTECUCCO, C. 2000. Neurotoxins affecting neuroexocytosis. *Physiol Rev,* 80**,** 717-66.

SCHIAVO, G. G., BENFENATI, F., POULAIN, B., ROSSETTO, O., DE LAURETO, P. P., DASGUPTA, B. R. & MONTECUCCO, C. 1992. Tetanus and botulinum-B neurotoxins block neurotransmitter release by proteolytic cleavage of synaptobrevin. *Nature,* 359**,** 832-835.

SCHLAKE, T. & BODE, J. 1994. Use of mutated FLP recognition target (FRT) sites for the exchange of expression cassettes at defined chromosomal loci. *Biochemistry,* 33**,** 12746-51.

SCHMAHMANN, J. D. 2004. Disorders of the cerebellum: ataxia, dysmetria of thought, and the cerebellar cognitive affective syndrome. *J Neuropsychiatry Clin Neurosci,* 16**,** 367-78.

SCHONIG, K., SCHWENK, F., RAJEWSKY, K. & BUJARD, H. 2002. Stringent doxycycline dependent control of CRE recombinase in vivo. *Nucleic Acids Res,* 30**,** e134.

SCHUMAN, E. M., DYNES, J. L. & STEWARD, O. 2006. Synaptic regulation of translation of dendritic mRNAs. *The Journal of neuroscience : the official journal of the Society for Neuroscience,* 26**,** 7143-6.

SEGAL, M., VLACHOS, A. & KORKOTIAN, E. 2010. The spine apparatus, synaptopodin, and dendritic spine plasticity. *Neuroscientist,* 16**,** 125-31.

SELEMON, L. D. & GOLDMAN-RAKIC, P. S. 1999. The reduced neuropil hypothesis: a circuit based model of schizophrenia. *Biol Psychiatry,* 45**,** 17-25.

SELKOE, D. J. 2002. Alzheimer's disease is a synaptic failure. *Science,* 298**,** 789-91.

SENECOFF, J. F. & COX, M. M. 1986. Directionality in FLP protein-promoted site-specific recombination is mediated by DNA-DNA pairing. *J Biol Chem,* 261**,** 7380-6.

SENECOFF, J. F., ROSSMEISSL, P. J. & COX, M. M. 1988. DNA recognition by the FLP recombinase of the yeast 2 mu plasmid. A mutational analysis of the FLP binding site. *J Mol Biol,* 201**,** 405-21.

SHANER, N. C., CAMPBELL, R. E., STEINBACH, P. A., GIEPMANS, B. N., PALMER, A. E. & TSIEN, R. Y. 2004. Improved monomeric red, orange and yellow fluorescent proteins derived from Discosoma sp. red fluorescent protein. *Nat Biotechnol,* 22**,** 1567-72.

SHANKAR, G. M., LI, S., MEHTA, T. H., GARCIA-MUNOZ, A., SHEPARDSON, N. E., SMITH, I., BRETT, F. M., FARRELL, M. A., ROWAN, M. J., LEMERE, C. A., REGAN, C. M., WALSH, D. M., SABATINI, B. L. & SELKOE, D. J. 2008. Amyloid-beta protein dimers isolated

directly from Alzheimer's brains impair synaptic plasticity and memory. *Nat Med,* 14**,** 837-42.

SHEN, K. & SCHEIFFELE, P. 2010. Genetics and cell biology of building specific synaptic connectivity. *Annu Rev Neurosci,* 33**,** 473-507.

SHENG, M. & HOOGENRAAD, C. C. 2007. The postsynaptic architecture of excitatory synapses: a more quantitative view. *Annu Rev Biochem,* 76**,** 823-47.

SHENG, M. & KIM, E. 2011. The postsynaptic organization of synapses. *Cold Spring Harb Perspect Biol,* 3.

SHEPHERD, G. M. 2004. *The synaptic organization of the brain,* Oxford, Oxford University Press.

SHIMSHEK, D. R., KIM, J., HUBNER, M. R., SPERGEL, D. J., BUCHHOLZ, F., CASANOVA, E., STEWART, A. F., SEEBURG, P. H. & SPRENGEL, R. 2002. Codon-improved Cre recombinase (iCre) expression in the mouse. *Genesis,* 32**,** 19-26.

SIA, G. M., BEIQUE, J. C., RUMBAUGH, G., CHO, R., WORLEY, P. F. & HUGANIR, R. L. 2007. Interaction of the N-terminal domain of the AMPA receptor GluR4 subunit with the neuronal pentraxin NP1 mediates GluR4 synaptic recruitment. *Neuron,* 55**,** 87-102.

SIKORRA, S., HENKE, T., GALLI, T. & BINZ, T. 2008. Substrate recognition mechanism of VAMP/synaptobrevin-cleaving clostridial neurotoxins. *J Biol Chem,* 283**,** 21145-52.

SILVEIRA, C., MARQUES-TEIXEIRA, J. & DE BASTOS-LEITE, A. J. 2012. More than one century of schizophrenia: an evolving perspective. *J Nerv Ment Dis,* 200**,** 1054-7.

SINGH, K. K., PARK, K. J., HONG, E. J., KRAMER, B. M., GREENBERG, M. E., KAPLAN, D. R. & MILLER, F. D. 2008. Developmental axon pruning mediated by BDNF-p75NTR-dependent axon degeneration. *Nat Neurosci,* 11**,** 649-58.

SLIMKO, E. M., MCKINNEY, S., ANDERSON, D. J., DAVIDSON, N. & LESTER, H. A. 2002. Selective electrical silencing of mammalian neurons in vitro by the use of invertebrate ligand-gated chloride channels. *J Neurosci,* 22**,** 7373-9.

SOKAL, R. R. & ROHLF, F. J. 1995. *Biometry: The principles and practice of statistics in biological research,* New York, W.H. Freeman.

SORIANO, P. 1999. Generalized lacZ expression with the ROSA26 Cre reporter strain. *Nat Genet,* 21**,** 70-1.

SPACEK, J. & HARRIS, K. M. 1997. Three-dimensional organization of smooth endoplasmic reticulum in hippocampal CA1 dendrites and dendritic spines of the immature and mature rat. *The Journal of neuroscience : the official journal of the Society for Neuroscience,* 17**,** 190-203.

SPITZER, N. C. 2006. Electrical activity in early neuronal development. *Nature,* 444**,** 707-12.

SRINIVASAN, S., VAISSE, C. & CONKLIN, B. R. 2003. Engineering the melanocortin-4 receptor to control G(s) signaling in vivo. *Ann N Y Acad Sci,* 994**,** 225-32.

ST-ONGE, L., FURTH, P. A. & GRUSS, P. 1996. Temporal control of the Cre recombinase in transgenic mice by a tetracycline responsive promoter. *Nucleic Acids Res,* 24**,** 3875-7.

STAR, E. N., KWIATKOWSKI, D. J. & MURTHY, V. N. 2002. Rapid turnover of actin in dendritic spines and its regulation by activity. *Nat Neurosci,* 5**,** 239-46.

STEPHAN, A. H., BARRES, B. A. & STEVENS, B. 2012. The complement system: an unexpected role in synaptic pruning during development and disease. *Annu Rev Neurosci,* 35**,** 369-89.

STEVENS, B., ALLEN, N. J., VAZQUEZ, L. E., HOWELL, G. R., CHRISTOPHERSON, K. S., NOURI, N., MICHEVA, K. D., MEHALOW, A. K., HUBERMAN, A. D., STAFFORD, B., SHER, A., LITKE, A. M., LAMBRIS, J. D., SMITH, S. J., JOHN, S. W. & BARRES, B. A. 2007. The classical complement cascade mediates CNS synapse elimination. *Cell,* 131**,** 1164-78.

STORNETTA, R. L. & ZHU, J. J. 2011. Ras and Rap signaling in synaptic plasticity and mental disorders. *Neuroscientist,* 17**,** 54-78.

STRATHDEE, C. A., MCLEOD, M. R. & HALL, J. R. 1999. Efficient control of tetracycline-responsive gene expression from an autoregulated bi-directional expression vector. *Gene,* 229**,** 21-9.

SUDHOF, T. C. 1995. The synaptic vesicle cycle: a cascade of protein-protein interactions. *Nature,* 375**,** 645-53.

SUTTON, R. B., FASSHAUER, D., JAHN, R. & BRUNGER, A. T. 1998. Crystal structure of a SNARE complex involved in synaptic exocytosis at 2.4 A resolution. *Nature,* 395**,** 347-53.

SVOBODA, K., TANK, D. W. & DENK, W. 1996. Direct measurement of coupling between dendritic spines and shafts. *Science,* 272**,** 716-9.

SWEET, R. A., HENTELEFF, R. A., ZHANG, W., SAMPSON, A. R. & LEWIS, D. A. 2009. Reduced dendritic spine density in auditory cortex of subjects with schizophrenia. *Neuropsychopharmacology,* 34**,** 374-89.

SWEGER, E. J., CASPER, K. B., SCEARCE-LEVIE, K., CONKLIN, B. R. & MCCARTHY, K. D. 2007. Development of hydrocephalus in mice expressing the G(i)-coupled GPCR Ro1 RASSL receptor in astrocytes. *The Journal of neuroscience : the official journal of the Society for Neuroscience,* 27**,** 2309-17.

SWITZER, R. C., 3RD 2000. Application of silver degeneration stains for neurotoxicity testing. *Toxicol Pathol,* 28**,** 70-83.

TACKENBERG, C., GHORI, A. & BRANDT, R. 2009. Thin, stubby or mushroom: spine pathology in Alzheimer's disease. *Curr Alzheimer Res,* 6**,** 261-8.

TAKAI, Y., SASAKI, T. & MATOZAKI, T. 2001. Small GTP-binding proteins. *Physiol Rev,* 81**,** 153-208.

TAKASHIMA, S., BECKER, L. E., ARMSTRONG, D. L. & CHAN, F. 1981. Abnormal neuronal development in the visual cortex of the human fetus and infant with down's syndrome. A quantitative and qualitative Golgi study. *Brain Res,* 225**,** 1-21.

TAKASHIMA, S., IESHIMA, A., NAKAMURA, H. & BECKER, L. E. 1989. Dendrites, dementia and the Down syndrome. *Brain Dev,* 11**,** 131-3.

TAN, E. M., YAMAGUCHI, Y., HORWITZ, G. D., GOSGNACH, S., LEIN, E. S., GOULDING, M., ALBRIGHT, T. D. & CALLAWAY, E. M. 2006. Selective and quickly reversible inactivation of mammalian neurons in vivo using the Drosophila allatostatin receptor. *Neuron,* 51**,** 157-70.

TASIC, B., MIYAMICHI, K., HIPPENMEYER, S., DANI, V. S., ZENG, H., JOO, W., ZONG, H., CHEN-TSAI, Y. & LUO, L. 2012. Extensions of MADM (mosaic analysis with double markers) in mice. *Plos One,* 7**,** e33332.

TERRY, R. D., MASLIAH, E., SALMON, D. P., BUTTERS, N., DETERESA, R., HILL, R., HANSEN, L. A. & KATZMAN, R. 1991. Physical basis of cognitive alterations in Alzheimer's disease: synapse loss is the major correlate of cognitive impairment. *Annals of neurology,* 30**,** 572-80.

TESSIER-LAVIGNE, M. & GOODMAN, C. S. 1996. The molecular biology of axon guidance. *Science,* 274**,** 1123-33.

THORPE, H. M. & SMITH, M. C. 1998. In vitro site-specific integration of bacteriophage DNA catalyzed by a recombinase of the resolvase/invertase family. *Proc Natl Acad Sci U S A,* 95**,** 5505-10.

THYAGARAJAN, B., OLIVARES, E. C., HOLLIS, R. P., GINSBURG, D. S. & CALOS, M. P. 2001. Site-specific genomic integration in mammalian cells mediated by phage phiC31 integrase. *Mol Cell Biol,* 21**,** 3926-34.

TOJIMA, T. 2012. Intracellular signaling and membrane trafficking control bidirectional growth cone guidance. *Neurosci Res,* 73**,** 269-74.

TRACHTENBERG, J. T., CHEN, B. E., KNOTT, G. W., FENG, G., SANES, J. R., WELKER, E. & SVOBODA, K. 2002. Long-term in vivo imaging of experience-dependent synaptic plasticity in adult cortex. *Nature,* 420**,** 788-94.

TRAYNELIS, S. F., WOLLMUTH, L. P., MCBAIN, C. J., MENNITI, F. S., VANCE, K. M., OGDEN, K. K., HANSEN, K. B., YUAN, H., MYERS, S. J. & DINGLEDINE, R. 2010. Glutamate receptor ion channels: structure, regulation, and function. *Pharmacol Rev,* 62**,** 405-96.

TRONCHE, F., KELLENDONK, C., KRETZ, O., GASS, P., ANLAG, K., ORBAN, P. C., BOCK, R., KLEIN, R. & SCHUTZ, G. 1999. Disruption of the glucocorticoid receptor gene in the nervous system results in reduced anxiety. *Nat Genet,* 23**,** 99-103.

TSAY, D. & YUSTE, R. 2004. On the electrical function of dendritic spines. *Trends Neurosci,* 27**,** 77-83.

TSIEN, J. Z., CHEN, D. F., GERBER, D., TOM, C., MERCER, E. H., ANDERSON, D. J., MAYFORD, M., KANDEL, E. R. & TONEGAWA, S. 1996. Subregion- and cell type-restricted gene knockout in mouse brain. *Cell,* 87**,** 1317-26.

TSIEN, R. Y. 1998. The green fluorescent protein. *Annu Rev Biochem,* 67**,** 509-44.

TURAN, S. & BODE, J. 2011. Site-specific recombinases: from tag-and-target- to tag-and-exchange-based genomic modifications. *FASEB J,* 25**,** 4088-107.

TURAN, S., GALLA, M., ERNST, E., QIAO, J., VOELKEL, C., SCHIEDLMEIER, B., ZEHE, C. & BODE, J. 2011. Recombinase-mediated cassette exchange (RMCE): traditional concepts and current challenges. *J Mol Biol,* 407**,** 193-221.

TURRIGIANO, G. 2011. Too many cooks? Intrinsic and synaptic homeostatic mechanisms in cortical circuit refinement. *Annu Rev Neurosci,* 34**,** 89-103.

TURRIGIANO, G. 2012. Homeostatic synaptic plasticity: local and global mechanisms for stabilizing neuronal function. *Cold Spring Harb Perspect Biol,* 4**,** a005736.

TYLER, W. J., PETZOLD, G. C., PAL, S. K. & MURTHY, V. N. 2007. Experience-dependent modification of primary sensory synapses in the mammalian olfactory bulb. *The Journal of neuroscience : the official journal of the Society for Neuroscience,* 27**,** 9427-38.

UDIN, S. B. & FAWCETT, J. W. 1988. Formation of topographic maps. *Annu Rev Neurosci,* 11**,** 289-327.

UESAKA, N., HAYANO, Y., YAMADA, A. & YAMAMOTO, N. 2007. Interplay between laminar specificity and activity-dependent mechanisms of thalamocortical axon branching. *The Journal of neuroscience : the official journal of the Society for Neuroscience,* 27**,** 5215-23.

UMEMORI, H., LINHOFF, M. W., ORNITZ, D. M. & SANES, J. R. 2004. FGF22 and its close relatives are presynaptic organizing molecules in the mammalian brain. *Cell,* 118**,** 257-70.

VALTSCHANOFF, J. G. & WEINBERG, R. J. 2001. Laminar organization of the NMDA receptor complex within the postsynaptic density. *The Journal of neuroscience : the official journal of the Society for Neuroscience,* 21**,** 1211-7.

VAN DEN POL, A. N. & GHOSH, P. K. 1998. Selective neuronal expression of green fluorescent protein with cytomegalovirus promoter reveals entire neuronal arbor in transgenic mice. *J Neurosci,* 18**,** 10640-51.

VAN DER BLIEK, A. M. & MEYEROWITZ, E. M. 1991. Dynamin-like protein encoded by the Drosophila shibire gene associated with vesicular traffic. *Nature,* 351**,** 411-4.

VAN DEURSEN, J., FORNEROD, M., VAN REES, B. & GROSVELD, G. 1995. Cre-mediated site-specific translocation between nonhomologous mouse chromosomes. *Proc Natl Acad Sci U S A,* 92**,** 7376-80.

VLACHOS, A. 2012. Synaptopodin and the spine apparatus organelle-regulators of different forms of synaptic plasticity? *Ann Anat,* 194**,** 317-20.

VOLGRAF, M., GOROSTIZA, P., NUMANO, R., KRAMER, R. H., ISACOFF, E. Y. & TRAUNER, D. 2006. Allosteric control of an ionotropic glutamate receptor with an optical switch. *Nat Chem Biol,* 2**,** 47-52.

VOZIYANOV, Y., KONIECZKA, J. H., STEWART, A. F. & JAYARAM, M. 2003. Stepwise manipulation of DNA specificity in Flp recombinase: progressively adapting Flp to individual and combinatorial mutations in its target site. *J Mol Biol,* 326**,** 65-76.

WEINGARTEN, M. D., LOCKWOOD, A. H., HWO, S. Y. & KIRSCHNER, M. W. 1975. A protein factor essential for microtubule assembly. *Proceedings of the National Academy of Sciences of the United States of America,* 72**,** 1858-62.

WEN, Q., STEPANYANTS, A., ELSTON, G. N., GROSBERG, A. Y. & CHKLOVSKII, D. B. 2009. Maximization of the connectivity repertoire as a statistical principle governing the shapes of dendritic arbors. *Proceedings of the National Academy of Sciences of the United States of America,* 106**,** 12536-41.

WILKIE, T. M., BRINSTER, R. L. & PALMITER, R. D. 1986. Germline and somatic mosaicism in transgenic mice. *Developmental biology,* 118**,** 9-18.

WILSON, M. C., MEHTA, P. P. & HESS, E. J. 1996. SNAP-25, enSNAREd in neurotransmission and regulation of behaviour. *Biochem Soc Trans,* 24**,** 670-76.

WITKOVSKY, P., PATEL, J. C., LEE, C. R. & RICE, M. E. 2009. Immunocytochemical identification of proteins involved in dopamine release from the somatodendritic compartment of nigral dopaminergic neurons. *Neuroscience,* 164**,** 488-96.

WOJTOWICZ, W. M., FLANAGAN, J. J., MILLARD, S. S., ZIPURSKY, S. L. & CLEMENS, J. C. 2004. Alternative splicing of Drosophila Dscam generates axon guidance receptors that exhibit isoform-specific homophilic binding. *Cell,* 118**,** 619-33.

WONG, R. O. 1999. Retinal waves and visual system development. *Annu Rev Neurosci,* 22**,** 29-47.

WOODS, G. F., OH, W. C., BOUDEWYN, L. C., MIKULA, S. K. & ZITO, K. 2011. Loss of PSD-95 enrichment is not a prerequisite for spine retraction. *The Journal of neuroscience : the official journal of the Society for Neuroscience,* 31**,** 12129-38.

WULFF, P., GOETZ, T., LEPPA, E., LINDEN, A. M., RENZI, M., SWINNY, J. D., VEKOVISCHEVA, O. Y., SIEGHART, W., SOMOGYI, P., KORPI, E. R., FARRANT, M. & WISDEN, W. 2007. From synapse to behavior: rapid modulation of defined neuronal types with engineered GABAA receptors. *Nat Neurosci,* 10**,** 923-9.

WULFF, P. & WISDEN, W. 2005. Dissecting neural circuitry by combining genetics and pharmacology. *Trends Neurosci,* 28**,** 44-50.

WUNDERLICH, F. T., WILDNER, H., RAJEWSKY, K. & EDENHOFER, F. 2001. New variants of inducible Cre recombinase: a novel mutant of Cre-PR fusion protein exhibits enhanced sensitivity and an expanded range of inducibility. *Nucleic Acids Res,* 29**,** E47.

XU, H. T., PAN, F., YANG, G. & GAN, W. B. 2007. Choice of cranial window type for in vivo imaging affects dendritic spine turnover in the cortex. *Nat Neurosci,* 10**,** 549-51.

XU, T. & RUBIN, G. M. 1993. Analysis of genetic mosaics in developing and adult Drosophila tissues. *Development,* 117**,** 1223-37.

XU, T., YU, X., PERLIK, A. J., TOBIN, W. F., ZWEIG, J. A., TENNANT, K., JONES, T. & ZUO, Y. 2009. Rapid formation and selective stabilization of synapses for enduring motor memories. *Nature,* 462**,** 915-9.

XU, X. & KIM, S. K. 2011. The early bird catches the worm: new technologies for the Caenorhabditis elegans toolkit. *Nat Rev Genet,* 12**,** 793-801.

YAMAMOTO, M., WADA, N., KITABATAKE, Y., WATANABE, D., ANZAI, M., YOKOYAMA, M., TERANISHI, Y. & NAKANISHI, S. 2003. Reversible suppression of glutamatergic neurotransmission of cerebellar granule cells in vivo by genetically manipulated

expression of tetanus neurotoxin light chain. *The Journal of neuroscience : the official journal of the Society for Neuroscience,* 23**,** 6759-67.

YANG, G., PAN, F. & GAN, W. B. 2009. Stably maintained dendritic spines are associated with lifelong memories. *Nature,* 462**,** 920-4.

YANG, Y., WANG, X. B., FRERKING, M. & ZHOU, Q. 2008. Spine expansion and stabilization associated with long-term potentiation. *J Neurosci,* 28**,** 5740-51.

YARON, A., HUANG, P. H., CHENG, H. J. & TESSIER-LAVIGNE, M. 2005. Differential requirement for Plexin-A3 and -A4 in mediating responses of sensory and sympathetic neurons to distinct class 3 Semaphorins. *Neuron,* 45**,** 513-23.

YASUDA, M., JOHNSON-VENKATESH, E. M., ZHANG, H. L., PARENT, J. M., SUTTON, M. A. & UMEMORI, H. 2011. Multiple Forms of Activity-Dependent Competition Refine Hippocampal Circuits In Vivo. *Neuron,* 70**,** 1128-1142.

YOUNG, P. & FENG, G. 2004. Labeling neurons in vivo for morphological and functional studies. *Curr Opin Neurobiol,* 14**,** 642-6.

YOUNG, P., QIU, L., WANG, D., ZHAO, S., GROSS, J. & FENG, G. 2008. Single-neuron labeling with inducible Cre-mediated knockout in transgenic mice. *Nat Neurosci,* 11**,** 721-8.

YU, C. R., POWER, J., BARNEA, G., O'DONNELL, S., BROWN, H. E., OSBORNE, J., AXEL, R. & GOGOS, J. A. 2004. Spontaneous neural activity is required for the establishment and maintenance of the olfactory sensory map. *Neuron,* 42**,** 553-66.

YU, W. & LU, B. 2012. Synapses and dendritic spines as pathogenic targets in Alzheimer's disease. *Neural Plast,* 2012**,** 247150.

YUSTE, R. 2011. Dendritic spines and distributed circuits. *Neuron,* 71**,** 772-81.

YUSTE, R. & BONHOEFFER, T. 2001. Morphological changes in dendritic spines associated with long-term synaptic plasticity. *Annu Rev Neurosci,* 24**,** 1071-89.

ZAMBROWICZ, B. P., IMAMOTO, A., FIERING, S., HERZENBERG, L. A., KERR, W. G. & SORIANO, P. 1997. Disruption of overlapping transcripts in the ROSA beta geo 26 gene trap strain leads to widespread expression of beta-galactosidase in mouse embryos and hematopoietic cells. *Proceedings of the National Academy of Sciences of the United States of America,* 94**,** 3789-94.

ZAR, J. H. 1999. *Biostatistical analysis,* Upper Saddle River, NJ, Prentice Hall.

ZARITSKY, J. J., ECKMAN, D. M., WELLMAN, G. C., NELSON, M. T. & SCHWARZ, T. L. 2000. Targeted disruption of Kir2.1 and Kir2.2 genes reveals the essential role of the inwardly rectifying K(+) current in K(+)-mediated vasodilation. *Circ Res,* 87**,** 160-6.

ZEMELMAN, B. V., LEE, G. A., NG, M. & MIESENBOCK, G. 2002. Selective photostimulation of genetically chARGed neurons. *Neuron,* 33**,** 15-22.

ZHANG, J., ZHAO, J., JIANG, W. J., SHAN, X. W., YANG, X. M. & GAO, J. G. 2012. Conditional gene manipulation: Cre-ating a new biological era. *J Zhejiang Univ Sci B,* 13**,** 511-24.

ZHANG, Y., RIESTERER, C., AYRALL, A. M., SABLITZKY, F., LITTLEWOOD, T. D. & RETH, M. 1996. Inducible site-directed recombination in mouse embryonic stem cells. *Nucleic Acids Res,* 24**,** 543-8.

ZHAO, S., TING, J. T., ATALLAH, H. E., QIU, L., TAN, J., GLOSS, B., AUGUSTINE, G. J., DEISSEROTH, K., LUO, M., GRAYBIEL, A. M. & FENG, G. 2011a. Cell type-specific channelrhodopsin-2 transgenic mice for optogenetic dissection of neural circuitry function. *Nat Methods,* 8**,** 745-52.

ZHAO, Y., ARAKI, S., WU, J., TERAMOTO, T., CHANG, Y. F., NAKANO, M., ABDELFATTAH, A. S., FUJIWARA, M., ISHIHARA, T., NAGAI, T. & CAMPBELL, R. E. 2011b. An expanded palette of genetically encoded Ca(2)(+) indicators. *Science,* 333**,** 1888-91.

ZHOU, Q., HOMMA, K. J. & POO, M. M. 2004. Shrinkage of dendritic spines associated with long-term depression of hippocampal synapses. *Neuron,* 44**,** 749-57.

ZHU, H. & LUO, L. 2004. Diverse functions of N-cadherin in dendritic and axonal terminal arborization of olfactory projection neurons. *Neuron,* 42**,** 63-75.

ZIMMERMAN, L., PARR, B., LENDAHL, U., CUNNINGHAM, M., MCKAY, R., GAVIN, B., MANN, J., VASSILEVA, G. & MCMAHON, A. 1994. Independent regulatory elements in the nestin gene direct transgene expression to neural stem cells or muscle precursors. *Neuron,* 12**,** 11-24.

ZIPURSKY, R. B., LIM, K. O., SULLIVAN, E. V., BROWN, B. W. & PFEFFERBAUM, A. 1992. Widespread cerebral gray matter volume deficits in schizophrenia. *Arch Gen Psychiatry,* 49**,** 195-205.

ZONG, H., ESPINOSA, J. S., SU, H. H., MUZUMDAR, M. D. & LUO, L. 2005. Mosaic analysis with double markers in mice. *Cell,* 121**,** 479-92.

ZOU, Y. & LYUKSYUTOVA, A. I. 2007. Morphogens as conserved axon guidance cues. *Curr Opin Neurobiol,* 17**,** 22-8.

ZUO, Y., LIN, A., CHANG, P. & GAN, W. B. 2005. Development of long-term dendritic spine stability in diverse regions of cerebral cortex. *Neuron,* 46**,** 181-9.

IV. Acknowledgments

This thesis is dedicated to my wonderful husband, Brendan, and to my two beautiful daughters, Saoirse Teresa and Elena Louise. They are my inspiration and my reason for persevering, and I love you with all my being. Thank you, Brendan, for all your loving support and understanding, this thesis is as much yours as it is mine.

Thank you to my supervisor, Paul, who has shaped me into the scientist that I am today. As one of his first PhD students, I admire and congratulate your hard work during the last four years. You have challenged us, encouraged us, and most of all helped us in times of need. Thank you to Kate and Orthis for enduring the journey with me and making it a fun one!

Thank you to my parents, Grace, Hakon, Alden, and Jim, for all your love, support, encouragement, care, and help. I am who I am because of you and I owe this work to all four of you. Special thanks to Mama for always being by my side; for all your advice, all the sleepless nights finishing school projects, all the discipline you taught me and, in the last three months, for all the babysitting! I literally could not have done it without you. Special thanks to my chief editor and best writing instructor, Hakon; thank you for giving me the confidence to write this dissertation and thank you for editing all my work throughout the years!

Finally, thank you to my grandparents, whose lives have paved the way for my success. To my kind and loving grandmother, Mami (may she rest in peace), I am grateful for all the tender, beautiful memories. Thank you, Papi, for being my #1 fan and always encouraging me to succeed in anything I do. Farmor (RIP), I thank you for the fun memories and for teaching me about the world in your own way, I know myself better because of you. Farfar (RIP), you are my inspiration and role model, thank you for teaching me that a good scientist always doubts him/herself.